

Multilevel Assessment of The Role of Moisture and Temperature in ASR-Induced Expansion and Deterioration

Olusola David Olajide

A Thesis

In the Department

of

Building, Civil and Environmental Engineering (BCEE)

Presented in Partial Fulfillment of the Requirements for the Degree of

Doctor of Philosophy in Civil Engineering

at

Concordia University

Montréal, Québec, Canada

January 2025

© Olusola David Olajide, 2025

Concordia University
School of Graduate Studies

This is to certify that the thesis prepared

By: Olusola David Olajide

Entitled: Multilevel Assessment of the Role of Moisture and Temperature in ASR-induced Expansion and Deterioration

and submitted in partial fulfillment of the requirements for the degree of

DOCTOR OF PHILOSOPHY (Civil Engineering)

Complies with the regulations of the University and meets the accepted standards with respect to originality and quality.

Signed by the final examining committee:

_____	Chair
Dr. Rabin Raut	
_____	External Examiner
Dr. Kevin Folliard	
_____	External to Program
Dr. Mamoun Medraj	
_____	Examiner
Dr. Bruno Lee	
_____	Examiner
Dr. Ahmed Soliman	
_____	Thesis Supervisor
Dr. Michelle Nokken	
_____	Thesis Supervisor
Dr. Leandro Sanchez	

Approved by _____
Graduate Program Director

January, 2025 _____
Dean of Faculty

ABSTRACT

Multilevel Assessment of the Role of Moisture and Temperature in ASR-induced Expansion and Deterioration

Olusola David Olajide, PhD

Concordia University, 2025

Alkali silica reaction (ASR) is a widely known deterioration mechanism in concrete; sufficient moisture and temperature are crucial for initiating and sustaining the reaction. The influence of these factors on ASR-induced expansion has been previously studied. However, little is known about their influence on ASR-induced damage. This work aims to apply a multi-level assessment protocol combining microscopic and mechanical properties tools to evaluate the impact of a wide range of moisture conditions and temperatures on ASR-induced expansion and deterioration. Concrete specimens were manufactured in the laboratory incorporating aggregates displaying different levels of reactivity (i.e., moderate, high, and very-high) and containing two alkali loadings (i.e., 3.82kg/m^3 and $5.25\text{kg/m}^3 Na_2O_{eq}$ by mass of cement). The specimens were conditioned at five relative humidities (i.e., 100%, 90%, 82%, 75%, and 62%) and three temperatures (i.e., 21°C , 38°C , and 60°C) and monitored for internal and external moisture, and ASR expansion over time. A time-based assessment was conducted, and upon reaching pre-defined ages (i.e., 3, 6, and 12 months), the Damage Rating Index (DRI), Stiffness Damage Test (SDT), Direct Shear, and compressive strength tests were conducted to appraise ASR-induced deterioration in the specimens. The results show that moisture inside concrete is typically around 90% RH from batching, which enables rapid ASR-induced expansion. However, lower external moisture reduces internal moisture and may induce shrinkage cracks that influence the overall

damage pattern. Moreover, at elevated temperatures, ASR-induced cracks exhibit greater density but shorter length and narrower width compared to lower temperatures despite similar expansion levels. These conditions influence the microscopic and mechanical properties of ASR-affected concrete, with the DRI and SDT outcomes presenting a strong correlation to expansion. Through the multi-level assessment protocol, this study establishes that the moisture threshold required to trigger ASR is temperature- and aggregate-dependent. While the 80% RH has been widely used in the past, the findings of this study suggest that a lower range (62-75% RH) might be required for high temperatures and reactivity of the aggregates. A novel damage classification table that accounts for a wider range of exposure conditions is thus proposed, offering a more comprehensive tool for the condition assessment of ASR-affected concrete.

ACKNOWLEDGMENTS

First and foremost, I would like to express my sincere gratitude to my supervisor, Prof. Michelle Nokken, and my co-supervisor, Prof. Leandro Sanchez, for their continuous support and guidance throughout my Ph.D. studies. Prof. Nokken believed in me even before I saw my potential. Her confidence in my success was a constant source of motivation during this roller-coaster journey. Prof. Sanchez took a chance on me when he didn't have to. He welcomed me into his research group as if I were one of his students and ensured I had everything I needed to make this study successful. I could not have imagined better supervisors for my Ph.D.

I would like to express my heartfelt appreciation to my wife, Shakirat. Your love, unwavering support, and belief in me have been my pillars of strength. The late nights, prayers, and mental support you provided were instrumental in my success. And to my son, Ethan, your smiles brightened my day and gave me every reason to keep going. I am truly grateful for your presence in my life.

I must express my undiluted gratitude to my parents (Mr. Kolawole Olajide and Mrs. Veronica Olajide) for all your sacrifices. You allowed me to fulfill my dreams. I also want to thank my siblings (Omolola Alagbado, Bolanle Faluade, and Mary Olajide); you guys rock. I can't ask for better siblings.

Also, I must express my sincere appreciation to my colleagues in the uOttawa concrete microstructure research team; you all welcomed me with open arms and even allowed me to serve as a group leader. My Ph.D. story would never be complete without this team. Special recognitions (in no specific order) to Cassandra, Rennan, Ana, Mayra, Diego, Andisheh, Leah, Agnes and Luan. Thank you for all your support.

Finally, I would like to recognize two important Civil Engineering Materials and Structures lab members in uOttawa: Drs. Muslim Majeed and Gamal Elnabelsya. You are both instrumental in the success of my experimental program. Thank you very much for your support.

CONTRIBUTION OF AUTHORS

This dissertation is manuscript-based, consisting of five papers in various stages of publication. With the support of my supervisors, I designed the experimental program for the study and performed all the experimental work. Furthermore, I analyzed all the data, wrote the first drafts of all five scientific papers, and were reviewed by my main and co-supervisors. Chapter two has been published in the Materials journal. Chapter seven has been published in the Journal of Cement and Concrete Composites (CCC). Chapters six and eight have been submitted for publication in scientific journals. Moreover, Chapter nine is expected to be submitted for publication in Winter 2025.

Chapter 9:

Rennan Medeiros wrote the Python code for the multiply imputation chained equations (MICE) and Response surface methodology (RSM).

All authors reviewed the final manuscripts and approved the contents.

TABLE OF CONTENTS

LIST OF FIGURES	xiv
LIST OF TABLES.....	xviii
CHAPTER ONE: INTRODUCTION.....	1
CHAPTER TWO: ALKALI–SILICA REACTIONS: LITERATURE REVIEW ON THE INFLUENCE OF MOISTURE AND TEMPERATURE AND THE KNOWLEDGE GAP ..	4
2.1 Introduction	5
2.1.1 Background.....	5
2.1.2 The mechanism of the ASR	8
2.2 Review objectives	10
2.3 Moisture in concrete.....	10
2.4 The role of moisture in the alkali–silica reaction	13
2.4.1 Relative humidity threshold.....	14
2.4.2 The role of alternate drying and wetting on the availability of moisture for the alkali–silica reaction.....	16
2.5 The role of temperature in the kinetics of the ASR.....	18
2.2.6 The influence of moisture and temperature on the microstructure properties of ASR-affected concrete	24
2.7 Conclusions	28
CHAPTER THREE: MULTILEVEL ASSESSMENT OF ASR-INDUCED DAMAGE.....	30
3.1 Stiffness Damage Test (SDT).....	30
3.2 Damage Rating Index (DRI)	32
3.3 Direct shear	34
3.4 Compressive strength	35
CHAPTER FOUR: PROBLEM STATEMENT AND OBJECTIVES OF THE STUDY	37
CHAPTER FIVE: RESEARCH PROGRAM AND CORE OF THE THESIS.....	39
5.1 Experimental procedures.....	40
5.1.1 Control of relative humidity (RH).....	40
5.1.3 Stiffness Damage Test (SDT)	43
5.1.4 Damage Rating Index (DRI).....	43
5.1.5 Direct shear.....	44

5.1.6 Compressive strength	44
5.2 Core of the thesis – scientific paper	44
CHAPTER SIX: MOISTURE DYNAMICS AND INFLUENCE ON ALKALI-SILICA REACTION-INDUCED EXPANSION: A COMPREHENSIVE LABORATORY STUDY	47
6.1 Introduction	48
6.2 Background	49
6.2.1 Scope of work.....	51
6.3 Materials and methods	52
6.3.1 Concrete mixture design and materials	52
6.3.2 Experimental program	53
6.3.2.1 Control and measurement of relative humidity	53
6.3.2.2 Concrete cylinders conditioned at the selected testing temperatures.....	56
6.4 Results	57
6.4.1 Relative humidity and temperature measurements.....	57
6.4.2 Mass and length change and ASR kinetics.....	60
6.5 Discussion	63
6.5.1 Influence of exposure conditions on ASR-induced length change rates	63
6.5.2 Understanding moisture dynamics in concrete and the influence of ASR-induced expansion	67
6.5.3 Assessing the moisture threshold for ASR	72
6.6 Conclusion.....	74
Supplementary materials	76
Overview of chapter six	78
CHAPTER SEVEN: EVALUATION OF THE INDUCED MECHANICAL DETERIORATION OF ASR-AFFECTED CONCRETE UNDER VARIED MOISTURE AND TEMPERATURE CONDITIONS	79
7.1 Introduction	80
7.2 Background	81
7.2.1 Overview of ASR.....	81
7.2.2 ASR and mechanical properties reduction.....	82
7.2.3 Influence of temperature and RH on ASR-induced development	84
7.2.4 Mechanical property protocols to appraise ASR-induced deterioration.....	85
7.2.4.1 Stiffness Damage Test (SDT).....	85

7.2.4.2 Direct shear test.....	87
7.2.4.3 Compressive strength.....	88
7.2.5 Scope of work.....	89
7.3 Materials and Method.....	89
7.3.1 Concrete mix design and materials.....	89
7.3.2 Testing conditions.....	90
7.3.3 Manufacturing of concrete specimens and storage.....	91
7.3.4 Experimental procedures.....	91
7.3.4.1 Stiffness Damage Test (SDT).....	91
7.3.4.2 Direct shear test.....	92
7.3.4.3 Compressive strength test.....	92
7.4 Results.....	93
7.4.1 ASR development.....	93
7.4.2 Mechanical Properties.....	97
7.4.2.1 Stiffness Damage Test.....	97
7.4.2.1.1 Modulus of elasticity.....	97
7.4.2.1.2 Stiffness Damage Test – Indices.....	98
7.4.2.2 Direct Shear.....	101
7.4.2.3 Compressive strength.....	102
7.5 Discussion.....	103
7.5.1 Mechanical properties of ASR affected concrete and influence of moisture and temperature.....	105
7.5.2 Statistical analysis of data.....	109
7.5.3 Validation of ASR distress development using microscopic assessment.....	112
7.5.4 Assessing moisture threshold for ASR using mechanical properties reductions.....	115
7.6 Conclusion.....	118
Overview of chapter seven.....	119
CHAPTER EIGHT: EVALUATION OF THE INFLUENCE OF MOISTURE AND TEMPERATURE ON THE MICROSTRUCTURAL PROPERTIES OF ASR.....	120
8.1 Introduction.....	121
8.2 Background.....	122
8.2.1 Overview of ASR.....	122
8.2.2 Microstructure of ASR-affected concrete.....	122

8.2.3 Influence of moisture and temperature on ASR-induced development.....	124
8.2.4 Damage Rating Index (DRI).....	125
8.2.5 Scope of work.....	128
8.3 Materials and method.....	129
8.3.1 Materials and mix proportion.....	129
8.3.2 Selection of exposure conditions, durations, and concrete manufacture.....	130
8.3.3 Experimental procedures.....	132
8.3.3.1 Damage Rating Index (DRI).....	132
8.3.3.2 Image analysis – crack patterns.....	132
8.4 Results.....	134
8.4.1 ASR kinetics at numerous exposure conditions.....	134
8.4.2 Microscopic distress features.....	137
8.4.3 Crack width, length and density.....	140
8.4.4 Crack orientation analysis.....	142
8.4.5 Damage Rating Index (DRI).....	143
8.5 Discussion.....	144
8.5.1 Effect of moisture and temperature on ASR kinetics.....	144
8.5.2 Understanding the influence of RH and temperature on the microstructural properties of ASR-affected concrete.....	146
8.5.2.1 Time-based assessment.....	147
8.5.2.1.1 DRI number and Crack properties.....	147
8.5.2.1.2 Influence of moisture and temperature on distress features.....	149
8.5.2.2 Expansion-based assessment.....	152
8.5.3 Relative humidity threshold for significant ASR damage.....	157
8.6 Conclusion.....	159
Supplementary materials.....	161
Overview of chapter eight.....	164
CHAPTER NINE: MULTILEVEL ASSESSMENT OF ASR-INDUCED DAMAGE IN CONCRETE: EFFECTS OF RELATIVE HUMIDITY, TEMPERATURE, AGGREGATE REACTIVITY AND ALKALI CONTENT.....	165
9.1 Introduction.....	166
9.2 Background.....	167
9.2.1 ASR-induced development.....	167

9.2.2 Effect of moisture and temperature on ASR.....	168
9.2.3 Effect of aggregate reactivity level and alkali content on ASR.....	168
9.2.4 Tools for assessing ASR-induced damage.....	171
9.2.5 Scope of work.....	171
9.3 Materials and method.....	172
9.3.1 Statistical design of experiment (DOE).....	172
9.3.2 Materials.....	173
9.3.3 Experimental Methods.....	176
9.3.3.1 Stiffness Damage Test (SDT).....	176
9.3.3.2 Damage Rating Index (DRI).....	176
9.3.3.3 Compressive strength.....	177
9.4 Results.....	178
9.4.1 ASR kinetics.....	178
9.4.1.1 Concrete cylinders conditioned at 21°C and 38°C.....	178
9.4.1.2 Concrete cylinders conditioned at 60°C.....	180
9.4.2 Stiffness Damage Test (SDT).....	181
9.4.2.1 Modulus of elasticity reduction (MER).....	182
9.4.2.2 Stiffness Damage Index (SDI).....	186
9.4.3 Compressive strength reduction (CSR).....	189
9.4.4 Damage Rating Index (DRI).....	193
9.5 Discussion.....	196
9.5.1 Understanding the overall influence of aggregate reactivity, alkali loading and exposure conditions on ASR kinetics and damage development.....	196
9.5.1.1 ASR kinetics.....	196
9.5.1.2 Microscopic assessment.....	197
9.5.1.3 Mechanical properties.....	201
9.5.2 Influence of exposure conditions, alkali loading, and aggregate reactivity on ASR damage classification degree.....	203
9.5.3 Exploring the influence of exposure conditions, alkali content and aggregate reactivity on ASR-induced damage using the response surface methodology (RSM).....	207
9.5.4 Damage-based RH threshold assessment.....	210
9.6 Conclusion.....	216
Supplementary materials.....	218

Overview of Chapter nine	226
CHAPTER TEN: SCIENTIFIC AND ENGINEERING CONTRIBUTIONS OF THE PHD THESIS	227
10.1 Scientific contributions	227
10.2 Engineering contributions	228
CHAPTER ELEVEN: CONCLUSIONS AND RECOMMENDATIONS.....	229
11.1 Conclusions	229
11.2 Recommendations	231
References	

LIST OF FIGURES

Figure 1.1: Descriptive model for crack propagation in ASR-affected concrete [6] (reproduced with permission of Elsevier).....	1
Figure 2.1: ASR induced cracks (a) A (Open crack in aggregate with reaction product; OCAG), B (Crack in cement paste with reaction product; CCPG); (b) C (Closed crack in aggregate; CCA), D (Open crack in aggregate; OCA)	7
Figure 2.2: Sequence of ASR: (a) factors needed for ASR; (b) initiation of cracks; (c) propagation of cracks. Modified from [6,53].....	8
Figure 2.3: Relative humidity threshold as a function of temperature, specimen type, and reactive content from several studies [8,13,26,46–48,93,94].....	16
Figure 2.4: ASR-induced ultimate expansion at different temperatures reported by several authors [89,95,100,106,108–111].....	22
Figure 2.5: Damage features counted in CPT (38°C, >95% RH) and ACPT (50°C, >95% RH) at 0.1% and 0.20% expansion levels: (a) comparison of DRI results at 0.1% expansion; (b) comparison of DRI results at 0.2% expansion. Adapted from[6,100]	28
Figure 3.1: The Stiffness Damage Test [133]	31
Figure 3.2: Damage Rating Index: (a,b) ASR distress features (c) Distress features with corresponding weighting factors [140]	33
Figure 3.3: The direct shear test [148].....	35
Figure 5.1: Experimental set up: (a) Framework for internal and external RH measurement (b) storage bucket with sensor for external RH measurement (c) iButton sensor [151] (d) test cylinder for internal RH measurement.....	41
Figure 5.2: Core of the PhD. Thesis-link between scientific papers	45
Figure 6.1: Experimental set up: (a) Framework for internal and external RH measurement (b) storage bucket with sensor for external RH measurement (c) iButton sensor [151] (d) test cylinder for internal RH measurement.....	55
Figure 6.2: Testing Matrix.	56
Figure 6.3: Internal RH (IRH) and External RH (ERH) as a function of time: (a) 21°C (b) 38°C (c) 60°C	59
Figure 6.4: Mass and length change as a function of time at three different temperatures: (a) mass change-21°C (b) length change-21°C (c) mass change-38°C (d) length change-38°C (e) mass change-60°C (f) length change-60°C	63
Figure 6.5: Length change rate over time at five different relative humidity: (a) 21°C (b) 38°C (c) 60°C	64
Figure 6.6: Length change rate over time at three different temperatures: (a) 100% RH (b) 90% RH (c) 82% RH (d) 75% RH (e) 62% RH.....	65
Figure 6.7: RH difference as a function of age (Abs [IRH-ERH]): (a) 21°C (b) 38°C (c) 60°C ..	68
Figure 6.8: K values (IRH/ERH) and length change as a function of maturity: (a) 100% RH (b) 90% RH (c) 82% RH (d) 75% RH (e) 62% RH	70
Figure 6.9: Assessing the influence of temperature on RH threshold for ASR	73
Figure S6.1: Surface plot - 21°C: (a) 3D response surface plot of interaction between time and ERH (b) 3D response surface plot of interaction between time and IRH.....	77

Figure S6.2: Surface plot - 38°C: (a) 3D response surface plot of interaction between time and ERH (b) 3D response surface plot of interaction between time and IRH.....	77
Figure S6.3: Surface plot - 60°C: (a) 3D response surface plot of interaction between time and ERH (b) 3D response surface plot of interaction between time and IRH.....	78
Figure 7.1: Descriptive model for crack propagation in ASR-affected concrete[6] (reproduced with permission of Elsevier)	82
Figure 7.2: Reduction in mechanical properties involving aggregates of varying levels of reactivity, aggregate type, and concrete strength: (a) Compressive strength (b) modulus of elasticity (c) direct shear [17,141] (used with permission from Elsevier).....	84
Figure 7.3: The Stiffness Damage Test [133] (reproduced with permission of Elsevier).....	86
Figure 7.4: The direct shear test.....	88
Figure 7.5: ASR kinetics at numerous relative humidities, including both decoupled expansion and non-decoupled length changes: (a) 21°C (b) 38°C (c) 60°C	94
Figure 7.6: Modulus of Elasticity reduction versus relative humidity: (a) at 21°C (b) at 38°C (c) at 60°C	98
Figure 7.7: Stiffness Damage Index versus relative humidity: (a) at 21°C (b) at 38°C (c) at 60°C	100
Figure 7.8: Plastic Deformation Index versus relative humidity: (a) at 21°C (b) at 38°C (c) at 60°C	101
Figure 7.9: Direct shear reduction versus relative humidity: (a) at 21°C (b) at 38°C (c) at 60°C	102
Figure 7.10: Compressive strength results: (a) at 21°C (b) at 38°C (c) at 60°C	103
Figure 7.11: Mechanical properties reduction as a function of expansion (i.e., total and net), relative humidity (RH), and temperature (°C): (a,b) modulus of elasticity reduction (c,d) SDI (e,f) PDI (g,h) shear strength reduction (i,j) Compressive strength reduction.....	107
Figure 7.12: Microscopic features count at numerous RH and temperature as a function of time: (a) 21°C (b) 38°C (c) 60°C.....	114
Figure 7.13: Mechanical properties reductions as a function of relative humidity: (a) 21°C (b) 38°C (c) 60°C	117
Figure 8.1: Qualitative AAR damage model vs. levels of expansion between 0.05 and 0.30% aggregates [6] [reproduction with permission from Elsevier]	123
Figure 8.2: Damage Rating Index: (a,b) ASR distress features (c) Distress features with corresponding weighting factors [140]	127
Figure 8.3: Flow chart of crack pattern analysis.....	133
Figure 8.4: Image processing: (a) ASR-affected specimen surface (b) traced image (c) cracks on a black layer (d) thresholding of only ASR-induced cracks on ImageJ	133
Figure 8.5: ASR kinetics at numerous relative humidities, including both decoupled expansion and non-decoupled length changes: (a) 21°C (b) 38°C (c) 60°C	136
Figure 8.6: Count of microscope features: (a,b) 21°C (c,d) 38°C (e,f) 60°C	138
Figure 8.7: Percentage of counts: (a,b) 21°C (c,d) 38°C (e,f) 60°C	140
Figure 8.8: Damage Rating Index results: (a) 21°C and 38°C (b) 60°C.....	144

Figure 8.9: Influence of RH and temperature on ASR-induced expansion at different ages: (a) 3 months expansion (b) 6 months expansion (c) ultimate expansion: 21°C and 38°C at six months and 60°C at six months.	145
Figure 8.10: DRI results with decoupled ASR-induced expansion: (a) 21°C-6months (b) 21°C-12 months (c) 38°C-6months (d) 38°C-12 months (e) 60°C-3months (f) 60°C-6months.....	147
Figure 8.11: Decoupled DRI results with decoupled ASR-induced expansion: (a) 21°C-6months (b) 21°C-12 months (c) 38°C-6months (d) 38°C-12 months (e) 60°C-3months (f) 60°C-6months	150
Figure 8.12: Heat maps of damage assessment at similar expansion levels: (a) High expansion, (b) Moderate expansion, (c) low expansion	154
Figure 8.13: Crack properties at similar expansion: (a) crack density (b) max. crack width (c) max. crack length.....	155
Figure 8.14: Some maximum crack widths recorded in the study.....	157
Figure 8.15: Assessment of RH humidity threshold for ASR damage at three different temperatures comparing DRI with: (a) Expansion, (b) Crack density, (c) Maximum crack width, (d) Maximum crack length.....	158
Figure S8.1: Directionality histogram at 21°C	162
Figure S8.2: Directionality histogram at 38°C	163
Figure S8.3: Directionality histogram at 60°C	164
Figure 9.1: Qualitative model for crack propagation in ASR-affected concrete[6] (reproduced with permission of Elsevier)	167
Figure 9.2: Distress features with corresponding weighting factors [140].....	177
Figure 9.3: ASR expansions results at 21°C and 38°C: (a) Sudbury-21°C (b) Sudbury-38°C (c) Spratt-21°C (d) Spratt-38°C (e) Springhill-21°C (f) Springhill-38°C.....	179
Figure 9.4: ASR expansions results at 60°C: (a) Sudbury-60°C (b) Spratt-60°C	181
Figure 9.5: Modulus of elasticity reduction as a function of time, relative humidity and aggregates: (a) 21°C-boosted alkalis (b) 21°C-non-boosted alkalis (c) 38°C-boosted alkalis (d) 38°C-non-boosted alkalis (e) 60°C-boosted alkalis (f) 60°C-non-boosted alkalis	185
Figure 9.6: Stiffness Damage Index (SDI) as a function of time, relative humidity and aggregates: (a) 21°C-boosted alkalis (b) 21°C-non-boosted alkalis (c) 38°C-boosted alkalis (d) 38°C-non-boosted alkalis (e) 60°C-boosted alkalis (f) 60°C-non-boosted alkalis	189
Figure 9.7: Compressive strength reduction (CSR) as a function of time, relative humidity and aggregates: (a) 21°C-boosted alkalis (b) 21°C-non-boosted alkalis (c) 38°C-boosted alkalis (d) 38°C-non-boosted alkalis (e) 60°C-boosted alkalis (f) 60°C-non-boosted alkalis	193
Figure 9.8: Microscopic distress features of deterioration (counts): (a) 21°C-6 Months (b) 21°C-12 Months (c) 38°C-6 Months (d) 38°C-12 Months (e) 60°C-3 Months (f) 60°C-6 Months	194
Figure 9.9: Damage Rating Index: (a) DRI number of ASR-affected concrete incorporating aggregates of different levels of reactivity at numerous exposure conditions (b) Expansion range as a function of RH, temperature, and aggregate type.....	197
Figure 9.10: DRI results for specimens containing three aggregates (SP, SB, and SPH) with two alkali levels in numerous RH conditions: (a,b) 21°C (c,d) 38°C (e,f) 60°C	200

Figure 9.11: Mechanical properties of ASR-affected concrete incorporating aggregates of different levels of reactivity at numerous exposure conditions: (a) compressive strength reduction (b) modulus of elasticity reduction (c) SDI (d) RH, temperature, and expansion.....	202
Figure 9.12: 3D surface and 2D contour plot of expansion model: (a,b) effects of aggregate reactivity and RH (c,d) effects of temperature and RH (e,f) effects of alkali content and RH...	209
Figure 9.13: Damage-based (ultimate expansion, DRI and modulus loss) evaluation of RH threshold for ASR: (a,b) 21°C (c,d) 38°C (e,f) 60°C	211
Figure 9.14: Pareto plot: (a) Expansion (b) DRI (c) Modulus.....	215
Figure S9.1: 3D surface and 2D contour plot of DRI model: (a,b) effects of aggregate reactivity and RH (c,d) effects of temperature and RH (e,f) effects of alkali loading and RH.....	221
Figure S9.2: 3D surface and 2D contour plot surface of modulus of elasticity reduction model: (a,b) effects of aggregate reactivity and RH (c,d) effects of temperature and RH (e,f) effects of alkali loading and RH	222

LIST OF TABLES

Table 2.1: Moisture measurement techniques.....	11
Table 2.2: Database of ASR expansion at different temperatures.....	20
Table 2.3: Microstructure assessment of ASR	24
Table 2.4: Damage features used in Damage Rating Index [6]	26
Table 5.1: Testing matrix	39
Table 5.2: Control of relative humidity.....	40
Table 6.1: Characterization of aggregates.....	52
Table 6.2: Mixture design of concrete	53
Table 6.3: Control of relative humidity.....	54
Table 6.4: Early age external RH (ERH) and internal (RH) readings	59
Table S6.1: Moisture and length change measurements for high alkali concrete at 21°C for numerous relative humidity	76
Table S6.2: Moisture and length change measurements for high alkali concrete at 38°C for numerous relative humidity	76
Table S6.3: Moisture and length change measurements for high alkali concrete at 60°C for numerous relative humidity	77
Table 7.1: Aggregates used in the study.....	90
Table 7.2: Characteristics of the two mixtures.....	90
Table 7.3: Classification of damage[141] [Reproduced with permission from Elsevier].....	106
Table 7.4: ANOVA results.....	110
Table 7.5: Tukey post hoc test results: (a) compressive strength (b) Modulus of elasticity (c) SDI (d) PDI	111
Table 7.6: Damage features and corresponding weighting factors [140]	113
Table 8.1: Properties of aggregates used.....	129
Table 8.2: Characteristics of the two mixtures.....	130
Table 8.3: Control of relative humidity.....	131
Table 8.4: Crack length, width, and density.....	141
Table 8.5: Crack orientations	142
Table 8.6: Expansion-based assessment of the role of RH and temperature	152
Table 9.1: Relative humidity thresholds	170
Table 9.2: Factors and associated level for the design of experiment	173
Table 9.3: Aggregates used in the study.....	174
Table 9.4: Characteristics of the seven mixtures	174
Table 9.5: Control of relative humidity.....	175
Table 9.6: Comparison of the classification of ASR-induced damage in concrete [141] (<i>Reproduced with permission of Elsevier</i>)	205
Table 9.7: Classification of ASR-induced damage coupled with shrinkage in concrete [141] (<i>Reproduced with permission of Elsevier</i>)	207
Table 9.8: Influence of temperature and aggregate reactivity on damage-based RH threshold for ASR.....	213
Table S9.1: Influence of RH on damage.....	218

Table S9.2: Influence of temperature on damage	219
Table S9.3: ANOVA Table for expansion	219
Table S9.4: ANOVA Table for DRI.....	220
Table S9.5: ANOVA Table for modulus loss	220
Table S9.6: Tukey test for damage assessment: (a) expansion. (b) modulus of elasticity reduction. Chi-squared test for (c) DRI	223
Table S9.7: Experimental plan.....	224

CHAPTER ONE: INTRODUCTION

Alkali-silica reaction (ASR) is a well-known deterioration mechanism in concrete. It involves a physicochemical reaction between certain siliceous phases in aggregates and the alkali ions (i.e., Na^+ , K^+ , and OH^-) in the concrete pore solution. This leads to the generation of a secondary reaction product (i.e., often referred to as ASR gel) that exhibits swelling characteristics and can potentially induce cracks in affected concrete, especially in humid environments. Since the discovery of this reaction several decades ago [1], numerous concrete structures suffering from ASR have been reported, and they are often prone to an early loss of serviceability [2–5]. ASR is typically initiated within the aggregate particles (i.e., fine or coarse), as illustrated by the descriptive model by Sanchez et al. [6]; sharp and onion skin cracks represented by A and B, respectively, in Fig. 1.1, are generated in the aggregates at low expansion (i.e., 0.05%). The existing cracks increase in length and width as expansion increases, and some of these cracks can propagate into the cement paste at moderate expansion levels (i.e., $\sim 0.12\%$). At high expansion levels (i.e., $\geq 0.20\%$), most of the cracks originating in the aggregates propagate to the cement paste, and some network of cracks in the cement paste can be observed. At very high expansion levels (i.e., $\geq 0.30\%$), the cement paste cracks are quite dense, with cracks originating from distinct aggregate particles connecting to one another [6,7].

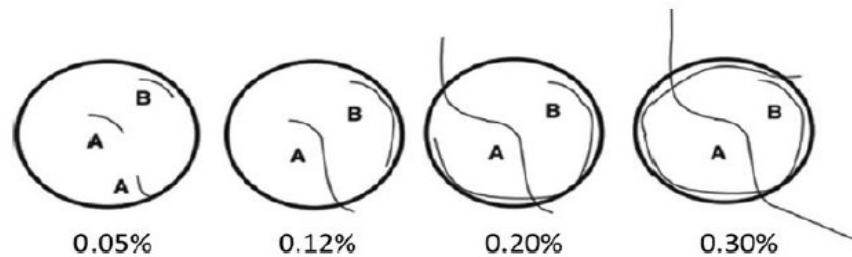


Figure 1.1: Descriptive model for crack propagation in ASR-affected concrete [6] (reproduced with permission of Elsevier)

Moisture and temperature play a critical role in the development of the reaction, along with other factors like aggregate reactivity level and alkali content [8–16] While the impact of these factors on ASR-induced expansion is more established, little is known about how they affect ASR-induced damage.

Several tools have been employed to appraise damage in concrete affected by ASR. Promising tools such as the Damage Rating Index, Stiffness Damage Test (SDT) are of significant importance and have proven reliable in assessing the condition (i.e., the extent of deterioration) of ASR-affected concrete. Notably, the combination of outcomes from the tests, such as DRI number, distress features, crack counts, modulus of elasticity (ME), Stiffness Damage Index (SDI), and Plastic Deformation Index (PDI), alongside the non-linearity index (NLI), have contributed to the extensive assessment of damage. Other tools, such as the direct shear strength [17], tensile strength [18] and compressive strength [19] have successfully been used complementarily with the DRI and SDT to evaluate induced deterioration in ASR-affected concrete. However, most existing studies on ASR-induced deterioration were conducted on specimens stored in very humid environments (RH >95%) and standard temperatures (i.e., 38°C-CPT and 60°C-ACPT) [19–21]. Thus, limited studies have been performed to understand the influence of other exposure conditions on ASR-induced expansion and deterioration.

Furthermore, the most reliable strategy for mitigating ASR remains avoiding or reducing the availability of one or more factors causing ASR (i.e., reactive silica, moisture, and alkali). Among these, moisture limitation can be considered the easiest, especially in existing concrete members. As a result, the concept of minimum moisture (referred to as relative humidity [RH] threshold) required to trigger or sustain ASR has been widely used. However, numerous contradicting RH

thresholds have been reported [8,10,13,22–27]. Even so, these critical moisture threshold studies have been limited to expansion measurements.

In this context, this study focuses on detailed laboratory investigations aiming first to understand the moisture dynamics in concrete along with the influence of temperature. It introduces a metric that relates the moisture state in concrete to ASR-induced expansion. Furthermore, the unique role of temperature on concrete properties inspires an assessment of the applicability of the maturity concept to ASR development. Building upon the thorough understanding of moisture dynamics and temperature on ASR kinetics, this study evaluates how these factors influence ASR-induced deterioration, particularly their influence on the physical integrity of ASR-affected concrete and associated mechanical property losses in aggregates with different reactivity levels. The study subsequently proposes a damage-based assessment table for evaluating ASR-induced damage under different exposure conditions. Moreover, a damage-based RH threshold assessment is conducted.

This Ph.D. thesis is organized into chapters, with the core consisting of five scientific papers that address specific but interrelated research topics. To ensure clarity for readers, chapter one provides a brief introduction and the structure of the study. Chapter two presents a comprehensive literature review on ASR and the role of moisture and temperature, and the concluding part of the literature review focused on an overview of ASR-induced damage assessment is presented in Chapter three. The problem statement and objectives of the study are presented in Chapter four, followed by Chapter five, which summarizes the experimental program and briefly describes how the findings from the study are divided into scientific papers. Four scientific papers are presented in sequence from chapters six to nine. The scientific and engineering contributions from this study are outlined in chapter ten, and finally, chapter eleven presents the conclusions and recommendations.

CHAPTER TWO: ALKALI–SILICA REACTIONS: LITERATURE REVIEW ON THE INFLUENCE OF MOISTURE AND TEMPERATURE AND THE KNOWLEDGE GAP

Olusola D. Olajide¹, Michelle R. Nokken¹ and Leandro F. M. Sanchez^{2,*}

¹ Department of Building, Civil & Environmental Engineering, Concordia University, Montreal, QC H3G 1M8, Canada; olusola.olajide@concordia.ca (O.D.O.); m.nokken@concordia.ca (M.R.N.)

² Department of Civil Engineering, University of Ottawa, Ottawa, ON K1N 6N5, Canada

Published in Materials Journal

Abstract

The alkali–silica reaction is a universally known destructive mechanism in concrete that can lead to the premature loss of serviceability in affected structures. Quite an enormous number of research studies have been carried out focusing on the mechanisms involved as well as the mitigation and prevention of the reaction. A few in-depth discussions on the role of moisture and temperature exist in the literature. Nevertheless, moisture and temperature have been confirmed to play a vital role in the reaction. However, critical assessments of their influence on ASR-induced damage are limited. The available moisture in concrete needed to initiate and sustain the reaction has been predominantly quantified with the relative humidity as a result of difficulties in the use of other media, like the degree of capillary saturation, which is more scientific. This paper discussed the current state of understanding of moisture measurement in concrete, the role of moisture and temperature in the kinetics of the reaction, as well as the moisture threshold needed for the reaction. Furthermore, the influence of these exposure conditions on the internal damage caused by ASR-induced deterioration was discussed.

Keywords: alkali–silica reaction; moisture; relative humidity; temperature; Damage Rating Index; relative humidity threshold

2.1 Introduction

2.1.1 Background

The alkali–silica reaction (ASR) has been a menace to the durability of concrete infrastructure since its discovery several decades ago [28]. The ASR is a chemical reaction that results from the interaction between reactive silica and alkalis in a humid environment; this reaction generates a gel that swells upon moisture uptake, leading to induced expansion and cracking in the affected concrete. The occurrence of ASR depends on many factors and although the failure of ASR-affected structures is not common, it can induce several durability and serviceability issues [29]. Extensive research has been conducted on the mechanism of the ASR and the development of maintenance strategies [8,28,29]. However, in many cases, locally available aggregates exhibit some level of reactivity, necessitating the need to prevent the reaction. Unfortunately, there is currently no known technique to completely prevent the reaction once all the required conditions are met. Nevertheless, supplementary cementitious materials (SCMs) [30–33] and lithium compounds [34–37] have often been incorporated into new concrete structures to slow down the reaction. However, due to the reported shortages in the supply of SCMs like fly ash [38] and the cost of using available admixtures [35], there is an urgent need to explore additional SCMs or admixtures that could be used [39,40]. In existing structures already affected by ASR, there is no known method to halt the reaction. Common mitigation measures include controlling moisture availability through the application of coatings/sealers [41,42], the impregnation of lithium, the release of stresses through slot cutting, and external restraint by post-tensioning [43]. However, new cracks have been reported to appear years after the application of such techniques [44,45].

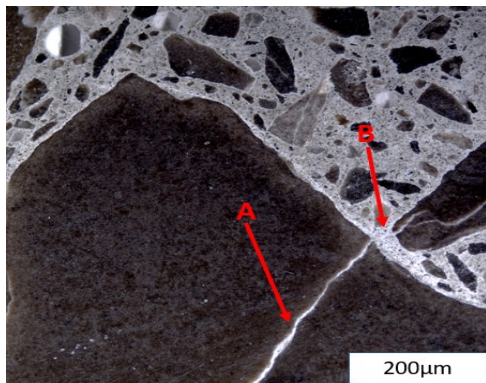
Given the challenges posed by the unavailability of non-reactive aggregates, especially in areas prone to ASR; diminishing SCMs; the availability of high-alkali cement; and limitations to existing coating systems; exploring the influence of moisture and environmental conditions like temperature remains crucial for preventing the ASR and selecting effective maintenance strategies. Moisture is an important factor for the ASR and its availability in concrete has been often appraised with the aid of relative humidity (RH), which is not the true indicator of available water in concrete. Other methods like the degree of capillary saturation, chemical reactions, electrical resistance, etc., have also been used. Nonetheless, various researchers have reported numerous RH thresholds for the onset of the reaction. Some conclusions were based on the external RH, while others were based on the internal RH, i.e., relative humidity outside or inside the concrete, respectively [8,27,46]. Furthermore, some authors have claimed the threshold is dependent on the temperature [47], while others have suggested that the reactivity level of the aggregates is paramount [8,48]. Some of these conclusions were inferred from tests using reactive fine aggregates [25] and others with reactive coarse aggregates [26]. Other factors, such as size, drying and wetting cycles, etc., can also affect the availability of moisture in concrete and, subsequently, the kinetics of the reaction.

Temperature plays a pivotal role in the ASR as with other durability problems in concrete. Concrete exposed to high temperatures is more likely to experience the ASR as a result of the increase in the rate of expansion aided by the rapid dissolution of silica and the diffusion of ions. However, temperature could also play a counter role by improving drying and thereby reducing the absorption of water by ASR gel [24]. Furthermore, temperature can significantly affect the relative humidity of the air that concrete is exposed to; the higher the temperature, the higher the capacity

of the air to take in more moisture, thereby reducing the relative humidity. The impact of this relationship and its influence on ASR-induced expansion are yet to be well studied.

The ASR is initiated in the concrete microstructure and produces internal cracks long before the manifestation of surface cracks or other symptoms. The internal cracks in ASR-affected concrete can be correlated to its induced expansion [49], thus emphasizing the need to assess the influence of various exposure conditions on the microstructural behaviour of the reaction. Cracks due to ASR, as shown in Fig. 2.1, were observed as being initiated within the aggregate particles (i.e., fine or coarse) and propagating to the cement paste. Coarse aggregates have been known to have a different effect on induced expansion when compared to fine aggregates [50]; cracks generated by the latter propagate faster into the cement paste due to their small size [51]. Thus, the physical integrity determined by the inner damage (pattern and extent of cracks) of affected concrete at different moisture and temperature conditions, bearing distinct aggregates with different reactivity levels, can vary.

(a)



(b)

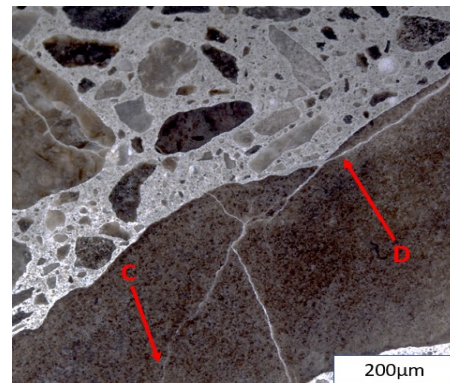


Figure 2.1: ASR induced cracks (a) A (Open crack in aggregate with reaction product; OCAG), B (Crack in cement paste with reaction product; CCPG); (b) C (Closed crack in aggregate; CCA), D (Open crack in aggregate; OCA)

This paper aims to review the influence of moisture and temperature on the ASR. To provide a comprehensive overview, the available methods for measuring moisture in concrete, the moisture

threshold needed for the reaction, the influence of cyclic conditions, and the multifaceted role of temperature in the ASR will be discussed. While the influence of these conditions in the kinetics of ASR is well known, existing studies have primarily focused on expansions recorded over time. This study seeks to broaden the discussion by exploring the evaluation of damage due to the ASR under various moisture and temperature conditions using microscopic assessment.

2.1.2 The mechanism of the ASR

In the presence of adequate moisture, the alkalis present in cement—mainly sodium and potassium oxides—react with poorly crystallized siliceous phases in aggregates. According to Juliana et al. [52], the high alkalinity of concrete pore solutions promotes the exchange of hydroxyl ions (OH^-) with either sodium or potassium through an ion exchange process, and calcium-rich ASR gel is formed when amorphous or poorly crystallized silica is attacked. The ASR gel formed has a great affinity to water and swelling and exerts pressure in all directions. This mechanism leads to stresses which, in turn, generate cracks that initiate from the aggregates and propagate into the cement paste, as schematically shown in Fig. 2.2.

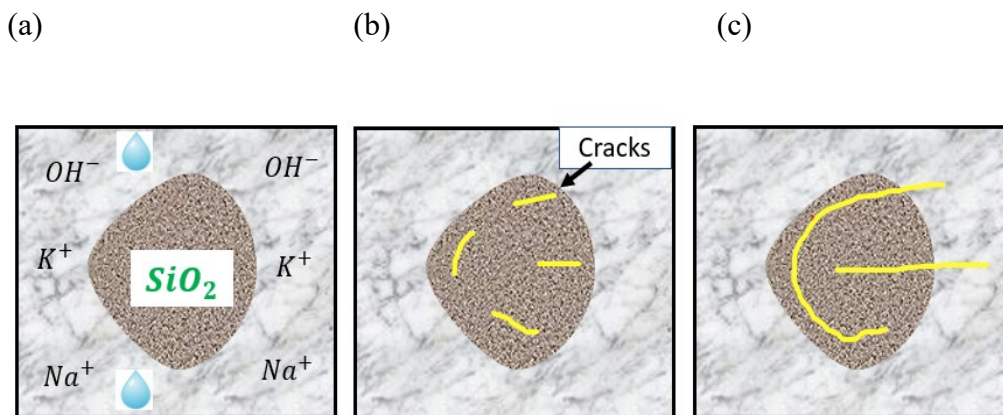


Figure 2.2: Sequence of ASR: (a) factors needed for ASR; (b) initiation of cracks; (c) propagation of cracks. Modified from [6,53]

The hydroxyl ions (OH^-) present in the pore solution from the hydration of cement attack the silica in aggregates, leading to the decomposition of the silica structure. The OH^- disrupt the siloxane bonds ($\equiv Si-O-Si \equiv$) and break the network to form a silanol group ($\equiv Si-OH$). The progressive attack of the hydroxyl ions on the silanol group ($\equiv Si-OH$) results in the network dissolution of silica. According to Rajabipour et al. [28], this dissolution can be hastened with an increase in temperature and/or alkalinity. The high alkalinity of the pore solution promotes the exchange of hydroxyl ions (OH^-) from the silica surface with alkali ions, such as sodium (Na^+) or potassium (K^+), in the pore solution [54]. The presence of alkali ions triggers the formation of an ASR gel composed of alkali silicates. The reaction mechanism is time-dependent [19]; at the inception of the reaction, the ASR gel is deficient in calcium. However, as the reaction progresses, the dissolution of solid portlandite ($Ca(OH)_2$) in the cement occurs. Although the role of calcium ions remains controversial [55], popular claims remain stating that calcium hydroxide ($Ca(OH)_2$) serves two primary roles: it functions as a “buffer” by helping to sustain a high pH level, which corresponds to a significant concentration of hydroxyl ions within pore solutions [56], and allows for the potential exchange of Ca^{++} ions with alkali ions in the gel and forcing the return of the alkali ions into the pore solution, a phenomenon referred to as alkali recycling. Despite the controversial state of the role of calcium ions in the reaction, their availability remains vital for the expansive behaviour of the gel. Irrespective of this, ASR gels have been known to possess a low Ca/Si- ratio compared to C-S-H gel. The presence of Ca in the gel ensures its high viscosity and swelling upon the imbibition of water. Otherwise, the gel dissolves and remains in the solution [57].

The deficiency of calcium in the concrete pore solution will further lead to the disintegration of more portlandite from the cement. This, combined with the presence of alkali ions in the pore

solution, initiates a repetitive sequence, ultimately leading to the formation of additional alkali–silica gels. Buttressing the time dependency of the reaction, the reaction can be distinguished into two stages [58]. The first stage is composed of amorphous ASR products that are generated in the aggregates in proximity to the cement paste. The products move into the interior of the aggregates, generating pressure that results in cracks. Since the reaction is a continuous one, new ASR products formed in the second stage are crystalline in structure, filling the existing cracks and exerting swelling pressure that propagates the cracks into the cement paste. There exist several other analogies in the literature about the ASR gel swelling mechanism [59–61]. Nonetheless, the reactivity is endless and will continue until sufficient alkalis, calcium ions, siliceous phases, and moisture are no longer available [8].

2.2 Review objectives

The objective of this research was to conduct a thorough examination of the impact of moisture and temperature on the alkali–silica reaction (ASR). This review highlights the variations in the existing literature concerning the role of moisture in the reaction, as well as the limited availability of articles specifically addressing the influence of moisture and temperature on the microstructural properties of ASR-affected concrete.

2.3 Moisture in concrete

Moisture plays a vital role in the durability of concrete [62]. Its availability beyond a specific limit could be favourable for the alkali–silica reaction, freezing and thawing [27], carbonation [63], etc. Available water in concrete can be categorized into chemically bound water, physically bound water, and capillary (free) water [64]. Physically bound and free water are responsible for the transportation mechanism in concrete pore structures, and their distribution in this space is influenced by the moisture content, while chemically bound water is non-evaporable and fixed in

the hydrate phases [65]. The moisture content available in concrete can therefore be interpreted as the volumetric ratio of the sum of physically bound and free water to the pore space [64]. This moisture content has been measured using several methods.

The gravimetric method is the most dependable and accurate technique for measuring moisture in concrete, especially when representative samples can be collected from the body under investigation. However, the destructive nature of the test renders it unsuitable in some circumstances [66]. Some other relevant methods are itemized in Table 2.1, but most of these methods do not measure moisture in concrete directly, thus limiting their use. Other challenges include cost, calibration challenges, and ease of usage. Nevertheless, the relative humidity and degree of capillary saturation have been popularly used for such measurements.

Table 2.1: Moisture measurement techniques

Test	NDT	Location	Influencing Factor	Output
Gamma densitometry [67]	Yes	Different depth	Geometry	Density of concrete
Electrical resistance [68]	Yes	Surface	Degree of maturity	Electrical conductivity
Hygrometry [69]	Yes	Location of choice	Calibration, temperature	Relative humidity
Chemical reactions [70]	No	Representative sample	Evaporation	Reaction with water
Thermalized neutrons [71]	Yes	Surface	Chemical composition	Thermal neutron detector
Microwave absorption [72]	Yes	Few inches deep	Mix proportion	Electromagnetic waves
Infrared thermography [73]	Yes	No contact	Concrete density	Surface temperature
Gravimetric [74]	No	Representative sample	Depth of collection, incomplete drying	Surface temperature

The choice of relative humidity or degree of capillary saturation measurement is dependent on the type of moisture (water vapour or liquid water) under consideration. The assessment of frost damage in concrete can be further emphasized with the use of the degree of capillary saturation, which illustrates the number of filled pores. Whereas, in describing concrete deterioration involving chemical reactions influenced by the activity of moisture in the pores, the relative humidity measurement can be more efficient [75].

The RH considers the amount of water vapour in the air. The internal RH of early-age concrete is hugely dependent on the water-to-cement ratio (w/c), and the readings can be obtained with hygrometers [76]. The RH is assumed to be 100% at complete saturation after casting (liquid-like condition). According to Zhang et al. [77], this condition exhibits a continuous liquid network, and the RH of the air is close to 100% [78]. After some time, the RH starts dropping due to hydration and/or evaporation. As hydration continues, the formerly continuous liquid network gets breached, secluding the pore water and leading to the decrement in the internal RH.

The degree of capillary saturation (DCS) of concrete, on the other hand, can be obtained through the ratio of the volume of water available in the concrete to the volume taken up when the concrete is subjected to capillary suction until equilibrium is reached [75]. A handful of strategies have been adopted to measure the DCS in the literature, most of which are focused on obtaining the weights of the sample before and after drying as well as the weight after capillary water absorption, which can be achieved by submerging the sample or with one surface of the sample in contact with water [79,80]. The procedure (weighing and drying) for DCS can limit its use for in situ measurements, unlike that for RH [81,82].

The DCS and RH focus on different properties of moisture in concrete and are affected by distinct factors. However, there exists a seemingly linear relationship between them. According to a study

by Weiss [83] on concrete specimens with a w/c of 0.42, the degree of saturation increases as the RH increases. Despite the challenges involved in performing the DCS, this test seems to be more scientific; the actual amount of water in concrete can be determined. However, the RH is more suitable for use in ASR-affected concrete due to the ease of measurement. This can be performed easily with the aid of sensors. Furthermore, the ability to carry out RH measurements in situ, especially in the laboratory, without interfering with the ASR-accelerated performance tests through the drying of samples and the capillary water absorption procedures required for DCS makes the RH more suitable.

2.4 The role of moisture in the alkali–silica reaction

Moisture is a critical factor for the initiation and sustenance of the ASR [84]. The moisture present in ASR-affected concrete is largely due to the mixing water (w/c) and ingress of water from external sources. Such ingress could be from rain, ambient environmental conditions, drainage, etc., or a combination of these.

The role of moisture in the reaction has been well documented [85]. Its availability serves as a transportation medium for the ions involved in the reaction and for the formation/swelling of the resulting ASR gel. The transportation of ions can be further enhanced in a highly porous and permeable medium obtainable in concrete with high w/cm [86]. As a result, the reduction in the available moisture has been used to mitigate the reaction. On the other hand, a reduction in the w/cm could potentially aid the reaction. During hydration at low w/cm, the products are less heterogeneous and less portlandite is produced. Hydroxyl ions are dissolved from the Ca(OH)_2 in order to maintain equilibrium with the high alkali concentration in the pore solution as a result of the release of Na^+ and K^+ from the cement, leading to an abundance of ions in the pore solution [80]. According to Nilsson and Peterson [87], the reaction can be initiated even at a low RH of

80%, but progresses slowly due to the low rate of diffusion. The ASR gel swelling that can arise in this condition may not be sufficient to exert significant pressure on the surrounding paste. If the concrete is re-exposed to water or moved to a more saturated condition, the rate of the reaction is improved, and expansion is significantly improved [11,88].

The moisture needed for the ASR has been prominently measured using the RH [8,13,47]. Poyet et al. [47] examined the kinetics of the ASR and resulting expansion in cylindrical mortar samples stored in different external relative humidity conditions and, based on their studies, ASR expansion increases as RH increases. Few researchers have argued that the degree of DCS is a better means of moisture measurement for the reaction [75,89]. Nonetheless, damage due to the ASR intensifies as the DCS increases [75], and a DCS threshold of 90% has been reported to be needed [89].

2.4.1 Relative humidity threshold

The availability of a sufficient amount of water has been confirmed as a crux for the reaction [24]. Based on the discussion in the previous sections, no significant distress can be recorded at low moisture conditions. As a result, the concept of the RH threshold has been introduced for the prevention and maintenance of ASR-affected structures.

The absorption of water and expansion of the ASR gel are dependent on the RH. According to a work carried out by Bažant and Steffens [90], the absorption capacity of the gel greatly diminishes when the RH of the air in the pores falls below 85%. Furthermore, expansion is impeded at low RH levels. According to the studies in [91], no expansion was recorded when mortar samples were stored at 65% RH and 38°C, while considerable expansion was reported in those stored at similar temperatures but at 85% RH, buttressing the claims that a minimum RH of 80–85% is needed for the reaction [92]. Some other authors have posited a threshold of 80% [27,87]. Yet, numerous RH

thresholds exist in the literature. Olafsson [13] reported 80% at 23°C, which falls to 75% at 38°C, while Ludwig [46] reported it to be between 80–85% at a lower temperature of 20°C.

Some researchers have worked at higher temperatures. Tomosawa et al. [26] and Kurihara and Katawaki [25] investigated the reaction at 40 °C and reported a threshold of 75%. Poyet et al. [47] reported a threshold of less than 59% at 60°C as an expansion of 0.06% was recorded in cylindrical concrete specimens exposed to 60°C after just 100 days. Thus, the RH threshold could depend on the temperature [47]. As indicated by Fig. 2.3, which includes various studies on RH thresholds at different temperatures, it is evident that the moisture needed for the reaction at room temperature surpasses that required at the standard conditioning temperature of 38°C. Moreover, the moisture requirement is even lower at a higher temperature of 60°C. Consequently, the critical RH for ASR-induced expansion decreases with increasing temperature, confirming the claims in [47]. However, in a report by Pedneault [48], the author stated that the critical RH depends on the form of siliceous minerals of the aggregate. Given the different reactivity levels of aggregates, some aggregates are expected to have a faster rate of expansion. As a result, very highly reactive aggregates could expand at a moisture level where moderately reactive aggregates would not. Furthermore, the reactive content (fine versus coarse) of the mix could influence the kinetics of the reaction, as clearly shown in Fig. 2.3.

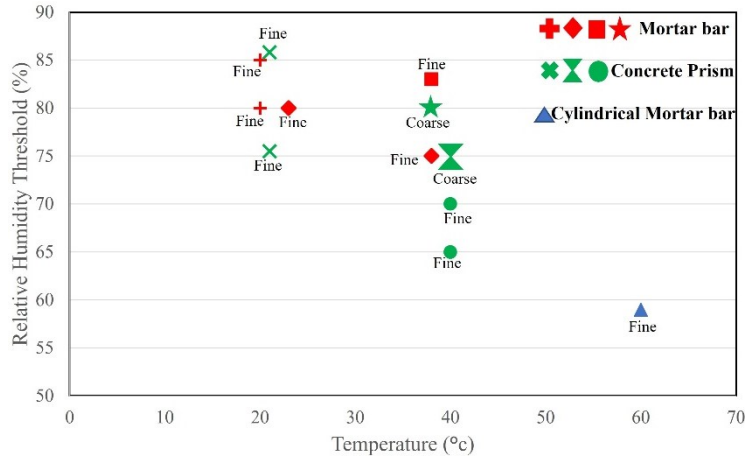


Figure 2.3: Relative humidity threshold as a function of temperature, specimen type, and reactive content from several studies [8,13,26,46–48,93,94]

According to the studies [26,93] carried out on concrete prisms stored at 40°C, as shown in Fig. 2.3, specimens containing reactive coarse content have an RH threshold of 75% compared to the 65–70% RH needed for the mix prepared using a reactive fine aggregate. Hence, a lower moisture level could be sufficient to initiate the reaction in specimens involving reactive fine aggregate. After all, ASR-induced cracks propagate faster in reactive fine aggregates due to their small size. Lastly, the RH threshold required for the reaction could vary depending on the sample size and shape. After all, the rate of the reaction and ultimate ASR-induced expansion differ in concrete prisms, cubes, and cylinders incorporating reactive aggregates [95]. Thus, the varying sample types used in the available studies may play a role in the varying thresholds reported in the literature.

2.4.2 The role of alternate drying and wetting on the availability of moisture for the alkali–silica reaction

Concrete exposed to natural environmental conditions is subjected to several drying and wetting cycles during its service life; these conditions have an influence on the available moisture in the concrete and the development of the ASR. According to Zhang et al. [78], when concrete is

exposed to moisture (wetting), the interior RH increases rapidly within a short period of time and then reaches a stable level; this, however, is dependent on the concrete grade, permeability, size, and other properties of hardened concrete; duration of the wetting cycle; etc. Conversely, during drying, the interior RH reduces gradually [78]. According to the study by Zhang et al. [78], concrete cubes with 28 days of compressive strength of 30 MPa were subjected to a dry and wet cycle (14 and 7 days, respectively) and the internal RH at the centre of the $60 \times 100 \times 350$ mm cubes of the samples was measured. As expected, the RH reduced during the drying cycle but failed to reach the initial moisture level when subjected to wetting. This could have been due to the duration of the wetting cycle. As a result, such a phenomenon could influence the available moisture in concrete for the ASR [41,96].

To discuss the influence of the cyclic condition on ASR, Stark et al. [24] confirmed that cyclic wetting and drying conditions could stimulate the initiation and sustenance of the reaction. Of course, there was less moisture to be absorbed by ASR gel during drying; nevertheless, the increase in temperature improved the concentration of hydroxyl ions in the pore solution, which exacerbated the attack on the poorly crystallized aggregates. As a result, expansion progressed exponentially in the following wetting cycle. Furthermore, in the next dry period, more non-expansive reaction products were formed and drying increased the extent of the cracks formed in the prior wetting cycle. Thus, minimizing wetting and drying cycles is vital in controlling the reaction [97].

Evidently, expansion due to the ASR is significantly retarded in the drying cycle, especially towards the surface of the concrete. The reaction can, however, progress actively in the inner depth but not close to the outer surface due to the moisture gradient. According to Kagimoto and Kawamura [98] in their study on lab-conditioned concrete specimens, a relative humidity of up to

80–90% (a moisture level sufficient to initiate the ASR) was measured in the middle of the concrete cylinders during drying; such variations in expansion across the depth of affected concrete were responsible for surface cracks due to the ASR [99]. A similar observation was recorded in field samples by Stark et al. [24]. It is, however, worth noting that this phenomenon could be dependent on the size of the concrete member. Slender members would experience a rather quicker drop in RH across their depth.

2.5 The role of temperature in the kinetics of the ASR

Increases in moisture, temperature, alkalinity, or a combination of any of these factors have been adopted in the laboratory to accelerate the rate of ASR-induced expansion, among which, increases in temperature have been reported to be the most efficient [100]. Although temperature has not been noted as one of the primary factors (alkalis, silica, water) needed for the ASR, its influence can affect the availability of these factors. Its influence extends even further into the structure of the gel produced upon the initiation of the reaction. An increase in temperature has proven to be effective in enhancing the dissolution of silica, thereby accelerating the formation of ASR gel [101,102]. The influence of temperature on the accelerated dissolution of silica was reported in [103]; the authors recorded an increase in the rate of dissolution of siliceous particles from 71% to 100% when their storage temperature was increased from 25°C to 80°C. The role of temperature on the availability of alkalis in concrete pore solutions can be categorized into two groups. An increase in temperature enhances the mobility of the alkali ions (K and Na); aside from that, the concentration of ions in concrete pore solutions increases at elevated temperatures. On the other hand, some reactive aggregates have been found to contribute alkalis to concrete pore solutions, and temperature has been reported to affect the release of such additional alkalis. In [95], elevated temperatures resulted in a greater total alkali content released from the three tested aggregates

(Sudbury, Spratt, and Springhill) into the alkaline solutions at three different temperatures (21°C, 38°C, and 60°C), with the highest release occurring at 60°C. An exponential increase in alkali release was reported when the temperature was increased from 20°C to 80°C [104]. It is, however, worth noting that after considering other studies in the literature [105] and the comprehensive table of available works in the literature on aggregates and alkali release put together in [106], the amount of alkali release can also be influenced by the mineralogy of the aggregates and the type of aggregate (coarse versus fine).

The improved properties due to elevated temperature can influence the properties of the resulting ASR gels. As noted in the study on synthesized gel in [107], gels at elevated temperatures and higher molarities exhibit notable differences in both their microstructure and macrostructure when compared to those generated under milder conditions. For instance, the structure of the crystalline product formed at 38°C/40°C was different from that formed at 60°C using the Raman spectra [58]. The differences in the mobility/dissolution parameters and structure of the gels can influence the kinetics of the reaction, leading to a possible rise in the expansion rate by 1.7 times when the temperature is increased from 38°C to 50°C [100]. As a result, several laboratory performance tests were conducted at high temperatures to increase the rate of expansion and reduce their duration [108–110]. Table 2.2 comprises a database of several ASR tests that have been conducted at different temperatures, highlighting the uniqueness of each test. The table includes the test conditions, durations, and ultimate expansion results. Furthermore, the 28-day expansion results are highlighted to show the influence of temperature on the evolution of the reaction over time.

Table 2.2: Database of ASR expansion at different temperatures

Ref.	Aggregate Type	Sample Size	Reactive content	Alkali (Na_2O_{eq})	Temp.	Test Duration	Final Expansion	Expansion @ 28 days
[8]	Highly reactive fine	75 x 75 x 285 mm (prism)	Fine agg.	1.25%	21°C	167 Days	0.14%	0.010%
					40°C		0.55%	0.020%
[47]	Reactive limestone	16 x 2cm (cylinder)	Fine agg.	1.84%	60°C	200 days	0.24%	0.220%
[89]	Highly reactive Quartz	75 x 75 x 285 mm (prism)	Coarse agg.	0.925%	38°C	365 days	0.24%	0.010%
					60°C	273 days	0.18%	0.040%
[95]	Sudbury	100 x 285 mm (cylinder)	Coarse agg.	1.25%	38°C	365 days	0.20%	0.010%
					60°C		0.16%	0.040%
		75 x 75 x 285 mm (prism)			38°C		0.170%	0.015%
		60°C			0.080%		0.030%	
	Spratt	100 x 285 mm (cylinder)	Coarse agg.	1.25%	38°C	365 days	0.26%	0.018%
					60°C		0.18%	0.110%
		75 x 75 x 285 mm (prism)			38°C		0.21%	0.020%
		60°C			0.17%		0.100%	
[100]	Spratt	75 x 75 x 285 mm (prism)	Coarse agg.	1.25%	38°C	730 days	0.26%	0.013%
					50°C	187 days	0.248%	0.085%
[106]	Spratt	75 x 150 mm (cylinder)	Fine agg.	1.07%	38°C	365 days	0.160%	0.033%
					60°C		0.074%	0.058%
	Springhill				38°C		0.230%	0.028%
					60°C		0.103%	0.050%
[108]	Spratt	75 x 75 x 285 mm (prism)	Coarse agg.	1.25%	38°C	365 days	0.257%	-----
					60°C	91 days	0.160%	-----
	Sudbury				38°C	365 days	0.171%	-----
					60°C	91 days	0.138%	-----
[109]	Spratt	75 x 75 x 285 mm (prism)	Coarse agg.	1.25%	38°C	365 days	0.229%	-----
					60°C	182 days	0.167%	0.103%
	Sudbury				38°C	365 days	0.150%	-----

					60°C	182 days	0.187%	0.022%
[110]	Limestone	75 x 75 x 285 mm (prism)	Coarse agg.	1.25%	38°C	365 days	0.22%	0.000%
					60°C	150 days	0.19%	0.065%
[111]	Highly reactive andesite	75 x 75 x 250 mm (prism)	Coarse agg.	0.94%	40°C	365 days	0.140%	0.035%
					60°C		0.110%	0.070%
[112]	Highly reactive Jobe sand	25 x 25 x 285mm (prism)	Fine agg.	1.04%	38°C	600 days	0.800%	0.050%
					55°C		0.790%	0.350%
[113]	Silica sand and Pyrex Glass	28 x 28 x 180 mm (Prism)	Fine agg.	1.20%	30°C	100 days	0.650%	0.350%
					60°C		0.420%	0.410%

Despite the pros of the accelerated performance tests conducted at high temperatures, some shortcomings have been identified. As a matter of fact, the ultimate expansion can be lower at high temperatures [100,108,111]. Significant reductions in the ultimate expansion recorded from several accelerated tests are in Fig. 2.4. At similar ages of exposure, specimens conditioned at 38°C all had a higher final expansion than at 60°C, even in tests involving the use of similar aggregates. Based on findings from the literature, increased alkali leaching, non-reactive sand, improved porosity, and reduced calcium content [108,114] are factors that could be deemed responsible for a lower final expansion.

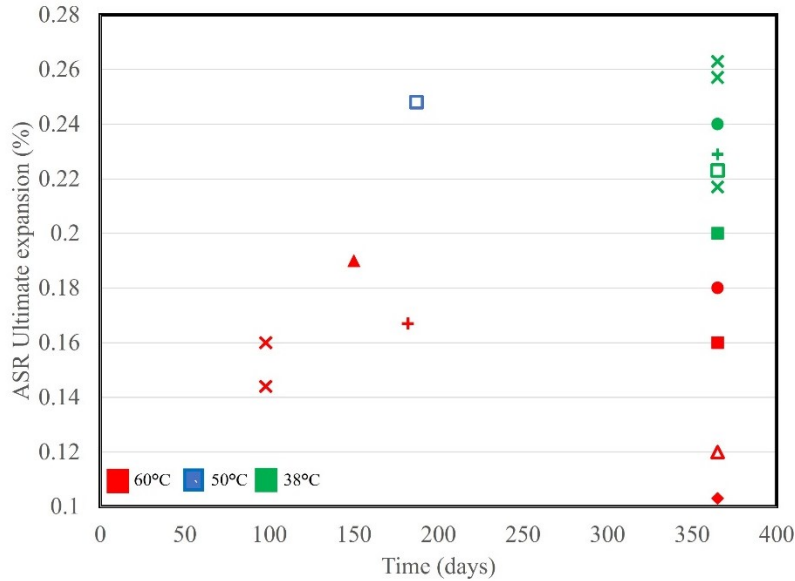


Figure 2.4: ASR-induced ultimate expansion at different temperatures reported by several authors [89,95,100,106,108–111]

The curing temperature to which concrete specimens are exposed before being conditioned for the ASR can affect their expansion. High curing temperatures tend to result in a high degree of hydration, consequently reducing the porosity of concrete and thereby reducing water uptake properties and the mobility of ions [80]. Although this does not stop expansion, the final expansion can be much lower [89]. Considering this, some researchers [115] developed a micro-mechanical expansion model that assessed the effect of ASR gel in cement paste in terms of hydrostatic pressure in the microstructure of cement at different temperatures. Porosity is considered an important characteristic of concrete microstructure, and experimental results prove its reduction at high temperatures because of hydration. According to the authors, the hydrostatic pressure decreases with increases in temperature due to improved porosity, leading to a reduced diffusion of alkali and ASR expansion. However, since hydration is a continuous process, the rate of expansion could be higher at early ages and dwindle at later ages.

An increase in temperature can indirectly lead to a reduction in calcium concentration and accelerate various chemical reactions, including the dissolution of alkali compounds and their

mobility, thus enhancing the concentration of the alkalis in the pore solution [58] and the ASR reaction. The absorption of Ca by existing gel reduces the concentration of Ca ions in the pore solution. Hence, new ASR gels generated may lack the required expansive properties that can be acquired by reactions with Ca ions. In fact, a less viscous gel has been reported to be produced in such conditions that flows into the concrete matrix without an accompanied swelling pressure [80,112]. In the same context, several authors have reported the instability of ettringite at high temperatures greater than 60°C leading to the presence of sulfate ions and aluminium in the pore solution [116]. The presence of these ions lowers the concentration of Ca and, consequently, the ASR expansion.

Other factors like the drying of the ASR gel leading to the reduced absorption of water by the gel [24] and alkali leaching have been studied [111,116–119]. The role of alkali leaching has been the most studied from the above factors. The existing literature on notable possible solutions includes the adoption of a maximum testing temperature of 50°C/60°C [100], wrapping of test samples [80], and reduction of the testing duration [105]. Nevertheless, most of these solutions have proven to be abortive. Of notable importance is the wrapping of concrete specimens during testing. For instance, in the study carried out by Kawabata et al. [111], concrete prisms containing highly reactive aggregates wrapped with alkaline cloth to reduce alkali leaching were conditioned to 20°C, 40°C, and 60°C in accordance with [117]. The correlation of the results was confirmed by calculating the total alkali content in the wrapping cloth and assessing the water at the bottom of containers. The kinetics of the reaction differed at different temperature levels and no linear relationship existed between the temperature and ultimate expansion; specimens at 60°C yielded the highest early expansion, but the highest final expansion was achieved at 40°C, which was only slightly higher than the ultimate expansion at 20°C. Since this method [117] made provisions for

the recycling of alkalis, other factors that have been previously discussed or combinations of these factors might be hypothesized to be responsible for the low ultimate expansion at 60°C.

2.2.6 The influence of moisture and temperature on the microstructure properties of ASR-affected concrete

The ASR is known to induce the degradation of the microstructure of concrete before its appearance on the macroscale. This facilitates the need to understand the behaviour of the mechanism from a microstructural point of view. Several microscopic methods have been established for such assessment, some of which are highlighted in Table 2.3. The scanning electron microscope has been the most used tool; this has often been coupled with other tools like the EDS and XRF among others to assess the properties of ASR gel and induced cracks. Other tools such as the TEM and CT scan are also becoming popular for the diagnosis of the ASR. It should be noted that while some of the assessments from these tests are quantitative, they are somewhat relative [111]. Furthermore, these tools have been proven reliable in determining the cause of deterioration (the ASR, in this case), and visual descriptions of the extent of damage can be made. However, a quantitative output for assessing the extent of damage is lacking. The Damage Rating Index (DRI) has so far proven reliable in determining the cause (using the location, features, and propagation of cracks) and extent of damage in concrete (using the DRI number) [120–122].

Table 2.3: Microstructure assessment of ASR

Ref.	Study	Test and Methods	Findings
[58]	Characterization of amorphous and crystalline ASR products formed in concrete aggregates	SEM, X-ray spectroscopy, and Raman microscopy	The morphology of crystalline ASR products is influenced by temperature.
[100]	The effect of elevated conditioning temperature	Damage Rating Index	Similar ASR-induced expansion can result in different levels of damage as temperature increases.

	on the ASR expansion, cracking, and properties of reactive Spratt aggregate concrete		
[123]	Failure criteria and microstructure evolution mechanism of the alkali-silica reaction of concrete	Scanning electron microscopy (SEM) and X-ray computed microtomography	Microcracks propagate from voids in the aggregate into the cement paste. Presence of ASR gel in the pores leads to a reduction in porosity.
[124]	Quantitative analysis of the evolution of ASR products and crack networks in the context of the concrete mesostructure	Time-lapse X-ray tomography	Visualization of the movement of ASR products from the aggregates into the cement paste in 4D.
[125]	Diagnosis of ASR damage in highway pavement after 15 years of service in wet-freeze climate region	Thin section, SEM, and electron dispersive spectroscopy (EDS)	Cracks were identified in the grains of coarse quartzite aggregate. Gel-like products in the cracks were confirmed to be ASR products by EDS.
[126]	Assessment of the alkali-silica reactivity potential in granitic rocks	X-ray diffraction (XRD) and SEM/EDS	Contents of strained quartz in quartz were determined using image analysis and correlated with AMBT results. There existed a linear correlation between the two observations.
[127]	Composition of alkali-silica reaction products at different locations within concrete structures	Thin section and SEM/EDS	Structure and qualitative properties of ASR gel in different structures were verified. Composition of gel varied with location. Gels that had propagated into the cement paste contained a higher amount of calcium than those in the aggregates.
[128]	Application of electron backscatter diffraction to evaluate the ASR risk of concrete aggregates	SEM and electron backscatter diffraction (EBSD)	The dissolution of quartz at high pH was observed to occur along its grain and sub-grain boundaries. This technique can be used to assess the properties of slow-late reactive aggregates.
[129]	Microstructure, crystallinity, and composition of alkali-silica reaction	SEM, EDS, focused ion beam (FIB), and transmission	The morphology of ASR products differs with location. Products located in thin grains are amorphous while those in larger widths are crystalline.

products in concrete determined by transmission electron microscopy	electron microscopy (TEM)	
---	---------------------------	--

The DRI is a petrographic-based semi-quantitative analysis performed on a polished surface using a stereomicroscope with a magnification of 15-16x, and damage features - as highlighted in Table 2.4 - are counted in a 1 cm² square grid. The count of each feature is multiplied by the corresponding weighting factor. The DRI number is obtained by taking the sum of the weighted features and normalizing it to 100 cm² [130].

Table 2.4: Damage features used in Damage Rating Index [6]

Features	Weighting Factors
CCA: Closed cracks in aggregates	0.25
OCA: Open cracks in aggregates	2
OACG: Open cracks in aggregates with reaction products	2
CAD: Coarse aggregate debonded	3
DAP: Disaggregated/corroded aggregate particle	2
CCP: Cracks in cement paste	3
CCPG: Cracks in cement paste with reaction products	3

Quite a huge amount of work has been conducted to evaluate the reliability of the DRI in assessing damage due to ASR and other internal swelling reactions. In summary, the DRI number has been reported to increase as ASR-induced deterioration increases [49]. Cracks in aggregates have been categorized into two types, namely, sharp cracks and onion skin cracks [131]. Furthermore, a qualitative model for crack propagation in ASR-affected concrete has been developed: it highlights the development of several single sharp and onion cracks in aggregates at low expansion levels. These cracks increase in length, connect, and propagate into the cement paste at moderate to high expansion levels [130]. Despite the enormous work that has been conducted with this tool, most studies have been limited to concrete/mortar samples conditioned at high and constant moisture levels. No study has been carried out to directly evaluate the influence of moisture on ASR-induced

damage features. An assessment of the few microstructural studies [6,100] that have been conducted at different temperatures shows that an increase in temperature can lead to changes in the pattern, location, and number of cracks, even at similar expansion levels. Comparing the DRI results of samples affected by the ASR through the accelerated concrete prism test (ACPT) carried out [100] at 50°C and the concrete prism test (CPT) carried out [6] at 38°C, at ~0.1% and 0.2% expansion levels, a higher DRI number was recorded in the ACPT than in their counterparts in the CPT. Fig. 2.5 combines the data from published sources and shows that the damage features are different; more open cracks in aggregates with reaction products (OCAG) were counted in ACPT than in CPT at similar expansion levels. This is because of the fast rate of expansion leading to more induced cracks. Another interesting point is the influence of temperature on the number of cracks in the cement paste at similar expansion levels. Fewer CCPs were recorded at 60 °C compared to 38 °C. This interesting result validates the hypothesis that exposure conditions can influence the microstructural properties of ASR-affected samples, even at similar expansion levels. Since this comparison is based on ASR-induced expansion and DRI results from two different authors, research is needed to improve our understanding of the influence of these exposure conditions on internal damage caused by ASR-induced expansion.

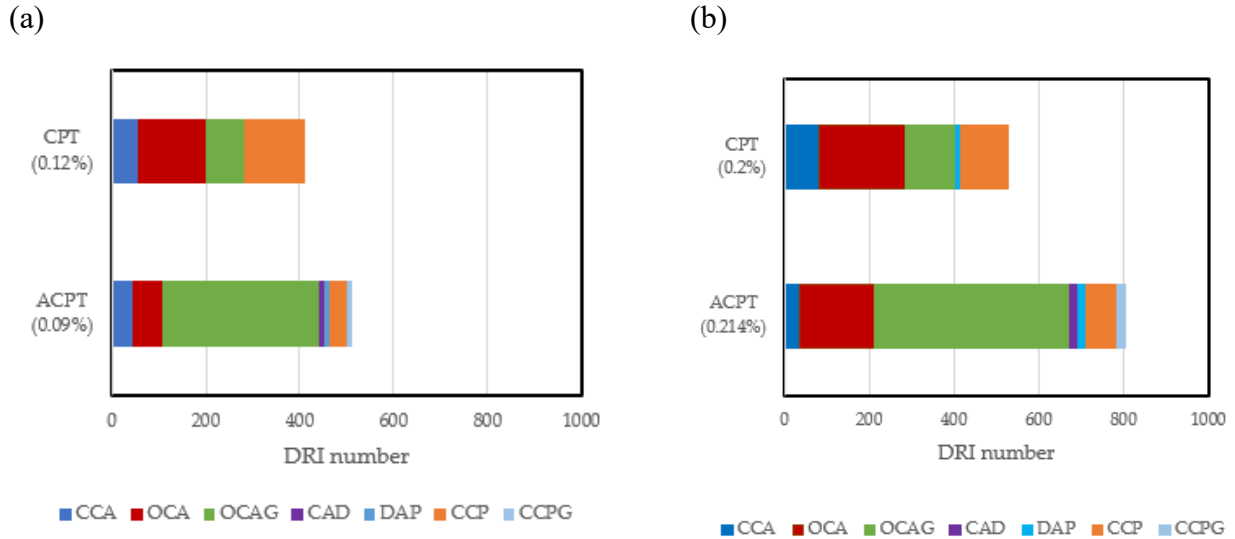


Figure 2.5: Damage features counted in CPT (38°C, >95% RH) and ACPT (50°C, >95% RH) at 0.1% and 0.20% expansion levels: (a) comparison of DRI results at 0.1% expansion; (b) comparison of DRI results at 0.2% expansion. Adapted from[6,100]

2.7 Conclusions

- Moisture is an important factor for the reaction and an ample amount is needed. The utilization of relative humidity, an indirect technique measuring the quantity of water vapour in the air, has been both commonly employed and scrutinized. However, it has been preferred as a means of moisture measurement in ASR-affected concrete due to the ease of measurement compared to other methods like the degree of capillary saturation.
- A moisture threshold of 80% RH has been generally agreed to be required to initiate and sustain the reaction. However, based on reviewed works in the literature, there exist studies that report thresholds lower and higher than this value. The threshold could be dependent on the reactivity of the aggregate, temperature, or other factors that differed among the existing studies.
- Concrete subjected to wet and dry cycles are prone to exhibiting moisture gradients, and their impact on ASR expansion may vary depending on the size of the concrete member, with slender members experiencing a quicker drop in RH across their depth. In managing

the reaction, minimizing the number of wetting and drying cycles is critical. Furthermore, understanding the combined influence of moisture availability, cyclic conditions, and concrete properties is essential for developing effective strategies to mitigate the deleterious effects of the ASR.

- The influence of temperature on the ASR is multifaceted and extends beyond its direct inclusion among the primary factors (alkalis, silica, moisture) necessary for the initiation and continuation of the reaction. An increase in temperature has been identified as the most efficient factor for accelerating ASR-induced expansion in laboratory conditions. However, the ultimate expansion can be lower at higher temperatures. Efforts to address these complexities have not consistently proven to be effective. Hence, the relationship between temperature and ASR-induced expansion is complex and non-linear.
- The assessment of the ASR in concrete has evolved to include a detailed assessment of the influence of induced expansion on microstructural properties, recognizing that ASR induces microstructural degradation before visible signs appear at the macroscale. This shift in focus emphasizes the need to comprehend the influence of moisture and temperature in ASR-affected concrete from a microstructural standpoint rather than just the induced expansion. The availability of moisture and temperature has been reviewed to have a possible influence on the properties of cracks induced by the ASR.

CHAPTER THREE: MULTILEVEL ASSESSMENT OF ASR-INDUCED DAMAGE

Expansion and external signs of damage resulting from alkali-silica reaction have often been used to determine the degree of ASR development. However, this may not accurately reflect the internal condition of the distressed concrete, leading to uncertainties in the condition assessment of the affected concrete. Hence, the multi-level assessment protocol has been developed to address these challenges [130]. This protocol entails using microscopic and mechanical advanced techniques, namely the Damage Rating Index (DRI), Stiffness Damage Test (SDT), and other mechanical property tools like shear strength and compressive strength, to appraise the cause(s) and extent (i.e., diagnosis) of concrete deterioration.

3.1 Stiffness Damage Test (SDT)

The Stiffness Damage Test (SDT) has been confirmed to be a reliable tool for evaluating ASR-induced deterioration in concrete [132,133]. The test is a non-destructive method used to assess the response of concrete to cycles of uniaxial loading/unloading. Walsh originally conceptualized the test [134] based on a correlation between crack density and the loading and unloading cycles in rock specimens. The test was later adapted for concrete specimens by Crouch [135] in 1987. Building upon those developments, in 1993, the test was adapted explicitly by Chrisp [136] to evaluate concrete affected by ASR using a fixed stress of 5.5 MPa at a loading rate of 0.10 MPa/s. The authors proposed parameters like the average secant modulus (using the last four cycles) and the hysteresis area over the five cycles, which reflect energy loss in the system. The Nonlinearity Index (NLI) was also introduced to illuminate the damage pattern based on the slope of the stress-strain curve. Smaoui et al. [137] later proposed a fixed load of 10 MPa to improve the diagnostic

nature of the test and they found a correlation between expansion and plastic deformation from the five loading/unloading cycles.

Sanchez et al. [138] further refined the test through a comprehensive experimental campaign, evaluating numerous concrete mixtures of varying compressive strength ranges and reactive aggregate types (i.e., fine versus coarse) for the use of SDT in appraising concrete affected by ASR. Other internal swelling reactions like delayed ettringite formation (DEF), and freezing and thawing (FT), single or combined were investigated as well. The authors proposed conducting the SDT at 40% of the 28-day compressive strength of the concrete at the loading rate of 0.10 MPa/s and established indices like the Stiffness Damage Index (SDI), Plastic Deformation Index (PDI), Non-Linearity Index (NLI), and the modulus of elasticity which can be obtained from Fig. 3.1. The SDI (Equation 3.1) and PDI (Equation 3.2) represent the ratio of dissipated energy/plastic deformation to the total energy/deformation implemented over the five loading cycles in the system, respectively. The NLI computed from the first loading cycle (obtained by taking the ratio of the secant modulus at half load to the peak load; sec1/sec 2) is efficient in evaluating the orientation of inner cracks, and the modulus of elasticity (Equation 3.3) is computed from the average of the secant modulus of 2nd and 3rd cycles.

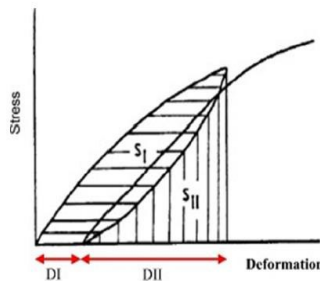


Figure 3.1: The Stiffness Damage Test [133]

$$SDI = \frac{\sum_{i=1}^5 S_{I_i}}{\sum_{i=1}^5 (S_{I_i} + S_{II_i})} \dots\dots\dots(3.1)$$

$$PDI = \frac{\sum_{i=1}^5 DI_i}{\sum_{i=1}^5 (DI_i + DII_i)} \dots \dots \dots (3.2)$$

$$MOE = \frac{\sum_{i=2}^{3^{rd}} \frac{stress_{40\%}}{strain_{40\%}}}{2} \dots \dots \dots (3.3)$$

SI = Dissipated energy over the five cycles.

SI + SII = Total energy placed in the system (i.e., the area under the entire stress/strain curve)

DI = Plastic deformation

DI + DII = Total deformation of the system

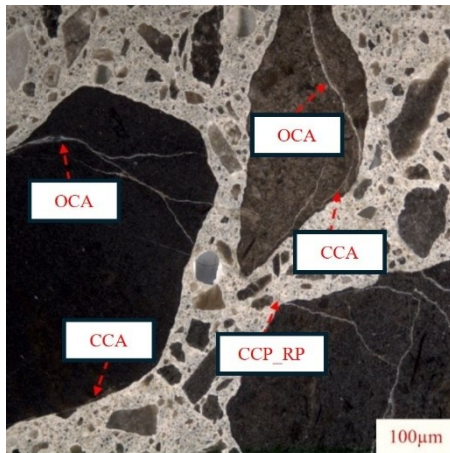
*stress*_{40%} = stress at 40% of maximum load

*strain*_{40%} = strain at 40% of maximum load

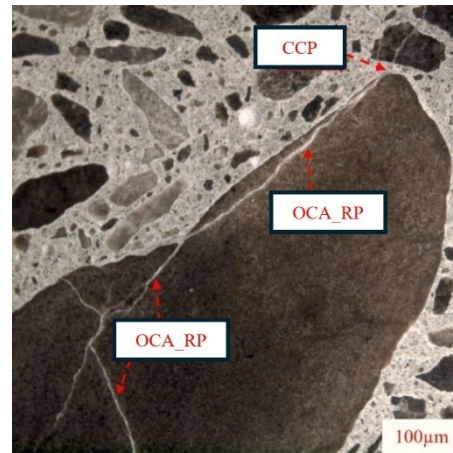
3.2 Damage Rating Index (DRI)

The Damage Rating Index (DRI) has proven reliable for its semi-quantitative role in assessing internal swelling reactions (ISR) such as ASR. It is a simple-to-use technique proposed by Grattan-Bellew [139] that can evaluate the cause of distress through its damage features, and the extent of damage can be quantified using its result along with other mechanical properties of affected concrete. ASR-induced cracks are counted in 1 by 1 cm squares drawn on the surface of polished concrete sections using a stereomicroscope at 15-16X magnification, and the count for each damage feature can be multiplied with their respective weighting factor as shown in Fig. 3.2 to balance their relative importance towards the ASR distress mechanism, as proposed by Villeneuve & Fournier [140] to obtain the DRI number that is normalized to 100 cm². The DRI number has been proven to increase as ASR-induced deterioration increases [121]. Some of the damage features that can be counted are shown in Fig. 3.2.

(a)



(b)



(c)

Distress feature	Description	Weighting factor
CCA	Closed crack in aggregate	0.25
OCA	Opened crack in aggregate	2
OCA_RP	Opened crack in aggregate with reaction product	2
CAD	Debonded aggregate	3
DAP	Disaggregated/corroded aggregate particle	2
CCP	Crack in the cement paste	3
CCP_RP	Crack in the cement paste with reaction product	3

Figure 3.2: Damage Rating Index: (a,b) ASR distress features (c) Distress features with corresponding weighting factors [140]

A closed crack in the aggregate (CCA) is given the lowest importance with a weighting factor of 0.25 as they are most likely a product of pre-existing flaws in aggregate particles before their use in concrete, commonly originating from natural erosion or during the processing of the aggregates. The open cracks in the aggregates with or without reaction product (OCA_RP and OCA) are given a factor of 2 since their occurrence can be related to ASR development. Similarly, the disaggregated particle (DAP) with a factor of 2 represents an aggregate particle exhibiting evidence of disintegration, characterized by the breakdown into loose rock grains. Finally, a crack in the cement paste with or without reaction product (CCP or CCP_RP) and debonded aggregate

(CAD) is assigned the highest weighting factor of 3 since these types of distress are associated with concrete with high damage. The DRI can be conducted in its traditional form using the DRI number and the weighted distress feature to appraise damage as proposed by [140]. However, the extended version proposed by [6] can provide a more detailed overall assessment. Specifically, microscopic distress features can be evaluated in absolute (i.e., counts) and relative (i.e., percentage-%) methods without multiplying with weighting factors, thus contributing to a robust understanding of the mechanism of the reaction. Furthermore, the extended DRI also involves the assessment of the crack lengths, widths, and density, all of which have been reported to be sensitive to ASR development [7]. These would contribute to an extensive overall appraisal of ASR development in affected concrete.

DRI has been adopted to assess damage from concrete containing aggregates of different levels of reactivity [141], concrete with different strengths [6], concrete undergoing free expansion [7], and concrete undergoing different forms of restraint [142–144]. Moreover, its reliability in assessing damage in existing infrastructures has been verified [145]. However, there is a lack of research on the influence of varying moisture and temperature conditions on the microstructural properties of ASR-affected concrete and the influence of these exposure conditions on the DRI results.

3.3 Direct shear

Shear strength in concrete is controlled by tensile and compressive forces [146]. Concrete inherently contains some internal cracks and flaws, and it can transfer shear forces across these cracks via two primary mechanisms: a) the dowel effect through the reinforcement and b) shear friction through the characteristics of the concrete. The latter can be defined as the “frictional resistance to crack,” popularly called “aggregate interlock,” which can be affected by ASR-induced deterioration [147]. Several methods exist for assessing direct shear capacity in concrete

[148,149]. The recently developed technique [17] is of significant relevance to this study due to its extensive testing on unreinforced lab-made concrete cylinders. Moreover, the tool is less variable than tensile strengths, leading to its preference in this work. Furthermore, unlike the compressive strength test, the direct shear strength (obtained using Equation 3.4) is more diagnostic for low and moderate expansion levels [17]. Thus, the tool looks promising for evaluating ASR-induced deterioration, especially at low RH levels where low to moderate expansions are expected. The test is conducted on concrete cylinders of 100 x 200mm, as displayed in Fig. 3.3. Notches of about 20 - 25 mm have been reported to be reliable to reduce discrepancies that may arise from leaving a too-small or big area for the test [148].

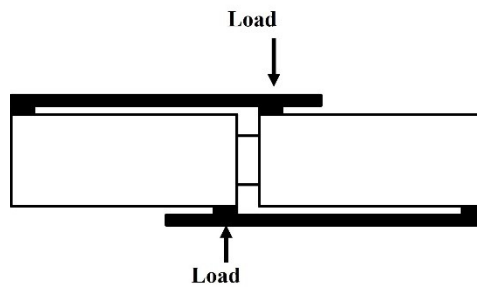


Figure 3.3: The direct shear test [148]

$$\text{Direct shear strength} = \frac{4 * \text{load}}{\pi * (\phi_{\text{cylinder}} - 2a)^2} \dots\dots\dots(3.4)$$

ϕ_{cylinder} : cylinder diameter (mm)

a: depth of notch (mm)

3.4 Compressive strength

Studies have reported a low reliability of the compressive strength in assessing ASR-induced development. This is because the reaction is initiated in the aggregate particles and cracks only propagate into the cement paste at moderate/high expansion levels. Hence, since cracks in the cement paste largely influence compressive strength, the tool is less effective in assessing damage, especially at low to moderate expansion. Therefore, significant reductions have only been reported

for high ASR-induced expansion levels; up to a 25% reduction in compressive strength is expected [141]. Nevertheless, this tool has been selected for use in this study because of its structural design importance (i.e., ultimate capacity). Moreover, it could account for the possible occurrence of shrinkage cracks at low RH.

CHAPTER FOUR: PROBLEM STATEMENT AND OBJECTIVES OF THE STUDY

As previously mentioned, moisture and temperature play crucial roles in ASR development. While extensive research exists on their influence on the kinetics of ASR, there is a lack of in-depth understanding of how these factors contribute to induced deterioration. Specifically, a thorough and quantitative analysis of their effect on ASR-induced damage (i.e., cracks generation and propagation and associated mechanical properties reduction) is necessary.

The multi-level assessment protocol proposed by Sanchez et al. in 2017 proved effective for assessing damage development in ASR-affected concrete but has been limited to specimens subjected to high moisture conditions and standard temperatures, particularly in laboratory settings. The physical integrity of concrete may behave differently at low moisture conditions. For instance, concrete specimens stored in low humidity environment are susceptible to shrinkage cracks [10,13]. Shrinkage-induced cracks could lead to an occurrence of coupled mechanisms and can be expected to exacerbate overall ASR-induced damage. Given the peculiarity of moisture reduction as a strategy for mitigating ASR, this study will focus on the following objectives to enhance an in-depth understanding of the role of moisture and temperature in ASR:

- Understanding the relationship between internal and external RH and their effect on ASR development,
- Assessing the mechanical properties of ASR-affected concrete exposed to varying moisture (low versus high moisture) and temperature conditions,
- Understanding the impact of exposure conditions on the physical integrity (crack generation, properties, and propagation) of ASR-affected concrete,

- Assessing the impact of aggregate reactivity level on the role of moisture and temperature on ASR-induced damage,
- Propose a damage-based assessment of the RH threshold needed to trigger ASR.

CHAPTER FIVE: RESEARCH PROGRAM AND CORE OF THE THESIS

The comprehensive experimental program for this study involves three reactive coarse aggregates with different levels of reactivity (i.e., moderate; Sudbury, high; Spratt, and very high; Springhill), one non-reactive coarse aggregate, one non-reactive fine aggregate (i.e., manufactured sand), two alkali levels (i.e., 3.82kg/m³ and 5.25kg/m³), three temperatures (i.e., 21°C, 38°C and 60°C) and five relative humidities (i.e., 100%, 90%, 82%, 75%, and 62%). Several combinations of these factors were divided into four scientific papers (Chapters 6-9). The testing matrix for each chapter is illustrated in Table 5.1. The mix proportions and aggregate properties are presented in the scientific papers.

Table 5.1: Testing matrix

	Aggregates (coarse)				Alkali loading		Testing conditions		ASR-induced expansion		ASR-induced damage			
	Sudbury (SB)	Spratt (SP)	Springhill (SPH)	Nonreactive aggregates*	5.25kg/m ³ $N a_2 O_{eq}$	3.82kg/m ³ $N a_2 O_{eq}$	Relative humidity (62% - 100%)	Temperature (21°C, 38°C, 60°C)	IRH and ERH**	ASR-induced expansion	Stiffness Damage Test (SDT)	Damage Rating Index (DRI)	Direct shear (DS) test	Compressive strength (CS) test
Chapter 6		+			+		+	+	+	+				
Chapter 7		+		+	+		+	+		+	+		+	+
Chapter 8		+		+	+		+	+		+		+		
Chapter 9	+	+	+	+	+	+	+	+		+	+	+		+

*Specimens made with nonreactive coarse aggregates are used to account for shrinkage at low moisture levels

**IRH and ERH represent the internal relative humidity (in concrete) and external relative humidity (in the surrounding environment), respectively.

Concrete cylinders of 100mm x 200mm were manufactured and proportioned as per ASTM C1293.

After casting, the specimens were de-molded and moist-cured at room temperature for 48 hours;

holes were drilled on both sides, and studs were installed using a fast-setting cement slurry during the first 24 hours. The initial length readings were conducted after 48 hours, and specimens were ready for storage. Concrete specimens were placed in sealed buckets, each containing four concrete cylinders, and a minimum of 12 specimens were prepared for each RH (i.e., a minimum of three buckets per RH) at each temperature and relative humidity for each aggregate type.

5.1 Experimental procedures

5.1.1 Control of relative humidity (RH)

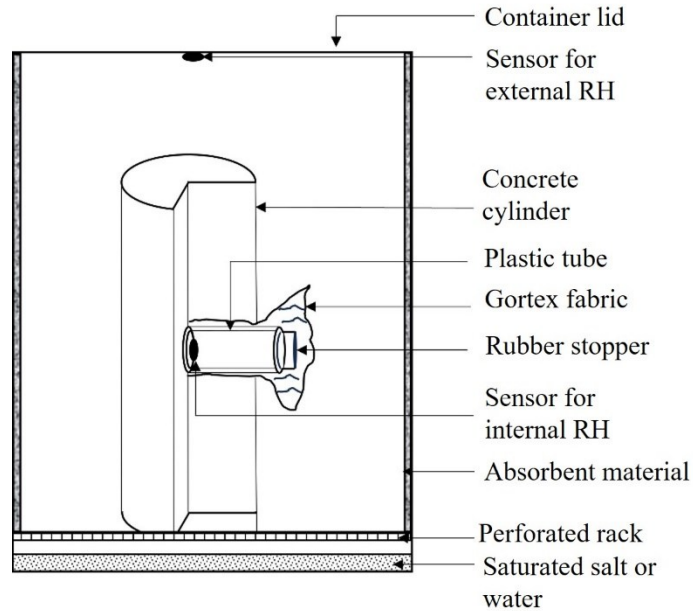
Fifteen relative humidity (RH) and temperature combinations, as shown in Table 5.2, were prepared for this study. Each condition was achieved with distilled water or salt solutions as stipulated in ASTM E104 [150]. The procedure was initiated by selecting the appropriate salt based on the desired RH condition and preparing saturated solutions using distilled water. Subsequently, the salt solution was placed at the bottom of a 20L container, and each container was stored at a specific temperature.

Table 5.2: Control of relative humidity

RH/Temperature	21°C	38°C	60°C
100%	Distilled water	Distilled water	Distilled water
90%	Barium chloride	Potassium nitrate	Potassium sulfate
82%	Ammonium sulfate	Potassium chloride	Potassium nitrate
75%	Sodium chloride	Sodium chloride	Sodium chloride
62%	Sodium bromide	Sodium nitrite	Sodium nitrite

iButton DS1293 sensors, as shown in Fig. 5.1, were placed in the containers to monitor the RH and temperature readings over time; the framework for the measurement is illustrated in Fig. 5.1.

(a)



(b)



(c)



(d)



Figure 5.1: Experimental set up: (a) Framework for internal and external RH measurement (b) storage bucket with sensor for external RH measurement (c) iButton sensor [151] (d) test cylinder for internal RH measurement

The iButton sensors are made of stainless steel to ensure their durability. Functioning as self-collecting data loggers, the iButton sensors operate within an RH range of 0% to 100%, providing reliable measurements with an RH accuracy level of $\pm 5\%$ and temperature accuracy of $\pm 0.5\%$. Data readings are stored directly within the iButton's memory, and retrieval is facilitated by

connecting the sensor to a computer through a data logger hardware and software. Despite its capability to measure relative humidity every 1 second, a 24-hour time interval was selected for this study to optimize the sensors' battery life, and 15 containers were monitored over up to one year.

To measure the external RH, a sensor was attached to the lid of each container to track the RH inside the container, representing the RH external to the cylinder. To monitor the internal RH within the concrete, a hole was perforated into the cylindrical mold before batching, and a plastic tube was inserted into the mold, extending to the middle of the mold. This setup allowed for the measurement of internal RH at the center of the concrete. Before batching, a Gortex material, similar to the approach outlined in [152], was attached to the end of the tube to prevent concrete spillage during the batching process. After demolding, the Gortex material was retained in the concrete specimen since it facilitates the passage of water vapor through its pores. The iButton sensor was then introduced into the tube to monitor internal RH, and a rubber stopper was attached to the opposite end of the tube to ensure air tightness. This procedure was repeated using the appropriate salt solutions or water for all fifteen conditions. One of the specimens for each condition was configured for internal RH measurements. Additional cylinders were also stored in the same bucket for length change measurements. This approach was adopted to balance the costs of acquiring multiple sensors while ensuring reliability and consistency in data collection. The reactive aggregate used exhibited minimal variability [153]. Moreover, testing and calibration procedures were employed to validate the reliability of the iButton sensor reported in [154].

5.1.2 Expansion measurements

Length and mass change measurements were taken over 6 months (i.e., 60°C) or 12 months (i.e., 21°C and 38°C). Specimens were collected after 3 and 6 months (i.e., for those stored at 60°C) and

after 6 and 12 months (i.e., for those conditioned at 21°C and 38°C) for the multi-level assessment protocol (i.e., SDT, DRI, Shear, and compressive strength).

5.1.3 Stiffness Damage Test (SDT)

The SDT procedure was performed as per the methodology proposed by Sanchez et al. [138], which involves subjecting concrete specimens to five loading/unloading cycles at a controlled rate of 0.10 MPa/s, with a maximum load equivalent to 40% of the 28-day concrete compressive strength. Tests were conducted on specimens from each relative humidity (RH) condition after 6 and 12 months (i.e., for specimens conditioned at 21°C and 38°C) and after 3 and 6 months (i.e., for those stored at 60°C). It is noted that three separate specimens were tested for each RH level, temperature, and age combination. Before the initiation of the test, specimens from each condition were stored in a humid environment at room temperature for 48 hours as per [138], and each end of the specimens was mechanically ground to ensure a flat surface. This study reports an average of three specimens for each result (i.e., ME, SDI, and PDI).

5.1.4 Damage Rating Index (DRI)

This study conducted a microscopic evaluation involving the conventional and extended Damage Rating Index (DRI) versions. A time-based assessment was selected to monitor the evolution of ASR-induced expansion and damage. The concrete specimens conditioned at 21°C and 38°C were tested at 6 and 12 months. The 60°C specimens were, however, assessed after three months and six months. Before the assessment, a specimen from each setup at each predetermined age was cut into half longitudinally. One half was polished using a mechanically operated table polish with grit sizes 30, 60, 120, 240, 600, 1200, and 3000. A square grid of 1cm² was drawn on the polished surface, and the DRI was conducted using a stereomicroscope at a magnification of 16x. Considering each square at a time, the number of each damage feature, as shown in Fig. 3.7, is

counted. The sum of the total count per feature is multiplied by weighting factors specified by Villeneuve and Fournier [140]. Furthermore, a more comprehensive assessment was conducted to determine maximum crack length, width, and density.

5.1.5 Direct shear

The direct shear test was performed as illustrated by De Souza et al. [17]. Specimens similar to the SDT were collected at the predetermined testing age. The specimens were conditioned at 100% RH and room temperature 48 hours before testing as per [155]. Then, a notch of 5mm width and 20 – 22mm depth was carefully made around the circumference of the cylinder using a masonry saw. The concrete cylinders were then loaded to failure at an applied loading rate of 100 N/s. It is worth noting that only two specimens were selected for each test condition.

5.1.6 Compressive strength

The 28-day compressive strength of the concrete mix utilized in this study was assessed by employing the maturity concept due to the reactivity potential of the aggregate, which could potentially trigger ASR at room temperature and above, thereby impacting the strength of the concrete. Six concrete specimens were enclosed in a plastic wrap and stored at 12°C for 47 days (i.e., the maturity is equivalent to 28 days at standard temperature), after which they were tested. To assess compressive strength reductions, the specimens tested for SDT underwent an additional 48-hour reconditioning at 21°C. This approach was facilitated by the non-destructive nature of the SDT, as confirmed by Sanchez et al. [138].

5.2 Core of the thesis – scientific paper

Five scientific papers were prepared to effectively assess and present the findings from the experimental work conducted in this Ph.D. study. Each paper addresses key aspects of the research,

allowing them to fulfill the objectives of the Ph.D. study collectively. The connections of these papers are shown in Fig. 5.2.

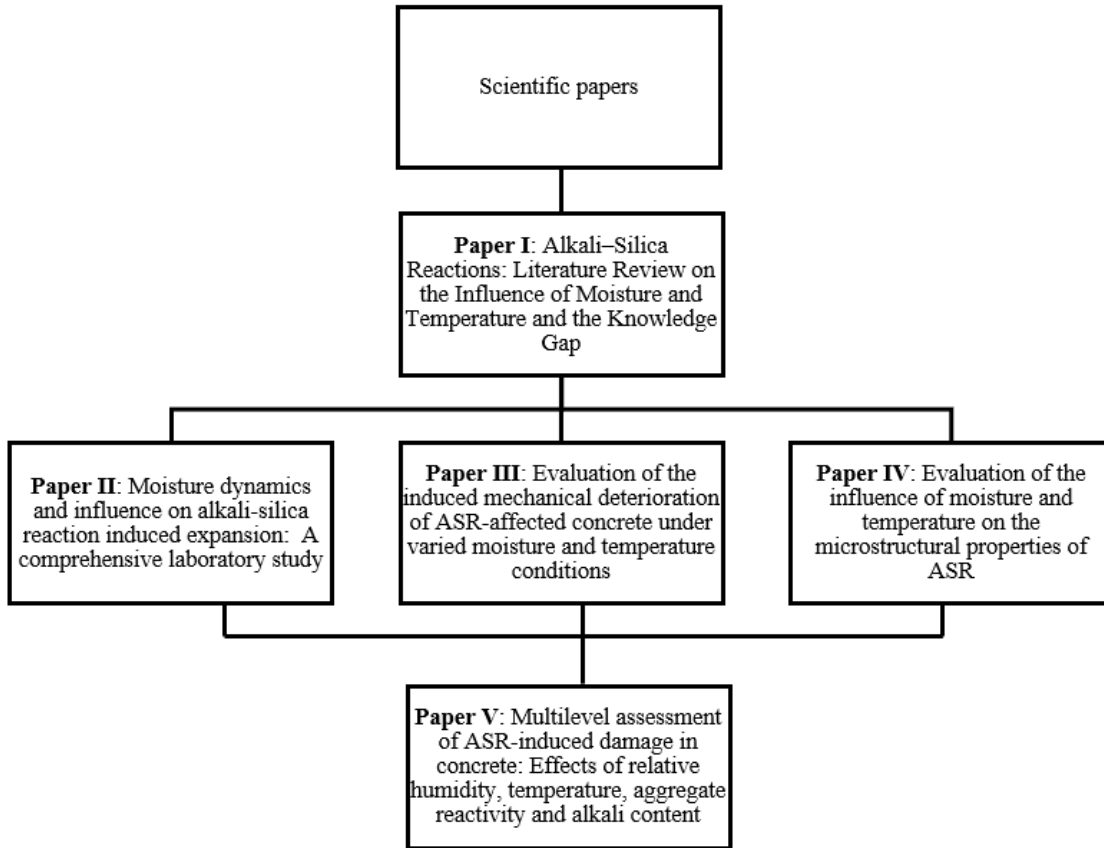


Figure 5.2: Core of the PhD. Thesis-link between scientific papers

Paper I (Chapter two) reviews the current understanding of the influence of moisture and temperature on alkali-silica reaction (ASR). It highlights the key role these exposure conditions play in ASR kinetics and identifies research gaps, particularly the lack of studies on the interaction between internal and external moisture and its impact on ASR development. Additionally, the paper discussed the moisture limitation as a mitigation strategy for ASR. Relative humidity (RH) threshold is commonly used for this purpose. However, the review notes the variability of this threshold in the literature. Furthermore, it indicates that most research on exposure conditions

primarily focuses on assessing expansion which might not give the actual state of ASR-induced damage. These identified gaps inspired the subsequent studies conducted and reported in Papers II through V (Chapters 6 to 9).

Paper II (chapter 6) focuses on the dynamics between external and internal moisture at various temperatures and examines how this interaction influences ASR kinetics. Observed shrinkage at low moisture levels led to the decoupling of shrinkage from total expansion, as presented in Paper III (chapter 7). Additionally, Paper III evaluates the impact of ASR-induced expansion under different moisture and temperature conditions on the mechanical properties of affected concrete. Building on the identified differences in mechanical properties, Paper IV (chapter 8) investigates the microscopic properties to understand how these exposure conditions affect the physical integrity of concrete.

Given that Papers II through IV were limited to one aggregate and alkali loading, the findings from these papers motivated a comprehensive analysis using a multi-level assessment protocol to evaluate the influence of moisture and temperature on ASR-induced deterioration in concrete with aggregates of varying reactivity and alkali loading in Paper V (chapter 9). This thorough assessment enables the proposal of a damage classification table and a damage-based evaluation of the RH threshold necessary to trigger ASR.

CHAPTER SIX: MOISTURE DYNAMICS AND INFLUENCE ON ALKALI-SILICA REACTION-INDUCED EXPANSION: A COMPREHENSIVE LABORATORY STUDY

Olusola Olajide ⁽¹⁾, Michelle Nokken ⁽²⁾, Leandro Sanchez ⁽³⁾

(1) Concordia University, Montreal/University of Ottawa, Ottawa, Canada, olusoladavid2013@gmail.com

(2) Concordia University, Montreal, Canada, m.nokken@concordia.ca

(3) University of Ottawa, Ottawa, Canada, leandro.sanchez@uottawa.ca

Submitted to a scientific journal for publication

Abstract

Moisture availability is crucial for initiating and progressing alkali-silica reaction (ASR) in concrete. As a result, moisture control has often been adopted as a mitigation strategy in maintaining ASR-affected concrete. Selecting effective maintenance strategies requires a deep understanding of the moisture dynamics between internal moisture in concrete and its environment, and influence on ASR, which remains incompletely explored. To evaluate this interplay, 180 concrete cylinders incorporating a reference reactive aggregate (i.e., Spratt) were manufactured and stored at distinct conditions: i.e., three different temperatures (21°C, 38°C and 60°C) and five relative humidities (100% RH, 90% RH, 82% RH, 75% RH, and 62% RH). The internal and external relative humidity, length, and mass change were monitored for up to a year. Results indicate that the amount of water used for cement hydration is sufficient to trigger the reaction, regardless of the subsequent exposure condition. However, the rate of ASR-induced development is influenced by the internal relative humidity, which changes with time based on the external relative humidity and temperature. Additionally, the minimum moisture (i.e., RH threshold) required to cause significant deleterious effects from ASR was assessed and confirmed to be temperature-dependent.

Keywords: Alkali-Silica reaction (ASR), Moisture, Relative humidity, Internal relative humidity, External relative humidity, Temperature.

6.1 Introduction

Alkali-silica reaction (ASR) is a well-known deterioration mechanism in concrete. It involves a physicochemical reaction between certain siliceous phases present in aggregates and the alkali ions (i.e., Na^+ , K^+ , and OH^-) in the concrete pore solution. This leads to the generation of a secondary reaction product (i.e., often referred to as ASR gel) that exhibits swelling characteristics and can potentially induce cracks in affected concrete, especially in humid environments. Since the discovery of this reaction several decades ago [1], numerous concrete structures suffering from ASR have been reported, and they are often prone to an early loss of serviceability [2–5].

Moisture significantly influences ASR kinetics, acting as a transport medium for alkali ions and facilitating ASR gel absorption [10]. When sufficient moisture is available, ASR-induced expansion and deterioration are exacerbated. To mitigate this, maintenance strategies often focus on limiting water ingress into affected concrete structures [156]. A key strategy in ASR maintenance is maintaining an internal relative humidity (IRH) below 80%, which has been reported to control ASR effectively [8]. Some studies even suggest that lower thresholds might be needed [13,25]. Equally critical to ASR kinetics is the external relative humidity (ERH); ASR-induced expansion has been shown to be significantly reduced in less humid environments [97,157]. Hence, the external moisture condition of ASR-affected concrete would notably influence its internal moisture dynamics [158]. Concrete exposed to varying environmental conditions, such as submerged, drying and wetting cycles, etc., may experience changes in their internal moisture over time. Therefore, understanding how environmental moisture affects internal moisture in concrete is crucial for selecting effective ASR maintenance strategies.

While several studies have assessed the internal RH of concrete in various indoor/outdoor environments, as well as in controlled laboratory settings [69,159,160], limited research has focused specifically on how internal RH influences ASR. Furthermore, numerous studies have explored the influence of external RH on the kinetics of ASR [8,10], highlighting the impact of increasing ERH on ASR kinetics. Yet, there remains a significant gap in understanding the interaction between internal and external RH and its effects on ASR. This gap emphasizes the need for further research to understand the evolution of the internal RH as a function of the external RH, which is crucial in ensuring the robustness of ASR-affected concrete maintenance protocols in the face of diverse environmental conditions.

Considering the knowledge gap that has just been identified, this paper aims to assess the time-dependent evolution of internal and external moisture conditions and their influence on the initiation and progression of ASR. Furthermore, the role of temperature on moisture interplay (i.e., internal RH versus external RH) and subsequent impact on the kinetics of the reaction was explored.

6.2 Background

Alkali-silica reaction (ASR) has been a significant concern for the durability of concrete infrastructure for many years [19,22,52,59,61,161,162]. The resulting ASR gel from the reaction has a strong affinity with water, inducing swelling and exerting volumetric pressure. Whenever the pressure generated overcomes the material's capacity in tension, cracks are generated in the aggregates and propagate to the cement paste [141], resulting in durability issues and premature loss of serviceability. In structures already affected by ASR, no known method exists to stop the reaction. The only reliable mitigation measure involves controlling moisture availability. Hence,

establishing an effective moisture management strategy in ASR-affected concrete requires a broad understanding of moisture dynamics in concrete [163].

As a porous material, concrete can absorb (i.e., absorption) and release moisture (i.e., desorption) [164]. Furthermore, capillary pores facilitate moisture movement through capillary action [165–167]. In conjunction with diffusion and permeation, these mechanisms can all be influenced by relative humidity, temperature, and, consequently, the moisture state in concrete. Additionally, environmental factors such as relative humidity and temperature significantly affect external moisture availability by influencing the evaporation rate and the amount of moisture available for absorption by the concrete. Hence, the interaction between internal and external moisture conditions creates a dynamic system that can impact concrete properties [168–172].

The influence of relative humidity on ASR has been well-studied [36]. Available findings revealed that elevated relative humidity levels speed up ASR-induced expansion and damage in concrete; otherwise, it has been found that significant ASR deterioration is unlikely to occur in dry concrete. Some studies have reported that ASR is not prone to occur in concrete with an internal relative humidity below 80% [13,27,46]. Most studies highlighting the threshold at 80% RH were conducted within a temperature range of 20 - 24°C. As earlier reported, environmental conditions like temperature can influence moisture dynamics in concrete, potentially explaining why some authors have reported a lower threshold at higher temperatures [93]. For instance, values close to 75% RH were reported at 38-40°C [13,25,26] or even as low as 59% RH at 60°C [10]. Nevertheless, a threshold of 80% RH has been widely accepted in the literature. The above reveals discrepancies in the literature regarding a single threshold. Increased temperature enhances the diffusion rate in concrete microstructure, thereby improving the mobility of ions, the movement of moisture, and the solubility of silica [102,103], all of which are crucial for ASR development.

Hence, the reaction is more rapid at higher temperatures, potentially requiring lower moisture levels to initiate ASR, which might explain why RH thresholds might be lower at higher temperatures.

All the highlighted studies on the role of moisture only considered the ERH in their assessment, disregarding the IRH, which is expected to influence ASR kinetics directly. Although the ERH is more straightforward to measure, the IRH accurately reflects the conditions influencing ASR within the concrete. Measuring the IRH may be challenging due to factors such as moisture gradients within the concrete [173], poor reliability of some sensors [169,174], etc. Nevertheless, understanding the IRH is required to improve current ASR management strategies. It could even lead to reassessing our current conclusions on moisture thresholds.

The above clearly illustrates the need to study the IRH in concrete and its interaction with the environment to further our understanding of the influence of moisture on ASR. Several studies [69,98,99,160,175–180] exist on the impact of exposure conditions (i.e., natural or simulated) on the moisture conditions in concrete. However, only a few [98,99] are related to ASR. Yet, they are all limited to a handful temperature and relative humidity combinations, limiting a comprehensive understanding of the moisture interplay across a broader range of exposure conditions.

6.2.1 Scope of work

This study aims to improve our understanding of internal relative humidity (IRH), external relative humidity (ERH), their interaction and how they influence ASR kinetics. To accomplish this goal, concrete specimens incorporating a highly reactive coarse aggregate (i.e., Spratt) were fabricated in the lab and conditioned in three temperatures (i.e., 21°C, 38°C and 60°C) and five relative humidities (i.e., 100%, 90%, 82%, 75%, and 62%). Relative humidity sensors were placed in the

storage container and embedded inside the specimens, and the moisture dynamics (i.e., changes in the IRH and ERH) were monitored over time. Furthermore, the mass and length change of the specimens were measured during the storage period. The evolution of IRH and ERH as a function of time was then assessed, and the relative humidity threshold required for ASR-induced expansion was evaluated.

6.3 Materials and methods

6.3.1 Concrete mixture design and materials

The standard mixture design used in this study was based on ASTM C1293 [181]; the properties of the aggregates are presented in Table 6.1, and information on the proportioning of the mixture is shown in Table 6.2. The reference Spratt reactive aggregate was selected as the reactive coarse aggregate, and a non-reactive manufactured sand was used as fine aggregate. The concrete was fabricated with a conventional GU cement (i.e., equivalent to ASTM Type I) with a total alkali content of 0.86% Na_2O_{eq} . The alkali content of the mixture was raised to 1.25% Na_2O_{eq} by cement mass by adding reagent-grade NaOH pellets. The details of the mixture are presented in Table 6.2.

Table 6.1: Characterization of aggregates

Aggregate	Location	Lithotype	Specific gravity (kg/m^3)	Absorption (kg/m^3)	AMBT-14 Days expansion (%)	CPT-365 Days, Expansion (%)
Reactive coarse	Ontario (Canada)	Siliceous limestone (Spratt)	2.70	0.62	0.310	0.211 [182]
Non- Reactive fine	Ontario (Canada)	Crushed limestone	2.76	0.65	0.04	0.025

Table 6.2: Mixture design of concrete

Cement (kg/m ³)	Water (kg/m ³)	Coarse aggregate (kg/m ³)			Fine Aggregate (kg/m ³)	Alkali Pellet (kg/m ³)
		4.75-9.5mm	9.5-12.5mm	12.5-19mm		
420	177.4	334.12	334.12	344.24	833.46	2.12

6.3.2 Experimental program

The experimental program was designed to simultaneously monitor internal and external relative humidities (IRH and ERH) along with length and mass changes in concrete specimens over time. This study was conducted at three different temperatures (i.e., 21°C, 38°C, and 60°C) and five relative humidity conditions (i.e., 100%, 90%, 82%, 75%, and 62%).

6.3.2.1 Control and measurement of relative humidity

Fifteen relative humidity (RH) and temperature combinations, as shown in Table 6.3, were prepared for this study. Each RH condition was achieved with saturated salt solutions as stipulated in ASTM E104 [150]. The procedure was initiated by selecting the appropriate salt based on the desired RH condition and preparing saturated solutions using distilled water. Subsequently, the salt solution was placed at the bottom of a 20L container, and each container was stored at a specific temperature. iButton DS1293 sensors, as shown in Fig. 6.1, were placed in the containers to monitor the RH and temperature readings over time; the framework for the measurement is illustrated in Fig. 6.1. The iButton sensors are made of stainless steel to ensure their durability. Functioning as self-collecting data loggers, the iButton sensors operate within an RH range of 0% to 100%, providing reliable measurements with an RH accuracy level of $\pm 5\%$ and temperature accuracy of $\pm 0.5\%$. Data readings are stored directly within the iButton's memory, and retrieval is facilitated by connecting the sensor to a computer through a data logger hardware and software. Despite its capability to measure relative humidity every 1 second, a 24-hour time interval was

selected for this study to optimize the sensors' battery life, and 15 containers were monitored over up to one year.

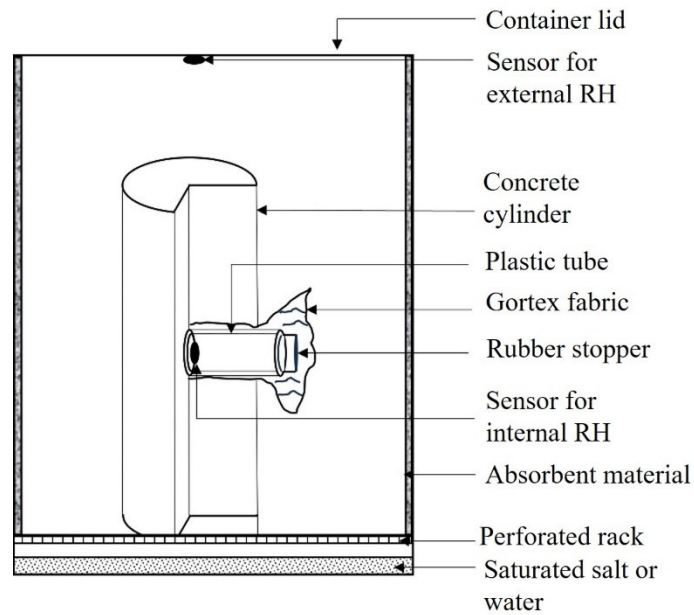
Table 6.3: Control of relative humidity

RH/Temperature	21°C	38°C	60°C
100%	Distilled water	Distilled water	Distilled water
90%	Barium chloride	Potassium nitrate	Potassium sulfate
82%	Ammonium sulfate	Potassium chloride	Potassium nitrate
75%	Sodium chloride	Sodium chloride	Sodium chloride
62%	Sodium bromide	Sodium nitrite	Sodium nitrite

To measure the external RH, a sensor was attached to the lid of each container to track the RH inside the container, representing the RH external to the cylinder. To monitor the internal RH within the concrete, a hole was perforated into the cylindrical mold before batching, and a plastic tube was inserted into the mold, extending to the middle of the mold. This setup allowed for the measurement of internal RH at the center of the concrete. Before batching, a Gortex material, similar to the approach outlined in [152], was attached to the end of the tube to prevent concrete spillage during the batching process. After demolding, the Gortex material was retained in the concrete specimen since it facilitates the passage of water vapor through its pores. The iButton sensor was then introduced into the tube to monitor the internal RH, and a rubber stopper was attached to the opposite end of the tube to ensure air tightness. This procedure was repeated using the appropriate salt solutions or water for all fifteen conditions. One of the specimens for each condition was configured for internal RH measurements. Additional cylinders were also stored in the same bucket for length change measurements. This approach was adopted to balance the costs of acquiring multiple sensors while ensuring reliability and consistency in data collection. The

reactive aggregate used exhibited minimal variability [153]. Moreover, testing and calibration procedures were employed to validate the reliability of the iButton sensor reported in [154].

(a)



(b)



(c)



(d)



Figure 6.1: Experimental set up: (a) Framework for internal and external RH measurement (b) storage bucket with sensor for external RH measurement (c) iButton sensor [151] (d) test cylinder for internal RH measurement.

6.3.2.2 Concrete cylinders conditioned at the selected testing temperatures

A total of 180 cylinders (i.e., 60 each for 21°C, 38°C, and 60°C), 100 mm in diameter by 200 mm in length, were manufactured using the mixtures presented in Table 6.2. After 24 hours of moist-curing (100% RH and 21°C), the specimens were de-molded, small holes were drilled in both ends, and stainless-steel gauge studs were bonded in place with a fast-setting cement slurry. The specimens were then moist-cured for another 24 hours to ensure the hardening of the slurry, after which the initial longitudinal reading was taken. For each temperature, the specimens were placed in sealed containers with four cylinders per container. Distilled water or salt solutions were added at the bottom of each container, depending on the desired RH. A detailed experimental plan is illustrated in Fig. 6.2. Typically, 12 concrete cylinders were prepared per RH condition at each temperature. Of these, one specimen was dedicated to monitoring the internal RH, while the remaining eleven (11) cylinders were monitored for length and mass variations over 182 days (for 60°C) and 365 days (for 21°C and 38°C).

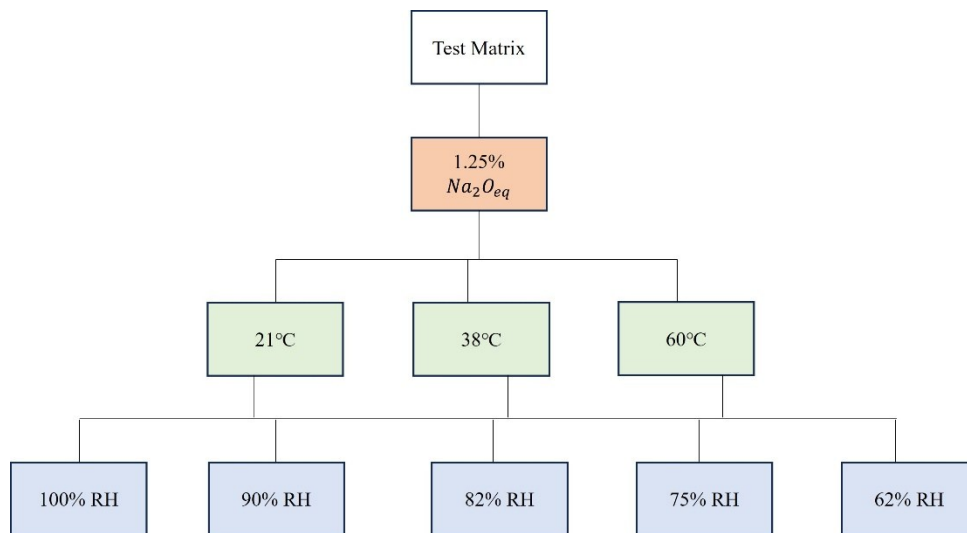


Figure 6.2: Testing Matrix.

6.4 Results

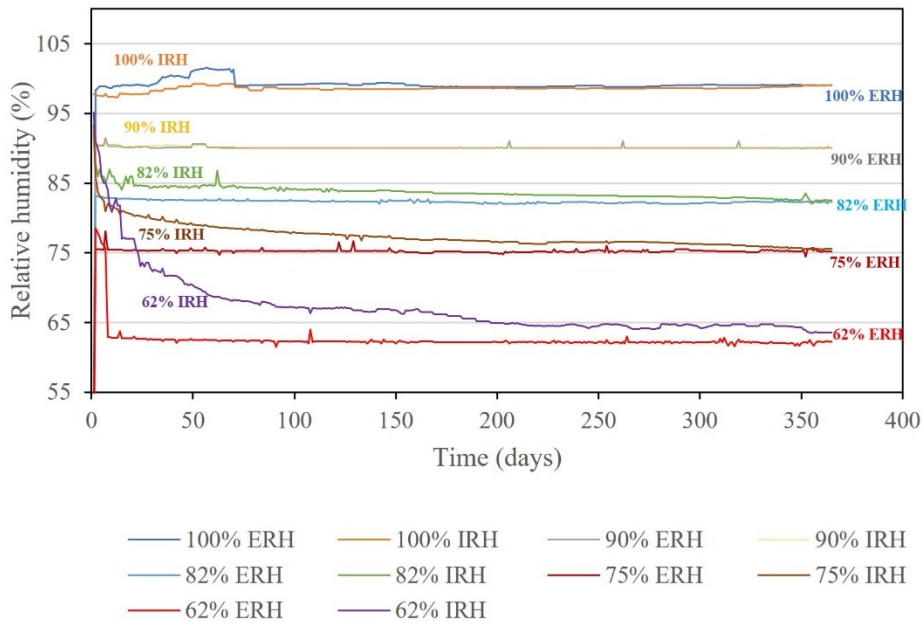
6.4.1 Relative humidity and temperature measurements

The IRH and ERH (i.e., RH inside the specimen and the storage container, respectively), as well as temperature readings as a function of time for specimens incorporating the Spratt reactive coarse aggregate stored in numerous RH (i.e., 100%, 90%, 82%, 75%, and 62%) and temperature (i.e., 21°C, 38°C and 60°C) combinations, are presented in Fig. 6.3. In all conditions, the ERH tends to converge towards the targeted RH over time. Moreover, the IRH initially showed a higher value than the ERH. The ERH in the storage buckets on day 1 before placing the specimens ranges between 28.08% - 58.22%. As shown in Table 6.4, it is interesting to note that these values increase towards the targeted RH, showing a significant increase by day 7. Meanwhile, the initial IRH in the concrete specimens on day 1 is within the range of 90.08% – 97.77%, indicating a high moisture state in the concrete at an early age, which is expected. Additionally, the internal and external temperatures were always at the target temperature.

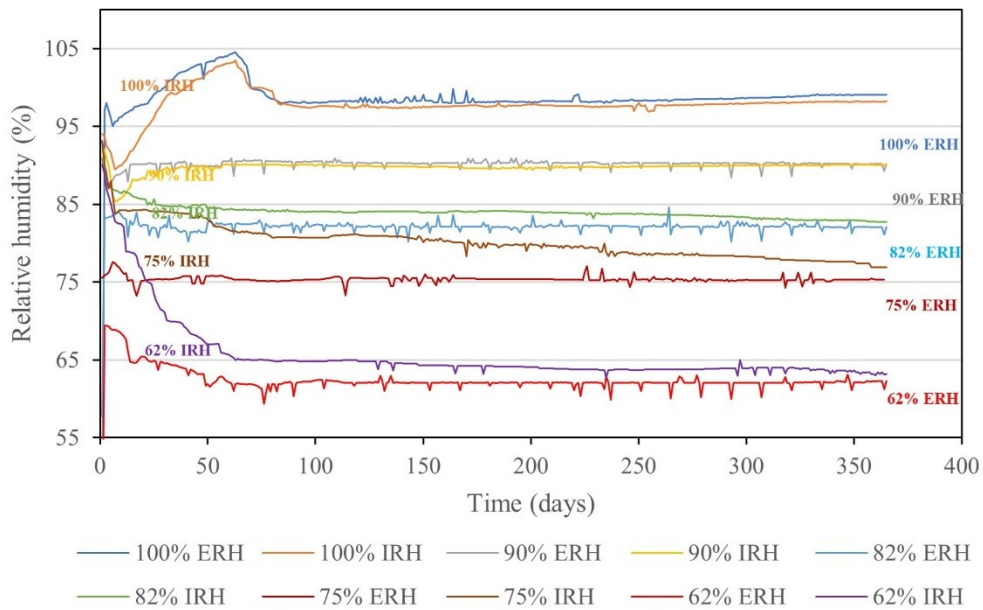
The ERH and IRH results at 21°C in Fig. 6.3a show that the targeted RH was achieved in less than 28 days for all conditions and sustained over time except for the 100% RH that recorded an ERH greater than 100% between 42-70 days. This situation was due to condensation and prevented in subsequent measurements by briefly removing and air drying the sensors bi-weekly. Consequently, an ERH of 98.80% – 99.30% was recorded afterward for the 100% RH target. As mentioned earlier, the early-age IRH in the specimens was high and is highlighted in Table 6.4. Subsequently, these values either increase (in the case of 100% RH condition) or decrease (for all other conditions) towards equilibrium with the ERH. The duration for equilibrium is shorter in high moisture than in low moisture conditions. Interestingly, the 62% RH condition at 21°C did not equilibrate

throughout the study despite the sharp drop in IRH between 1-50 days. However, all the other RH conditions bear less than a 1% difference between the ERH and IRH at day 365.

(a) 21°C



(b) 38°C



(c) 60°C

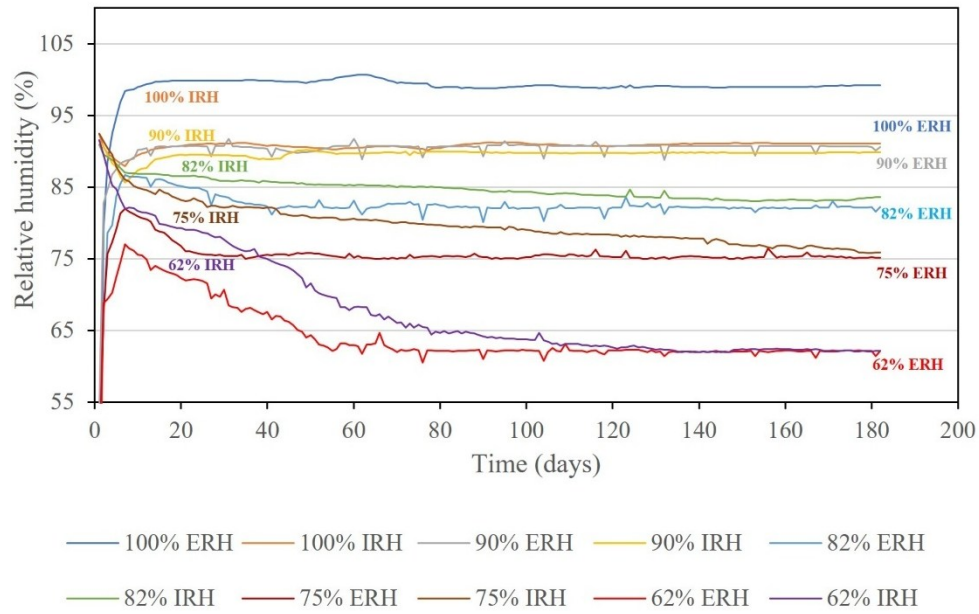


Figure 6.3: Internal RH (IRH) and External RH (ERH) as a function of time: (a) 21°C (b) 38°C (c) 60°C

Table 6.4: Early age external RH (ERH) and internal (RH) readings

Temp.	Day	100% RH		90% RH		82% RH		75% RH		62% RH	
		ERH	IRH	ERH	IRH	ERH	IRH	ERH	IRH	ERH	IRH
21°C	Day 2	98.34	97.65	90.47	90.46	83.19	87.97	75.53	86.10	78.54	91.42
	Day 7	98.90	97.81	91.48	90.72	82.88	84.94	78.13	80.94	75.71	85.04
38°C	Day 2	97.37	93.73	87.10	92.11	83.19	88.67	75.53	90.00	69.43	89.00
	Day 7	95.57	89.44	88.62	85.34	83.68	86.77	77.54	83.83	68.86	82.78
60°C	Day 2	78.96	90.54	82.69	90.65	66.78	89.54	67.43	91.43	68.78	89.56
	Day 7	98.34	87.93	88.66	85.66	86.66	87.00	82.00	86.00	77.00	82.00

Fig. 6.3b and 6.3c display the IRH and ERH under tests conducted at 38°C and 60°C, respectively.

In Fig. 6.3b, over 365 days at 38°C, ERH showed a significant increment towards the target RH, ranging from 68.86% to 95.57% by day 7. At the same time, IRH remained higher than 82% across

all conditions despite some early losses, likely due to hydration effects within the first week. Subsequently, the IRH in 100% RH and 90% RH conditions increased to equilibration with the ERH, while other conditions experienced a reduction in IRH towards the ERH. Meanwhile, Fig. 6.3c details a 182-day study at 60°C, showing a rapid convergence of ERH to the target RH across all conditions, with high moisture setups like 100% and 90% RH achieving this within just 21 days and 62% RH taking up to 75 days. The 100% RH condition failed to fully equilibrate, mirroring the IRH at 90% RH, while lower RH setups, such as 62% RH, reached equilibrium in less than 150 days, quicker than at lower temperatures.

It is worth noting that some temporal changes (i.e., increase/decrease) in ERH can be observed in the plots in Fig. 6.3. These changes might have occurred due to excess water diluting the saturated salt solutions, typically resulting from condensation since fluctuations in temperature cause water to accumulate in the solution. Additional salt was added to mitigate this issue and to maintain consistent RH levels. Furthermore, some observed drops can be attributed to the 18-24 hours transfer of storage buckets to room temperature before expansion measurements. This was limited to the 38°C and 60°C setups.

6.4.2 Mass and length change and ASR kinetics

The average induced mass and length changes as a function of time for concrete specimens containing Spratt reactive aggregates stored at three temperatures (i.e., 21°C, 38°C and 60°C) under numerous RH conditions (i.e., 100% RH, 90% RH, 82% RH, 75% RH and 62% RH) are presented in Fig. 6.4. The data presented represents the average of 11 cylinders for each data point. Standard deviations are presented in supplementary materials (Table S6.1-3), which fall within 0.01-0.04% depending on the exposure conditions. It is interesting to note that conditions below 100% RH displayed a significant initial shrinkage during the test. The recovery duration from shrinkage

depends on the moisture level and exposed temperature. However, the 62% RH conditions failed to achieve a net positive expansion throughout the study for any temperature appraised. Fig. 6.4a, 6.4c, and 6.4e illustrate the average mass change for all conditions, and the mass change presents a generally similar behavior across all temperatures.

The influence of moisture conditions and temperature on concrete specimens over different durations highlights significant trends in mass changes and ASR kinetics, as illustrated in Fig. 6.4. At 21°C over 365 days, the plots (Fig. 6.4a and 6.4b) show distinct behaviors influenced by RH levels. In the most humid condition (i.e., 100% RH), specimens gained up to 0.97% mass due to moisture gain and, therefore, enhanced ASR activity. In comparison, the driest condition (i.e., 62% RH) experienced a substantial mass loss of about 1.6%, indicative of a moisture-driven mass reduction. Interestingly, specimens at 90% RH maintained nearly constant mass throughout the test. Similarly, ERH influences ASR-induced expansion, and ultimate expansion reduces with ERH; the highest ultimate expansion of 0.1113% was reached at 100% RH, and notably, the lowest RH condition, 62% RH, led to a net shrinkage of -0.0096%. At 38°C over the same duration (Fig. 6.4c and 6.4d), ASR kinetics varied more significantly with ERH than at 21°C, especially for high RH conditions. Specimens at 100% RH displayed the highest ultimate expansion of 0.210%. Contrastingly, 62% RH conditions only showed minor shrinkage (i.e., -0.002%). Lower RH conditions (i.e., 82%, 75%, and 62%) initially suffered from early age shrinkage, transitioning to expansion later during the test. The shift from shrinkage to expansion became more prolonged and less significant with decreasing RH, leading to the 62% RH specimens failing to achieve a net positive ultimate expansion. Nevertheless, the switch from a high negative length change at around 3 months to close to 0% length change at 12 months indicates the occurrence of ASR for this exposure. At 60°C (Fig. 6.4e and 6.4f), the mass and length change trend over 182 days echoed

earlier temperatures, but the behavior was accelerated. For instance, specimens conditioned at 62% RH attained up to 2.5% mass loss, the highest among all conditions, likely due to intensified drying effects at elevated temperatures. Remarkably, the ultimate expansion at 90% RH exceeded that of 100% RH, suggesting possible increased alkali leaching, a widely known drawback of accelerated ASR testing [14,100,183].

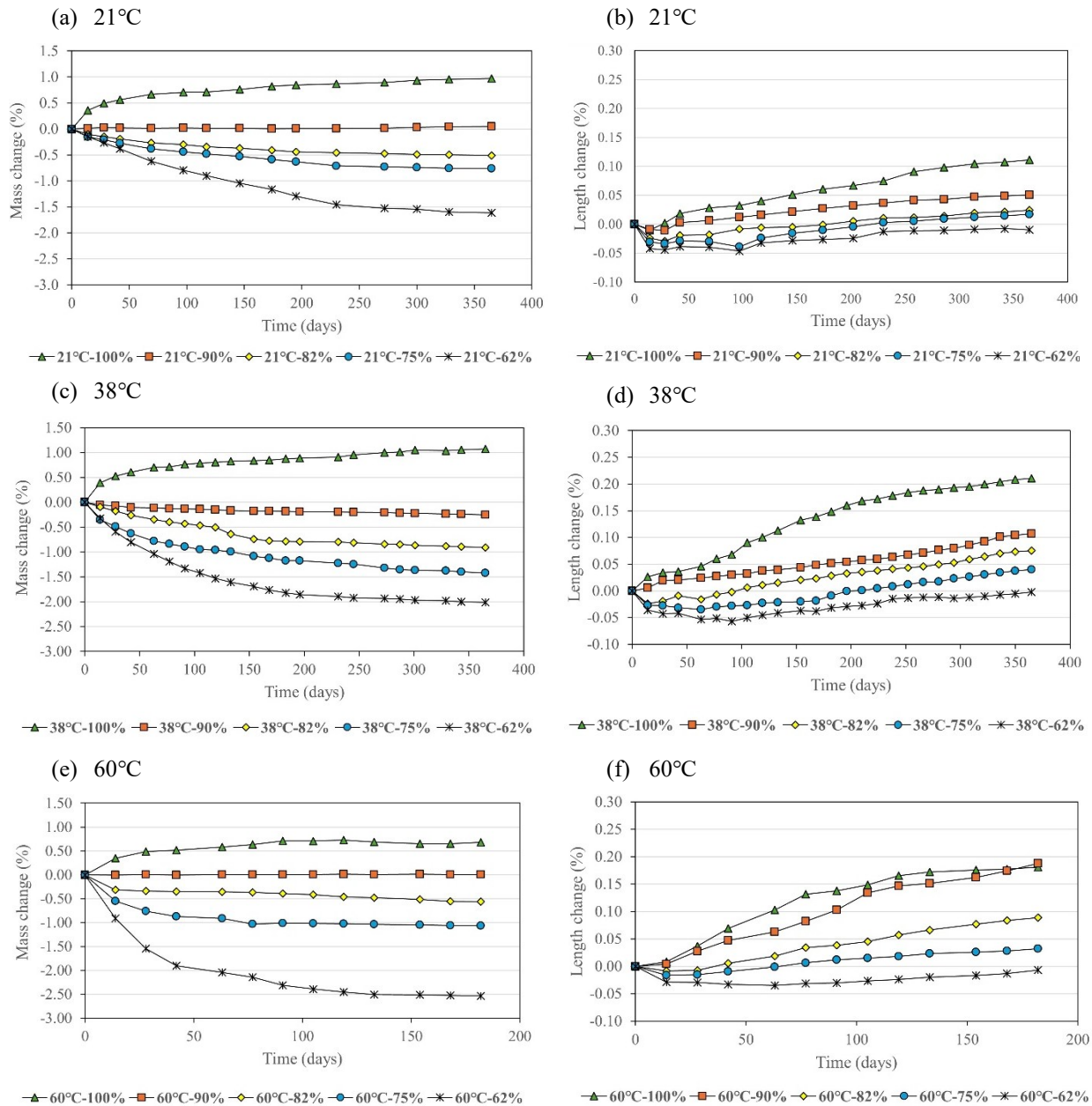
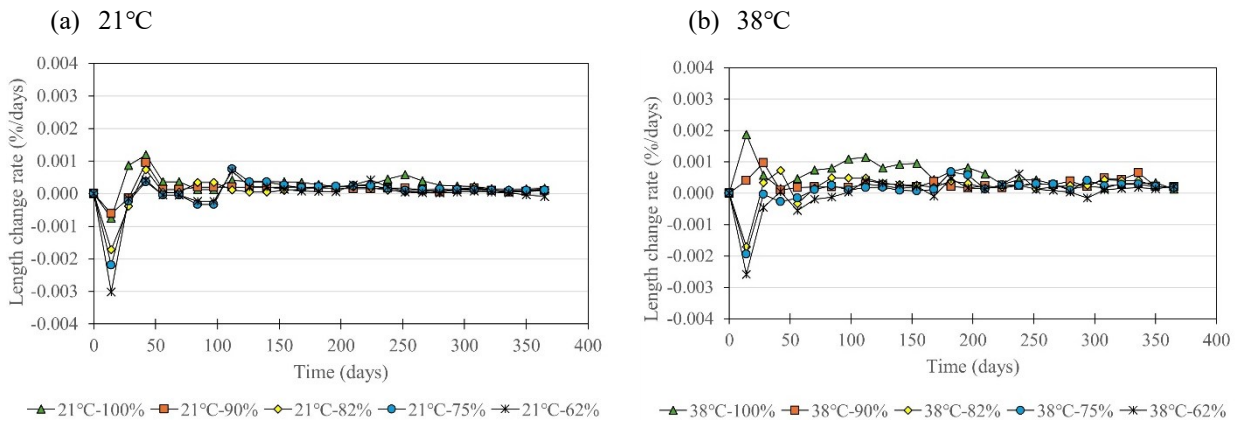


Figure 6.4: Mass and length change as a function of time at three different temperatures: (a) mass change-21°C (b) length change-21°C (c) mass change-38°C (d) length change-38°C (e) mass change-60°C (f) length change-60°C

6.5 Discussion

6.5.1 Influence of exposure conditions on ASR-induced length change rates

The rate of ASR-induced expansion can provide deeper insights into ASR kinetics, which is crucial for predicting how quickly ASR-induced expansion might occur in different environments. Different temperatures and RH levels can significantly alter the kinetics of ASR, as already shown in the results and as per [13,46], making it essential to study these factors in detail. Furthermore, understanding how ASR-induced length change rate is affected by measurable environmental factors, such as the ERH and temperature, is critical for identifying periods of rapid ASR progression, which can inform maintenance schedules and mitigation strategies. Therefore, a time series analysis involving the rate of expansion change over time, based on the external RH and temperature, is presented in Fig. 6.5 (i.e., length change rate at fixed temperature) and Fig. 6.6 (i.e., length change rate at fixed ERH).



(c) 60°C

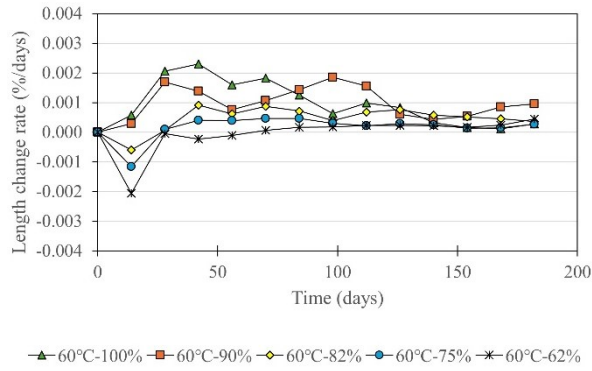
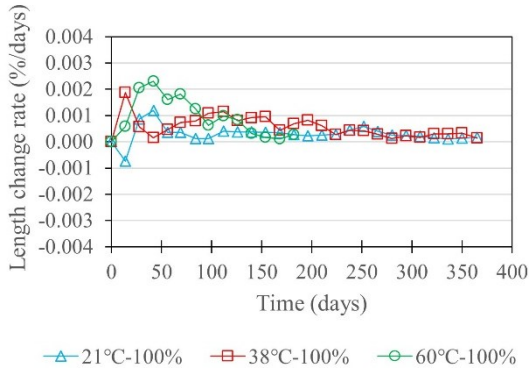
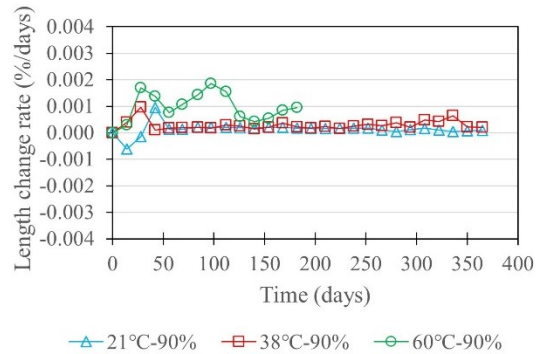


Figure 6.5: Length change rate over time at five different relative humidity: (a) 21°C (b) 38°C (c) 60°C

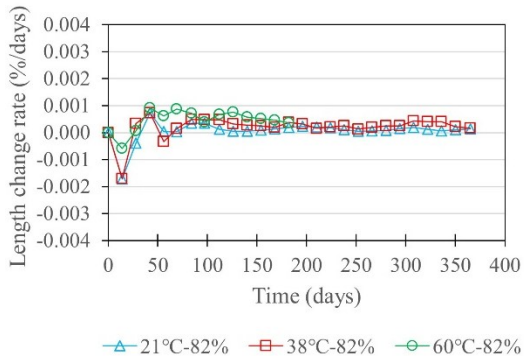
(a) 100% RH



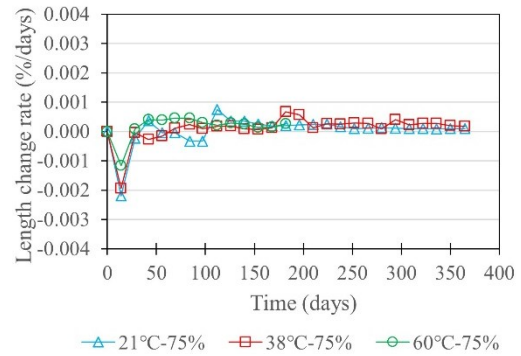
(b) 90% RH



(c) 82% RH



(d) 75% RH



(e) 62% RH

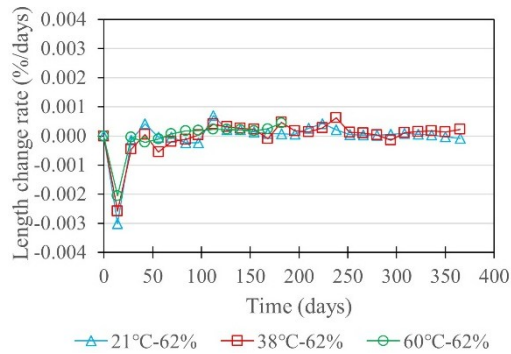


Figure 6.6: Length change rate over time at three different temperatures: (a) 100% RH (b) 90% RH (c) 82% RH (d) 75% RH (e) 62% RH

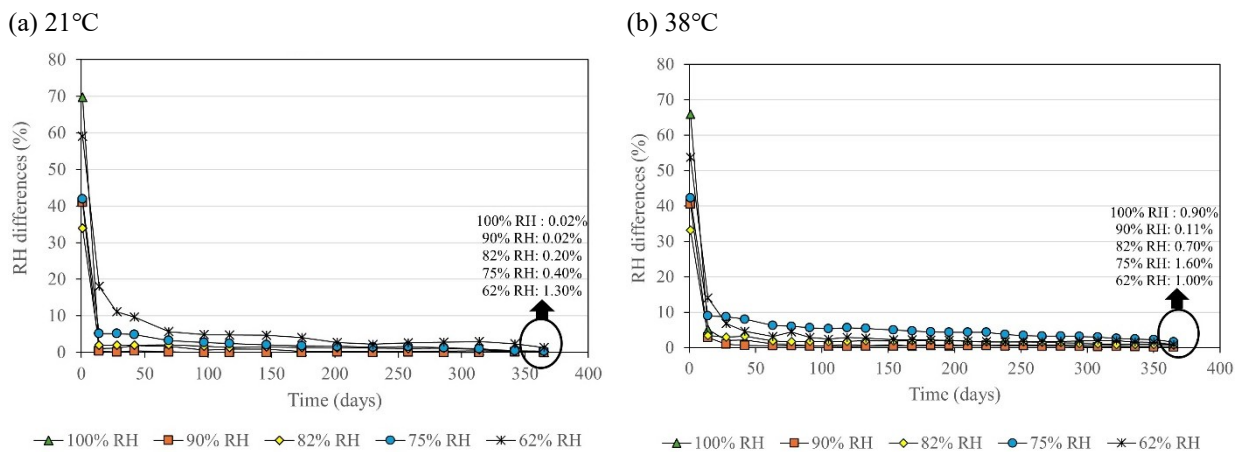
Each point on the plots represents the linear length change (i.e., expansion/shrinkage) over 14 days (i.e., the time between measurements). Analyzing Fig. 6.6, higher temperatures (i.e., 38°C and 60°C) and moisture (i.e., 90%RH and 100%RH) lead to positive initial length change rates from the onset of the reaction. This can be attributed to the optimal moisture availability and enhanced chemical reactivity potentials at elevated temperatures. Furthermore, the rate of expansion/shrinkage for all conditions increases and converges over time. As displayed in Fig. 6.5 and 6.6, the combination of the highest moisture and temperature (i.e., 60°C and 100% RH) presents the highest positive rate of 0.0023%/day. This demonstrates the influence of the exposure conditions on ASR-induced expansion, especially the role of elevated temperature in enhancing the dissolution of silica and mobility of ions for the reaction. On the other hand, the combination of the lowest moisture and temperature (i.e., 21°C and 62% RH) considered in this study presents the highest negative slope of -0.003% (i.e., shrinkage) recorded at an early age of 14 days. Despite the low ERH in this condition, the IRH was reasonably high (i.e., ~82%), which can be considered enough to initiate ASR-induced expansion as per [12,27]. However, the observed shrinkage can be attributed to the sharp decrease in the IRH from 95% recorded on day 1. Exploring Fig. 6.5 and 6.6, such magnitude of negative slope was not attained again throughout the study. This can be

attributed to the subsequent steady drop in IRH over time. Moreover, as illustrated in Fig. 6.6e, there are instances of positive slope even at later ages, confirming an expansive behavior and a recovery from shrinkage at low moisture conditions.

Another interesting point about the length change rate is the initial rise and steady decline over time, evident in most conditions, correlating with the expansive behavior of ASR. Typically, ASR is known to possess fast kinetics in its early stages, which tends to diminish over time until leveling off [16]. For instance, 60°C attained the highest rate of 0.0023%/days, while 38°C and 21°C attained 0.0019%/days and 0.0012%/days, respectively, all at 100% RH. All of these are within the first two months of the reaction. The length change rates became slower towards the mid-duration of the test and leveled off after that. The stabilization of the length change rate can be interpreted differently depending on the exposure conditions. As displayed in Fig. 6.6a and 6.6c, considering 90% RH and 100% RH (i.e., high moisture condition), the rates stabilized around 200 days; this stabilization can be attributed to the reaction nearing its completion. Alkali leaching will likely influence the ultimate expansion, preventing further expansion in these conditions. Other reasons can be attributed to the properties of the ASR gel, such as viscosity, especially in the case of 38°C and 60°C as per [14,100]. On the other hand, for low RH conditions (i.e., 62% RH and 75% RH), as displayed in Fig. 6.6d and 6.6e, the relatively stable rates, except for a few spikes recorded, suggest that these exposure conditions limit ASR-induced expansion. Although some expansion can be recorded in this condition, the kinetics appear stable and less sensitive to temperature changes. As a result, maintenance strategies need to be focused on this moisture level.

6.5.2 Understanding moisture dynamics in concrete and the influence of ASR-induced expansion

Moisture has been established to play a vital role in ASR kinetics [10,16]. Fig. 6.3 provides insight into moisture evolution in a controlled environment and its influence on moisture availability in concrete specimens at different temperatures as ASR develops. Concrete inherently contains a high moisture content from batching, which is reduced by hydration and environmental conditions over time. While the rate of hydration is unknown in this study, the latter is quantified by monitoring the IRH as a function of ERH and temperature. Fig. 6.7 provides a simplified influence of ERH and temperature on IRH as a function of time by determining the absolute RH difference (i.e., ERH-IRH) for all exposure conditions over time. Each point shown represent the same day expansion measurements were taken. This highlights the rate and extent of moisture movement into and out of concrete specimens; furthermore, it highlights how quickly the concrete reaches equilibrium with its environment.



(c) 60°C

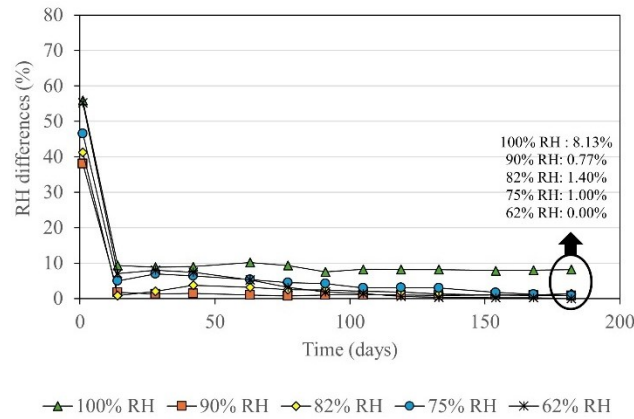


Figure 6.7: RH difference as a function of age (Abs [IRH-ERH]): (a) 21°C (b) 38°C (c) 60°C

Typically, concrete specimens subjected to 100% ERH and 90% ERH regained their moisture loss to hydration through the ERH, stabilizing their IRH. This stabilization is expected to depend on the hydration degree, which is temperature-dependent. Enhanced hydration at elevated temperatures leads to the need for more moisture from the ERH to maintain equilibrium. This can be attributed to the higher RH differences recorded at 38°C and 60°C compared to 21°C. However, this phenomenon is multifaceted. On the other hand, at 62% ERH, concrete requires a high moisture loss to maintain a stable IRH. This condition favors elevated temperatures where enhanced moisture loss due to hydration is possible. This leads to a lower RH difference of 62% RH at 60°C compared to 21°C and 38°C. Overall, reducing RH differences for all conditions over time highlights the importance of environmental factors such as ERH and temperature in governing concrete's IRH state. Hence, while ERH is not directly responsible for initiating ASR, it plays a critical role in the internal moisture level and would be vital for sustaining the reaction.

The trend of RH differences appears to be sensitive to temperature, as illustrated in Fig. 6.7. Hence, it is evident that the concrete specimens studied at different temperatures undergo different hydration rates, which might influence properties such as ions and moisture movement [184].

Since hydration can be related to concrete maturity [185], adapting this concept into the discussion would provide a more comprehensive understanding of the temperature-dependent behaviors observed in this study. Maturity is a well-established measure of the combined effects of temperature and time on concrete properties. Hence, properties such as the rate and amount of hydration can differ at the same age, leading to differences in moisture availability in the concrete pores (i.e., IRH) [186]. The above suggests that moisture availability should be assessed based on concrete maturity. Additionally, it serves as a critical parameter for explaining the accelerated ASR-induced expansion recorded at higher temperatures. Equation 6.1 describes the maturity method. Furthermore, a K value, as per Equation 6.2, defined as the ratio of Internal Relative Humidity (IRH) to External Relative Humidity (ERH), measures how the internal moisture content in the concrete specimen responds to the environment. Fig. 6.8 displays a dual-axis plot illustrating the length change and associated K-values as a function of maturity for all conditions to explore the interplay between moisture (i.e., IRH and ERH) and ASR-induced expansion.

$$\text{Maturity} = \sum_0^t (T - T_0) \Delta t \dots \dots \dots (6.1)$$

t = time

T = average temperature (°C) over the time interval Δt

T₀ = Datum temperature, taken as 0°C in this work

$$K = \frac{IRH}{ERH} \dots \dots \dots (6.2)$$

K = 1: equilibrium state

K < 1: ERH greater than IRH

K > 1: IRH greater than ERH

Several studies [187–189] have verified the importance of concrete maturity on various concrete properties. However, its applicability in discussing the moisture movement in concrete and ASR-induced expansion has not been quantified. Therefore, Fig. 6.8 describes the appraisal of moisture conditions and ASR-induced deterioration via concrete maturity.

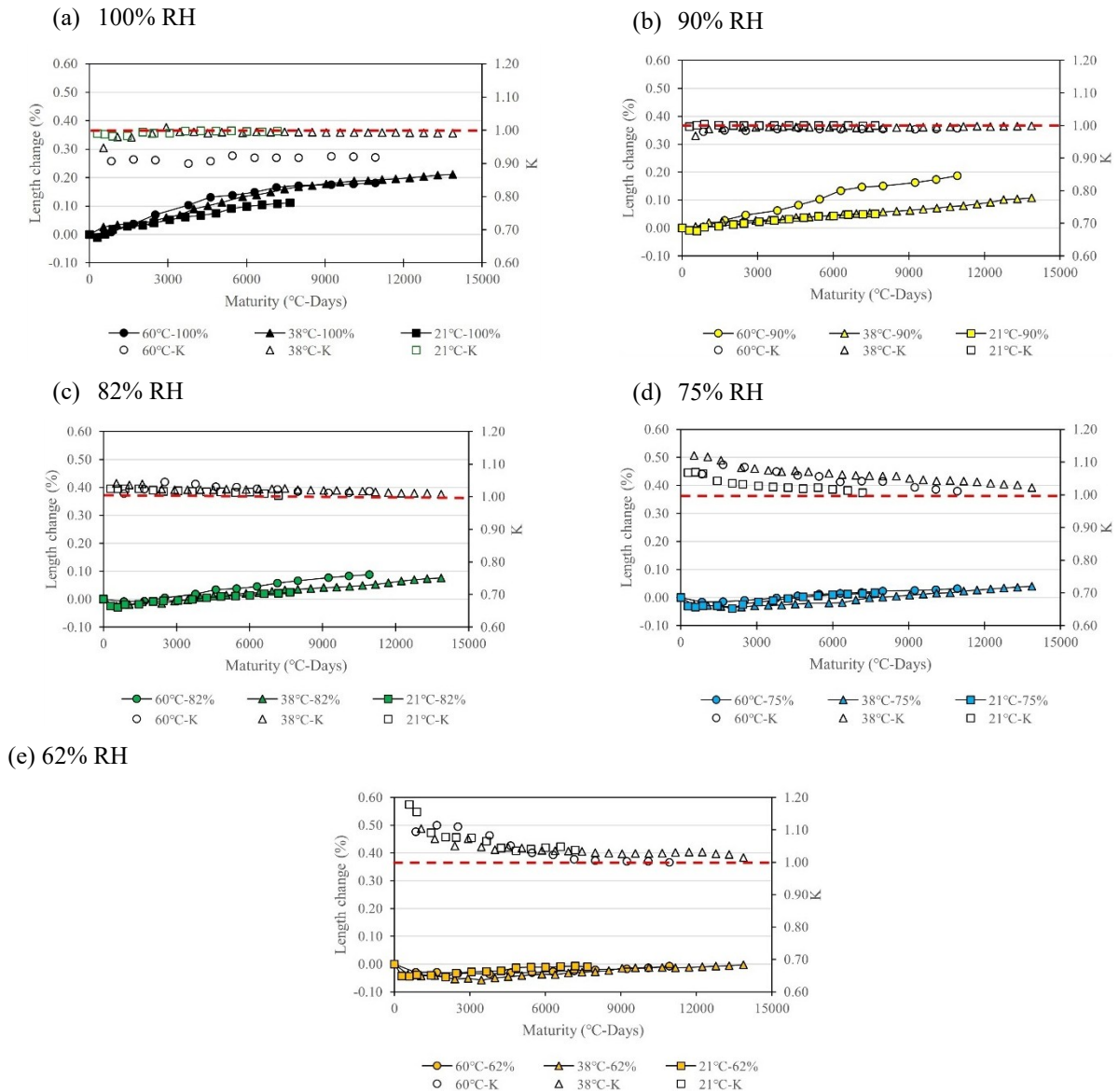


Figure 6.8: K values (IRH/ERH) and length change as a function of maturity: (a) 100% RH (b) 90% RH (c) 82% RH (d) 75% RH (e) 62% RH

Hydration, a unique, never-ending chemical reaction in concrete, results in moisture loss over time, coinciding with the densification of its microstructure. Hydration and the state of the microstructure can influence the availability of moisture in pores as well as the movement of ions and moisture. However, these conditions are expected to remain fairly similar in different concrete at similar maturity. As shown in Fig. 6.8, each RH has a different evolution for K; at high RH levels, the K is always near 1 except for 60°C at 100% RH. On the other hand, it takes more time for K to reach 1 for lower RH levels. This demonstrates that moisture equilibrium is RH-dependent at similar maturity as expected. Interestingly, the trends in K remain similar at each RH level, despite the difference in temperatures, highlighting the role of maturity. Furthermore, similar maturity ensures a similar porosity level for the migration of ions. While silica's dissolution rate might differ at different temperatures (e.g., 21°C versus 60°C), a similar amount of silica dissolution is expected at comparable maturity, leading to close ASR-induced expansion at each RH, as illustrated in Fig. 6.8.

The role of ERH in ASR has been well-documented [8,10]. Response surface analysis (RSA) plots illustrating the influence of ERH and IRH separately on ASR-induced expansion at numerous temperatures, confirming the uniqueness of both moisture states, are presented in supplementary materials (Fig. S6.1-3). However, discussions on the influence of the interplay between these states (i.e., IRH and ERH) on ASR-induced expansion are missing in the literature. Such interplay can be simplified using the K values. K value changes with maturity, reflecting a stabilization of moisture content within the concrete. This stabilization could either mitigate or exacerbate ASR, depending on the surrounding conditions. High RHs (i.e., 100% and 90% RH), as illustrated in Fig. 6.8a and b, remained in a high moisture state and close to equilibrium throughout the study, mainly due to the high ERH and initial IRH. The closeness to equilibrium ensures a steady increase

in ASR-induced expansion. Moreover, exploring the plots, 90% RH maintained a steady moisture state throughout the maturity period, emphasizing a minimal barrier to moisture exchange exists between the concrete and its surrounding environment. Hence, it is safe to assume that for environments with around 90% RH, the IRH of concrete can be similar to the ERH, irrespective of maturity (i.e., age and temperature). Furthermore, the K values play a significant role in length change. A sharp drop in K will mean a drop in internal moisture corresponding to considerable shrinkage in the affected concrete specimen. This scenario can be attributed to a high moisture loss due to hydration, which is not compensated by the environmental condition (i.e., low ERH). In contrast, a steady drop/increase or constant K value close to equilibrium will maintain or further enhance ASR-induced expansion depending on the IRH level. Hence, it can be deduced that ASR-induced expansion is sensitive to the interplay of the ERH and IRH.

6.5.3 Assessing the moisture threshold for ASR

A trident of factors (i.e., reactive silica, alkali, and moisture) is crucial for ASR, with moisture playing a pivotal role in the reaction. A relative humidity threshold of 80% has been widely referenced as sufficient for the reaction [13,46]. However, there have been other contrary opinions, with some suggesting different thresholds at varying temperatures [8,25,26]. This study has verified that the ERH and temperature play a crucial role in the state of moisture in concrete (i.e., IRH). Hence, the likely existence of a moisture threshold is assessed by preparing a plot of the ultimate expansion from 62% to 90% ERH at three temperatures (i.e., 21°C, 38°C, and 60°C), as shown in Fig. 6.9.

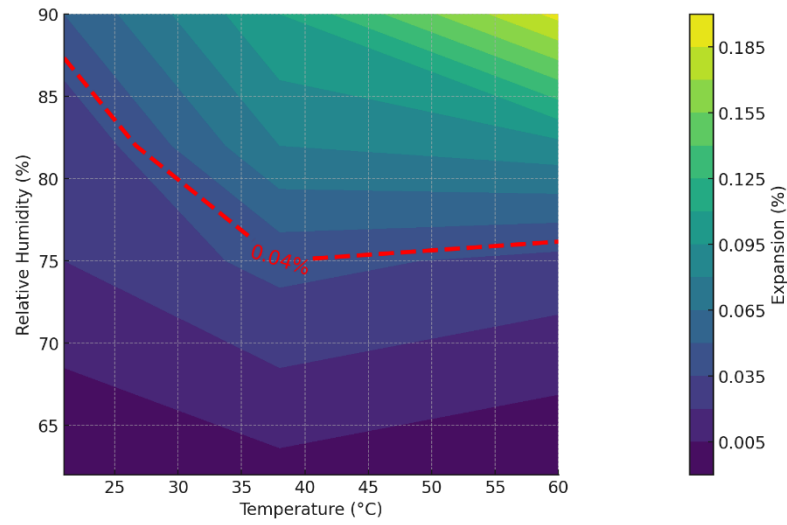


Figure 6.9: Assessing the influence of temperature on RH threshold for ASR

The surface plots suggest that the relationship between temperature, ERH, and ASR-induced expansion is non-linear. Thus, it can be deduced that the RH threshold is not a fixed value but varies depending on the combination of temperature and RH. This means ASR forecasting in the field via modeling or the selection of mitigation strategies should consider both factors together rather than relying on a single RH threshold for all conditions. Temperature can be noted to significantly influence ASR sensitivity to variations in RH when observing the plot. At higher temperatures (i.e., 38°C and 60°C), the reaction becomes more sensitive to RH changes, and length change rates increase more sharply above a certain ERH.

The threshold for ASR in this study is defined as an expansion below a limit (i.e., 0.04%) that causes deterioration in concrete. Overall, ultimate expansion is less susceptible to variability in temperature changes at 62% ERH. Although some expansions can be recorded at this RH despite the low moisture condition, the expansions recorded are negligible/marginal and all below 0.04% [24]. Hence, monitoring ASR-affected structures at this condition would sufficiently mitigate the reaction. However, observing the plot, the temperature dependence of the RH threshold is evident

above 62% ERH, with a steeper increase in expansion as RH increases from this level. At 21°C, the relatively low expansions, even at higher RH levels, suggest that the RH threshold at lower temperatures might be higher. Considering the well-referenced 80% threshold, 21°C failed to attain a 0.04% expansion. 85% - 90% ERH could be needed at this temperature to achieve 0.04%. For higher temperatures (i.e., 38°C and 60°C), they presented a reasonably similar expansion from 62% - 82% ERH, and the critical RH threshold for significant ASR expansion appears to decrease; 75% ERH is needed to achieve 0.04% in agreement with findings by [13]. These findings highlight the dependence of the RH threshold on temperature, as stated by [190]. Hence, the potential for ASR development might vary depending on the temperature. This further confirms the unique influence of exposure conditions on the reaction. Understanding this relationship will significantly influence our decision-making processes in maintaining ASR-affected structures. However, it is crucial to note that while ERH/IRH can be controlled through several available maintenance strategies, the temperature can not be controlled in the field. The results gathered in this work seem to indicate that limiting the ERH and thus IRH to 75% ERH can be considered an effective strategy to mitigate important induced deterioration in the field. However, these results need to be confirmed using a wide variety of aggregate types and concrete mixtures.

6.6 Conclusion

This study aimed to investigate how external moisture conditions influence internal moisture in concrete and the dependence of this interplay on temperature and, subsequently, the effects on ASR-induced expansions. The main findings can be highlighted hereafter:

- Concrete undergoes moisture loss or gain to achieve equilibrium with its surroundings, with temperature playing a vital role in this equilibration process. The relationship between temperature and equilibrium proves to be non-linear. In low moisture conditions, the

increase in temperature enhances drying and the rapid drop in internal moisture, leading to a quicker equilibration with the environment. On the other hand, in high moisture conditions, a reduction in temperature enhances the equilibration of external moisture with internal moisture.

- All concrete specimens studied have initial internal moisture more significant than 90% RH. Hence, sufficient moisture needed to initiate the reaction is available from batching. Provided all other factors required for ASR are met (i.e., alkali and reactive silica), the reaction can start irrespective of the storage condition. However, the rate depends on the evolution of the internal RH, which depends on external RH and temperature. As shown in the lowest moisture condition considered in this study (i.e., 21°C-62%), an expansion of 0.0367% was recorded between 97-365 days (i.e., after recovery from shrinkage). Hence, the reaction can not be stopped. Mitigating deleterious expansion becomes feasible by moderating the reaction rate, for how long would depend on the extent to which internal RH can be effectively reduced.
- Comparing internal and external RH, it was evident that ASR is more sensitive to internal RH, as a drop in the internal RH results in shrinkage. This suggests that maintaining lower internal RH could effectively control ASR. However, managing the external RH can make this possible. As a result, both internal and external RH are to be considered while assessing maintenance strategies.
- The moisture dynamics in concrete are influenced by temperature, leading to differences in ASR kinetics. Hence, the minimum moisture needed for substantial deleterious ASR depends on temperature. As a result, mitigative and preventive measures should be tailored to specific environmental conditions.

- The kinetics of the reaction are affected by moisture conditions. The rate is slow for low moisture conditions across all temperatures, leading to an early age combined mechanism including shrinkage, especially in 62% RH, 75% RH, and 82% RH. As a result, some of these conditions failed to attain positive net length change at the end of the study, but they were in an expansive state after recovery from shrinkage. Therefore, considering shrinkage-induced damage would be crucial in comprehensively assessing damage in ASR-affected structures across all moisture levels.

Supplementary materials

Table 6.5: Length change measurements for concrete specimens stored at 21°C and numerous relative humidities

Day	21°C-100%		21°C-90%		21°C-82%		21°C-75%		21°C-62%	
	Length Δ (%)	Std. Dev.								
28	0.0018	0.0191	-0.0106	0.0226	-0.0294	0.0177	-0.0339	0.0237	-0.0443	0.0250
97	0.0320	0.0218	0.0120	0.0203	-0.0084	0.0230	-0.0390	0.0279	-0.0463	0.0262
174	0.0607	0.0126	0.0275	0.0167	-0.0012	0.0170	-0.0105	0.0233	-0.0262	0.0275
286	0.0982	0.0109	0.0428	0.0102	0.0142	0.0108	0.0093	0.0128	-0.0108	0.0178
365	0.1113	0.0080	0.0507	0.0088	0.0244	0.0118	0.0172	0.0089	-0.0096	0.0147

Table 6.6: Length change measurements for concrete specimens stored at 38°C and numerous relative humidities

Day	38°C-100%		38°C-90%		38°C-82%		38°C-75%		38°C-62%	
	Length Δ (%)	Std. Dev.								
28	0.0341	0.0175	0.0192	0.0208	-0.0192	0.0222	-0.0277	0.0446	-0.0426	0.0233
91	0.0682	0.0171	0.0299	0.0281	-0.0023	0.0313	-0.0279	0.0365	-0.0570	0.0237
182	0.1483	0.0201	0.0517	0.0244	0.0285	0.0252	-0.0089	0.0418	-0.0317	0.0248
280	0.1898	0.0157	0.0765	0.0235	0.0493	0.0179	0.0175	0.0394	-0.0115	0.0100
365	0.2106	0.0162	0.1072	0.0210	0.0756	0.0124	0.0398	0.0328	-0.0023	0.0104

Table 6.7: Length change measurements for concrete specimens stored at 60°C and numerous relative humidities

Day	60°C-100%		60°C-90%		60°C-82%		60°C-75%		60°C-62%	
	Length Δ (%)	Std. Dev.								
28	0.0369	0.0189	0.0277	0.0195	-0.0074	0.0262	-0.0150	0.0223	-0.0295	0.0319
63	0.1028	0.0196	0.0629	0.0181	0.0184	0.0358	-0.0010	0.0299	-0.0349	0.0324
91	0.1378	0.0190	0.1030	0.0165	0.0384	0.0419	0.0120	0.0334	-0.0302	0.0249
182	0.1810	0.0149	0.1875	0.0152	0.0886	0.0211	0.0319	0.0306	-0.0070	0.0261

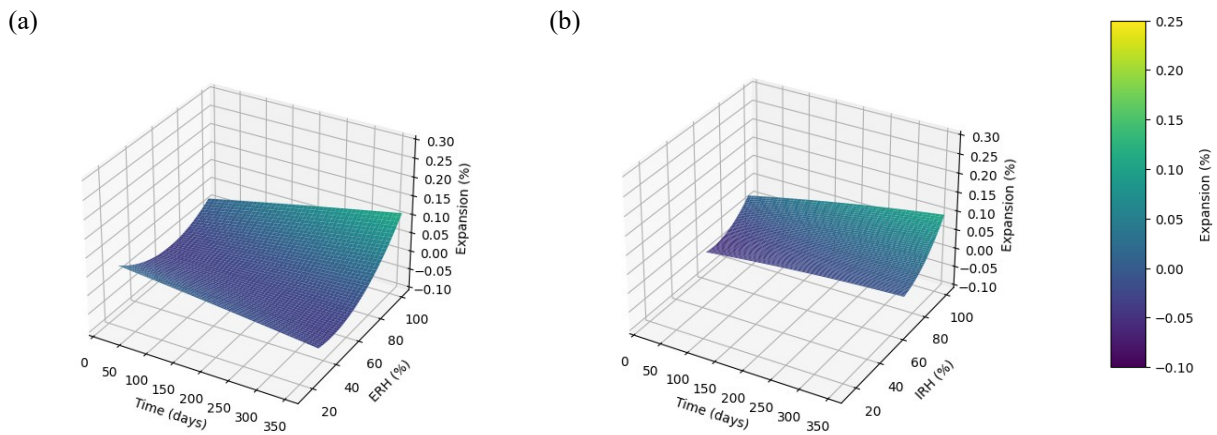


Figure S6.1: Surface plot - 21°C: (a) 3D response surface plot of interaction between time and ERH (b) 3D response surface plot of interaction between time and IRH

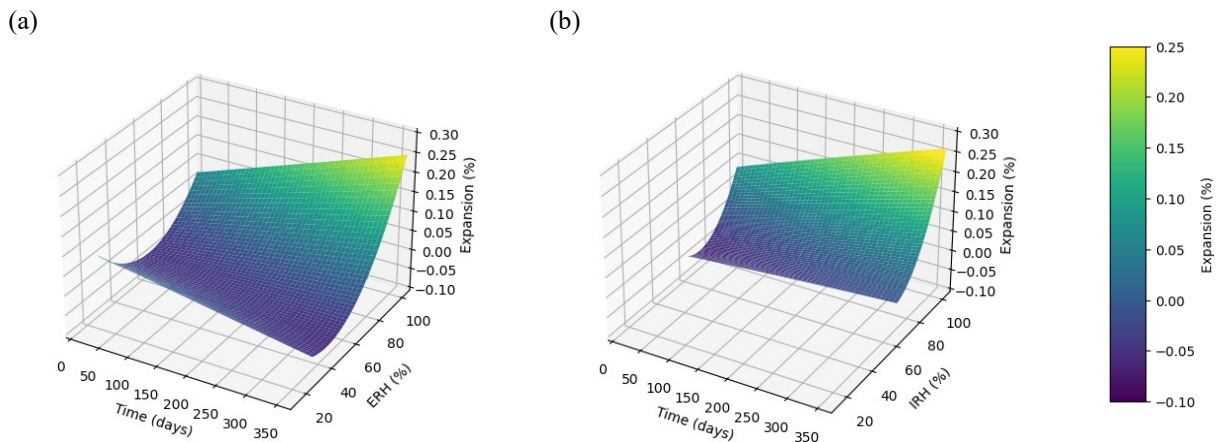


Figure S6.2: Surface plot - 38°C: (a) 3D response surface plot of interaction between time and ERH (b) 3D response surface plot of interaction between time and IRH

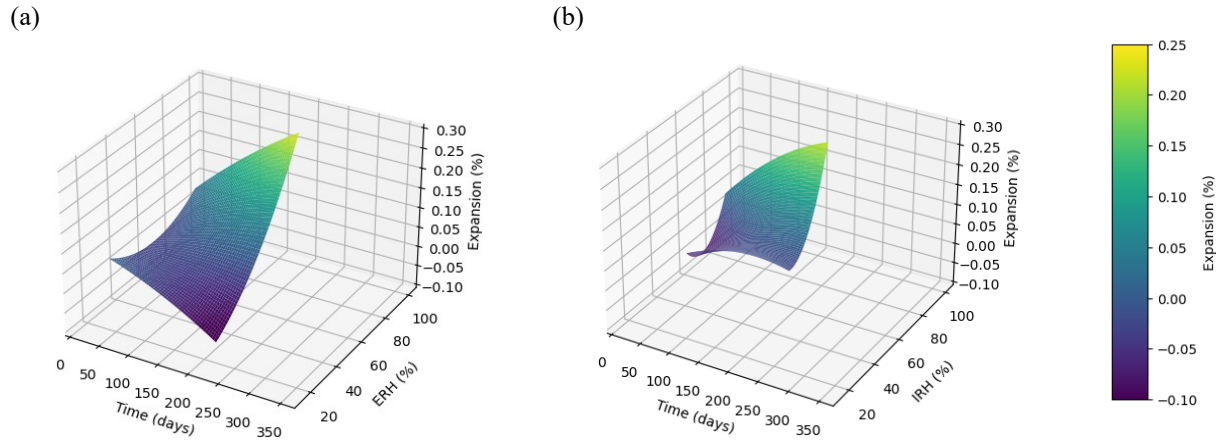


Figure S6.3: Surface plot - 60°C: (a) 3D response surface plot of interaction between time and ERH (b) 3D response surface plot of interaction between time and IRH

Overview of chapter six

Chapter six discusses the interplay between moisture in concrete and external moisture at numerous temperatures and how it evolves. The influence of such interplay on ASR development was evaluated, and such dynamics were confirmed to influence ASR kinetics. Results from this chapter motivate the assessment of the impact of moisture at different temperatures on the mechanical properties of ASR-affected concrete.

CHAPTER SEVEN: EVALUATION OF THE INDUCED MECHANICAL DETERIORATION OF ASR-AFFECTED CONCRETE UNDER VARIED MOISTURE AND TEMPERATURE CONDITIONS

O.D. Olajide^{*(a)}, M.R. Nokken^(b), L.F.M. Sanchez^(c)

(a) Concordia University, Montreal/University of Ottawa, Ottawa, Canada, olusola.olajide@concordia.ca

(b) Concordia University, Montreal, Canada, m.nokken@concordia.ca

(c) University of Ottawa, Ottawa, Canada, leandro.sanchez@uottawa.ca

Published in the Journal of Cement and Concrete Composites (CCC)

Abstract

Moisture and temperature are critical for developing alkali-silica reaction (ASR) in concrete. However, the influence of these exposure conditions on ASR-induced deterioration, specifically mechanical property losses, has not been well studied. To further our understanding, concrete cylinders made with Spratt reactive coarse aggregates and boosted in alkalis to $5.25\text{kg/m}^3 \text{Na}_2\text{O}_{eq}$ were manufactured and stored at three different temperatures (i.e., 21°C, 38°C, and 60°C) under numerous relative humidities (i.e., 100%, 90%, 82%, 75%, and 62%). The reduction in mechanical properties was assessed using the Stiffness Damage Test (SDT), direct shear and compressive strength tests. Overall, most results for mechanical properties showed a strong linear trend with expansion, with the exception of the modulus of elasticity and shear strength. In low moisture conditions that experienced both drying shrinkage and ASR, the expansion level associated with a given mechanical property loss differs from that in high moisture conditions due to early age cracks that developed in the cement paste. In most published research, expansion is the primary criteria used in assessing role of exposure conditions. However, it was found that expansion levels alone are not reliable indicators of induced deterioration due to the coupled mechanism. Furthermore, the impact of this phenomenon varies with the different mechanical properties assessed.

Additionally, the moisture threshold required for the reaction was evaluated by considering the impact on mechanical properties.

Keywords: Alkali silica reaction (ASR), Relative humidity (RH), Temperature, Mechanical properties, RH threshold

7.1 Introduction

Alkali-silica reaction (ASR) is a leading cause of aggregate-based concrete degradation. This phenomenon often leads to a loss in the mechanical properties of the affected concrete [191–193] and the initiation of other durability issues, ultimately resulting in the inevitable loss of serviceability of the affected structure [20,161]. Our comprehension of the underlying mechanisms and mitigation strategies has notably advanced after several decades of research. While a complete halt to the reaction within affected structures remains elusive [194], reducing moisture has been generally accepted as a preventive/mitigative approach [195]. Consequently, a relative humidity threshold (RH) of 80% has frequently been proposed for managing ASR-induced deterioration [196].

Several tools have been employed to appraise damage in concrete affected by ASR. Promising tools such as the Stiffness Damage Test (SDT) are of significant importance and have proven reliable in assessing the condition (i.e., the extent of deterioration) of ASR-affected concrete. Notably, the combination of outcomes from the test, such as modulus of elasticity (ME), Stiffness Damage Index (SDI), and Plastic Deformation Index (PDI), alongside the non-linearity index (NLI), have contributed to the extensive assessment of damage. Other tools like the direct shear strength [17], tensile strength [18] and compressive strength [19] have successfully been used to evaluate induced deterioration in specimens undergoing ASR in high moisture environments at standardized temperatures (i.e., particularly in laboratory settings at $\geq 95\%$ RH and $38^{\circ}\text{C}/60^{\circ}\text{C}$) [138,197,198]. While numerous studies have explored the interaction and influence of

other exposure conditions on the kinetics of ASR [8,80], there is a notable lack of data on the impact of lower moisture levels (i.e., which are crucial in mitigating ASR) on the mechanical properties deterioration caused by ASR at varying temperatures. Therefore, this study aims to appraise the influence of numerous exposure conditions on the induced mechanical deterioration associated with ASR through numerous mechanical test protocols. It is anticipated that a better understanding of how different moisture and temperature conditions affect ASR development and the subsequent mechanical property degradation will be gathered at the end of this work.

7.2 Background

7.2.1 Overview of ASR

Alkali-silica reaction (ASR) is a complex physicochemical process that significantly influences concrete infrastructure's long-term serviceability and durability worldwide. This reaction is triggered when poorly crystallized siliceous phases in aggregates are exposed to the alkalis in concrete from the pore solution [19,55,199]. A reaction product (i.e., ASR gel) is produced in the presence of sufficient moisture, which often induces expansion and cracking [10,200]. ASR is typically initiated within the aggregate particles (i.e., fine or coarse), as proven by the descriptive model by Sanchez et al. [6]; sharp and onion skin cracks represented by A and B, respectively, in Fig. 7.1, are generated in the aggregates at low expansion levels (i.e., 0.05%). The existing cracks increase in length and width as expansion increases, and some of these cracks can propagate into the cement paste at moderate expansion levels (i.e., ~0.12%). At high expansion levels (i.e., $\geq 0.20\%$), most of the cracks originating in the aggregates propagate to the cement paste, and some network of cracks in the cement paste can be observed. At very high expansion levels (i.e., $\geq 0.30\%$), the cement paste cracks are quite dense, with cracks originating from distinct aggregate particles connecting to one another [6,7]. The reaction described can subsequently reduce the

mechanical properties of the affected concrete. In most cases, the reduction in mechanical properties increases with an increase in expansion.

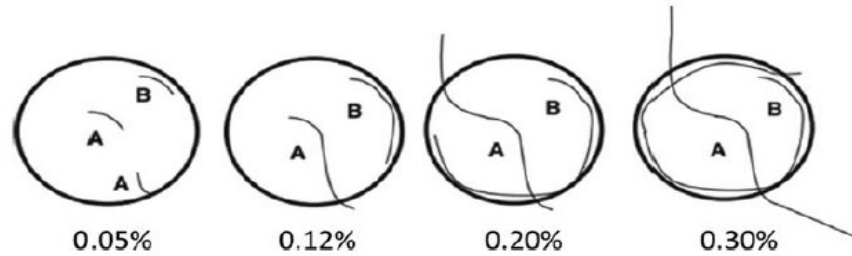


Figure 7.1: Descriptive model for crack propagation in ASR-affected concrete [6] (reproduced with permission of Elsevier)

7.2.2 ASR and mechanical properties reduction

Knowledge about the mechanical properties, such as modulus of elasticity, direct shear, tensile and compressive strength of ASR-affected concrete, has often been used as a criterion to assess the effects of the deleterious mechanism. The higher the induced expansion, the more significant the impact on the mechanical properties of the affected material. However, such a relationship does not appear linear, as displayed in Fig. 7.2. Rather, it varies depending on the mechanical property type. Typically, unlike compressive strength, ASR presents a high sensitivity to modulus of elasticity and direct shear [133,141], while the tensile strength test is found to have a high variability [64,201]. Since the modulus of elasticity (ME) of concrete is primarily influenced by the modulus of elasticity of aggregate particles, and ASR is a mechanism initiated within the aggregate particles, several studies [18,19,141,192,202–204] have reported a significant reduction in stiffness with ASR-induced expansion. The sensitivity of stiffness to ASR can already be observed even at low expansion levels [141]. Depending on the aggregate lithotype, an expansion of 0.05% can reduce stiffness by up to 40%. Likewise, around 20 – 50% loss is attainable at a moderate expansion of $\sim 0.12\%$, which can significantly lead to up to 70% loss at high and very

high expansion levels (i.e., 0.20% and >0.30%). Likewise, shear friction reduction, or “aggregate interlock” loss, which serves as a crack arrest mechanism in concrete, has been reported to be effectively measured using the direct shear setup [17,148,205]. In plain concrete, ASR-induced cracks within the aggregate particles can significantly diminish shear friction, especially during the initial reaction stages at low and moderate expansion levels. Studies [17,206] have reported reductions in shear strength ranging from 6% - 15% at low expansion levels (i.e., 0.05%), 12% - 30% at moderate expansion levels (i.e., 0.12%), and up to 18% - 33% at very high expansion levels (i.e., >0.30%) as illustrated in Fig. 7.2c. Thus, since ASR-induced cracks are initiated within the aggregate particles and only extend to the cement paste at later ages, ASR causes a progressive shear friction loss in affected concrete.

Conversely, contradictory compressive strength reductions have been reported in the literature as a function of ASR development. Some studies have found that compressive strength decreases as ASR-induced expansion increases [18,207,208], while others have found no significant relationship, and some even reported increased compressive strength with expansion [36,43,44]. Yet, it has been prominently verified that compressive strength is notably affected at high expansion levels [133,137]. The low sensitivity of the compressive strength to ASR-induced development at low expansion levels could be partially related to the strength gain due to the ongoing hydration superseding ASR deterioration. The reaction, as earlier mentioned, involves an aggregate-based mechanism. Microcracks resulting from the expansive properties of the gel do not propagate into the cement paste until a later stage of the reaction (i.e., moderate to high expansion), as illustrated in Fig. 7.1. Since the compressive strength of concrete is primarily governed by the cement paste, the compressive strength loss associated to ASR might not be noticeable at low expansion levels.

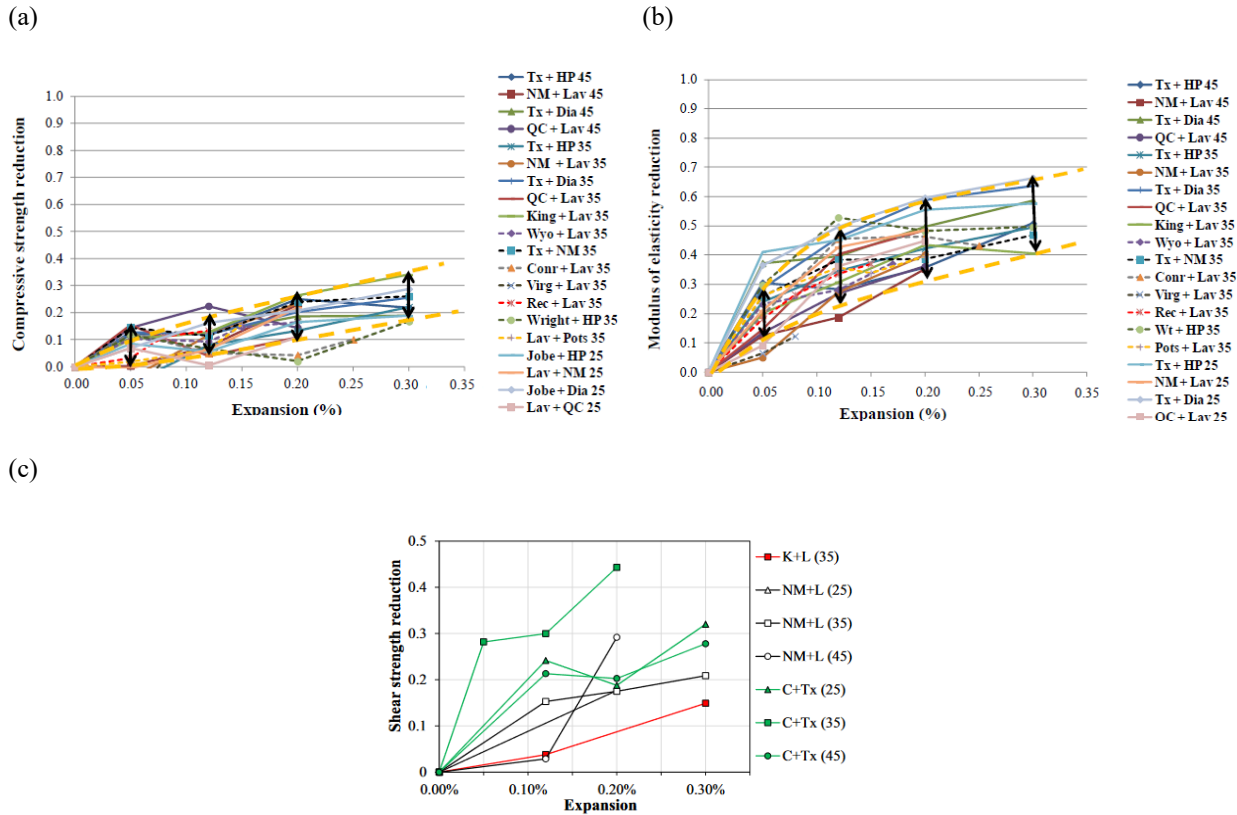


Figure 7.2: Reduction in mechanical properties involving aggregates of varying levels of reactivity, aggregate type, and concrete strength: (a) Compressive strength (b) modulus of elasticity (c) direct shear [17,141] (used with permission from Elsevier)

7.2.3 Influence of temperature and RH on ASR-induced development

Moisture and temperature play a critical role in the development of the reaction [8–16]. Moisture serves as a transportation medium for the alkali ions involved in the reaction and for the formation of ASR gel [10]. A humid environment, therefore, leads to significant ASR-induced expansion [16]. On the other hand, while temperature is not typically considered one of the primary factors (i.e., alkalis, silica, moisture) necessary to trigger ASR, its influence can affect the availability of these factors [101–103], the structure of the gel [58], rate, and ultimate expansion [209]. It has been found that ASR expansion can increase by 1.8 times when temperature is increased from 38°C to 50°C [15].

While the impact of moisture and temperature on ASR-induced expansion is more established, little is known about how these factors affect induced damage. Most existing studies on ASR-induced deterioration were conducted on specimens stored in a humid environment (RH >95%) and stored at standard conditioning temperatures (i.e., 38°C-CPT and 60°C-ACPT) [19–21]. Thus, limited studies have been performed to understand the influence of other exposure conditions. For instance, concrete specimens stored under low moisture conditions are susceptible to shrinkage [10,13]. Shrinkage-induced cracks or inner flaws could be expected to exacerbate overall damage. For context, shrinkage-induced cracks in the cement paste are known to increase the loss of compressive strength [210,211]. Moreover, since ASR-induced cracks are initiated in the aggregate particles at low expansion levels and propagate into the cement paste at higher expansion [7], a pre-existing network of shrinkage cracks could facilitate the interconnection/densification of ASR-related cracks when they propagate into the cement paste, increasing the overall damage. Still, the extent of this is mostly unknown.

7.2.4 Mechanical property protocols to appraise ASR-induced deterioration

7.2.4.1 Stiffness Damage Test (SDT)

The Stiffness Damage Test (SDT) has been confirmed to be a reliable tool for evaluating ASR-induced deterioration in concrete [132,133]. The test is a non-destructive method used to assess the response of concrete to cycles of uniaxial loading/unloading. Walsh originally conceptualized the test [134], based on a correlation between crack density and the loading and unloading cycles in rock specimens. The test was later adapted for concrete specimens by Crouch [135] in 1987. Building upon those developments, in 1993, the test was adapted explicitly by Chrisp [136] to evaluate concrete affected by ASR using a fixed stress of 5.5 MPa at a loading rate of 0.10 MPa/s. The authors proposed parameters like the average secant modulus (using the last four cycles) and

the hysteresis area over the five cycles, which reflect energy loss in the system. The Nonlinearity Index (NLI) was also introduced to illuminate the damage pattern based on the slope of the stress-strain curve. Smaoui et al. [137] later proposed a fixed load of 10 MPa to improve the diagnostic nature of the test and they found a correlation between expansion and plastic deformation from the five loading/unloading cycles.

Sanchez et al. [138] further refined the test through a comprehensive experimental campaign, evaluating numerous concrete mixtures presenting distinct compressive strength and reactive aggregate size (i.e., fine versus coarse) on the use of SDT for appraising concrete affected by ASR and other internal swelling reactions like delayed ettringite formation (DEF), and freezing and thawing (FT), single or combined. They proposed conducting the SDT at 40% of the 28-day compressive strength of the concrete at the loading rate of 0.10 MPa/s and established indices like the Stiffness Damage Index (SDI), Plastic Deformation Index (PDI), NLI, and the modulus of elasticity which can be obtained from Fig. 7.3. The SDI (Equation 7.1) and PDI (Equation 7.2) represent the ratio of dissipated energy/plastic deformation to the total energy/deformation implemented over the five loading cycles in the system, respectively. The NLI computed from the first loading cycle (obtained by taking the ratio of the secant modulus at half load to the peak load; $\sec 1/\sec 2$) is efficient in evaluating the orientation of inner cracks, and the modulus of elasticity (Equation 7.3) is computed from the average of the secant modulus of 2nd and 3rd cycles.

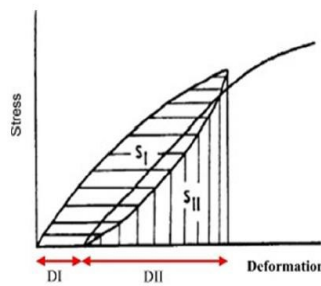


Figure 7.3: The Stiffness Damage Test [133] (reproduced with permission of Elsevier)

$$SDI = \frac{\sum_{i=1}^5 SI_i}{\sum_{i=1}^5 (SI_i + SII_i)} \dots\dots\dots(7.1)$$

$$PDI = \frac{\sum_{i=1}^5 DI_i}{\sum_{i=1}^5 (DI_i + DII_i)} \dots\dots\dots(7.2)$$

$$MOE = \frac{\sum_{i=2}^{3^{rd}} \frac{stress_{40\%}}{strain_{40\%}}}{2} \dots\dots\dots(7.3)$$

SI = Dissipated energy over the five cycles.

SI + SII = Total energy placed in the system (i.e., the area under the entire stress/strain curve)

DI = Plastic deformation

DI + DII = Total deformation of the system

*stress*_{40%} = stress at 40% of maximum load

*strain*_{40%} = strain at 40% of maximum load

7.2.4.2 Direct shear test

Shear strength in concrete is controlled by tensile and compressive forces [146]. Concrete inherently contains some internal cracks and flaws, and it can transfer shear forces across these cracks via two primary mechanisms: a) the dowel effect through the reinforcement and b) shear friction through the characteristics of the concrete. The latter can be defined as the “frictional resistance to crack,” popularly called “aggregate interlock,” which can be affected by ASR-induced deterioration [147]. Several methods exist for assessing direct shear capacity in concrete [148,149]. The recently developed technique [17] is of significant relevance to this study due to its extensive testing on unreinforced lab-made concrete cylinders. Moreover, the tool is less variable than tensile strengths, leading to its preference in this work. Furthermore, unlike the compressive strength test, the direct shear test (derived using Equation 7.4) was more diagnostic

for low and moderate expansion levels, as shown in Fig. 7.2c [17,133,141]. Thus, the tool looks promising for evaluating ASR-induced deterioration, especially at low RH levels where low to moderate expansions are expected. The test is conducted on concrete cylinders of 100 x 200mm, as displayed in Fig. 7.4. Notches of about 20 - 25 mm have been reported to be reliable to reduce discrepancies that may arise from leaving a too-small or big area for the test [148].

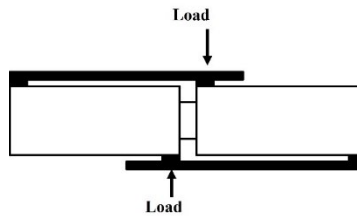


Figure 7.4: The direct shear test

$$\text{Direct shear strength} = \frac{4 * \text{load}}{\pi * (\phi_{\text{cylinder}} - 2a)^2} \dots\dots\dots(7.4)$$

ϕ_{cylinder} : cylinder diameter (mm)

a: depth of notch (mm)

7.2.4.3 Compressive strength

Studies on ASR have reported a low reliability of the compressive strength in assessing ASR-induced development. This is because the reaction is initiated in the aggregate particles and cracks only propagate into the cement paste at moderate/high expansion levels. Hence, since cracks in the cement paste largely influence compressive strength, the tool is less effective in assessing damage, especially at low to moderate expansion. Therefore, significant reductions have only been reported for high ASR-induced expansion levels; up to a 25% reduction in compressive strength is expected [141]. Nevertheless, this tool has been selected for use in this study because of its structural design

importance (i.e., ultimate capacity). Moreover, it could account for the possible occurrence of shrinkage cracks at low RH.

7.2.5 Scope of work

As already highlighted, there is a need to conduct a comprehensive assessment of the influence of numerous moisture and temperature on ASR development and associated mechanical properties losses. To achieve this objective, concrete cylinders containing a highly reactive coarse aggregate (i.e., Spratt) were manufactured in the laboratory and stored at distinct conditions; three different temperatures (i.e., 21°C, 38°C, and 60°C) and five relative humidities (i.e., 62%, 75%, 82%, 90%, and 100%) were selected as storage conditions for the specimens, which were monitored for length change as a function of time. Midway through the time-based assessment and at the end of the experiment, specimens were collected to conduct mechanical property tests (i.e., Stiffness Damage Test, shear strength and compressive strength). Finally, damage was compared at all distinct moisture and temperature setups.

7.3 Materials and Method

7.3.1 Concrete mix design and materials

Two sets of concrete cylinders were fabricated in the laboratory using a mixture design based on the concrete prism test (ASTM C1293). The first set is a reactive mix containing a highly reactive coarse aggregate (i.e., Spratt) and non-reactive fine aggregate (i.e., manufactured sand). The second set includes the same nonreactive fine aggregates but rather bears a nonreactive limestone to monitor shrinkage. The information about the aggregates is displayed in Table 7.1. A conventional GU cement (i.e., equivalent to ASTM type I) with a total alkali content of 0.86%

Na_2O_{eq} by mass of cement was used, and the alkali content of the mix was boosted to 5.25kg/m^3

Na_2O_{eq} by adding NaOH pellets to the mixing water, as presented in Table 7.2.

Table 7.1: Aggregates used in the study

Aggregates	Location	Rock type	Specific gravity (kg/m^3)	Absorption (%)	AMBT-14 Days expansion (%)
Spratt	Ottawa (Canada)	Crushed siliceous limestone	2.70	0.62	0.310
Non-reactive limestone	Ottawa (Canada)	Limestone	2.78	0.42	0.02
Sand (Nonreactive)	Ottawa (Canada)	Derived from limestone	2.76	0.65	0.04

Table 7.2: Characteristics of the two mixtures

Concrete Type	Cement (kg/m^3)	Water (kg/m^3)	Coarse aggregate (kg/m^3)			Fine Aggregate (kg/m^3)	Alkali Pellet (kg/m^3)
			4.75-9.5mm	9.5-12.5mm	12.5-19mm		
Reactive mix	420	177.4	334.12	334.12	344.24	833.46	2.12
Non-reactive mix			328.58	328.58	338.53	855.17	

7.3.2 Testing conditions

Five relative humidity conditions (i.e., 62% RH, 75% RH, 82% RH, 90% RH, and 100% RH) and three temperatures (i.e., 21°C , 38°C , and 60°C) were selected for this study. Specimens were stored and monitored over time for length change. Specimens at 21°C and 38°C were stored for twelve months based on the concrete prism test (CPT: ASTM C1293), while the specimens at 60°C were conditioned for six months following the accelerated concrete prism (ACPT: AAR-4.1) [212]. A time-based evaluation was selected; specimens were tested for mechanical property losses at 6 and 12 months (i.e., 21 and 38°C) and 3 and 6 months (i.e., 60°C).

7.3.3 Manufacturing of concrete specimens and storage

A total of 300 concrete cylinders (i.e., 180 and 120 for length change and shrinkage, respectively), each 100mm x 200mm, were fabricated in this study. After casting, the specimens were de-molded and moist-cured at room temperature for 48 hours; holes were drilled on both sides, and studs were installed using a fast-setting cement slurry during the first 24 hours. The initial length readings were conducted after 48 hours, then the specimens were ready for storage. Concrete specimens were placed in sealed buckets, each containing four concrete cylinders, and a minimum of 12 specimens were prepared for each RH/temperature combination (i.e., a minimum of three buckets per RH/temperature combination) for length change measurements. Three sets of complete RH (i.e., 62% RH, 75% RH, 82% RH, 90% RH, and 100% RH) were prepared; One set was stored at 21°C, the second at 38°C and the last set was stored at 60°C. A similar set was prepared using non-reactive coarse aggregate for shrinkage measurements, but each RH/temperature combination contains only eight specimens. The relative humidity conditions were targeted and maintained using a saturated salt solution as used by Poyet et al. [10]. Length change measurements were carried out after 14, 28, 97, 119, 182, 273, and 365 days for 21°C and 38°C. The specimens stored at 60°C were measured after 14, 28, 97, 119 and 182 days.

7.3.4 Experimental procedures

7.3.4.1 Stiffness Damage Test (SDT)

The SDT procedure was performed as per the methodology proposed by Sanchez et al. [138], which involves subjecting concrete specimens to five loading/unloading cycles at a controlled rate of 0.10 MPa/s, with a maximum load equivalent to 40% of the 28-day concrete compressive strength. Tests were conducted on specimens from each relative humidity (RH) condition after 6 and 12 months (i.e., for specimens conditioned at 21°C and 38°C) and after 3 and 6 months (i.e.,

for those stored at 60°C). It is noted that three specimens were tested for each RH level, temperature, and age combination. Before the initiation of the test, specimens from each condition were stored in a humid environment at room temperature for 48 hours as per [138], and each end of the specimens was mechanically ground to ensure a flat surface. This study reports an average of three specimens for each result (i.e., ME, SDI, and PDI).

7.3.4.2 Direct shear test

The direct shear test was performed as illustrated by De Souza et al. [17]. Similar to the SDT, specimens were collected at the predetermined testing age. The specimens were conditioned at 100% RH and room temperature 48 hours before testing as per [155]. Then, a notch of 5mm width and 20 – 22mm depth was carefully made around the cylinder's circumference using a masonry saw. The concrete cylinders were then loaded to failure at an applied loading rate of 100 N/s. It is worth noting that only two specimens were selected for each test condition.

7.3.4.3 Compressive strength test

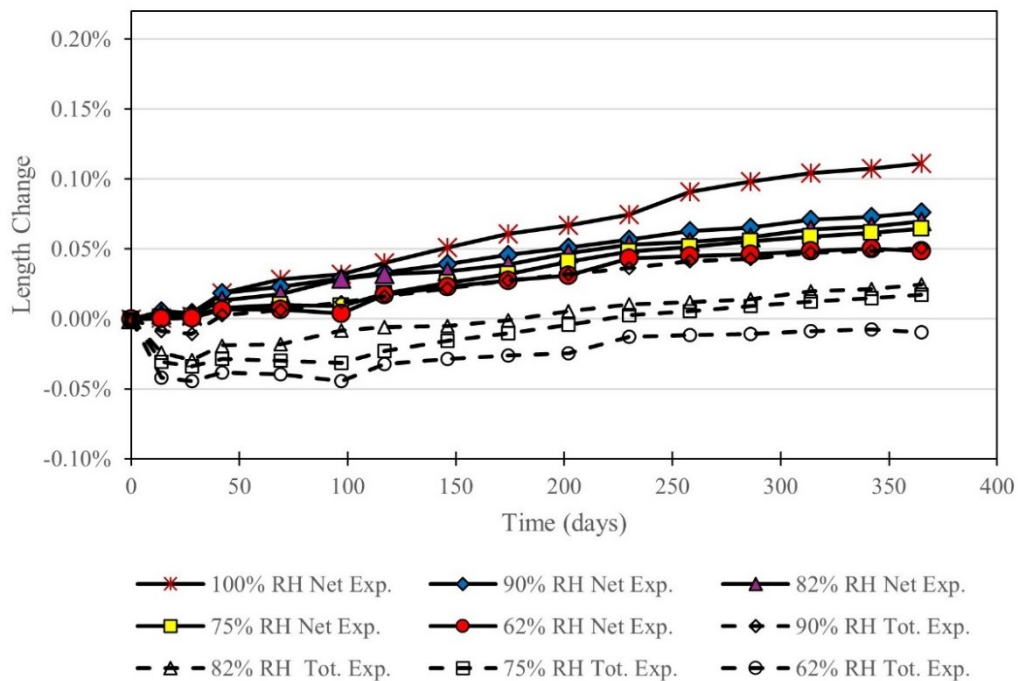
The 28-day compressive strength of the concrete mix utilized in this study was assessed by employing the maturity concept due to the reactivity potential of the aggregate, which could potentially trigger ASR at room temperature and above, thereby impacting the strength of the concrete. Six concrete specimens were enclosed in a plastic wrap and stored at 12°C for 47 days (i.e., the maturity is equivalent to 28 days at standard temperature), after which they were tested. To assess compressive strength reductions, the specimens tested for SDT underwent an additional 48-hour reconditioning at 21°C. This approach was facilitated by the non-destructive nature of the SDT, as confirmed by Sanchez et al. [138].

7.4 Results

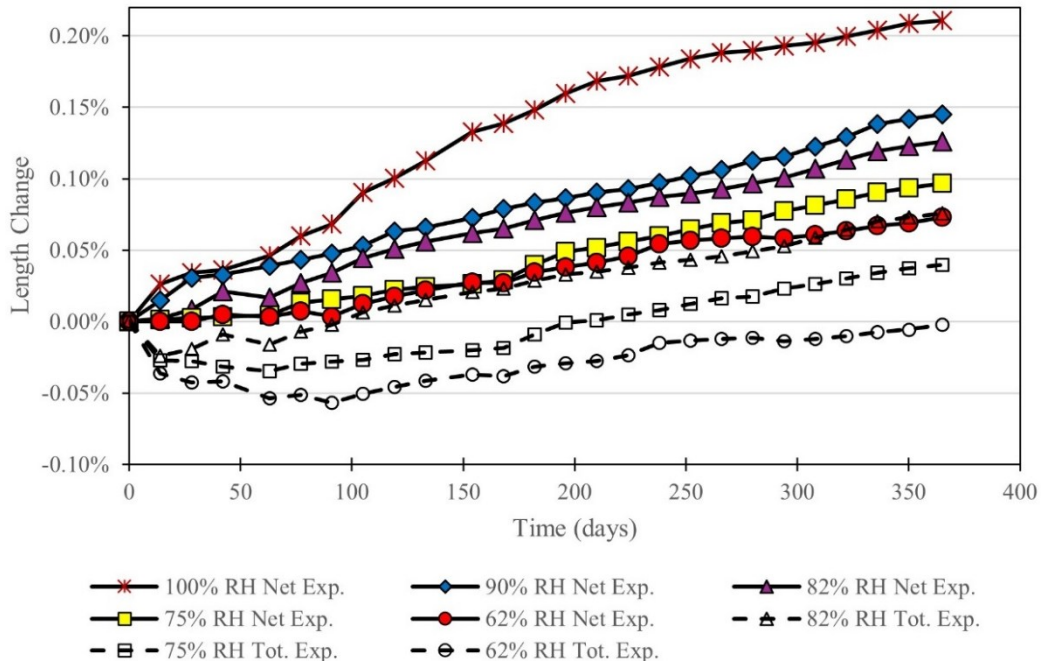
7.4.1 ASR development

The length change measurements as a function of time for concrete specimens incorporating a reactive coarse aggregate (i.e., Spratt) and nonreactive fine aggregate stored in numerous relative humidity conditions (i.e., 62% RH, 75% RH, 82% RH, 90% RH and 100% RH) and temperatures (i.e., 21°C, 38°C and 60°C) are presented in Fig. 7.5, with standard deviations ranging from 0.01% to 0.03%. Total expansion (i.e., Tot. Exp.) represents the overall length change readings from the reactive aggregate specimens, including the shrinkage effect. The net expansion (i.e., Net Exp.) represents the positive length change readings after accounting for the shrinkage measured from non-reactive aggregate specimens. It is important to highlight the overlapping of some conditions, such as 62%RH Net Exp. and 90% RH Tot. Exp. in Fig. 7.5a. This was retained to maintain clarity in the general trend presentation and comparison between the two length change types.

(a) 21°C



(b) 38°C



(c) 60°C

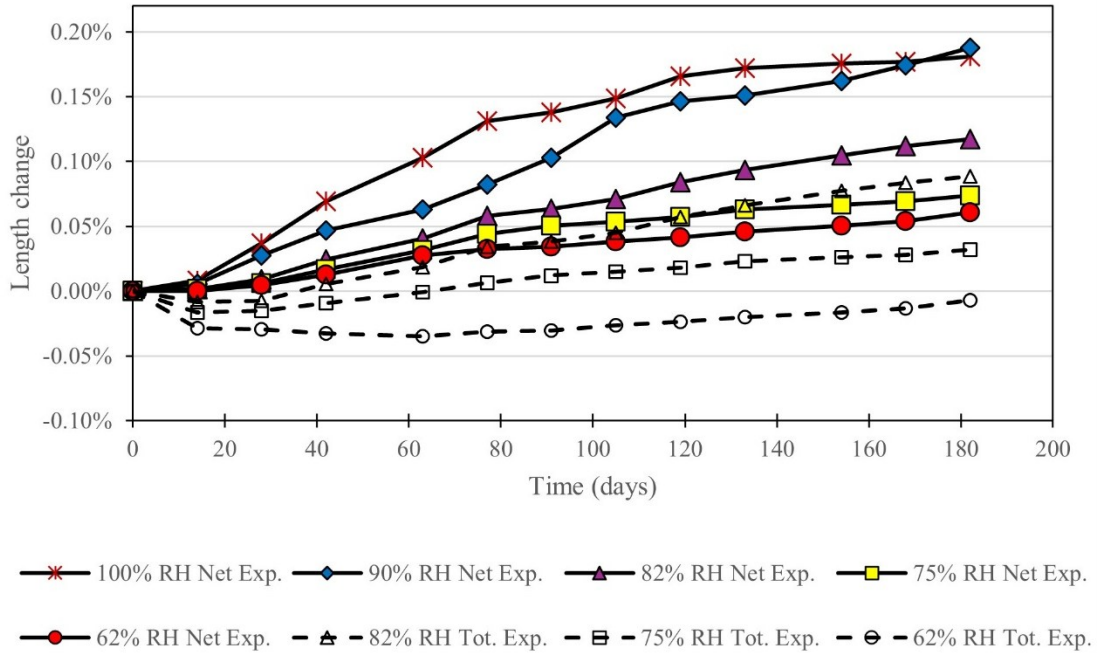


Figure 7.5: ASR kinetics at numerous relative humidities, including both decoupled expansion and non-decoupled length changes: (a) 21°C (b) 38°C (c) 60°C

As shown in Fig. 7.5, higher RH levels result in greater length change, indicating more significant ASR-induced expansion of the concrete specimens. Furthermore, length change measurements increase with age across all the distinct RH and temperature conditions, which means that ASR has been at least partially triggered in all scenarios studied. The significance of elevated temperature on ASR-induced expansion is more pronounced at 38°C and 60°C as illustrated in Fig. 6.5b and c with faster ASR kinetics. Moreover, specimens stored at high RH conditions (i.e., 100% RH and 90% RH) expanded significantly beyond those conditioned at lower RH conditions. Comparing the change in moisture from 90% RH to 100% across the three temperatures, ASR-induced expansion behaves differently upon the change in temperature from 21°C to 38°C. Despite both temperature conditions having sufficient moisture at 100% RH, there is a considerable gap in expansion between 90% RH and 100% RH at 38°C compared to 21°C. However, this behavior is not linear. There are lower differences between 90% RH and 100% RH when the temperature is increased to 60°C, which may be attributed to alkali-leaching [200,213,214] or reduced viscosity of gel [15,215].

Although changing exposure conditions (i.e., RH and temperature) often changes the kinetics of the reaction, as displayed in Fig. 7.5, specimens stored at low moisture conditions (i.e., low RHs) are susceptible to shrinkage. Hence, there is a need to decouple shrinkage from the total expansion (i.e., Tot. Exp.) to determine the net ASR-induced expansion (i.e., Net. Exp.). However, before decoupling, given that all the required factors for ASR are available, shrinkage switches to expansive behavior, leading to higher total ASR-induced expansion. For instance, at 62% RH and 21°C, the specimen initially exhibits peak shrinkage at 3 months, reaching -0.040% total expansion. However, the total expansion has increased to -0.010% by 12 months. This shift suggests that despite initial shrinkage, expansion is occurring. Similar initial shrinkage was

obtained in most conditions at 21°C but with different recovery ages and magnitudes; the higher the RH, the lower the magnitude and recovery duration. Hence, even at low RH, it is essential to highlight that the moisture required to trigger ASR was present in the mix. Comparing the shrinkage obtained across all temperatures, the recovery time from shrinkage appears shorter at higher temperatures, even in similar RH conditions. For instance, at 38°C (i.e., Fig. 7.5b), specimens stored at 82% RH and 75% RH experienced a negative length change over the first 98 days and 182 days, respectively, and a positive length change was obtained afterward, quicker than at 21°C and even more rapid at 60°C as displayed in Fig. 7.5c.

Although changing exposure conditions (i.e., RH and temperature) often changes the kinetics of the reaction, as displayed in Fig. 7.5, specimens stored at low moisture conditions (i.e., low RHs) are susceptible to shrinkage. Hence, there is a need to decouple shrinkage from the total expansion (i.e., Tot. Exp.) to determine the net ASR-induced expansion (i.e., Net. Exp.). However, before decoupling, given that all the required factors for ASR are available, shrinkage switches to expansive behavior, leading to higher total ASR-induced expansion. For instance, at 62% RH and 21°C, the specimen initially exhibits peak shrinkage at 3 months, reaching -0.040% total expansion. However, the total expansion has increased to -0.010% by 12 months. This shift suggests that despite initial shrinkage, expansion is occurring. Similar initial shrinkage was obtained in most conditions at 21°C but with different recovery ages and magnitudes; the higher the RH, the lower the magnitude and recovery duration. Hence, even at low RH, it is essential to highlight that the moisture required to trigger ASR was present in the mix. Comparing the shrinkage obtained across all temperatures, the recovery time from shrinkage appears shorter at higher temperatures, even in similar RH conditions. For instance, at 38°C (i.e., Fig. 7.5b), specimens stored at 82% RH and 75% RH experienced a negative length change over the first 98

days and 182 days, respectively, and a positive length change was obtained afterward, quicker than at 21°C and even more rapid at 60°C as displayed in Fig. 7.5c.

Comparing the three temperatures (i.e., 21°C, 38°C and 60°C) at all RH levels, it can be observed that at 21°C, the expansion is slower than at 38°C; 60°C has the highest rate of expansion. Furthermore, 21°C has the highest magnitude of early-age shrinkage, and all its RH conditions experienced some contraction at the beginning of the reaction. Specimens at 38°C and 60°C obtained net negative length change only in 82%, 75%, and 62% RH conditions with a quicker recovery time than 21°C, highlighting how temperature change can influence the initiation and progress of the reaction.

7.4.2 Mechanical Properties

The results presented in this section are those conducted on concrete specimens incorporating a reactive coarse aggregate (i.e., Spratt) and nonreactive fine aggregate at 6 and 12 months (i.e., 21°C and 38°C) and 3 and 6 months (i.e., 60°C).

7.4.2.1 Stiffness Damage Test

7.4.2.1.1 Modulus of elasticity

The modulus of elasticity reduction (MER) as a function of RH at three different temperatures is displayed in Fig. 7.6. A similar increasing trend of loss in modulus of elasticity against RH, similarly to expansion, was found for all temperatures; however, the specimens conditioned to 21°C present slightly lower losses than at 38°C and 60°C, as expected due to lower ASR-induced expansion. Generally, as shown in Fig. 7.6a for 21°C, a low to moderate ME loss (i.e., from 7% – 21% at six months to 16% – 33% at 12 months) was obtained. For higher temperatures at 38°C, the modulus of elasticity losses ranged from 12% – 38% at six months to 23% – 42% at 12 months. A similar trend is observed at 60°C (Fig. 7.6c), with ME losses of 12 – 37% at three months,

increasing to 20 – 40% at six months. Even though the modulus of elasticity losses varied with temperature, similar reduction trends were generally observed as a function of the relative humidity and expansion.

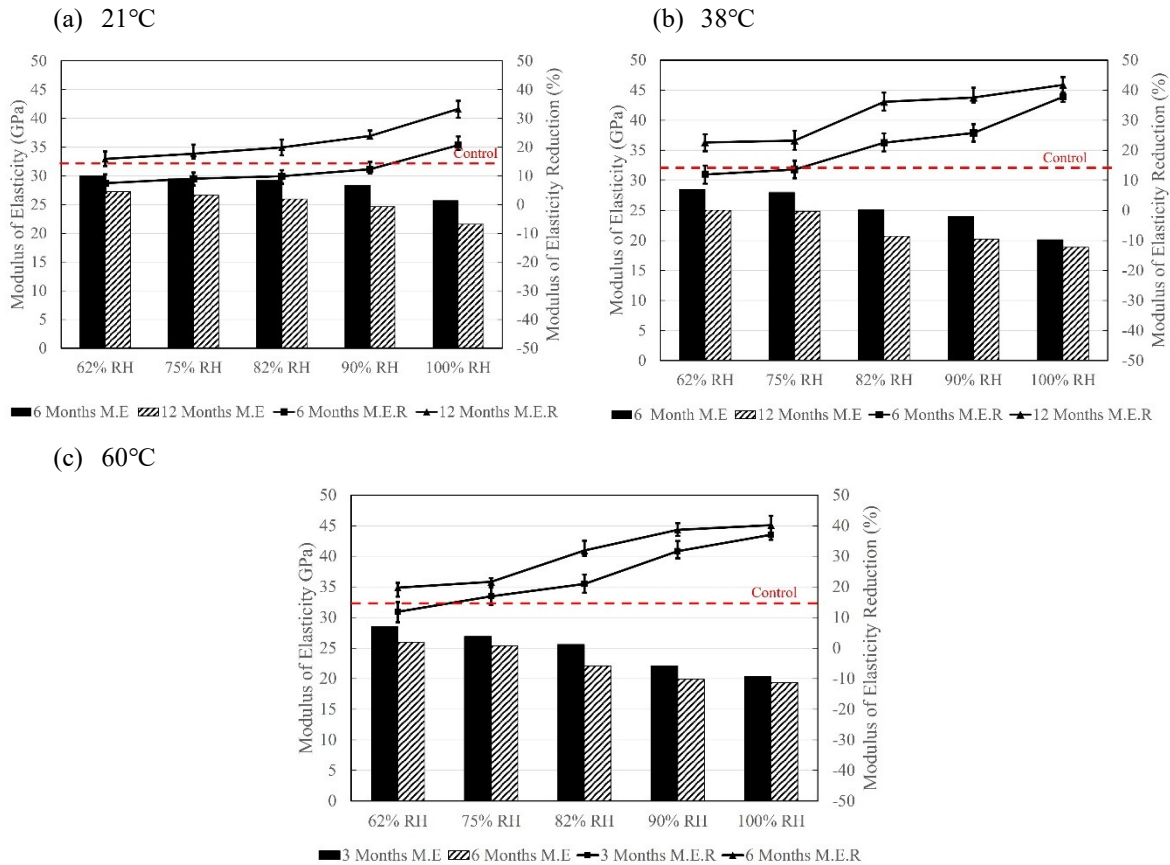


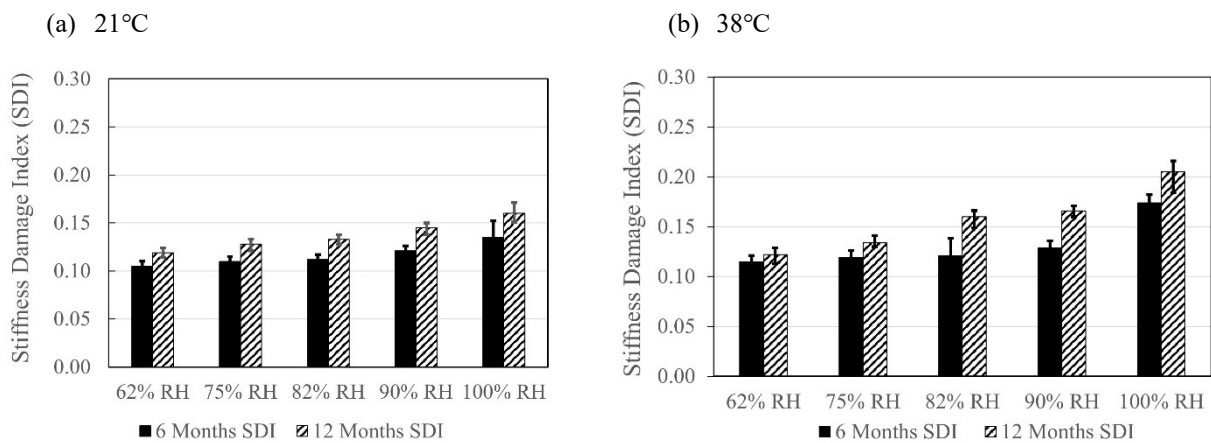
Figure 7.6: Modulus of Elasticity reduction versus relative humidity: (a) at 21°C (b) at 38°C (c) at 60°C

7.2.4.1.2 Stiffness Damage Test – Indices

Fig. 7.7 and 7.8 illustrate the SDI and PDI values over time for concrete specimens undergoing ASR-induced expansion under numerous RH and temperature conditions. SDI and PDI values of 0.093 and 0.087 were observed for the control samples (i.e., average of three samples). Generally, the SDI and PDI values increased towards the ultimate ASR expansion at each temperature; moreover, the higher the relative humidity and temperature, the higher the SDI and PDI. Evaluating the SDI data across all temperatures (i.e., Fig. 7.7), one observes that the SDI increases with age,

coinciding with the development of ASR. At 21°C, the SDI range increases from 0.105 – 0.135 at six months to 0.119 – 0.160 at 12 months. Likewise, a similar trend was observed at 38°C and 60°C. It is worth noting that the initial SDI values obtained (i.e., at 6 and 3 months for 21°C/38°C and 60°C respectively) at lower RHs (i.e., 62%, 75%, and 82% RH) are quite similar at high RHs (i.e., 90% and 100% RH).

Fig. 7.7 and 7.8 illustrate the SDI and PDI values over time for concrete specimens undergoing ASR-induced expansion under numerous RH and temperature conditions. SDI and PDI values of 0.093 and 0.087 were observed for the control samples (i.e., average of three samples). Generally, the SDI and PDI values increased towards the ultimate ASR expansion at each temperature; moreover, the higher the relative humidity and temperature, the higher the SDI and PDI. Evaluating the SDI data across all temperatures (i.e., Fig. 7.7), one observes that the SDI increases with age, coinciding with the development of ASR. At 21°C, the SDI range increases from 0.105 – 0.135 at six months to 0.119 – 0.160 at 12 months. Likewise, a similar trend was observed at 38°C and 60°C. It is worth noting that the initial SDI values obtained (i.e., at 6 and 3 months for 21°C/38°C and 60°C respectively) at lower RHs (i.e., 62%, 75%, and 82% RH) are quite similar at high RHs (i.e., 90% and 100% RH).



(c) 60°C

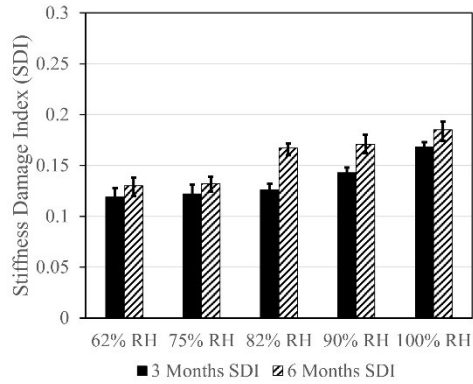
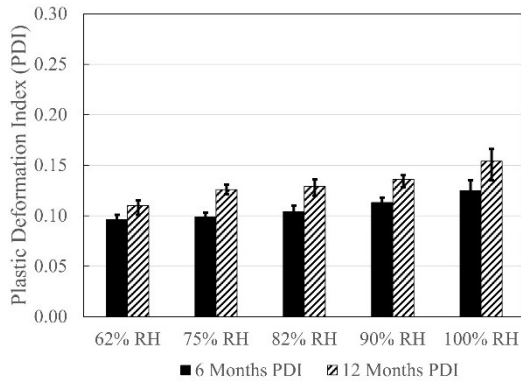


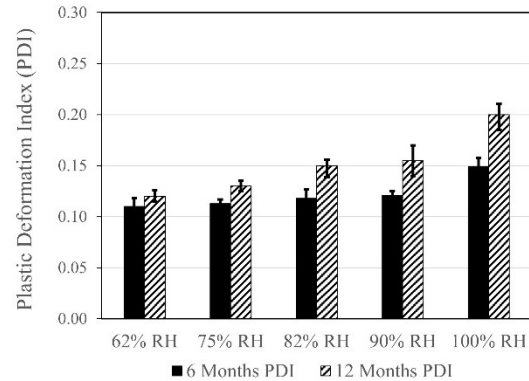
Figure 7.7: Stiffness Damage Index versus relative humidity: (a) at 21°C (b) at 38°C (c) at 60°C

Fig. 7.8 displays the PDI values obtained for all temperatures at distinct relative humidity conditions. At 21°C, the PDI range increased from 0.096 – 0.125 at six months to 0.110 – 0.154 after 12 months of exposure. The ASR-induced expansion was higher at 38°C, leading to higher PDI values of 0.110 – 0.149 and 0.119 – 0.201 after 6 and 12 months, respectively. Similarly, the PDI values at 60°C range from 0.110 – 0.157 at three months to 0.120 – 0.171 at six months.

(a) 21°C



(b) 38°C



(c) 60°C

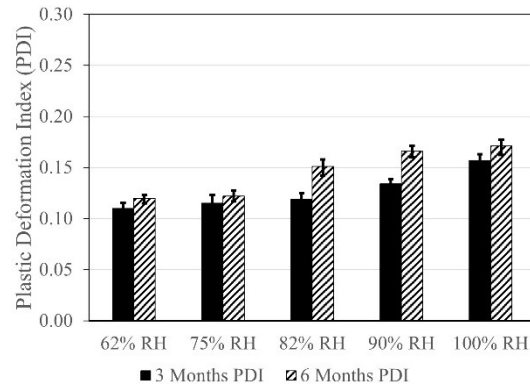


Figure 7.8: Plastic Deformation Index versus relative humidity: (a) at 21°C (b) at 38°C (c) at 60°C

7.4.2.2 Direct Shear

The direct shear strength reduction (DSR) results of specimens stored in numerous RH are illustrated in Fig. 7.9a (i.e., 21°C), Fig. 7.9b (i.e., 38°C), and Fig. 7.9c (i.e., 60°C). The overall behavior of the concrete specimens is quite similar across the three temperature conditions. The results present a shear strength decrease as a function of RH, as expected, due to an increase in ASR-induced expansion as RH increases. As shown in Fig. 7.9a, after six months of exposure at 21°C, a reduction in the range of 4% – 16% was obtained, which increased to 13% – 21% after 12 months, highlighting the progress of the reaction. Notably, specimens stored in 62% RH, 75% RH, and 82% RH showed similar reductions at six months compared to 90% RH and 100% RH. Higher reductions were obtained at 38°C and 60°C, as shown in Fig. 7.9b and c, respectively. Evaluating both plots, direct shear strength loss at 38°C ranged from 11% – 25% at six months to 17% – 34% after 12 months of exposure. Similarly, at 60°C, the reductions increased from 6% – 24% to 15% – 30% after 3 and 6 months. As displayed in Fig. 7.9c, it is interesting to note that 100% RH exhibited a higher reduction than 90% RH at three months. However, 90% RH obtained a higher reduction after six months of exposure, matching the expansion results reported in Fig. 7.5c.

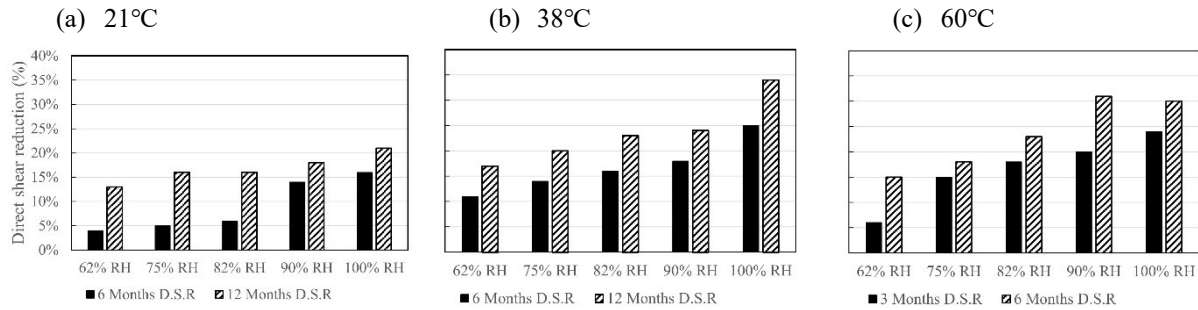


Figure 7.9: Direct shear reduction versus relative humidity: (a) at 21°C (b) at 38°C (c) at 60°C

7.4.2.3 Compressive strength

The compressive strength (CS) results as a function of numerous relative humidities (i.e., 62%, 75%, 82%, 90%, and 100%) at 21°C, 38°C, and 60°C are illustrated in Fig. 7.10. The equivalent 28-day compressive strength obtained in the control sample was 45.2 MPa (i.e., an average of 6 samples stored at 12°C for 47 days). After 6 and 12 months of exposure, the compressive strength results correspond to the average of at least three concrete specimens. As Fig. 7.10a displays, after six months of exposure at 21°C to different relative humidity conditions, the compressive strength reduced to 44.1 – 40.2 MPa (i.e., from low RH to high RH), representing a 2.4% – 11.1% reduction in compressive strength, respectively. The compressive strength reduction (CSR) increases with age, with 4.8% – 16.4% (i.e., from low to high RH) obtained after 12 months of exposure. Ultimately, the specimens exposed to the highest RH (i.e., 100% RH) with a final expansion of 0.111% were subjected to a 16.4% reduction in compressive strength. Furthermore, higher temperatures lead to enhanced expansion, which causes an increase in the compressive strength reduction. As shown in Fig. 7.10b, the reduction in compressive strength at 38°C is in the range of 3.3% – 20.5% at six months and increases to 8.3% – 25.9% after 12 months of exposure. Similarly, at 60°C, as presented in Fig. 7.10c, compressive strength reduction increases from 3.1% – 19.0% at three months to 6.6% – 24.5% after six months. The range in this section and subsequent sections

highlights values from low to high RH levels (i.e., corresponding to low to high ASR-induced expansion).

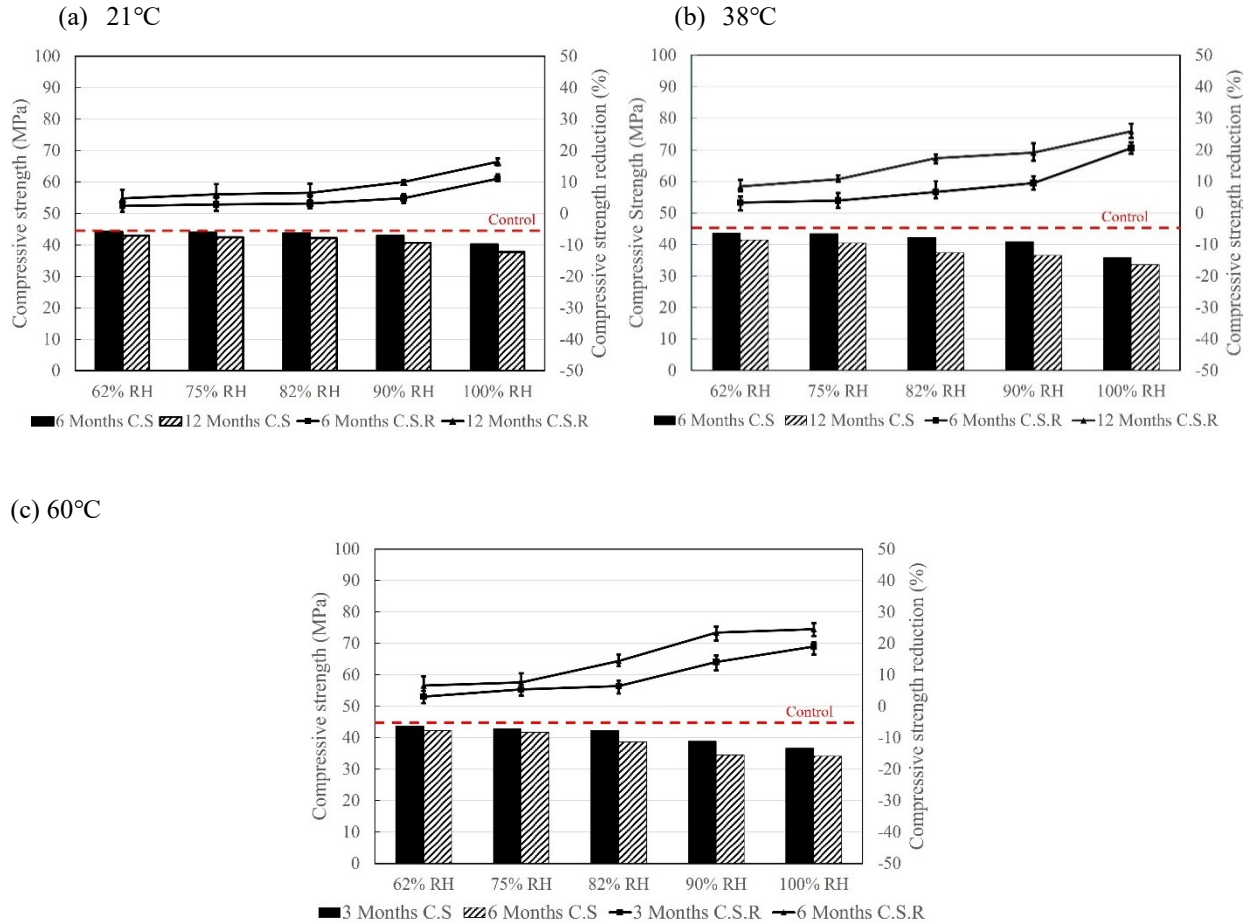


Figure 7.10: Compressive strength results: (a) at 21°C (b) at 38°C (c) at 60°C

7.5 Discussion

Exposure conditions such as relative humidity and temperature have been proven to be crucial to ASR [10,12,209]. Findings from this study agree with this fact. ASR kinetics is significantly reduced at low RHs and temperature and these conditions are of specific interest in this study. Specimens stored at low RH conditions experienced a delayed or slow initiation of ASR with an occurrence of shrinkage in their early ages. The switch from shrinkage to expansion means enough moisture to initiate the reaction is undoubtedly present in the mix, given the low RH environment

they are exposed to. Hence, it is safe to assume that ASR gel was generated from the expansion onset even while shrinkage was still ongoing, although the initiation time of the reaction is unknown; nevertheless, the build-up of expansive pressure is expected to be lower in low RH. The shrinkage obtained in the test can be attributed to the moisture loss to the dry environment (i.e., low RH), and the continued hydration, especially for specimens in 62% - 82% RH. During this period of length reduction, one may assume that ASR gel is still generated and swells slowly, counteracting the compressive forces due to shrinkage. Yet, this counteraction is not enough to supersede shrinkage. Therefore, the switch from shrinkage to expansion can be discussed in three distinct ways. First, it can be a result of the shrinkage reaching a plateau, making the slow expansion evident over time. This could be especially true for very low exposure conditions such as 62% RH at 21°C. Secondly, as hydration progresses, the alkalinity of the pore solution has been reported to increase over time [216], leading to the initiation or even acceleration of ASR, overcoming shrinkage before its plateau. This could be the case at high temperatures, which experienced an early switch to expansion in this study, for instance, 82% RH at 60°C. The third hypothesis is a change in the solubility of silica, which is known to increase with temperature rise [103]. The second and third hypotheses are significantly influenced by temperature [14,22]. Hence, it explains why lower moisture conditions could be sufficient to initiate the reaction at higher temperatures as obtained in this study and as per [59]. The switch from shrinkage to expansion is expected to induce shrinkage-induced cracks in the cement paste, which can potentially influence ASR-induced damage development. Hence, the following sections evaluate the potential contribution of these factors to the overall damage in ASR-affected concrete.

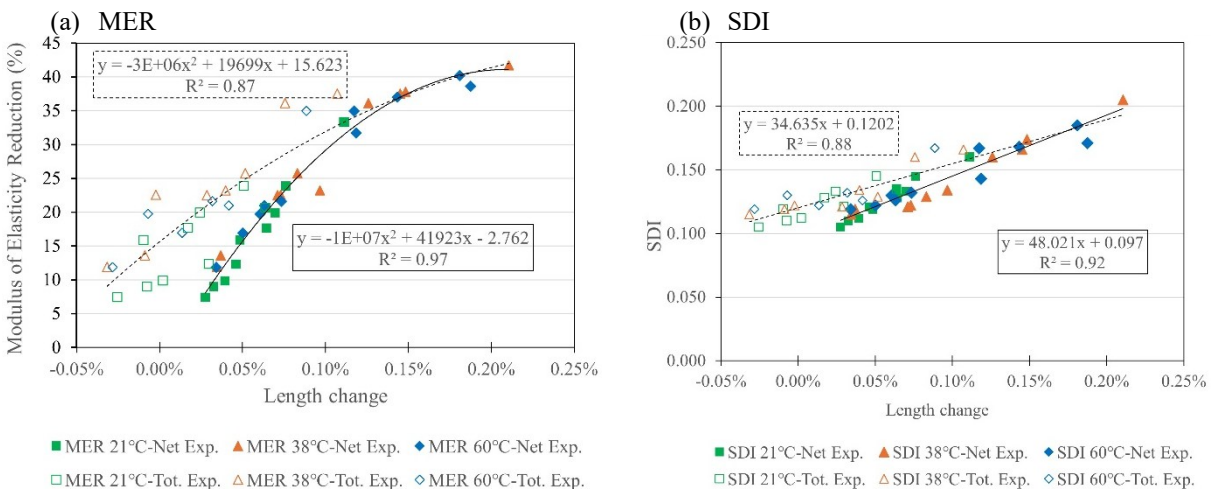
7.5.1 Mechanical properties of ASR affected concrete and influence of moisture and temperature

The evaluation of the ASR-induced distress in concrete specimens conditioned under numerous relative humidities (i.e., 100%, 90%, 82%, 75%, and 62%) and temperature conditions (i.e., 21°C, 38°C, and 60°C) through mechanical analyses provides results that align with expansion levels (i.e., total and net), as shown in Fig. 7.11. In general, the increase in expansion leads to an increase in losses of modulus of elasticity, shear and compressive strength; conversely, higher SDI and PDI values are obtained. The modulus of elasticity and direct shear reductions display a bilinear trend (i.e., reduction increases with expansion up to a certain point where it levels out – potentially indicating that the internal cracking has reached a critical point); however, SDI, PDI, and compressive strength reductions correlate linearly with expansion. The influence of ASR-induced expansion on the mechanical properties reduction has been well documented, most often in lab-made specimens conditioned at high moisture conditions [18,19]. By analyzing the mechanical properties results obtained in this study, one will notice that for all temperatures considered, concrete specimens conditioned at high RH (i.e., 100% RH and 90% RH) follow the same trend as proposed by Sanchez et al. [141]. Some of which are highlighted in Table 7.3.

Table 7.3: Classification of damage/[141] [Reproduced with permission from Elsevier]

Classification of ASR damage degree (%)	Reference expansion level (%)	Assessment of ASR			This Study				
		MER (%)	CSR (%)	SDI	Net Expansion (%)	Exposure condition	MER (%)	CSR (%)	SDI
Negligible	0.00 – 0.03	-	-	0.06-0.16					
Marginal	0.04 ± 0.01	5-37	10-15	0.11-0.25	0.08%	90% RH/21°C	23.87	10.03	0.15
Moderate	0.11 ± 0.01	20-50	0-20	0.15-0.31	0.11%	100%RH/21°C	33.29	16.44	0.16
High	0.20 ± 0.01	35-60	13-25	0.19-0.32	0.21%	100%RH/38°C	41.72	25.85	0.21
Very high	0.30 ± 0.01	40-67	20-35	0.22-0.36					

On the other hand, for low RH conditions, the early age shrinkage is anticipated to influence the losses obtained. Hence, the damage caused by low moisture is worth examining. Therefore, Fig. 7.11 displays the evolution of the mechanical properties reduction as a function of length change grouped by temperature for a comprehensive damage assessment. It is important to highlight that the grouping per temperature is intended to present the testing conditions and not a direct comparison between the testing conditions. Furthermore, the influence of total and net expansion on the mechanical properties is presented. A solid trend line represents net expansions with corresponding mechanical properties reductions, while the dashed line represents total expansion and associated reductions.



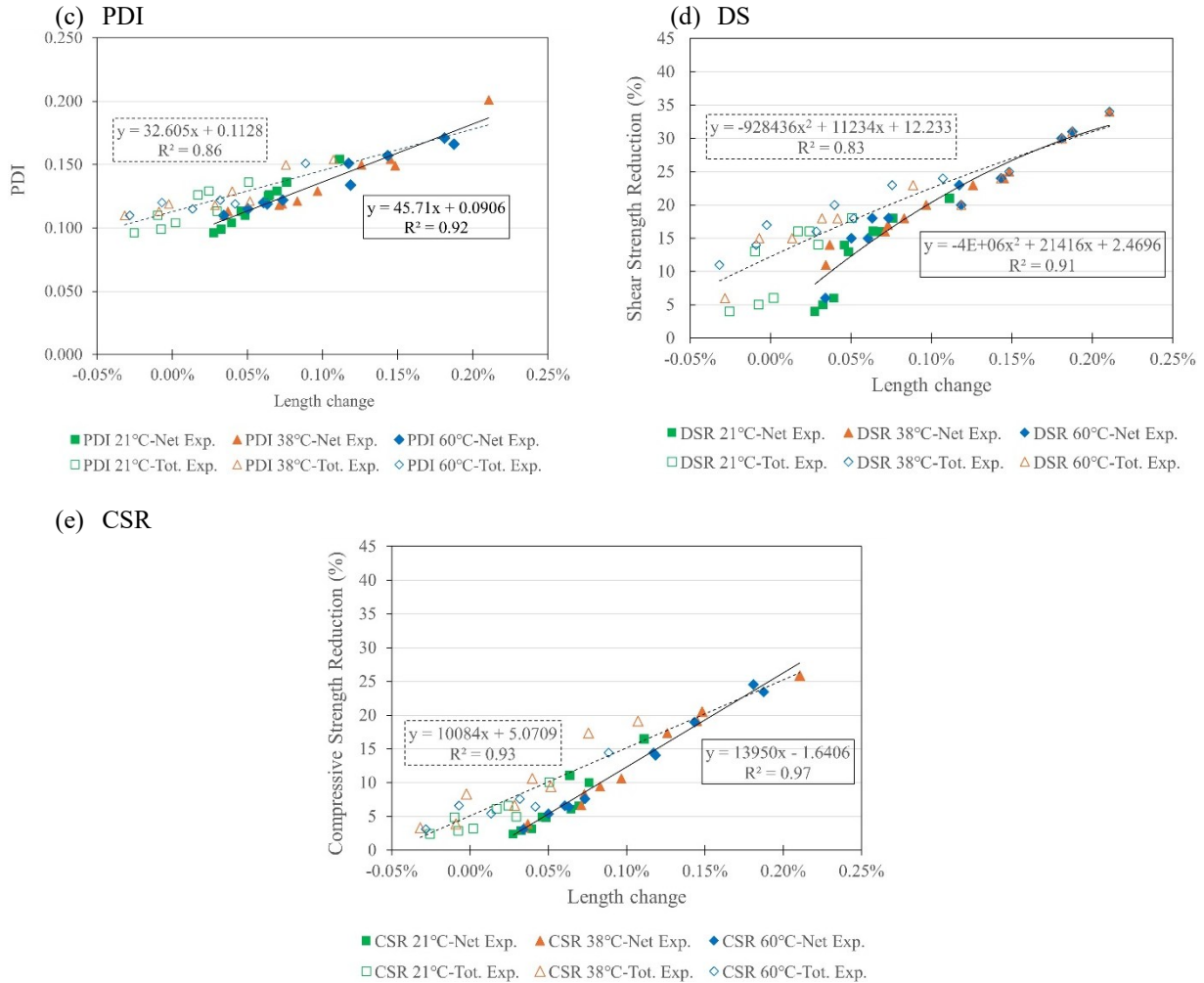


Figure 7.11: Mechanical properties reduction as a function of expansion (i.e., total and net), relative humidity (RH), and temperature (°C): (a,b) modulus of elasticity reduction (c,d) SDI (e,f) PDI (g,h) shear strength reduction (i,j) Compressive strength reduction

Pronounced shrinkage at low moisture levels, particularly 62%–82% RH, can sometimes offset the visible expansion caused by ASR. However, the induced deterioration might still be significant even if the total expansion (i.e., Tot. Exp.) is relatively low. This is the case when considering the modulus of elasticity reduction, for instance, where a total expansion of 0.01% could translate to a 15% loss in modulus. Such a phenomenon can influence the accurate evaluation of the damage extent of ASR-affected concrete. Hence, the total expansion does not give the actual state of damage. Yet, this expansion could be more representative of the real-world scenario where both ASR and shrinkage occur in concrete structures simultaneously; which makes the total expansion

a valuable metric for assessing the combined effects of environmental conditions on concrete deterioration.

By observing the difference between the total and net expansion in Fig. 7.11, the influence of shrinkage on mechanical properties outcomes appears to differ with tests. The modulus of elasticity and direct shear seem to be the most influenced by shrinkage, as expected, given their diagnostic nature at low expansions. Nevertheless, some influence is also captured in the compressive strength, which can be attributed to the pre-existing micro-cracks that weaken the cement paste properties and, thus, the concrete's response under compressive forces. Conversely, the Stiffness Damage Test indices (i.e., SDI and PDI) present a much lower difference, indicating a similar amount of inner cracks. It is worth noting that a similar amount of cracks does not attest equivalent mechanical properties' responses; the location of cracks (i.e., aggregates versus cement paste) and their features (i.e., length, width) are the major components associated with mechanical responses

Fig. 7.11 shows noticeable differences in mechanical properties reductions obtained at similar expansion levels due to shrinkage, particularly for low and moderate expansion levels (i.e., <0.15%). Total expansion, which accounts for shrinkage and ASR, presents higher losses than net expansions (i.e., ASR alone) at similar expansion levels. This effect is particularly significant in modulus of elasticity and direct shear reductions. For instance, at 0.05% expansion (i.e., x-axis), modulus loss due to net expansion is around 16%. However, the loss increases to close to 25% for total expansion. The influence of shrinkage appears to reduce as expansion increases, which coincides with higher levels of RH. Beyond 0.15% expansion, attained at RH levels of 90% and above, where minimal or no shrinkage was obtained, similar reductions were recorded in both expansion types (i.e., total and net expansion). Interestingly, while significant reduction differences exist in the modulus of elasticity and direct shear reductions, which can be related to their

effectiveness in assessing ASR-induced damage even at low expansion levels [17,141], a moderate difference is presented in the compressive strength reduction due to the inability of the test to diagnose ASR-induced damage at low expansions reliably [141]. On the other hand, the SDI and PDI show closer trends, capturing a similar number of cracks. These results show that the “amount of cracks” generated is similar in systems containing positive or negative (i.e., shrinkage) swelling. Yet, their impact on the mechanical responses of affected concrete may significantly differ. Although this might not be of concern in accelerated laboratory tests, where specimens are conditioned at high moisture, these tests will ideally be represented by the solid trend lines in Fig. 7.11. However, the dashed trendlines are more representative of field structures that could be subjected to some form of shrinkage over their life span.

Given that the management of ASR-affected concrete infrastructures has always been focused on maintaining RH below 80%, the result gathered from this study emphasizes the effectiveness of this approach. Specifically, these findings suggest that lowering RH to below 82% can effectively minimize ASR-induced damage from high to marginal damage levels with a reduction from 100% RH [141]. However, the temperature-dependent shrinkage associated with such RHs can compromise the long-term structural integrity of affected concrete through the development of microcracks that may aggravate the degradation of mechanical properties over time.

7.5.2 Statistical analysis of data

The statistical significance of the mechanical properties results (i.e., CS, ME, SDI, and PDI) obtained in this study was determined using a two-way analysis of variance (ANOVA) with a confidence level of 95%. Typically, the significance of each outcome (i.e., CS, ME, SDI, and PDI) across the numerous RH considered (i.e., 62% RH – 100% RH) over time was examined. According to the results, the test duration (i.e., time) significantly affects the response variables

(i.e., CS, ME, SDI, and PDI) as expected. Given that expansion and associated deterioration increased over time, as illustrated in Table 7.4, the influence of RH on the outcomes is statistically significant since all p-values are lower than 0.05 and F values are greater than F_{critic}. However, after a critical assessment of the average values and error bars associated with the mechanical property results presented in Fig. 7.6 – 7.10, a second statistical test was conducted to assess the significance of the RHs in pairs and to determine how each pair is statistically different from the others.

Table 7.4: ANOVA results

Temp.	RH	CS			ME			PDI			SDI		
		F	F _{crit}	P									
21°C	62%-100%	33.79	2.87	1.23E-08	33.79	2.87	1.23E-08	14.99	2.87	8.12E-06	19.46	2.87	1.14E-06
38°C	62%-100%	85.09	2.87	2.9E-12	85.09	2.87	2.9E-12	39.92	2.87	2.89E-09	41.77	2.87	1.94E-09
60°C	62%-100%	81.18	2.87	4.5E-12	81.18	2.87	4.5E-12	76.67	2.87	7.68E-12	42.87	2.87	1.54E-09

A Tukey’s honest significant difference (HSD) post hoc test was conducted for each mechanical property outcome obtained at three temperature levels over time. The RHs were paired, and their significance results are displayed in Table 7.5.

Table 7.5: Tukey post hoc test results: (a) compressive strength (b) Modulus of elasticity (c) SDI (d) PDI

(a)

Treatment	21°C		38°C		60°C	
	6M	12M	6M	12M	3M	6M
62% v 75%	x	x	x	x	x	x
62% v 82%	x	x	x	√	x	√
62% v 90%	x	x	x	√	√	√
62% v 100%	√	√	√	√	√	√
75% v 82%	x	x	x	√	x	√
75% v 90%	x	x	x	√	√	√
75% v 100%	√	√	√	√	√	√
82% v 90%	x	x	x	x	√	√
82% v 100%	√	√	√	√	√	√
90% v 100%	√	√	√	√	x	x

(b)

Treatment	21°C		38°C		60°C	
	6M	12M	6M	12M	3M	6M
62% v 75%	x	x	x	x	x	x
62% v 82%	x	x	√	√	√	√
62% v 90%	x	√	√	√	√	√
62% v 100%	√	√	√	√	√	√
75% v 82%	x	x	√	√	x	√
75% v 90%	x	x	√	√	√	√
75% v 100%	√	√	√	√	√	√
82% v 90%	x	x	x	x	√	x
82% v 100%	√	√	√	x	√	x
90% v 100%	√	√	√	x	x	x

(c)

Treatment	21°C		38°C		60°C	
	6M	12M	6M	12M	3M	6M
62% v 75%	x	x	x	x	x	x
62% v 82%	x	x	x	√	x	√
62% v 90%	x	√	x	√	√	√
62% v 100%	√	√	√	√	√	√
75% v 82%	x	x	x	x	x	√
75% v 90%	x	x	x	√	√	√
75% v 100%	√	√	√	√	√	√
82% v 90%	x	x	x	x	x	x
82% v 100%	√	√	√	√	√	x
90% v 100%	x	x	√	√	√	x

(d)

Treatment	21°C		38°C		60°C	
	6M	12M	6M	12M	3M	6M
62% v 75%	x	x	x	x	x	x
62% v 82%	x	x	x	√	x	√
62% v 90%	x	x	x	√	√	√
62% v 100%	√	√	√	√	√	√
75% v 82%	x	x	x	x	x	√
75% v 90%	x	x	x	x	x	√
75% v 100%	√	√	√	√	√	√
82% v 90%	x	x	x	x	x	x
82% v 100%	√	x	√	√	√	√
90% v 100%	x	x	√	√	√	√

√ Significant

x Insignificant

Overall, the mechanical property outcomes for all conditions and ages for 100% RH and 62% RH are statistically different as expected. Furthermore, mechanical reductions for 62% RH and 75% RH are statistically similar. This means that even though different net expansion levels were reached in both conditions, a comparable level of deterioration was attained. As discussed, 75% RH experiences more expansion than 62% RH. However, a higher shrinkage at 62% RH compensates for its lower expansion, leading to similar damage in both conditions. Considering

the ultimate mechanical property outcomes (i.e., outcomes after 12M and 6M for 21/38°C and 60°C respectively) at low moisture levels (i.e., 62% RH, 75% RH, and 82% RH), the significance of the pairs is dependent on temperature. For instance, in Table 7.5a, there is no significant difference in the CS reduction for 62% RH – 82% RH at 21°C, meaning that specimens conditioned in this environment can be said to possess similar levels of deterioration. However, this threshold is lower for 38°C and 60°C, where 62% RH – 75% RH are statistically equivalent. Table 7.5b – d shows a similar trend for other properties assessed. These findings further contribute to the existing literature on the influence of RH on ASR-induced deterioration and the existence of an RH threshold for the reaction, which could be dependent on temperature.

7.5.3 Validation of ASR distress development using microscopic assessment

To validate the mechanical deterioration observed in this study, particularly the data gathered at low RHs, microscopy evaluations using the Damage Rating Index (DRI) were performed on one specimen from each predetermined testing age from 62% to 90% at all temperatures. The Damage Rating Index (DRI) has proven reliable for its semi-quantitative role in assessing internal swelling reactions (ISR) such as ASR. It is a simple-to-use technique proposed by Grattan-Bellew [139] that can evaluate the cause(s) and the extent of damage by evaluating the number and features of cracks presented in the concrete under analysis. ASR-induced cracks are counted in 1 by 1 cm squares drawn on the surface of polished concrete sections using a stereomicroscope at 15-16X magnification, and the count for each damage feature can be multiplied by their respective weighting factor as shown in Table 7.6 to balance their relative importance towards the ASR distress mechanism, as proposed by Villeneuve & Fournier [140] to obtain a final DRI number that is normalized to 100 cm². The number has been proven to increase as ASR-induced deterioration increases [121].

Table 7.6: Damage features and corresponding weighting factors [140]

Features	Weighting factors
CCA: Cracks in aggregates	0.25
OCA: Open cracks in aggregates	2
<i>OCA_{RP}</i> : Cracks with reactive products in aggregates	2
CAD: Coarse aggregate debonded	3
DAP: Disaggregated/corroded aggregate particle	2
CCP: Cracks in cement paste	3
<i>CCP_{RP}</i> : Cracks with reaction products in cement paste	3

Each concrete specimen selected for this test was cut into half longitudinally, and one half was polished using a mechanically operated table polish with grit sizes 30, 60, 120, 240, 600, 1200, and 3000. The numbers of each crack feature – closed cracks in the aggregates (i.e., CCA), open cracks in aggregates with or without reaction product (i.e., OCA or OCA_{RP}), and cracks in the cement paste with or without reaction product (i.e., CCP or CCP_{RP}) – were counted and normalized to 100cm². Since the main goal of the microscopic analysis conducted in this project was to understand and validate the mechanical properties results obtained throughout this experimental campaign, it was decided to perform the extended version of the DRI, which involves disregarding the weighting factors proposed and focusing on quantifying the above mentioned distinct types of cracks. The results are illustrated in Fig. 7.12.

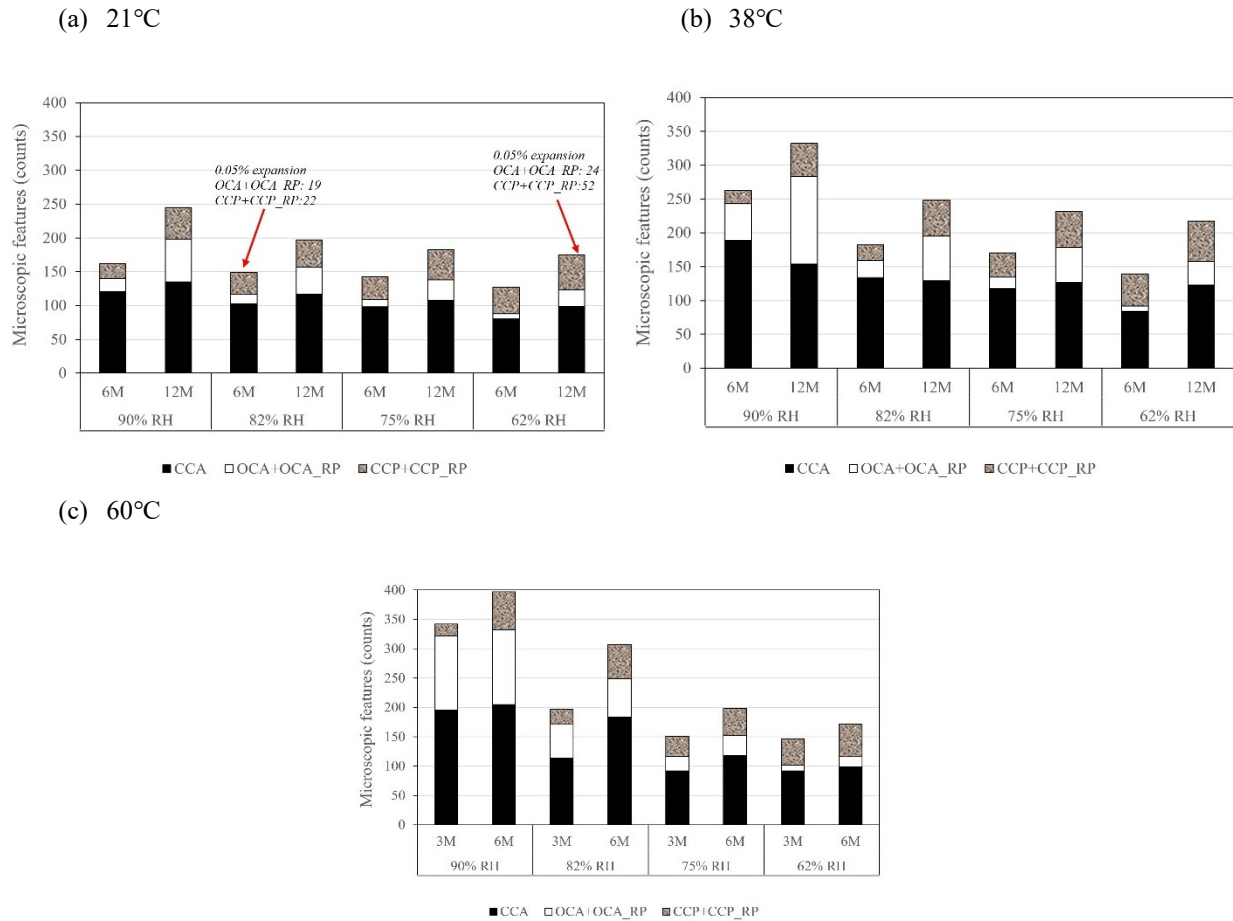


Figure 7.12: Microscopic features count at numerous RH and temperature as a function of time: (a) 21°C (b) 38°C (c) 60°C

In the case of low moisture conditions (i.e., 62% - 82% RH), a high count of cracks in the cement paste (i.e., CCP +CCP_RP) was obtained. Given that their ultimate net expansions are lower than 0.12% (i.e., expansion level above which ASR-induced cracks are expected to propagate to the cement paste), one may infer that the high counts of cracks in the cement paste are not related to ASR, validating the occurrence of early-age shrinkage obtained in this study. Moreover, exploring the DRI plots at six months (i.e., for 21°C and 38°C) and three months (i.e., for 60°C), the cracks count in the cement paste reduces with a rise in relative humidity, with 62% RH experiencing the highest count of CCP+CCP_RP. This further validates the claim of the influence of RH on the magnitude of shrinkage at early ages.

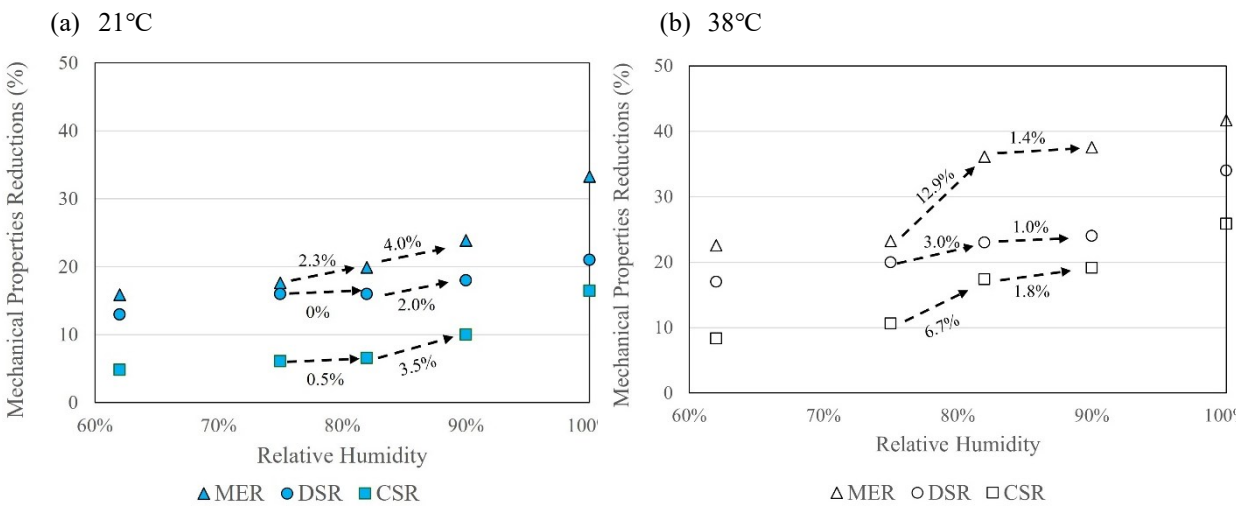
The development of the distress features in the aggregates explains the modulus of elasticity reduction obtained at low RHs despite their low total expansion (or negative net expansion). As one may notice, the plots in Fig. 7.11 show that the total expansion may underestimate the actual ASR-induced damage in systems preliminarily showing shrinkage. Yet, up to 15% reduction in modulus of elasticity are obtained at low RHs (i.e., 62% -75% RH). Considering the microscopic features count plots, some counts of cracks in the aggregates (i.e., OCA + OCA_RP) are obtained in these conditions, validating the modulus of elasticity loss. Furthermore, as mentioned earlier, similar expansions can result in different mechanical properties losses. Fig. 7.12a illustrates an instance where similar expansion leads to similar cracks count in the aggregates (i.e., OCA+OCA_RP) as expected, highlighting the damage due to ASR. However, the difference in their moisture conditions (i.e., 90% RH versus 62% RH) leads to a difference in crack count in the cement paste (i.e., CCP+CCP_RP), causing a difference in their mechanical properties.

Considering the microscopic features count obtained in this study, one realizes that at each temperature, the crack counts are similar for some RHs. For instance, at 21°C after 12 months, 62% RH – 82% RHs present similar counts within 175-197, while they undergo different levels of expansion and shrinkage, yet the damage is similar; this could explain the similarities in their mechanical properties. This similarity is limited to 62% RH and 75% RH at higher temperatures (i.e., 38°C and 60°C), which interestingly validates Tukey's post hoc test conclusions. This suggests a closer look at RH threshold for ASR-induced deterioration.

7.5.4 Assessing moisture threshold for ASR using mechanical properties reductions

As mentioned earlier, an RH level at which ASR-induced expansion is expected to be significantly impaired exists, called the RH threshold. Numerous authors [8,13,25,26] have reported different values, among which is the 80% RH that has been commonly cited. The post hoc test conducted

in Table 7.5 has highlighted the possible occurrence of a threshold in this study, which could be dependent on temperature, in agreement with the study by [10]. The available studies were limited to expansion assessments, but this study investigates the mechanical responses at different RHs to improve our understanding of such a threshold. This assessment focuses on the mechanical properties reductions around the 80% RH threshold; hence, the 75% RH, 82% RH, and 90% RH conditions were evaluated as shown in Fig. 7.13, comprising of the plot of final mechanical property reductions (i.e., MER, DSR, CSR) as a function of RH at three temperatures (i.e., 21°C, 38°C and 60°C). The difference between the 75% RH and 82% RH, as well as 82% RH and 90% RH, were calculated and highlighted in the figures to observe the trend of reductions. The RH threshold for this study is defined as an RH level where an increase in RH does not lead to a significant jump (i.e., $\leq 2\%$) in all mechanical property losses.



(c) 60°C

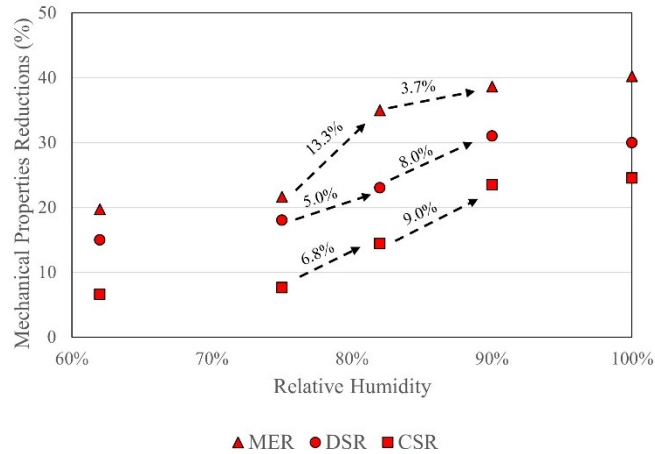


Figure 7.13: Mechanical properties reductions as a function of relative humidity: (a) 21°C (b) 38°C (c) 60°C

Overall, the reduction of mechanical properties over the studied RH levels depends on temperature; thus, the RH threshold is temperature-dependent. At 21°C, the increase in mechanical property loss from 75% RH to 82% RH was minimal; there was no change in direct shear reduction, and there was less than a 1% reduction in compressive strength reduction. Hence, the damage at these levels is similar (which has already been highlighted by the Tukey test and validated by the DRI) and falls short of the RH threshold definition. However, there is a considerable increase in losses at 90% RH. Hence, a possible threshold at 21°C could lie around 90% RH. The threshold is lower at 38°C with a sharp increase in all properties from 75% to 82% RH. For instance, the modulus of elasticity reduction has an approximately 13% increment. Hence, the threshold at 38°C could be around 82% RH. A similar threshold can also be observed at 60°C. Overall, based on the aggregate tested in this study, ASR-induced expansion is expected even at a low RH of 62%. However, an RH increase that could lead to significant damage in affected concrete is dependent on temperature. However, minimizing the RH to 75% would be effective for all temperatures.

7.6 Conclusion

This study aims to assess the influence of various exposure conditions on ASR development and the mechanical property losses in affected concrete specimens. Based on the experimental works and findings already discussed, the main conclusions are:

- Reduction of RH below 80% does not necessarily stop ASR; the inherent moisture from batching is enough to initiate the reaction. However, the kinetics can be impaired, leading to less expansion. Nevertheless, this is time-dependent; moderate to high expansion can be reached with time. It is also worth noting that specimens subjected to low moisture conditions often suffer from shrinkage, especially at early ages. ASR-induced expansion supersedes shrinkage over time depending on the available moisture and temperature.
- Overall, ASR-induced mechanical property loss changes as a function of RH and temperature. The mechanical property losses at high moisture conditions are in the range presented in the global ASR damage assessment table. Interestingly, there is no notable difference in the reduction of mechanical properties at 62% and 75% RH across all temperatures examined, indicating a consistent deleterious effect of ASR at and below these humidity levels. A similar crack count obtained in these conditions confirms this. However, at 82% RH and higher, the impact of ASR-induced deterioration is temperature-dependent, highlighting the role of temperature on the RH threshold needed for ASR.
- The reduction of relative humidity has often been used as a mitigating strategy for ASR. However, the results from this study highlight the occurrence of expansion and mechanical property losses at low RH conditions, even at a low moisture level of 62% RH. However, the reduction in this deleterious effect from 100% RH was significant.

- The crack count relatively increases as a function of RH. However, some of the damage features do not follow a linear trend. The occurrence of shrinkage induces more cracks in the cement paste at low RH, which decreases as the RH increases. On the other hand, the cracks in the aggregates increase with RH. The occurrence of a high number of cracks in the cement paste at low RH leads to up to 10% loss in compressive strength despite the low expansion in these conditions.
- Similar expansion does not necessarily lead to a similar level of ASR-induced damage. This is dependent shrinkage, which is influenced by temperature and relative humidity. The difference in the kinetics of the reaction through temperature can affect the quality of the microstructure, leading to a change in the mechanical and durability properties of the affected concrete. Furthermore, moisture could play an essential role in these properties. Nevertheless, the influence of these exposure conditions is not linear.

Overview of chapter seven

As reported in chapter six, the exposure of concrete specimens to numerous moisture conditions at different temperatures influences the kinetics of ASR. However, an intriguing observation from chapter six is the occurrence of shrinkage at low moisture levels, which was anticipated to influence the properties of affected concrete. Hence, this chapter evaluates this and reports exacerbated damage due to the coupled mechanism.

CHAPTER EIGHT: EVALUATION OF THE INFLUENCE OF MOISTURE AND TEMPERATURE ON THE MICROSTRUCTURAL PROPERTIES OF ASR

Olusola Olajide ⁽¹⁾, Michelle Nokken ⁽²⁾, Leandro Sanchez ⁽³⁾

(1) Concordia University, Montreal/University of Ottawa, Ottawa, Canada, olusoladavid2013@gmail.com

(2) Concordia University, Montreal, Canada, m.nokken@concordia.ca

(3) University of Ottawa, Ottawa, Canada, leandro.sanchez@uottawa.ca

Submitted to a scientific journal for publication

Abstract

The role of moisture and temperature in developing alkali-silica reaction (ASR) in concrete has been fairly well documented. While their influence on ASR-induced expansion is relatively well known, understanding the impact of these parameters on the microscopic damage features of ASR-affected concrete is crucial to comprehend its induced deterioration at distinct and more realistic exposure conditions. This study evaluates the influence of moisture and temperature on ASR-induced damage in concrete specimens containing a highly reactive coarse aggregate conditioned at three temperatures (i.e., 21°C, 38°C, and 60°C) and exposed to five relative humidity levels (i.e., 100%, 90%, 82%, 75%, and 62%). A time-based assessment was selected to monitor length changes, and upon reaching pre-determined ages of interest, microscopic evaluation via the Damage Rating Index (DRI) and image analysis were conducted. The findings demonstrate that temperature influences the microstructural properties (i.e., length, width, and density – of induced cracks). Moreover, moisture reduction, particularly to fairly low levels, exacerbates ASR-internal deterioration due to induced shrinkage. Furthermore, it has been found that the exposure conditions do not influence the orientation of cracks under free expansion.

Keywords: Alkali-silica reaction. Damage Rating Index (DRI), Image analysis, Relative humidity, Moisture, Temperature, crack properties

8.1 Introduction

Alkali-silica reaction (ASR) remains a crucial durability-related deterioration mechanism in concrete worldwide [217,218]. It occurs due to a chemical reaction between poorly crystallized siliceous phases within the aggregates and the alkalis present in the concrete pore solution [22,161]. ASR induces expansion that leads to crack formation [219], and diminishes the durability and serviceability of affected concrete members. Moreover, ASR can enhance other deterioration mechanisms, such as freezing and thawing, external surface attack, and corrosion. Hence, mitigating ASR is imperative for managing the integrity of affected concrete. While limiting moisture availability (i.e., moisture threshold) to less than 80% RH has been proposed as an effective maintenance strategy, temperature also plays a critical role. The dependency of the moisture threshold on temperature has been fairly well reported in the literature [10].

The significant challenges posed by ASR have necessitated assessing ASR-induced damage by conducting a multi-level assessment protocol involving evaluating the mechanical and microscopic properties of affected concrete. A standout microscopic tool from this protocol is the Damage Rating Index (DRI), a semi-quantitative method that evaluates internal damage features associated with ASR-affected concrete. If on the one hand, the influence of moisture and temperature on the dissolution of silica, release of alkalis from aggregates, mobility of ions, state of pore solution, structure of ASR gel, and the overall influence on the expansion has been well-documented [11,16,58,95,103,220–222], on the other hand, the impact of these exposure conditions on the microscopic features of affected concrete (i.e., damage generation and propagation, crack features, and pattern) is mostly unknown. For instance, the effect of rapid ASR

kinetics at elevated temperatures and the impact of induced shrinkage at low RH levels on the inner damage in ASR-affected concrete is still unknown. Therefore, this study uses the DRI and image-based analysis to evaluate the impact of varying moisture and temperature on ASR-induced damage.

8.2 Background

8.2.1 Overview of ASR

Alkali-silica reaction (ASR) remains amongst the most prominent deterioration mechanisms in concrete [102,200,223]. This reaction is initiated by the exposure of certain siliceous phases present within the aggregates used to make concrete and to the alkalis from the concrete's pore solution [100,224], which in turn generates an expansive product (i.e., ASR gel) that swells, leading to induced stresses and cracking. Different explanations exist regarding the ASR gel swelling process [59–61]. However, it is generally believed that ASR gel imbibes water and induces expansion and cracking in affected concrete. ASR-induced cracks are typically initiated within the aggregate particles (i.e., fine or coarse) and propagate into the cement paste [6]. The length and width of cracks increase with a rise in expansion, leading to a higher significance of the cracks. At very high expansion levels, cracks are largely present in the cement paste and connect to one another, significantly reducing the durability of the affected concrete.

8.2.2 Microstructure of ASR-affected concrete

Although the mechanism leading to ASR-induced expansion is still debatable, the development of cracks as a function of expansion is more understood, displaying a non-linear relationship with induced expansion. Several studies [225,226] highlighted natural openings (the so-called closed cracks) within the aggregates, which could have been generated during weathering or aggregate

processing; these cracks could act as preferential pathways, allowing alkali ions to migrate and thus generate ASR gel. Typically, two important crack types have been widely reported to be commonly observed in ASR-affected aggregates, as illustrated in Fig. 8.1: sharp and onion skin cracks, represented by A and B, respectively. The occurrence of either or both types of cracks depends on the properties (i.e., type and mineralogy of the rock) or the weathering process of the aggregates under study. Upon the initiation of ASR, cracks form within the aggregate particles, which may or may not be formed in zones previously displaying closed cracks, depending on the availability of siliceous phases in these regions. Nevertheless, the initial cracks (sharp and/or onion skin type) increase in width and length with the rise in expansion, along with new cracks being generated in the system; based on the minimum energy law, the old cracks propagate into the cement paste after a certain critical length and width are reached [7]. The evolution of these crack types provides a distinctive description of ASR development. Hence, a descriptive model that qualitatively explains the evolution of ASR-induced cracks as a function of expansion has been established [6].

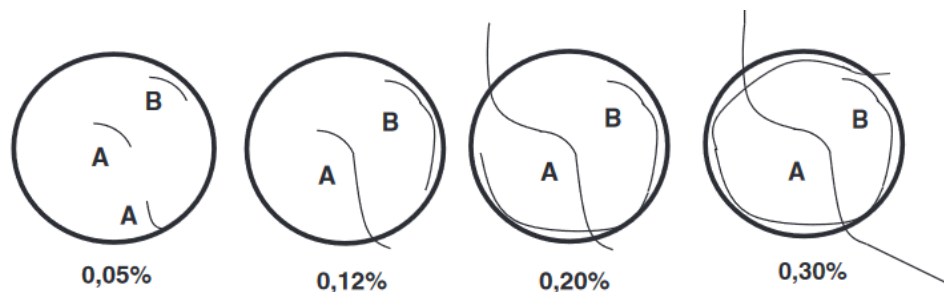


Figure 8.1: Qualitative AAR damage model vs. levels of expansion between 0.05 and 0.30% aggregates [6]
[reproduction with permission from Elsevier]

As illustrated in Fig. 8.1, sharp cracks are generally initiated within the aggregate particles at a low expansion level (i.e., 0.05%). These cracks extend towards the edge of the aggregates and slightly propagate into the cement paste, at least on one side of the aggregate particles, as the

reaction progresses to a moderate expansion level (i.e., 0.12%). At high expansion levels (i.e., 0.20%), the sharp cracks extend significantly beyond both sides of the aggregate particles, splitting it and propagating more into the cement paste. These cracks can be found linked with other existing cracks in the cement paste at very high expansion levels (i.e., 0.30%), decreasing the physical integrity of the affected material [6,141]. On the other hand, onion skin-type cracks are initiated along the aggregate's boundary, increasing in length with expansion until propagating into the cement paste. They may likely cause the debonding of the aggregate particles at very high expansion levels.

Studies have shown that while the development of ASR-induced damage presents a similar trend regardless of the aggregate type (i.e., fine versus coarse), as per Fig. 8.1 [227], the microstructure of concrete displays noticeable differences depending on the aggregate type [7]. Therefore, it is anticipated that other factors, such as enhanced kinetics at high temperatures and induced shrinkage at low moisture conditions, which have not been previously assessed, could impact the microstructure of affected concrete and should be investigated thus further.

8.2.3 Influence of moisture and temperature on ASR-induced development

Moisture and temperature are critical factors for the development of ASR [10,13,228]. Moisture is a transport medium for the ions involved in ASR and is needed for the swelling of ASR gel to induce expansion. As a result, a relative humidity threshold (RH) of 80% has often been stated as necessary to trigger the reaction. On the other hand, while temperature is not typically considered as one of the main factors (i.e., alkalis, silica, moisture) necessary to initiate ASR, it can affect the availability of these factors, the structure of ASR gel [58,107] and the kinetics of the reaction [111]. For instance, rising the temperature has been verified to promote the dissolution of silica [102]. It has been found that silica's dissolution rate increases from 71% to 100% with a rise in temperature

from 25°C to 80°C [103]. Similarly, the concentration and mobility of alkali ions (i.e., K⁺ and Na⁺) in the concrete pore solution increases at higher temperatures [229]. The above accelerates the formation of ASR gel and influences the rate and ultimate expansion of the concrete. However, in most cases, high moisture and temperature conditions are not encountered in the field. Concrete is often subjected to environmental variability in temperature and relative humidity [230], leading to fluctuating internal conditions. This highlights the need to understand the influence of numerous exposure conditions on ASR-induced development.

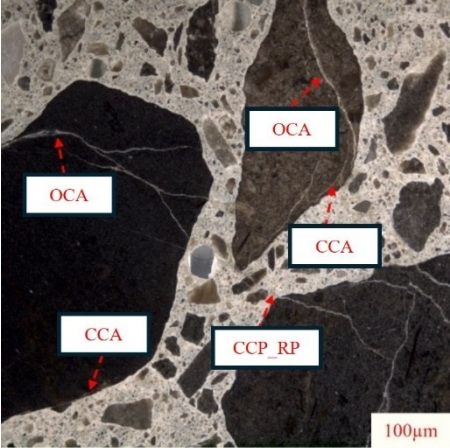
Most available studies on the role of moisture in ASR development primarily focus on expansion, with very limited information on its influence on deterioration. For instance, while the microstructural properties of ASR-affected concrete are considered a reliable means for assessing ASR-induced damage, especially in laboratory-made samples, much of the existing research has been focused on standard exposure conditions such as those adopted by the concrete prism test (CPT, >95% RH and 38°C) and, the accelerated concrete prism test (ACPT, >95% RH and 50/60°C); only a few works were conducted at lower temperature regimes (i.e., 21°C and 40°C) [6,100,111]. However, reducing RH to low levels necessary to mitigate ASR can induce shrinkage, potentially modifying the microstructural properties of ASR-affected concrete. Furthermore, temperature influences ASR kinetics, influencing the crack propagation rate. Hence, it can be hypothesized that a variation in kinetics might impact the microscopic damage features, such as length, width, and pattern of cracks. Yet, the influence of the temperature has either been rooted in expansion measurement or, at best, qualitative assessment of ASR-induced cracks [57,58,231].

8.2.4 Damage Rating Index (DRI)

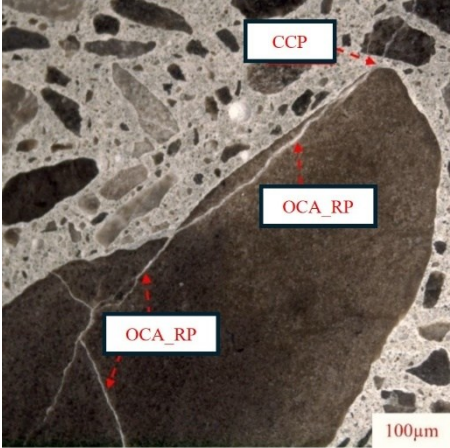
The Damage Rating Index (DRI) is a semi-quantitative microscopic procedure allowing the assessment of damage caused by internal swelling reactions (ISR) induced damage, such as ASR.

It is a simple-to-use technique proposed by Grattan-Bellew [139] that primarily evaluates the “extent” of ISR-induced damage, although the “cause” of distress (i.e., ASR, ACR, DEF, Freeze-Thaw, etc.) may also be recognized by experienced operators running the analysis. ASR-induced cracks are counted in 1 by 1 cm squares drawn on the surface of polished concrete sections using a stereomicroscope at 15-16X magnification; the count for each damage feature is then multiplied by weighting factors as shown in Fig. 8.2 to balance their relative importance towards the overall deterioration, as proposed by Villeneuve & Fournier [140]. The summation of cracks x weighting factors gives a DRI number; the higher this number, the higher the damage present in the evaluated specimen. The DRI number is normalized to 100cm², and has been proven to increase with ASR-induced expansion [121]. Some of the damage features along with their proposed weighting factors are shown in Fig. 8.2.

(a)



(b)



(c)

Distress feature	Description	Weighting factor
CCA	Closed crack in aggregate	0.25
OCA	Opened crack in aggregate	2
OCA_RP	Opened crack in aggregate with reaction product	2
CAD	Debonded aggregate	3
DAP	Disaggregated/corroded aggregate particle	2
CCP	Crack in the cement paste	3
CCP_RP	Crack in the cement paste with reaction product	3

Figure 8.2: Damage Rating Index: (a,b) ASR distress features (c) Distress features with corresponding weighting factors [140]

A closed crack in the aggregate (CCA) is given the lowest importance with a weighting factor of 0.25 as they are most likely a product of pre-existing flaws in the aggregate particles before their use in concrete, commonly originating from natural erosion or during the processing of the aggregates. The open cracks in the aggregates with or without reaction product (OCA_RP and OCA) are given a factor of 2 since their occurrence can be related to ASR-induced development. Similarly, the disaggregated particle (DAP) with a factor of 2 represents an aggregate particle exhibiting evidence of disintegration, characterized by the breakdown into loose rock grains. Finally, a crack in the cement paste with or without reaction product (CCP or CCP_RP) and debonded aggregate (CAD) is assigned the highest weighting factor of 3 since these types of distress are associated with concrete with high damage. The DRI can be conducted in its traditional form (i.e., using the DRI number and the weighted distress feature) to appraise damage as proposed by [140], or in its extended version proposed by [6] where a more detailed assessment is performed. Specifically, microscopic distress features are evaluated in absolute (i.e., counts) and relative (i.e.,

percentage-%) fashions without the use of weighting factors, thus contributing to a robust understanding of the mechanism of the reaction. Furthermore, the extended DRI also involves the assessment of the crack lengths, widths, and density, all of which have been reported to be sensitive to ASR-development [7]. These would contribute to an extensive overall appraisal of ASR development in affected concrete.

The DRI has been adopted to assess damage from concrete containing aggregates of different levels of reactivity [141], bearing different strengths [6], and undergoing free [7] or restrained expansion [142–144]. Moreover, its reliability in assessing damage in existing infrastructure has been verified [145]. However, there is a lack of research on the influence of varying moisture and temperature conditions on the microstructural damage features of ASR-affected concrete and their influence on the DRI results.

8.2.5 Scope of work

As previously stated, the influence of moisture and temperature on the microstructural properties of ASR-affected concrete is not well known. Moreover, the correlation of damage at similar expansion levels developed under different exposure conditions is unknown. Hence, to evaluate these gaps, concrete cylinders containing a highly reactive coarse aggregate (i.e., Spratt) were manufactured in the laboratory and stored at distinct conditions; three temperatures (i.e., 21°C, 38°C, and 60°C) and five relative humidities (i.e., 62%, 75%, 82%, 90%, and 100%). Length changes were monitored over 12 months for specimens stored at 21°C and 38°C, while those stored at 60°C were monitored for 6 months. At 3 and 6 months (i.e., for 60°C) and 6 and 12 months (i.e., for 21°C and 38°C), specimens were collected for conducting a comprehensive microscopic assessment (i.e., DRI complemented by image analysis using ImageJ). A time-based and expansion-based damage assessment was then performed, considering the influence of moisture

and temperature. Finally, discussions on the existence of a damage-based moisture threshold required for ASR-induced development were made.

8.3 Materials and method

8.3.1 Materials and mix proportion

Two sets of concrete mixtures were fabricated in the laboratory using a mix design based on the concrete prism test (ASTM C1293 [181]). The first set consists of a highly reactive coarse aggregate (i.e., Spratt) and a non-reactive fine aggregate (i.e., manufactured sand). While the second set combined non-reactive limestone (i.e., coarse aggregate content) and the same non-reactive manufactured sand (fine content). Table 8.1 provides information on the different aggregates used in this study. Both mixes contain conventional cement (i.e., CSA Type GU equivalent to ASTM Type I) with a total alkali content of 0.86% Na_2O_{eq} by mass of cement; their alkali content was boosted to 5.25kg/m³ Na_2O_{eq} by adding NaOH pellets to the mixing water. Table 8.2 displays the mix proportions for the two mixtures. Mixture B was designed to monitor shrinkage that is expected at low RH conditions. This shrinkage could interfere with accurately measuring ASR-induced expansion under these conditions.

Table 8.1: Properties of aggregates used

Aggregates	Location	Rock type	Specific gravity (kg/m ³)	Absorption (%)	AMBT-14 Days expansion (%)
Spratt	Ottawa (Canada)	Crushed siliceous limestone	2.70	0.62	0.310
Non-reactive limestone	Ottawa (Canada)	Limestone	2.78	0.42	0.02
Sand (Nonreactive)	Ottawa (Canada)	Derived from limestone	2.76	0.65	0.04

Table 8.2: Characteristics of the two mixtures

Mixture	Cement (kg/m ³)	Water (kg/m ³)	Coarse aggregate (kg/m ³)			Fine Aggregate (kg/m ³)	Alkali Pellet (kg/m ³)
			4.75-9.5mm	9.5-12.5mm	12.5-19mm		
A (reactive)	420	177.4	334.12	334.12	344.24	833.46	2.12
B (non-reactive)			328.58	328.58	338.53	855.17	

8.3.2 Selection of exposure conditions, durations, and concrete manufacture

To perform an extensive study of the role of numerous exposure conditions on ASR-induced development, five relative humidity conditions (i.e., 62% RH, 75% RH, 82% RH, 90% RH, and 100% RH) and three temperatures (i.e., 21, 38, and 60°C) were selected for this study. Samples stored at each temperature were investigated at all five relative humidity conditions, resulting in 15 conditions per mixture. The relative humidity conditions were targeted and maintained using saturated salt solutions, as per Poyet et al. [10]. Specific salt solutions for distinct RH/temperature setups were selected from ASTM E104[150]. Ibutton Sensors [151] were inserted into storage buckets to monitor the RH and temperature over time. Specimens were stored and continuously monitored for length change. Due to the aggregate’s reactivity, mixture A measured the expansion as per the standards and mixture B was used to separate the effect of shrinkage, particularly at low RH. The two results are vital for determining the net expansion. Specimens at 21°C and 38°C were stored for 12 months based on the concrete prism test (CPT), while the specimens at 60°C are to be conditioned for six months following the accelerated concrete prism (ACPT-AAR-4.1) [212].

A total of one hundred and eighty (180) and one hundred and twenty (120) 100mm x 200mm concrete cylinders were fabricated for mix A (reactive) and mix B (non-reactive), respectively. After 24 hours of moist-curing (i.e., at 100% RH and 20°C), the specimens were de-molded, small holes were drilled in both ends, and stainless-steel gauge studs were bonded in place with the aid of a fast-setting cement slurry. The specimens were then moist-cured for another 24 hours to ensure the hardening of the studs, after which the initial longitudinal reading was taken. Concrete specimens were placed in sealed buckets, each containing four concrete cylinders, and a minimum of 12 specimens were prepared for each RH at each temperature for the reactive mix (i.e., a minimum of three buckets per RH/temperature combination). However, for the non-reactive mix, eight specimens were prepared for each RH at each temperature. The buckets at 100% RH contained distilled water at the bottom to control RH, while water was replaced with the respective saturated salt solution as per ASTM E104 [150] for RHs lower than 100%, as highlighted in Table 8.3. Length change measurements were conducted out for 12 months (21°C and 38°C) or six months (60°C).

Table 8.3: Control of relative humidity

RH/Temperature	21°C	38°C	60°C
100%	Distilled water	Distilled water	Distilled water
90%	Barium chloride	Potassium nitrate	Potassium sulfate
82%	Ammonium sulfate	Potassium chloride	Potassium nitrate
75%	Sodium chloride	Sodium chloride	Sodium chloride
62%	Sodium bromide	Sodium nitrite	Sodium nitrite

8.3.3 Experimental procedures

8.3.3.1 Damage Rating Index (DRI)

The conventional and extended versions of the DRI were conducted on the affected specimens over time. A time-based assessment was selected to monitor the evolution of ASR-induced expansion and damage. The concrete specimens conditioned at 21°C and 38°C were tested at 6 and 12 months. The 60°C specimens were, however, assessed after three months and six months. Before the assessment, a specimen from each setup at each predetermined age was cut into half longitudinally. One half was polished using a mechanically operated table polish with grit sizes of 30, 60, 120, 240, 600, 1200, and 3000. A square grid of 1cm² was drawn on the polished surfaces, and the DRI was then conducted using a stereomicroscope at a magnification of 16x. Considering each square at a time, the number of each damage feature, as shown in Fig. 8.2, was counted. The sum of the total count per feature was multiplied by the weighting factors specified by Villeneuve and Fournier [140]. Furthermore, a comprehensive assessment as per the extended version of the DRI was conducted to determine some features of the cracks encountered such as maximum crack length, width, and density.

8.3.3.2 Image analysis – crack patterns

Concrete cylinders conditioned in three different temperatures and five distinct relative humidity conditions were further assessed using ImageJ following the flow chart presented in Fig. 8.3. A change in RH and temperature is anticipated to change the kinetics of the reaction, leading to the need to evaluate the possible influence of the change in exposure conditions on the cracking pattern and features such as crack orientation, density etc. The polished surface (used for DRI) from each setup and predetermined age was scanned using a paper scanner capable of 600 dots per inch (dpi) resolution and saved as a .jpg file (Fig. 8.4a). The images were transferred to an open-source photo

editing software, GIMP. Various damage features counted in the DRI were then traced, with each damage feature on a separate layer. The color code for each damage feature type was the same as that for the DRI charts in this study. Specifically, closed cracks in the aggregates; CCA (blue accent 1), open cracks in the aggregates with or without reaction products; OCA_RP (green), OCA (red) and cracks in the cement paste with or without reaction products; CCP_RP (blue accent 4), CCP (pink). The traced images were then exported to ImageJ. The traced images containing desired damage features (OCA, OCA_RP, CCP, and CCP_RP were used since only ASR-induced cracks are of interest) were converted to an 8-bit file before thresholding (Fig. 8.4d). The orientation of the traced cracks was assessed using the directionality plugin through a Fourier component method and a histogram starting and ending at 0° and 180° , respectively.

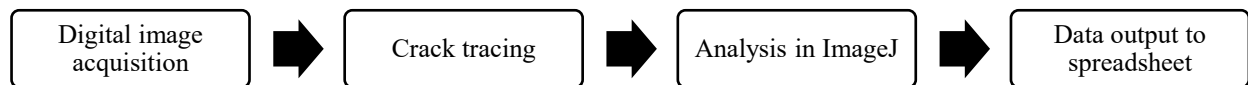


Figure 8.3: Flow chart of crack pattern analysis

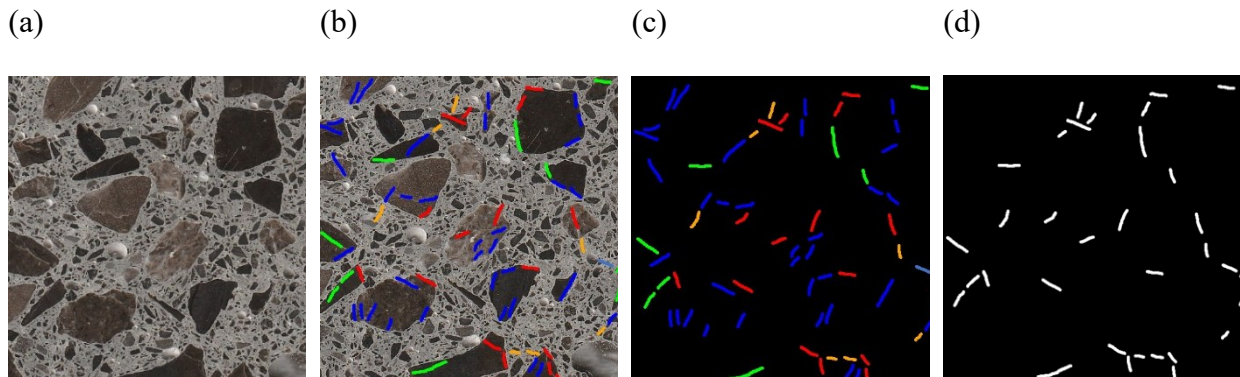


Figure 8.4: Image processing: (a) ASR-affected specimen surface (b) traced image (c) cracks on a black layer (d) thresholding of only ASR-induced cracks on ImageJ

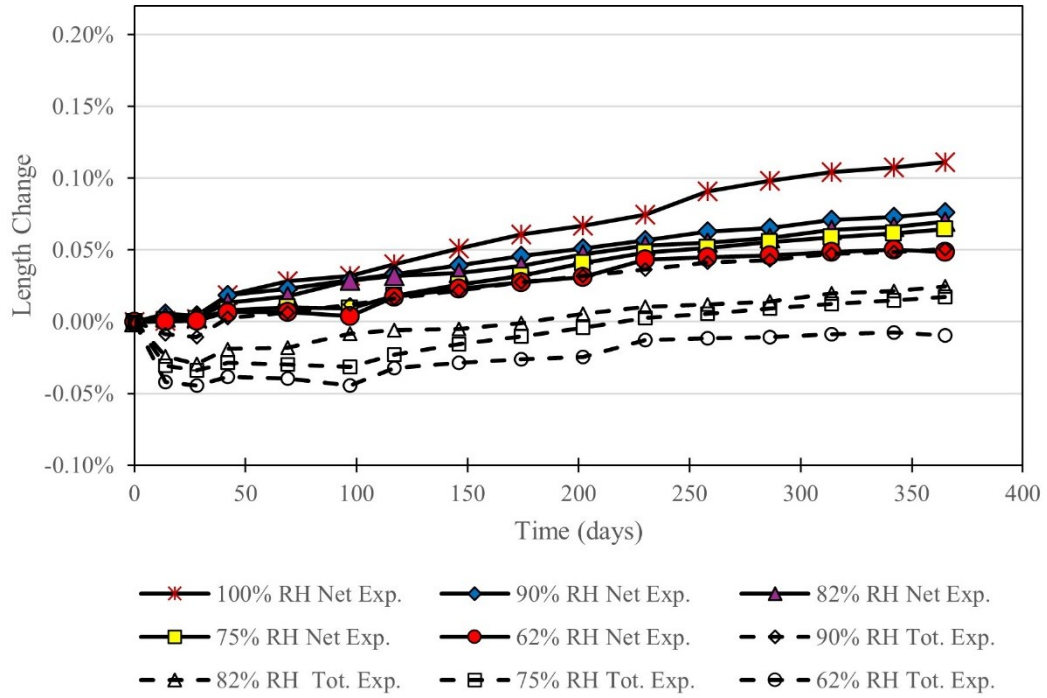
8.4 Results

8.4.1 ASR kinetics at numerous exposure conditions

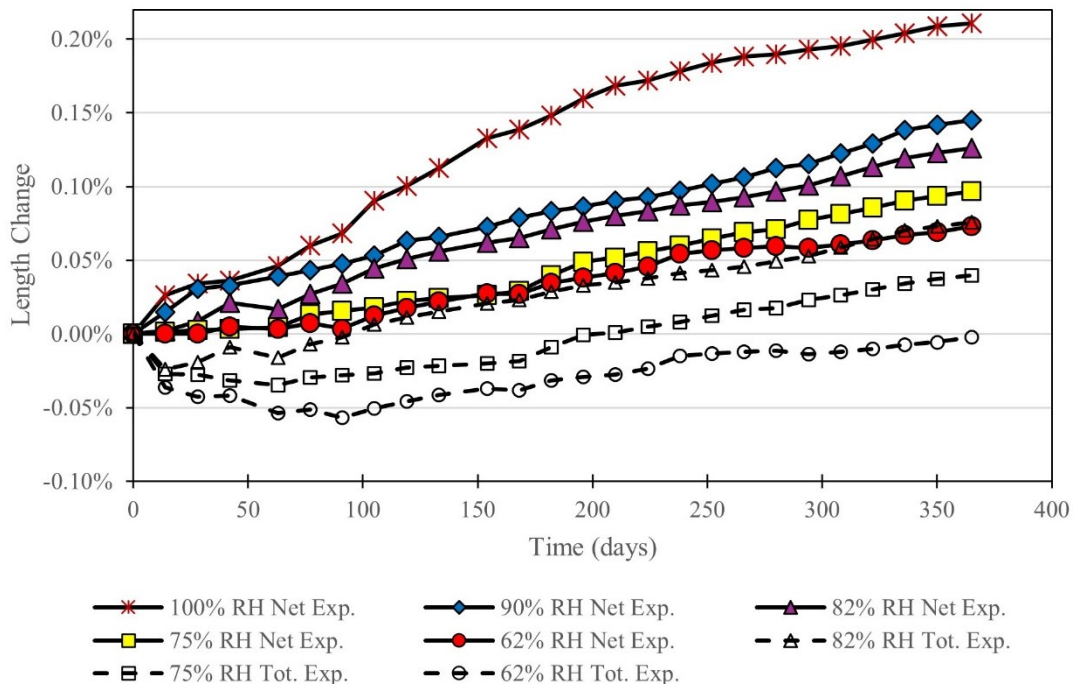
Fig. 8.5 presents the average length change as a function of time for ASR-affected concrete cylinders incorporating the reactive Spratt coarse aggregate at three different temperatures (i.e., 21°C, 38°C, and 60°C) and five relative humidity levels (i.e., 100% RH, 90% RH, 82% RH, 75% RH, and 62% RH), providing an overview of how varying exposure conditions influence ASR-induced expansion. The graph presents two distinct behaviors: (a) concrete mixtures displaying induced expansion throughout the whole monitoring process, and (b) concrete mixtures displaying an initial “shrinkage” process followed by induced expansion. Hence, the distinct mixtures evaluated are labeled as follows:

- Total expansion (Tot. Exp.): This represents the overall length change, including **ASR-induced expansion and shrinkage** for all RH conditions, particularly highlighting shrinkage at low RHs. These results were directly measured on Mixture A specimens.
- Net expansion (Net Exp.): This shows the net **ASR-induced expansion**, excluding any shrinkage effects, across all RH conditions. These results are the difference between Mixture A and Mixture B specimens.

(a) 21°C



(b) 38°C



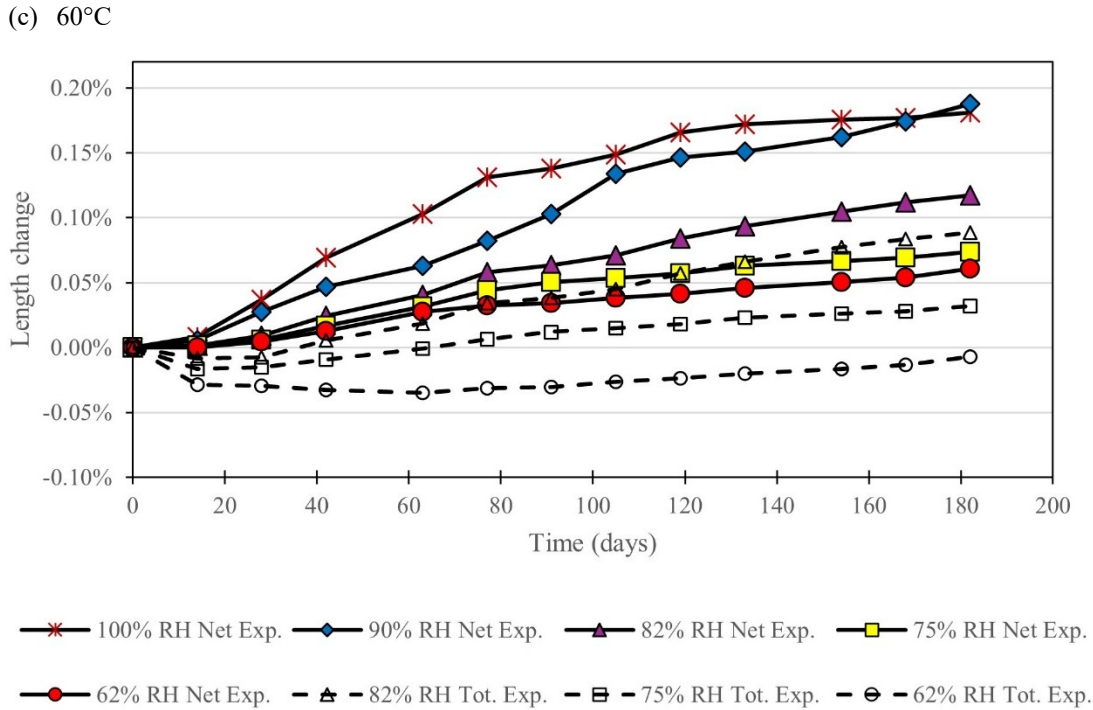


Figure 8.5: ASR kinetics at numerous relative humidities, including both decoupled expansion and non-decoupled length changes: (a) 21°C (b) 38°C (c) 60°C

Analyzing the above results, one observes that the kinetics of the reaction is affected by exposure conditions, leading to different rates and ultimate expansion. Furthermore, one notices that some mixtures exposed to conditions with RH lower than 100% experienced shrinkage at the beginning of the test. Upon decoupling of shrinkage, the net ASR-induced expansions follow the same trend as the total expansion.

Fig. 8.5a displays the length change measurements at 21°C. For all mixtures, the reaction presents a slow start; nevertheless, induced expansion increases with relative humidity. Noticeable initial shrinkage followed by steady expansion was recorded at RH lower than 100%. The magnitude of shrinkage and recovery time depends on the RH. A similar trend was observed at 38°C, as illustrated in Fig. 8.5b, but the kinetics of the reactions are enhanced, leading to higher ASR-induced expansions. For instance, the 0.111% ultimate expansion observed at 21°C under 100% RH after 365 days was achieved in less than 150 days at 38°C under the same RH condition. The

expansion rate is much faster at 60°C, as displayed in Fig. 8.5c. However, at the termination of the test after six months, 100% RH attained an ultimate expansion lower than 38°C due to apparent signs of alkali leaching.

Considering the difference in expansion among the three temperatures considered (i.e., 21°C, 38°C, and 60°C) at all RH levels, specimens conditioned at 21°C possess the slowest kinetics. Furthermore, all three temperatures exhibited some amount of shrinkage. The magnitude of shrinkage and recovery time is dependent on RH and temperature. Specimens conditioned at 62% RH experienced the most pronounced shrinkage. Yet, this condition attained an ultimate expansion higher than 0.04% across all temperatures.

8.4.2 Microscopic distress features

The ASR-induced microscopic distress features as a function of time for ASR-affected concrete cylinders incorporating the reactive Spratt coarse aggregate at three different temperatures (i.e., 21°C, 38°C, and 60°C) and five relative humidities (i.e., 100% RH, 90% RH, 82% RH, 75% RH, and 62% RH) were first assessed using the extended version of the DRI as proposed by [6]. This involves relatively appraising the distinct damage features (i.e., as counts, normalized to 100 cm²), as shown in Fig. 8.6. Fig. 8.7 displays the data in an absolute manner (i.e., percentage). To perform this assessment, damage features observed through the stereomicroscope were grouped into cracks in the aggregates (CCA), open cracks in the aggregates without and with reaction product (OCA + OCA_RP), and cracks in the cement paste with and without reaction product (CCP + CCP_RP). Furthermore, the number of counts is used directly without weighing factors, thus shedding more insights into the initiation and propagation of cracks in ASR development.

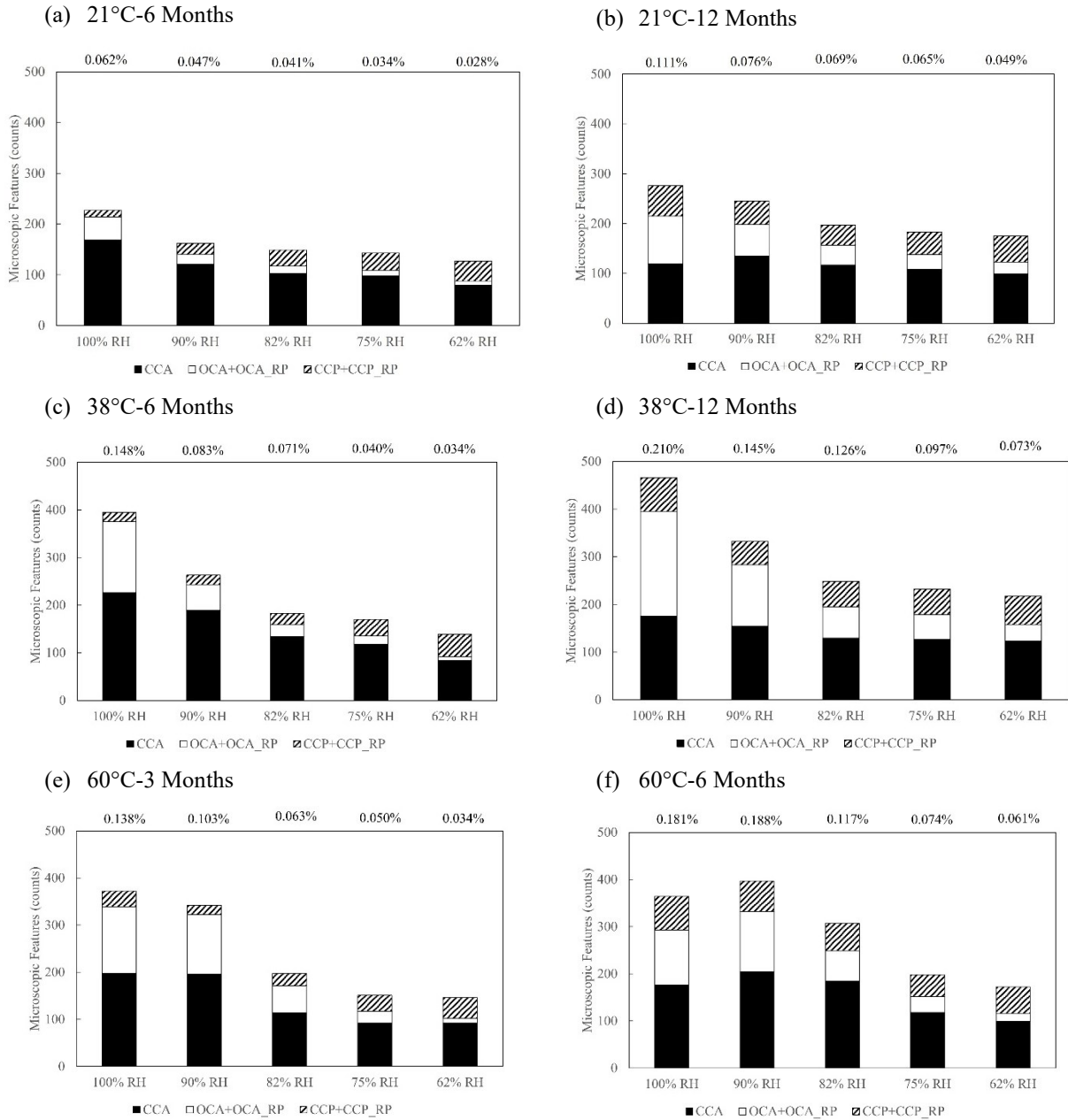
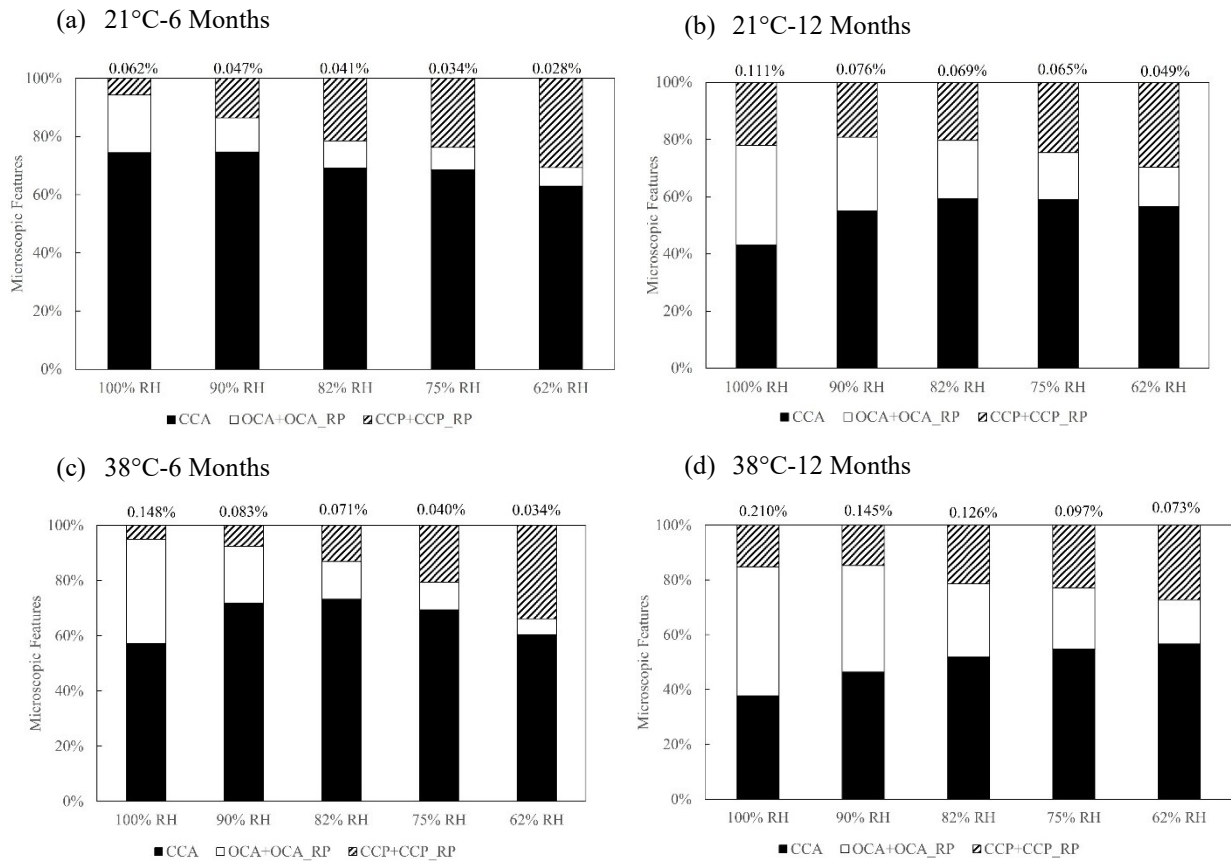


Figure 8.6: Count of microscope features: (a,b) 21°C (c,d) 38°C (e,f) 60°C

As displayed in Fig. 8.6, the total counts increase as the RH and expansion increase in most conditions. Typically, the most common feature observed was the closed crack in the aggregates (CCA) with up to 200 counts. This type of crack has been confirmed not to be an ASR-induced damage feature [7] but rather related to the crushing and weathering of the aggregates. Otherwise, open cracks in the aggregates without or with reaction products (OCA + OCA_RP) present a trend

across all conditions, with a consistent increase in the counts as RH and expansion rise. As clearly shown in the plots, specimens stored at low RH conditions (e.g., 62% RH and 75% RH) present few counts of the OCA + OCA_RP, which corresponds to their low ASR-induced expansion. Considering cracks in the cement paste without or with reaction products (CCP + CCP_RP), there is no clear pattern as RH increases. It is important to note that these crack types are most prominent in the 62% RH condition, highlighting induced shrinkage.

As displayed in Fig. 8.7, the cracks in the aggregates (i.e., CCA + OCA + OCA_RP) dominate across all setups, representing more than 60% of the total microscopic damage features.



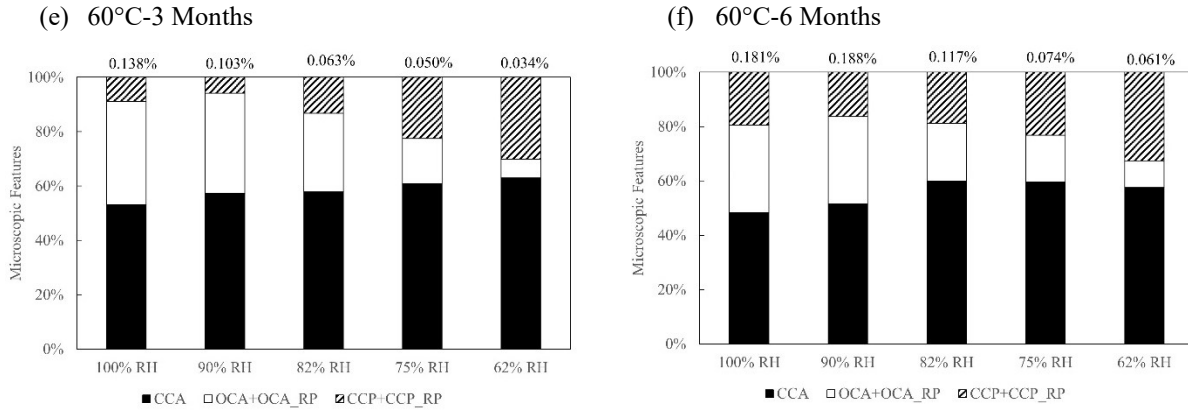


Figure 8.7: Percentage of counts: (a,b) 21°C (c,d) 38°C (e,f) 60°C

As expected, a significant increase in ASR-induced cracks in the aggregate was recorded over time at high RHs (e.g., 100% RH and 90% RH). However, only a fair increment was recorded at low RHs. For instance, at 21°C, the proportion of OCA + OCA_RP in specimens stored at 62% RH increases from 6% to 14% after 6 to 12 months, respectively. On the other hand, although the proportion of cracks in the cement paste is relatively high in specimens at low RHs compared to those at high RH conditions, confirming shrinkage, these proportions remain similar over time at low RHs, indicating no significant new cracks are formed. However, it increases significantly over time in specimens at high RH, implying the propagation of cracks into the cement paste.

8.4.3 Crack width, length and density

As Table 8.4 displays, the maximum crack length increases with RH over time for all temperatures, correlating with ASR-induced expansion. However, it is interesting to note that the maximum width is more influenced by high moisture and temperature.

Table 8.4: Crack length, width, and density

			Expansion (%)	Max. length (mm)	Max. width (mm)	Crack density (count/cm ²)	
21°C	100% RH	6 months	0.062%	16mm	0.05mm	0.60	
		12 months	0.111%	19mm	0.10mm	1.56	
	90% RH	6 months	0.047%	11mm	0.05mm	0.41	
		12 months	0.076%	12mm	0.05mm	1.10	
	82% RH	6 months	0.041%	10mm	0.05mm	0.46	
		12 months	0.069%	10mm	0.05mm	0.80	
	75% RH	6 months	0.034%	8mm	0.05mm	0.45	
		12 months	0.065%	9mm	0.05mm	0.75	
	62% RH	6 months	0.028%	7mm	0.05mm	0.46	
		12 months	0.049%	8mm	0.05mm	0.76	
	38°C	100% RH	6 months	0.148%	25mm	0.25mm	1.69
			12 months	0.210%	25mm	0.50mm	2.90
90% RH		6 months	0.083%	16mm	0.20mm	0.74	
		12 months	0.145%	19mm	0.25mm	1.78	
82% RH		6 months	0.071%	12mm	0.15mm	0.49	
		12 months	0.126%	14mm	0.15mm	1.18	
75% RH		6 months	0.040%	11mm	0.10mm	0.52	
		12 months	0.097%	12mm	0.10mm	1.05	
62% RH		6 months	0.034%	10mm	0.05mm	0.55	
		12 months	0.073%	11mm	0.10mm	0.94	
60°C		100% RH	3 months	0.138%	15mm	0.15mm	1.74
			6 months	0.181%	22mm	0.20mm	1.86
	90% RH	3 months	0.103%	15mm	0.15mm	1.47	
		6 months	0.188%	16mm	0.20mm	2.04	
	82% RH	3 months	0.063%	10mm	0.10mm	0.83	
		6 months	0.117%	12mm	0.15mm	1.24	
	75% RH	3 months	0.050%	10mm	0.05mm	0.60	
		6 months	0.074%	10mm	0.10mm	0.80	
	62% RH	3 months	0.034%	9mm	0.05mm	0.54	
		6 months	0.061%	10mm	0.05mm	0.73	

The crack density increases with time at all temperatures. However, there is no clear global pattern with RH. Yet, specimens conditioned at 100% RH at each temperature recorded the highest crack densities. At 21°C after six months of exposure, the crack density reduces with a change in RH from 100% to 90%. However, it increased for lower RHs. At 12 months, there is a consistent crack

density reduction from 100% RH to 75% RH. Yet it increased again for 62% RH. Thus, a nonlinear relationship between RH and crack density is highlighted despite a clear trend with ASR-induced expansion.

8.4.4 Crack orientation analysis

Table 8.5 illustrates the direction (i.e., in angles) of the cracks in specimens evaluated over time. Similar ASR-induced cracks considered for the crack length, width, and density (i.e., OCA, OCA_RP, CCP, and CCP_RP) are adopted for this assessment.

Table 8.5: Crack orientations

RH	Temperature					
	21°C		38°C		60°C	
	6 Months	12 Months	6 Months	12 Months	3 Months	6 Months
100%	30.99°	151.08°	22.39°	14.02°	157.74°	143.77°
90%	91.51°	163.28°	9.89°	2.80°	163.36°	177.33°
82%	66.72°	9.90°	10.95°	30.41°	163.90°	153.33°
75%	131.29°	97.85°	43.34°	154.58°	170.04°	28.35°
62%	18.59°	171.36°	11.74°	144.10°	109.85°	90.95°

The horizontal direction (0° and 180°) is perpendicular to the casting direction. Generally, the results show that cracks are oriented randomly, as expected in ASR-free expansion conditions. Nevertheless, peaks from the directionality analysis can indicate the preferred orientation of cracks. Analyzing the directionality histogram (see supplementary materials: Fig. S8.1-8.3) at 21°C, one will notice a more scattered peak, indicating the occurrence of various crack orientations across different angles. As shown in Table 8.5, no clear trend exists considering the preferred crack orientation. Instead, there is a dispersed crack distribution across the numerous RHs. At 38°C and 60°C, there are more concentrated peaks, especially at lower and higher angles, indicating cracks are more oriented toward horizontal directions (0° and 180°), which are perpendicular to the

casting direction except for 62% RH at 60°C. It is important to note that despite the preferred orientation, there is no strong pattern.

8.4.5 Damage Rating Index (DRI)

As Fig. 8.8 displays, the highest DRI values are consistently observed at the highest RH, while the lowest RH results in the lowest DRI values across all temperatures. Moreover, the onion skin crack type was found more frequently than the sharp cracks in all specimens assessed. Furthermore, isolated cracks that did not propagate from aggregate particles were found in the cement matrix. The crack types increase in length with expansion. Consequently, the DRI numbers increase over time (e.g., from 6 months to 12 months), corresponding to the increase in expansion over the same period, validating ASR-induced development in all conditions. It is, however, worth noting that a slower damage progression is identified at low RHs, as shown in the DRI plots. The increment in the DRI number over time is smaller at low RHs compared to high RHs. Considering the influence of temperature and comparing 21°C and 38°C (i.e., Fig. 8.8a) for the same RH and age, an increase in temperature results in a higher DRI number, similar to the trend observed with ASR-induced expansion. Even so, a temperature increment to 60°C (i.e., Fig. 8.8b) could result in a more substantial ASR development. For example, at 60°C, the DRI values for 100% RH after six months are comparable to or higher than those at 21°C after 12 months. Also, as one may notice, a similar DRI number was recorded at low RHs at 21°C after 6 months: 151 for 62% RH, 148 for 75% RH, and 151 for 82% RH. Interestingly, similar ASR-induced 11-microscopic damage feature counts (OCA + OCA_RP + CCP + CCP_RP) of 47, 45, and 46 were recorded, as shown in Fig. 8.6.

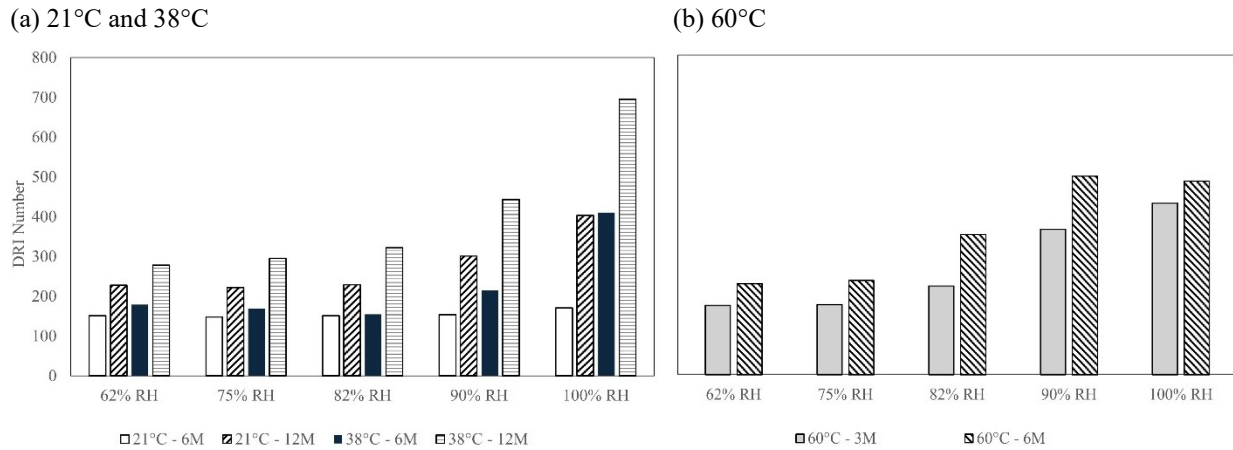


Figure 8.8: Damage Rating Index results: (a) 21°C and 38°C (b) 60°C

8.5 Discussion

8.5.1 Effect of moisture and temperature on ASR kinetics

The extensive assessment of ASR development at numerous RH and temperatures in this study brings about critical observations that would enable a better understanding of the reaction at different exposure conditions. As shown in the expansion plots, the kinetics of the reaction are significantly enhanced by high RH, leading to high ultimate expansions. Equally important is the exposure temperature, which can improve the expansion rate. However, temperature increases do not always lead to a higher ultimate expansion. It is instead dependent on the test duration [111,228]. Fig. 8.9 presents a time-based evolution of ASR-induced expansion as a function of RH and temperature to extensively assess this. Fig. 8.9a highlights the 3-month expansion for all RHs and temperatures, Fig. 8.9b displays the 6-month expansions, and Fig. 8.9c illustrates the ultimate expansions (i.e., 12 months for 21°C and 38°C and six months for 60°C).

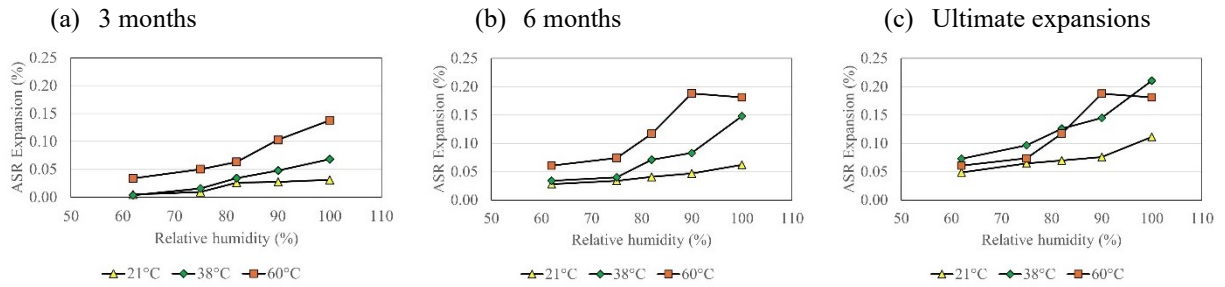


Figure 8.9: Influence of RH and temperature on ASR-induced expansion at different ages: (a) 3 months expansion (b) 6 months expansion (c) ultimate expansion: 21°C and 38°C at six months and 60°C at six months.

Comparing the expansion results across all temperatures and RHs, it can be concluded that the influence of temperature on the kinetics of ASR is less significant at low RHs. The change in RH from 62% to 75% would likely increase available moisture for ASR. However, the corresponding expansion increase is of low magnitude, even with a temperature rise. This highlights the sufficiency of moisture for the reaction. Despite the improved migration of ions and silica dissolution that can be attained at elevated temperatures, the ASR gel might be generated, but its expansive pressure will stay relatively low. On the other hand, a change in RH from 90% to 100% would lead to significant ASR-induced expansion upon a temperature rise [8]. However, this could exclude the 60°C. The 60°C presents a unique expansive scenario as per Fig. 8.9, due to its high susceptibility to alkali leaching [14,100]. As displayed in Fig. 8.9c, comparing the ultimate expansions across all temperatures at 100% RH, 38°C attained the highest ultimate expansion. Hence, the nonlinearity of the influence of temperature on ultimate expansion. Yet, considering the ultimate expansion plots, the expansions recorded at 38°C (12 months) and 60°C (6months) for all RHs appear to be close with $\pm 0.04\%$ difference across all RHs. This similarity suggests that the accelerated concrete prism test (ACPT) conducted at 60°C could be used effectively at lower or half the duration of the standard concrete prism test (CPT). This finding underscores the efficiency of the ACPT in evaluating ASR expansion within a shorter timeframe, providing valuable insights for faster assessment of aggregate reactivity.

Another interesting observation from the length change measurements as per Fig. 8.5 is the switch from shrinkage to expansive condition at low RHs. This interplay suggests combined mechanisms or a late start of ASR-induced expansion. For instance, in an environment of 82% RH, which is probably not the driest, the concrete specimen could undergo both drying shrinkage and ASR-induced expansion, but with the drying shrinkage leading at an early age. Over time, drying shrinkage will plateau as expected [232], and the slowly evolving ASR development supersedes after that. Conversely, a late start of ASR can be assumed at drier conditions (e.g. 62% RH) due to the late recovery of more than three months at 21°C and 38°C.

In general, it is interesting to note that a decrease in RH to 62% would not halt ASR-induced expansion. At the lowest temperature (i.e., 21°C), an expansion of 0.028% was recorded in specimens conditioned at 62% RH after six months. Although this can be classified as a negligible expansion according to the global ASR damage assessment table [141], it progressed to 0.049% after 12 months (i.e., a marginal expansion). Hence, the reaction can only be delayed.

8.5.2 Understanding the influence of RH and temperature on the microstructural properties of ASR-affected concrete

A time-based and expansion-based assessment is conducted to comprehensively describe the influence of exposure conditions on ASR-affected concrete at a microscopic level. The time-based assessment describes the evolution of inner damage, and the expansion-based evaluation focuses on how exposure conditions influence ASR-induced inner damage at similar expansion levels.

8.5.2.1 Time-based assessment

8.5.2.1.1 DRI number and Crack properties

Fig. 8.10 evaluates the distribution of distress features and DRI number across all exposure conditions. There are no considerable differences in DRI number at low RHs. However, the overall influence of ASR-induced expansion on damage is temperature-dependent.

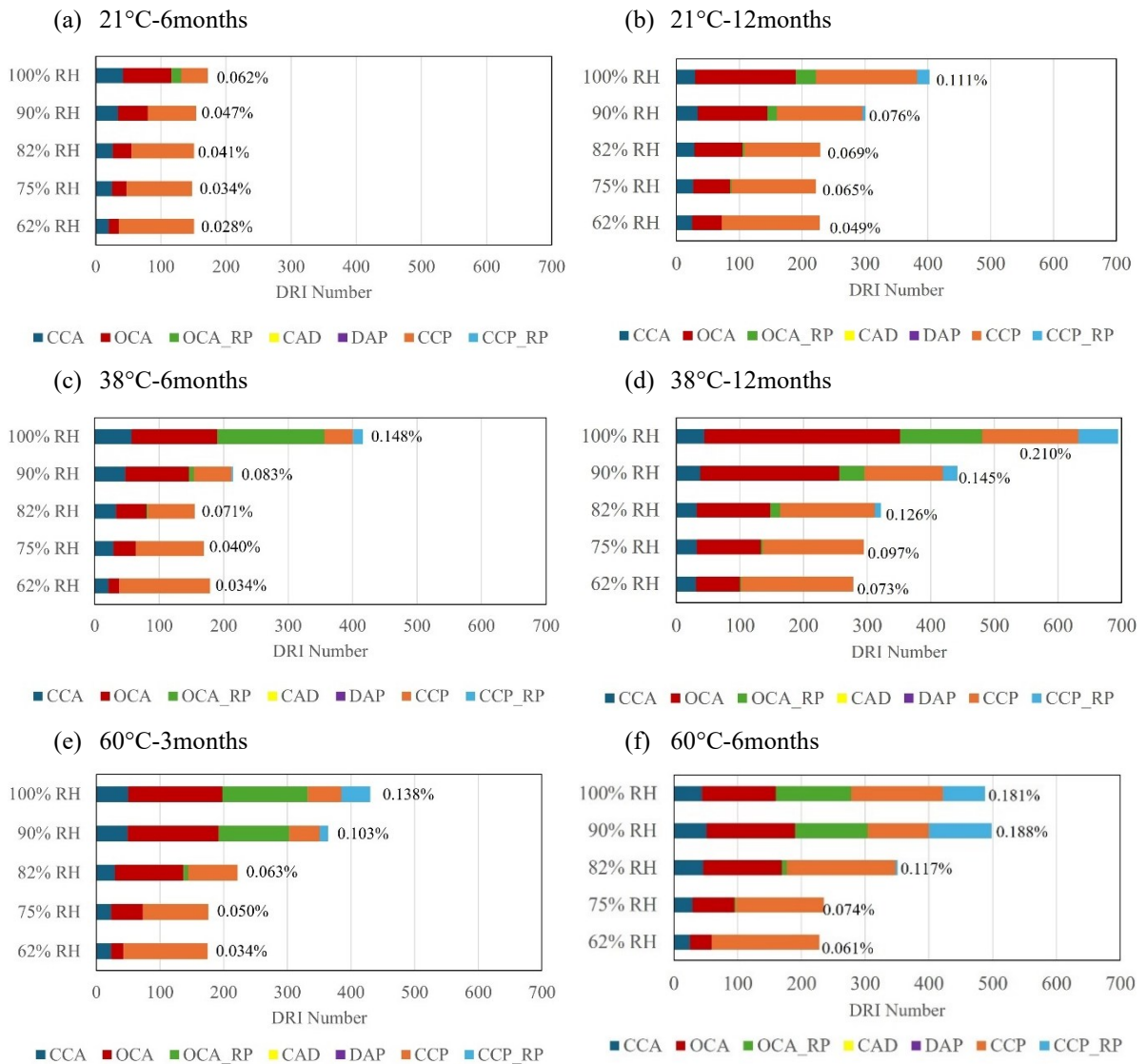


Figure 8.10: DRI results with decoupled ASR-induced expansion: (a) 21°C-6months (b) 21°C-12 months (c) 38°C-6months (d) 38°C-12 months (e) 60°C-3months (f) 60°C-6months

According to the DRI outcomes for 21°C and 38°C, as illustrated in Fig. 8.10 and Table 8.4, 100% RH recorded the highest ultimate DRI number and crack properties (i.e., length, width, and density) as expected, similar to the expansion trend. However, lower RHs (i.e., 90%-62%) present a dissimilar trend with expansion (i.e., DRI number and crack properties do not increase with RH). Considering the 21°C condition, a nonlinear trend, yet a similar DRI number of 151, 148, 151, and 154 were obtained at 62% RH, 75% RH, 82% RH, and 90% RH, respectively, at six months. A similar trend was observed in their crack density, which falls within 0.41-0.46 count/cm² at the same age. As a result, the DRI number or even the crack density alone is insufficient to describe/differentiate damage in these conditions. However, analyzing the DRI chart and crack types is vital in differentiating the damage levels for these conditions. Hence, the close DRI number can be attributed to the combined influence of ASR and shrinkage. The two mechanisms are at different levels, but their combined influence causes similar damage. For instance, comparing the 90% RH versus 62% RH, which have distinct ASR-induced expansions of 0.047% and 0.028%, respectively, 90% RH presents higher ASR-induced damage (i.e., cracks in the aggregates) and lower shrinkage (i.e., cracks in the cement paste), but vice versa at 62% RH as per their distress features count, leading to similar DRI number.

Another interesting observation from the DRI results is the influence of alkali leaching on inner damage. As noted in the expansion results and well reported in the literature [14,111,117,214], 100% RH attained a slightly lower ultimate expansion than 90% RH at 60°C. Interestingly, a similar trend was observed in inner damage, with 100% RH attaining a slightly lower DRI number and crack properties than 90% RH. Considering the magnitude of the distress features in both conditions, 90% RH presents a higher count of cracks in the aggregate and cement paste; this suggests the reaction proceeds in 90% RH after earlier termination at 100% RH due to the possible

depletion of sufficient alkalis in the system. Another possible explanation could be the loss of viscosity of gel, leading to a loss in expansive properties and flow into surrounding pores. The observation of several isolated pores containing gel deposits in this study might confirm this.

8.5.2.1.2 Influence of moisture and temperature on distress features

The DRI has proven reliable in assessing the cause of damage through its distress features described in Fig. 8.1. Typically, ASR-induced cracks are known to initiate in the aggregate particles and propagate into the cement paste. However, low moisture conditions have been established to introduce shrinkage cracks in the cement paste. As a result, more cracks in the cement paste than expected can be captured using the DRI, thus exaggerating the DRI number. To comprehensively assess the role of moisture and temperature in ASR development, the standard distress features were slightly modified by separating ASR-induced cracks in the cement paste without reaction product (i.e., CCP) from isolated cracks found in the bulk cement paste, referred to as CCP (Non ASR related) in this study. To conduct this, the number of CCP (Non ASR), which represents cracks that don't originate from aggregate particles (i.e., CCA, OCA, OCA_RP), were counted separately but assigned the same weighting factor of 3, given the importance of cracks in the cement paste in mechanical property reductions like compressive strength. The decoupled shrinkage DRI results, along with the decoupled ASR-induced expansion (i.e., net expansion), are presented in Fig. 8.11. Overall, the OCA + OCA_RP and CCP + CCPG increase with RH in most conditions. On the other hand, the CCP (Non ASR related) reduces as RH increases.

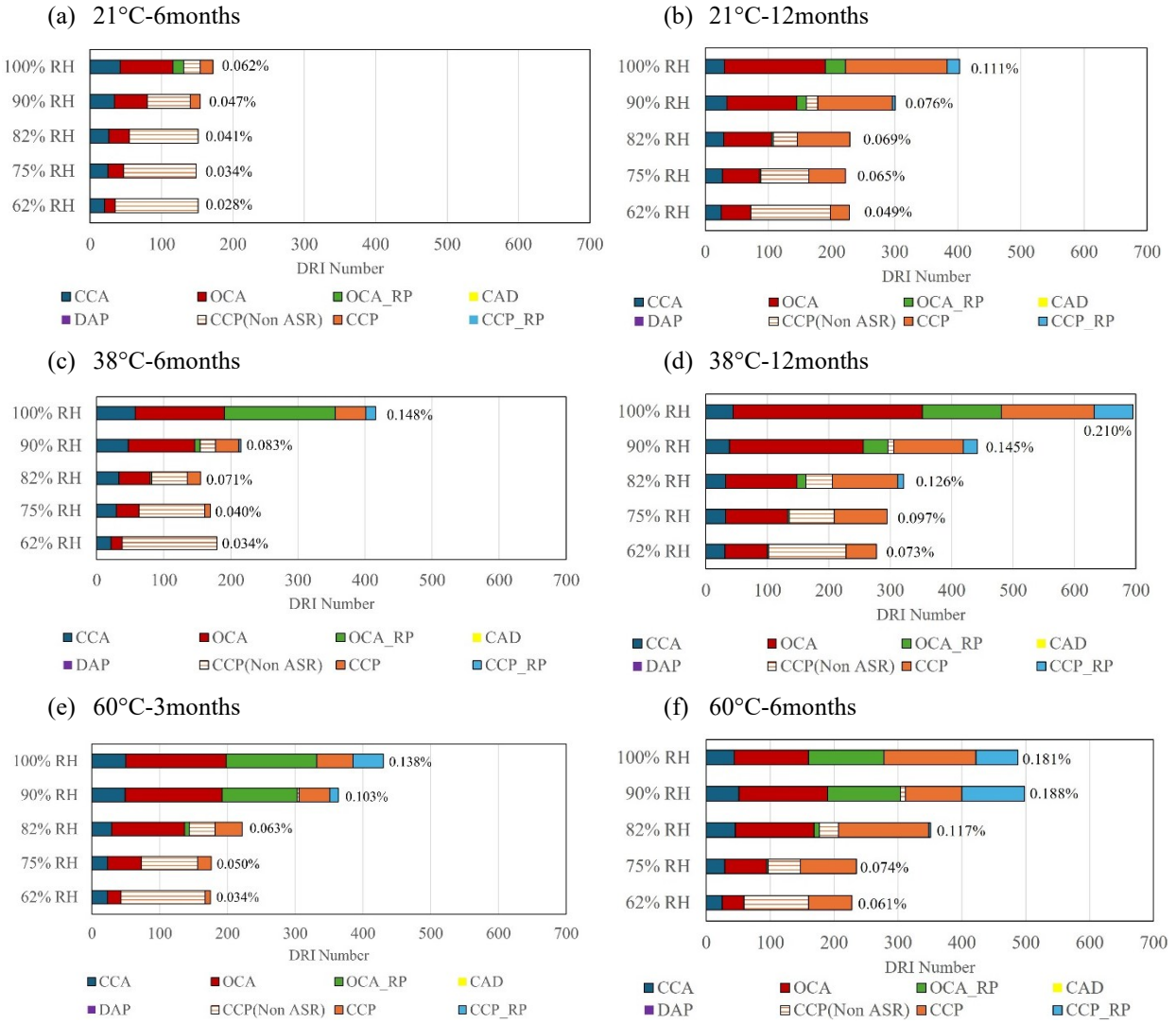


Figure 8.11: Decoupled DRI results with decoupled ASR-induced expansion: (a) 21°C-6months (b) 21°C-12 months (c) 38°C-6months (d) 38°C-12 months (e) 60°C-3months (f) 60°C-6months

Cracks in the aggregates and cement paste dominate all RH conditions at 21°C, as shown in Fig. 8.11a and b, but their magnitude and significance regarding ASR vary. As expected, the open cracks in the aggregates without reaction products (i.e., OCA) exhibit a linear trend with expansion, RH, and time. However, there is a lack of reaction products (i.e., ASR gel) in the coarse aggregates at low RH conditions. Possible reasons for this might include the magnification at which the DRI has been conducted (i.e., 15-16x). Another possibility is washing away gels during the specimens' preparation. Additionally, this finding might raise the question as to whether ASR-

induced cracks are caused by pressure from ASR gel upon moisture uptake, especially since the RH level in this condition is relatively low. Some researchers have proposed different theories that might support the existence of cracks without imbibition pressure from ASR gel [46].

On the other hand, the cracks in the cement paste consist of ASR and non-ASR related cracks. The occurrence and magnitude of the non-ASR related cracks is dependent on relative humidity. Specimens conditioned at 21°C present a dominant non-ASR related crack across all RH levels at six months coinciding with low ASR-induced expansion and high shrinkage. It is, however, interesting to know that as expansion increases at 12 months, some ASR-induced cracks have propagated from the coarse aggregates into the cement paste. However, a common feature of such CCP especially in specimens conditioned at low RH is that the CCP often propagates from closed coarse aggregates (i.e., CCA). This is unlike high RH conditions, where most CCP originates mainly from open cracks in the aggregates. Hence, the reduction in moisture influences the crack propagation. A possible explanation for this is a weaker cement paste due to shrinkage. As a result, the cement paste could not absorb the stresses caused by the expansion from the aggregate particles.

The increase in temperature influences the propagation of cracks as well. As shown in Fig. 8.11, the higher the temperature, the more the magnitude of ASR-induced distress features and lower the CCP (non-ASR related) across all RH levels. The changes in the microstructure at high temperatures can be attributed to enhanced hydration and ASR kinetics, which was significantly influenced at an elevated temperature of 60°C.

Overall, moisture and temperature are crucial in inner damage in ASR-affected concrete. Interestingly, while an increase in RH often leads to a rise in ASR-induced expansion, such a linear

trend is not the same for damage. For instance, considering the 62% RH and 75% RH per temperature, a similar DRI number was recorded for both RHs at all temperatures.

8.5.2.2 Expansion-based assessment

The RH-temperature combinations assessed in this study result in different ASR-induced expansions over time. Evaluating the influence of RH and temperature on the microscopic properties of affected concrete at similar expansion levels is essential for a comprehensive understanding of how these exposure conditions influence ASR. Temperature has been shown to have a more pronounced influence on the reaction, and as demonstrated in Fig. 8.9, 38°C and 60°C exhibit similar expansion behavior. Therefore, three expansion levels - high, moderate, and low - were selected across these two temperatures. This selection is based on the minimum and maximum expansions achieved in this study. For this evaluation, RH levels of 100%, 82%, and 75% are considered high, moderate, and low, respectively. The reference expansions are shown in Table 8.6.

Table 8.6: Expansion-based assessment of the role of RH and temperature

Classification of expansion	Temperature	RH	Age	Expansion	Expansion classification by [141]
High	38°C	100%	6 months	0.138%	Moderate - high
	60°C		3 months	0.148%	
Moderate	38°C	82%	6 months	0.071%	Marginal – moderate
	60°C		3 months	0.063%	
Low	38°C	75%	6 months	0.040%	Marginal
	60°C		3 months	0.050%	

Figure 8.12 displays heat maps illustrating the DRI pattern (i.e., the number in each square of the heatmaps represents the normalized DRI number in each of the 1cm² squares drawn on the surface

of the specimens) across the tested surface of the specimens at each expansion level selected. The damage in each square is formatted as follows based on the data range obtained in this study: 0 (i.e., no damage, green), 50 percentile (i.e., moderate damage, yellow), and 20.6 (i.e., high damage, red). The heat maps revealed the overall distribution of cracks and show that they are randomly distributed as expected for free ASR-induced expansion. However, low RH and temperature conditions have most of their cracks concentrated in the middle of the specimen. This indicates the higher state of moisture in the middle of concrete specimens, as verified by [99]. This occurrence can be expected because the external RH is usually lower than the internal RH as presented in chapter six.

38°C-100%RH

(a)

0.8	0.4	5.7	0.2	0.4	0.4	0.8	1.3	1.1	2.1	0.8	2.1	0.4	0.8	6.9	4.6	0.8
3.8	0.8	5.5	1.7	2.5	1.9	2.1	0.6	0.6	0.2	0.4	10.7	0.4	1.9	3.6	2.1	8.6
4.0	4.4	0.6	1.7	0.0	2.3	1.7	0.2	0.2	0.6	6.5	10.3	0.4	9.2	2.9	1.7	5.5
3.6	0.0	0.4	1.1	5.0	2.7	14.9	7.6	0.4	3.8	6.3	5.9	5.7	10.3	5.3	3.8	2.3
5.0	7.6	5.3	3.6	3.4	0.4	16.2	14.5	7.6	5.5	3.2	4.6	0.8	0.6	6.3	5.0	7.4
0.6	6.9	0.0	8.4	0.8	5.0	0.2	0.8	2.9	2.3	0.4	0.2	3.4	5.7	6.9	0.0	3.6
5.7	3.8	3.4	3.4	2.5	5.7	3.4	1.5	0.2	0.6	3.2	1.9	1.9	6.9	10.9	5.7	1.9

High expansion

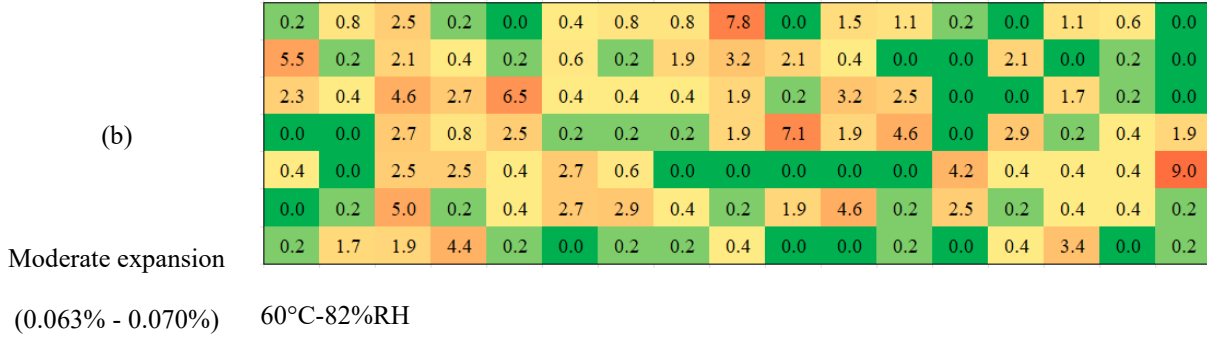
(0.138% - 0.148%)

60°C-100%RH

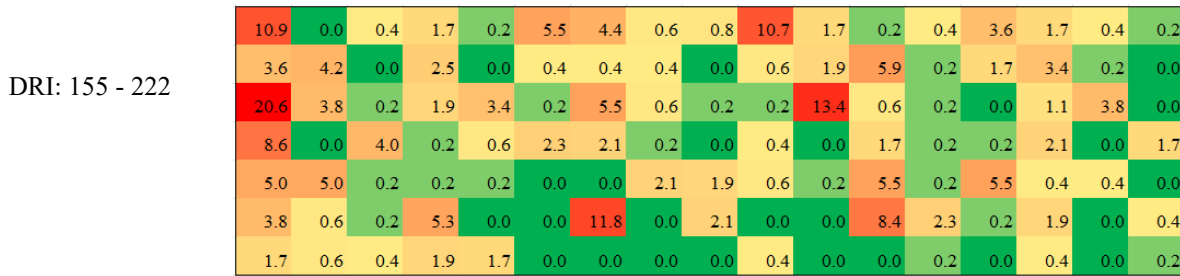
DRI: 416 – 430

4.8	13.0	2.1	7.1	12.8	3.2	6.3	3.8	4.2	13.4	5.5	12.2	0.4	5.3	16.6	3.6	7.4
3.8	6.7	0.6	4.6	0.0	3.8	2.1	2.1	1.5	6.9	0.4	5.5	0.2	4.2	0.4	12.6	7.8
8.4	5.3	0.0	0.6	0.0	8.2	0.8	4.6	1.7	8.2	0.8	3.6	0.0	2.3	0.8	2.7	3.2
4.2	0.2	0.2	2.7	8.4	0.4	0.2	0.0	3.6	0.8	5.3	0.6	2.5	4.2	3.4	2.3	2.1
1.9	0.0	3.8	0.0	9.9	2.3	2.1	5.0	5.9	2.7	2.3	0.4	3.2	6.1	3.4	5.3	4.0
0.6	0.4	0.2	1.7	5.3	0.2	0.6	2.1	9.5	0.4	0.2	5.7	0.8	5.5	0.6	3.4	1.7
10.3	0.6	9.2	0.0	7.4	0.2	6.9	0.2	0.2	0.0	2.1	4.2	0.8	0.6	2.1	3.6	7.4

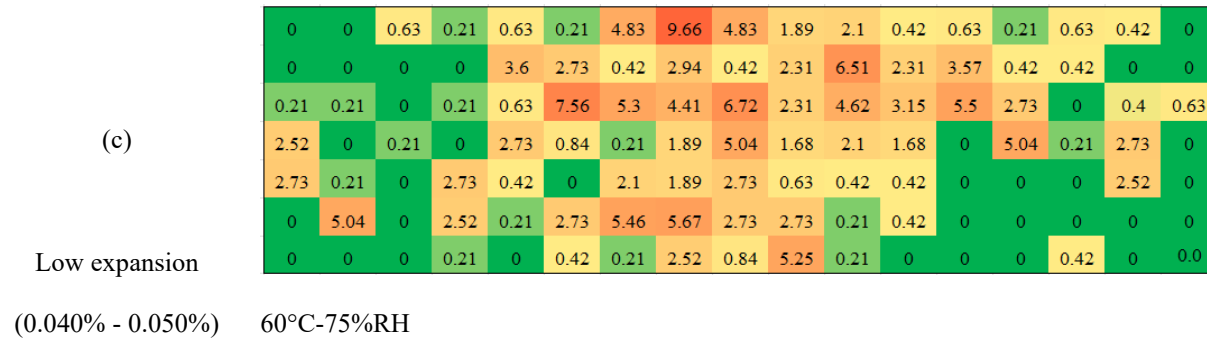
38°C-82%RH



60°C-82%RH



38°C-75%RH



60°C-75%RH

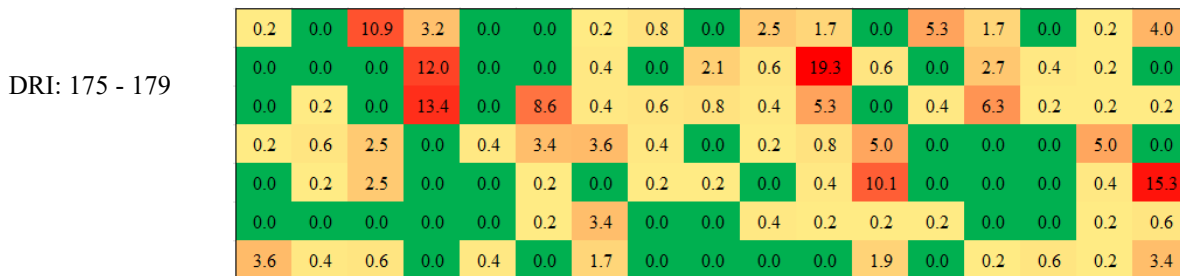


Figure 8.12: Heat maps of damage assessment at similar expansion levels: (a) High expansion, (b) Moderate expansion, (c) low expansion

At the high expansion and RH of 100% (i.e., 0.138% - 0.148%), 38°C obtained a total microscopic features count of 395. Similarly, 372 counts were recorded in the 60°C conditions. This leads to a

close DRI number of 416 and 430 at 38°C and 60°C, respectively. Hence, similar ASR-induced damage is attained at similar expansion, irrespective of the temperature change. However, considering the crack properties in these conditions, as displayed in Fig. 8.13, 38°C achieved a higher maximum crack length (i.e., 25mm) and width (i.e., 0.25mm) than 60°C, which attained a maximum crack length and width of 15mm and 0.15mm, respectively. Interestingly, a reversed scenario is seen for the crack density. Specimens conditioned at 60°C have a slightly higher crack density of 1.74 count/cm² than 1.69 count/cm² at 38°C.

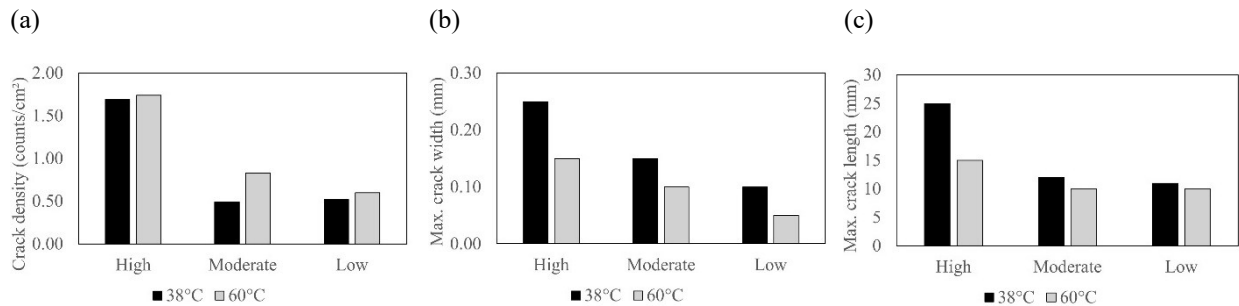
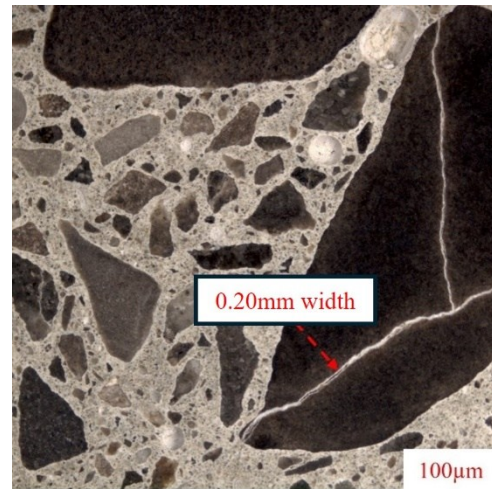
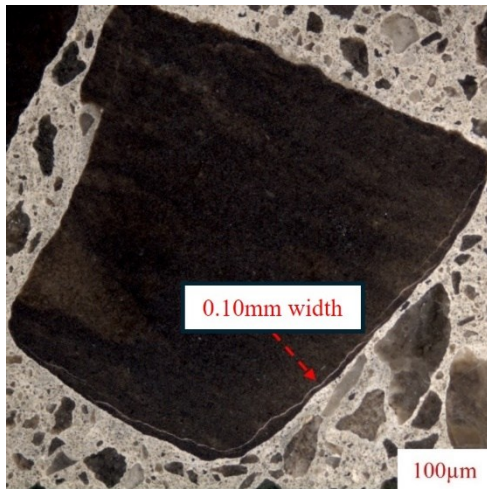


Figure 8.13: Crack properties at similar expansion: (a) crack density (b) max. crack width (c) max. crack length

Considering the microscopic properties at moderate expansion and RH of 82% (i.e., 0.63% - 0.71%), the expansion at 38°C results in a microscopic feature count of 183, slightly lower than the 197 counts at 60°C. It is, however, interesting to note that 60°C has a significantly higher open crack in the aggregates without or with reaction products (i.e., OCA + OCA_RP) with 57 counts compared to 25 counts recorded at 38°C, leading to 60°C having a higher DRI number of 222 compared to 155 for 38°C. Nevertheless, this falls within a close range. The crack properties follow a similar trend as the high expansion group. The 38°C cracks are longer (i.e., 12mm) and wider (0.15mm) compared to the maximum crack length (i.e., 10mm) and width (i.e., 0.10mm) at 60°C. Also, the crack counts at 60°C are denser, with 0.83 count/cm² compared to 0.49 count/cm² at 38°C.

The low expansion groups (i.e., 0.040% - 0.050%) at 75% RH follow the same pattern as the other groups. 38°C attained a similar DRI number (179) compared to 60°C (175). Yet, 60°C has higher crack density but lower maximum crack length and width.

Overall, the effect of temperature on ASR extends beyond the kinetics of the reaction. It influences the microstructure of ASR-affected concrete. Based on the differences highlighted, at a similar expansion level, ASR development at 38°C often leads to greater maximum crack length and width. In comparison, the development at 60°C leads to a higher crack density. This may be due to slower expansive pressure build-up at 38°C, allowing more significant stresses to develop in fewer locations before the concrete relieves the pressure by cracking. At 60°C, rapid reaction kinetics led to high micro-crack density; these cracks were numerous but smaller in width and length due to quick pressure relief through many tiny cracks. The findings in this study are similar to those from several authors on the occurrence of high crack counts/density at higher temperatures [100,111].



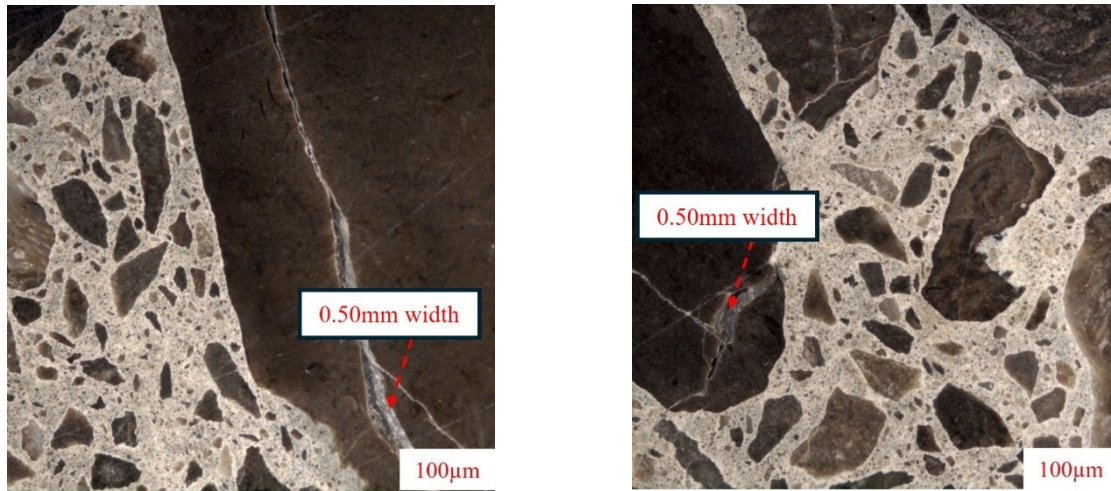


Figure 8.14: Some maximum crack widths recorded in the study

8.5.3 Relative humidity threshold for significant ASR damage

The critical role of high relative humidity (RH) in promoting ASR-induced expansion has been well-documented and corroborated by the findings of this study. It is well-established that significant ASR-induced expansion is effectively limited below certain RH levels. Consequently, the concept of an RH threshold has been introduced, which serves as a pivotal guideline for preventing and maintaining ASR-affected concrete [8,25,26]. Existing studies on the RH threshold required for ASR have primarily focused on expansion assessment over time. These assessments have led to the general adoption of a threshold of 80% RH for the reaction. The comprehensive assessment conducted by [10,48] indicates that this threshold could depend on temperature, among other factors. Furthermore, a close examination of ASR development at low RH levels in this study and those available in the literature [8,13] reveals the potential introduction of additional damage to the concrete microstructure, primarily due to shrinkage. Therefore, assessing the RH threshold by considering overall damage, not just expansion over time, is essential. Hence, conducting the RH threshold using the DRI can provide a more holistic assessment through the quantification of

various forms of deterioration that have been embedded in the various distress features of the DRI, including ASR-induced cracking and non-ASR-induced cracking that may be introduced through shrinkage. This study evaluates the RH threshold for significant ASR damage across three temperatures, as shown in Fig. 8.15, by comparing ultimate DRI number and crack properties (i.e., max. length, width, and crack density) at all temperatures.

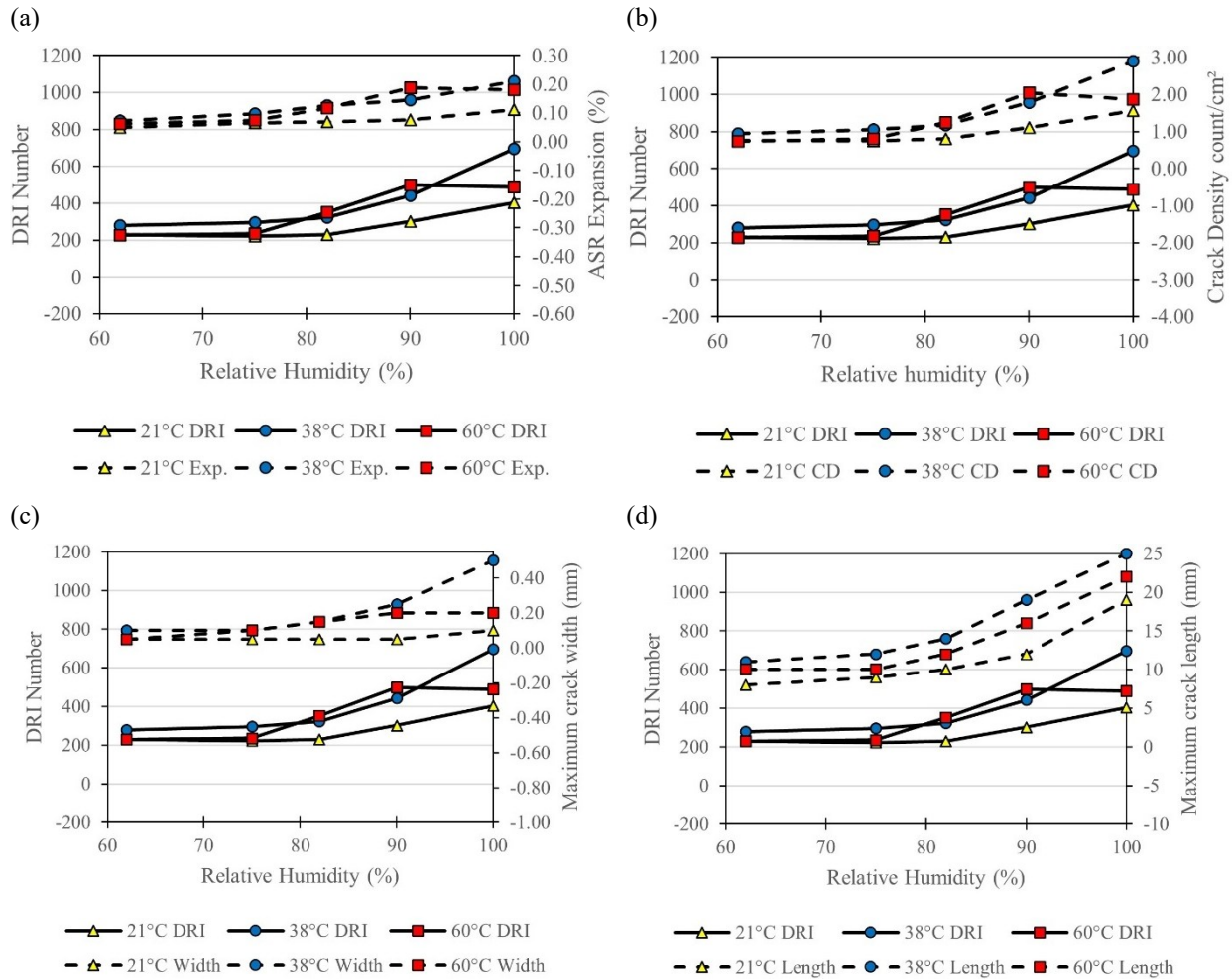


Figure 8.15: Assessment of RH humidity threshold for ASR damage at three different temperatures comparing DRI with: (a) Expansion, (b) Crack density, (c) Maximum crack width, (d) Maximum crack length

Due to the reactivity potential of the aggregate studied, all conditions attained an ultimate expansion of $\geq 0.04\%$. Hence, this study assumes an RH level showing a significant increment in ASR-induced deterioration (measured by DRI number and crack properties) as the threshold for

aggressive ASR damage. As illustrated in Fig. 8.15, at each temperature (i.e., 21°C, 38°C, and 60°C), the increase in RH from 62% to 75% does not significantly change ASR-induced deterioration. Exploring the Fig. 8.15 plot, a point of significant increase in ASR-induced deterioration appears to be dependent on temperature at $\geq 75\%$ RH. For instance, at 21°C, the change in DRI number only seems to be significant at 90% RH; a similar trend can be observed for the expansion, crack density, and maximum crack length, and an even more substantial increase at 100% RH can be noted. Based on this analysis, the threshold for substantial ASR damage using Spratt aggregate appears to be around 82 - 90% RH at 21°C. Interestingly, for 38°C and 60°C, pronounced damage starts at lower RH conditions. Both conditions seem to undergo a pronounced increase in damage indices around 75% - 82%RH. These findings indicate a lower threshold at higher temperatures. This confirms previous studies [10] that claim the dependence of the threshold on temperature. Overall, the interplay of RH and temperature leads to different RH thresholds needed for ASR for the reactive coarse aggregate considered in this study. At low temperatures, the solubility of silica and even the migration of alkalis are low, leading to the need for a high RH for the development of ASR damage. However, the moisture availability and pore saturation dynamics change at higher temperatures, leading to enhanced kinetics and lower RH needed for the reaction. Most importantly, irrespective of the temperature, an RH of $\leq 75\%$ will not stop the reaction but ASR-induced damage can be reduced.

8.6 Conclusion

The main goal of this study was to evaluate the microscopic properties of ASR-affected concrete incorporating reactive coarse aggregates conditioned at numerous relative humidity and temperatures. The main findings of this study are presented hereafter:

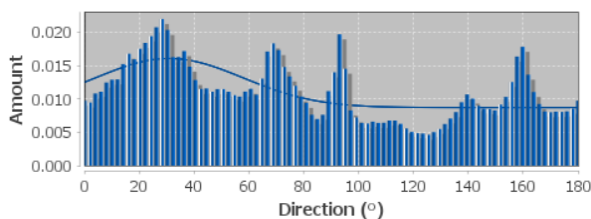
- Comparing the exposure conditions studied, one can verify that the kinetics of the reaction are influenced by relative humidity and temperature; both conditions lead to an increase in expansion rate and ultimate expansion. However, the potential of attaining very high ultimate expansion at elevated temperatures is limited by alkali leaching. Although the rise in temperature leads to improved kinetics, it conversely accelerates alkali leaching. Given that accelerated laboratory tests are being conducted to assess the reactivity potential of aggregates, an excessive increment of temperature could limit the realization of the full reactivity potential of aggregates.
- The Damage Rating Index is reliable for assessing ASR-induced deterioration in concrete irrespective of exposure conditions (e.g., moisture, and temperature). However, the DRI number alone is not sufficient to distinguish between damage at low RHs. Individual assessment of distress features has proven pivotal. Furthermore, the tool indicates different deterioration at low and high moisture levels. High moisture conditions are often limited to ASR-induced distress features. However, low moisture conditions show the occurrence of combined mechanisms.
- Mitigating ASR by reducing available moisture has often been used as a maintenance strategy for ASR-affected concrete. However, significant moisture reduction would result in shrinkage, especially at an early age. The DRI reliably verified the occurrence of shrinkage, and the tool can be used to decouple shrinkage from ASR-induced distress features.
- Elevated temperature has been well known to be influential in enhancing ASR kinetics. However, its role also influences the microstructure as well. Through the extended version of the DRI, it was possible to distinguish the influence of temperature on ASR-induced

crack properties. Concrete exposed to elevated temperatures (e.g., 60°C) experiences a rapid reaction, leading to many cracks. However, cracks generated at lower temperatures (e.g., 38°C) could be more significant, given their longer length and wider widths. The above differences highlight the possibility of having different inner damage even at similar expansion levels. This finding is essential for assessing ASR-affected concrete; assessments should not be limited to induced expansion.

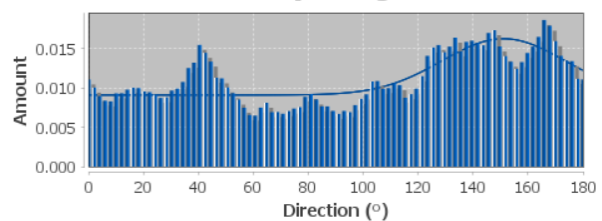
- Through the image analysis conducted in this study, it is safe to assume that while temperature can affect the width, length, and density of cracks in free expansion conditions, the orientation of cracks remains unchanged. They are always randomly distributed. However, the relative humidity might influence the location of cracks. At low RH, concrete experiences low moisture levels towards the outer surface; hence, most ASR activity occurs towards the middle of the concrete.
- Based on the assessment of the minimum moisture required to cause significant ASR-induced damage conducted in this study, the RH threshold appears to be dependent on temperature. This finding is essential to consider when deciding on proper ASR management techniques.

Supplementary materials

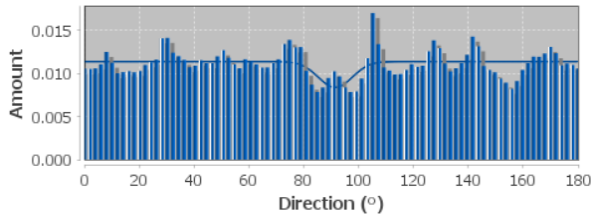
(a) 100% RH – 6 months



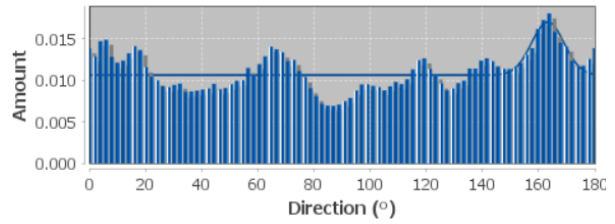
(b) 100% RH – 12 months



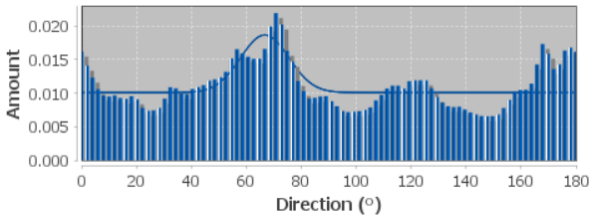
(c) 90% RH – 6 months



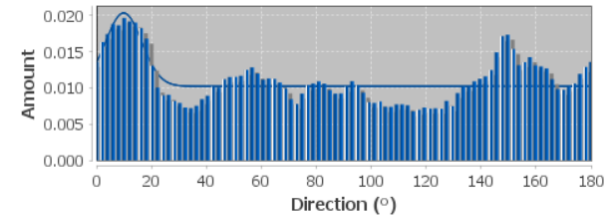
(d) 90% RH – 12 months



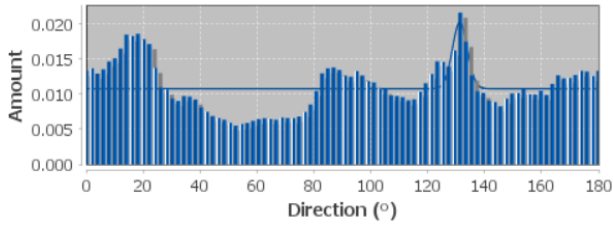
(e) 82% RH – 6 months



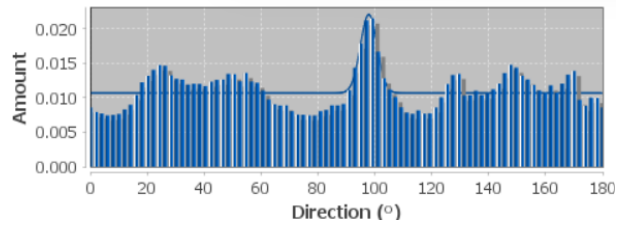
(f) 82% RH – 12 months



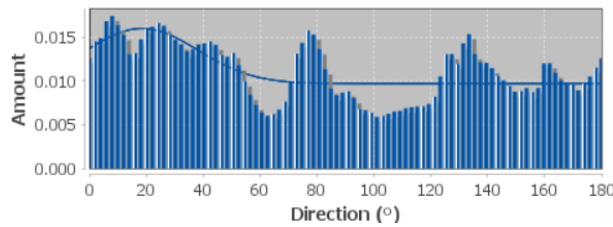
(g) 75% RH – 6 months



(h) 75% RH – 12 months



(i) 62% RH – 6 months



(j) 62% RH – 12 months

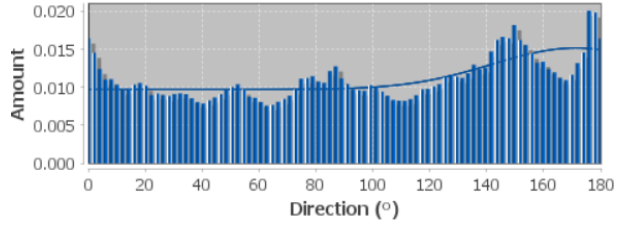
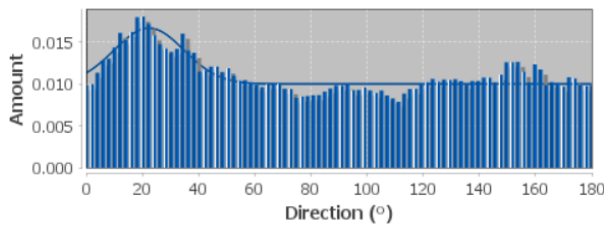
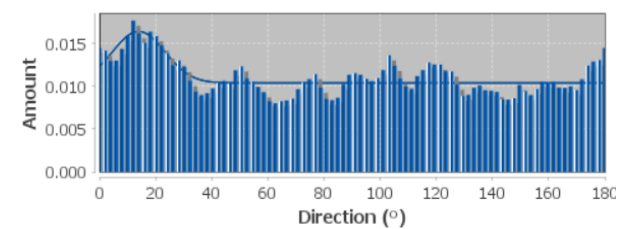


Figure S8.1: Directionality histogram at 21°C

(a) 100% RH – 6 months



(b) 100% RH – 12 months



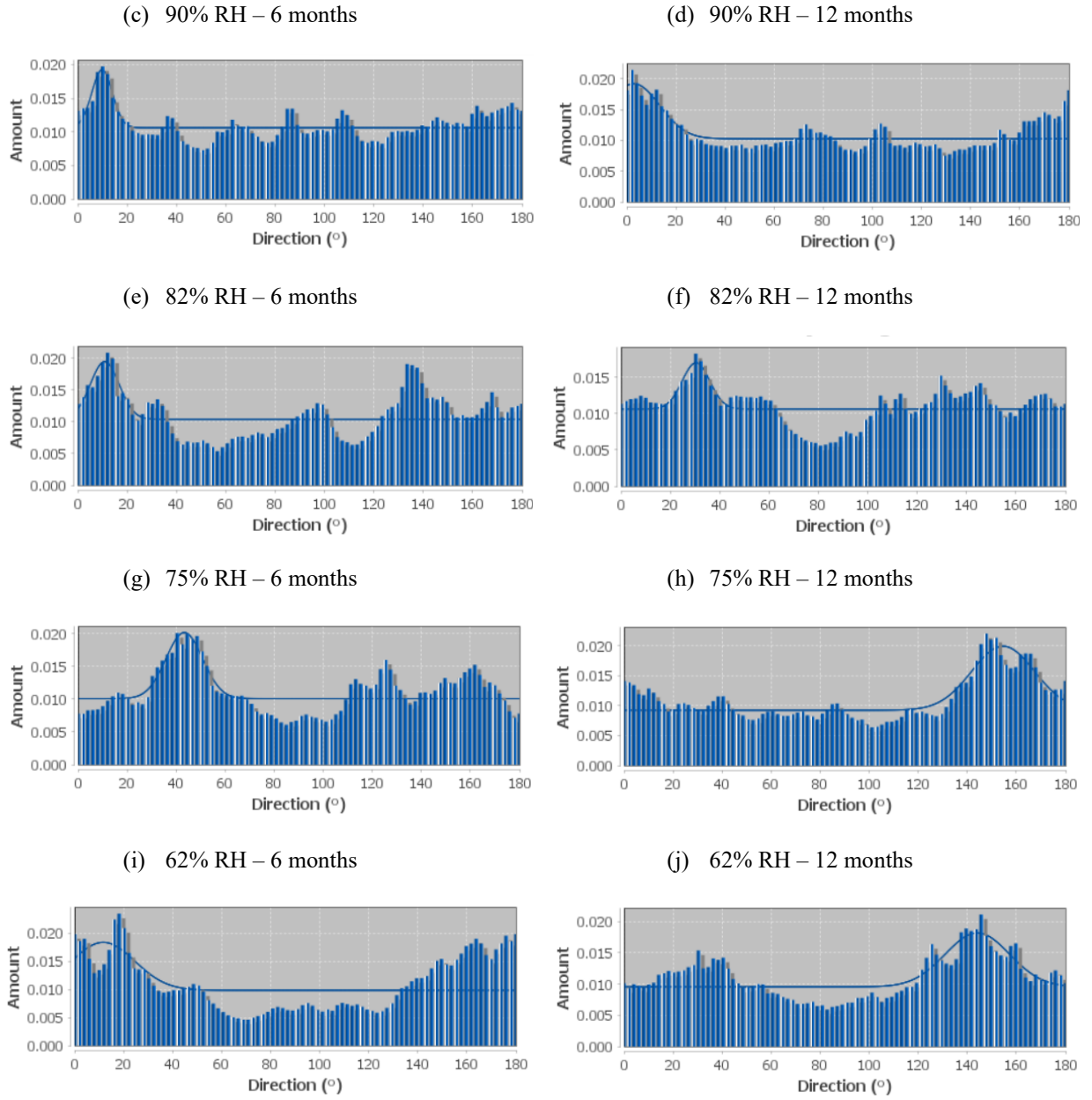
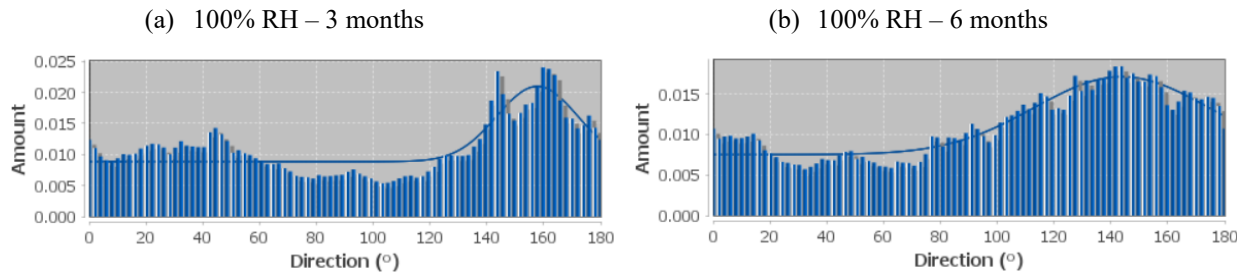


Figure S8.2: Directionality histogram at 38°C



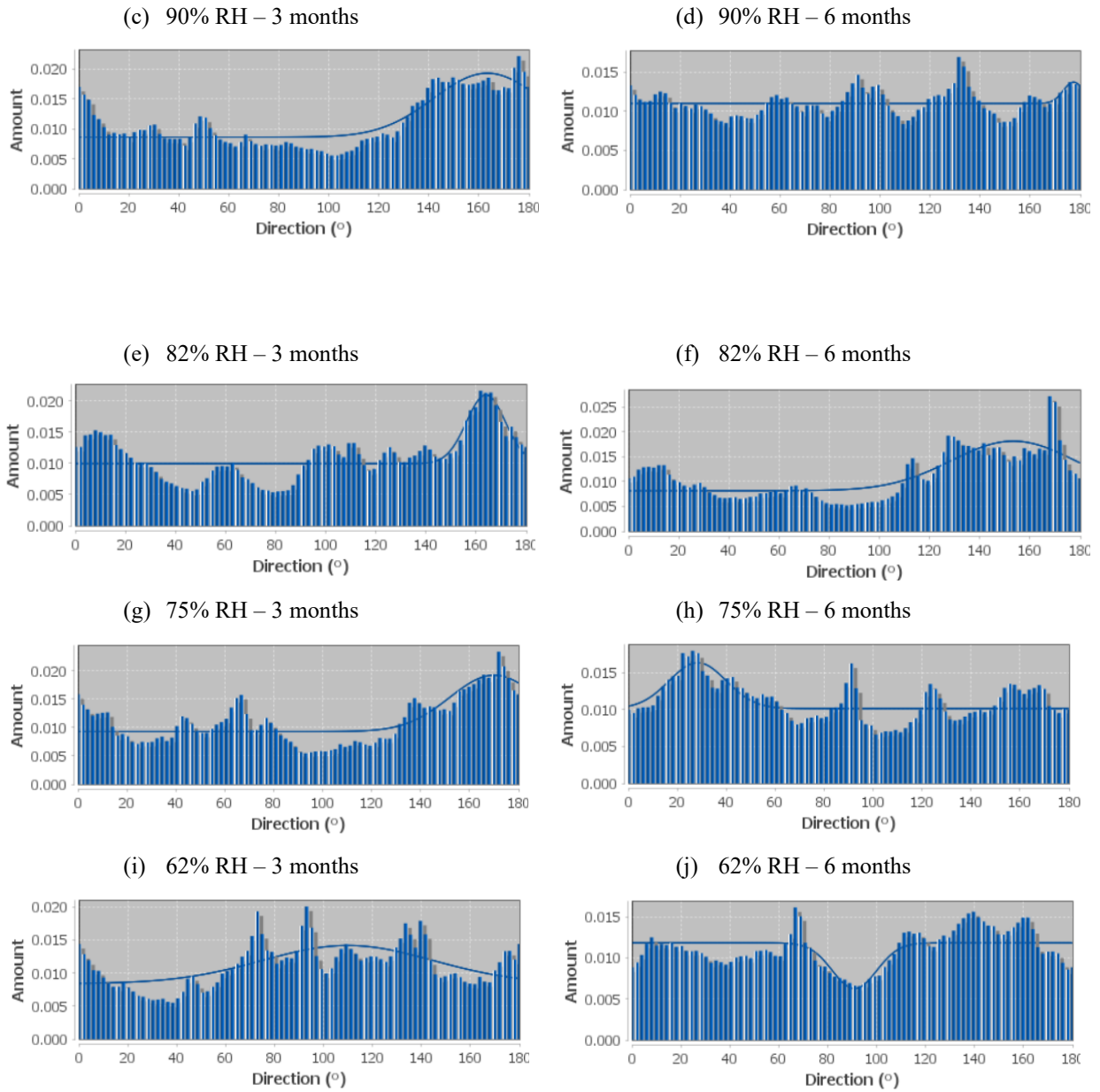


Figure S8.3: Directionality histogram at 60°C

Overview of chapter eight

Chapter eight discussed the microscopic assessment conducted to evaluate the influence of moisture and temperature on ASR development. The microscopic assessment was conducted using the Damage Rating Index (DRI) and image J. These exposure conditions were reported to influence the type, location and count of distress features, which can be attributed to the differences in mechanical properties reported in chapter seven.

**CHAPTER NINE: MULTILEVEL ASSESSMENT OF ASR-INDUCED DAMAGE
IN CONCRETE: EFFECTS OF RELATIVE HUMIDITY, TEMPERATURE,
AGGREGATE REACTIVITY AND ALKALI CONTENT**

Olusola Olajide ⁽¹⁾, Rennan Medeiros ⁽²⁾, Michelle Nokken ⁽³⁾, Leandro Sanchez ⁽⁴⁾

(1) Concordia University, Montreal/University of Ottawa, Canada, olusola.olajide@concordia.ca.

(2) University of Ottawa, Ottawa, Canada, rdasi077@uottawa.ca

(3) Concordia University, Montreal, Canada, m.nokken@concordia.ca

(4) University of Ottawa, Ottawa, Canada, leandro.sanchez@uottawa.ca

Abstract

Exposure conditions such as relative humidity and temperature, as well as alkali content and aggregate reactivity are deemed significant for ASR development. However, their assessment has focused on ASR-induced expansion, and little is known about their influence on deterioration. In this work, concrete specimens were manufactured in the laboratory incorporating aggregates of different levels of reactivity (i.e., moderate, high, and very-high) and containing two alkali levels (i.e., 3.82kg/m³ and 5.25kg/m³ Na₂O_{eq}). The specimens were conditioned at five relative humidities (i.e., 100%, 90%, 82%, 75%, and 62%) and three temperatures (i.e., 21°C, 38°C, and 60°C) and monitored for ASR expansion over time. A time-based assessment was conducted, and upon reaching the pre-defined age, the Damage Rating Index (DRI), Stiffness Damage Test (SDT), and compressive strength tests were conducted to assess ASR-induced damage in the specimens. Results showed that the influence of moisture, temperature, alkali content, and aggregate reactivity on damage outcomes (i.e., DRI, Modulus of elasticity, SDI, and compressive strength) varies. Moreover, these factors present quantitative (crack counts) and qualitative (crack type) changes to

the microstructure of affected concrete. Furthermore, it was observed that aggregate reactivity plays a more significant role in the minimum moisture required for critical ASR-induced damage.

Keywords: Alkali-Silica Reaction (ASR), Damage Rating Index (DRI), Stiffness Damage Test (SDT), Expansion, Damage, Moisture, Temperature, Aggregate reactivity

9.1 Introduction

Alkali silica reaction remains a crucial challenge to the durability and serviceability of concrete despite the vast existing research on its mechanism and mitigative measures [223]. Supplementary cementitious materials (SCMs) have been prominently incorporated in the construction of new infrastructure to prevent ASR [233–236], yet they only serve as a mitigative measure; ASR cannot be totally stopped when using reactive aggregates [237]. In fact, some SCMs have been reported to contain a high level of alkalis [80], which can potentially enhance ASR kinetics. Moreover, traditional SCMs like fly ash and blast furnace slag are facing a shortage [238,239], leading to ongoing research on discovering new alternative materials [238,240]. Given these challenges, the most reliable strategy for mitigating ASR remains avoidance or reduction in the availability of one or more of the factors responsible for the reaction (i.e., reactive silica, moisture, and alkali). Among these factors, moisture control can be considered the easiest, especially where there is an abundance of reactive aggregates and conventional cement containing high alkali content. Several studies have evaluated the role of moisture in the reaction, and numerous minimum moisture requirements for the initiation of ASR have been identified [8,10,13,22–27]. The minimum moisture condition (i.e., RH threshold) has often been reported to be dependent on temperature or aggregate reactivity [10,48]. However, these assessments have been focused on expansion assessment, disregarding the overall ASR-induced damage. This study aims to evaluate the role of moisture, temperature, alkali content, and aggregate reactivity using comprehensive multi-level

assessment techniques involving microscopic and mechanical properties reduction to further our understanding of ASR-induced damage. Furthermore, the paper seeks to establish a damage-based assessment of the RH threshold required to trigger ASR.

9.2 Background

9.2.1 ASR-induced development

Alkali silica reaction (ASR) is a widely known chemical reaction in concrete that can cause premature distress and lead to loss of serviceability in affected structures. Since its identification in the late 1930s, extensive research has been carried out for a better understanding of the mechanisms involved while also developing ways to prevent and manage already affected concrete [102,200,223]. ASR involves a chemical reaction initiated when poorly crystallized siliceous phases within the aggregate are exposed to alkalis present in the concrete pore solution [100,224], generating an expansive product (i.e., ASR gel). Most studies in the literature describe the ASR gel imbibing water, expanding, and exerting pressure on the surrounding matrix, leading to the generation of micro-cracks that propagate to cause severe durability and serviceability challenges as expansion increases. The reaction has been reported to initiate within the aggregate particles and propagate into the cement paste with a rise in expansion, as shown in Fig. 9.1 [6].

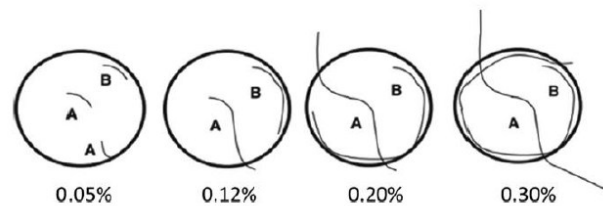


Figure 9.1: Qualitative model for crack propagation in ASR-affected concrete[6] (reproduced with permission of Elsevier)

9.2.2 Effect of moisture and temperature on ASR

The influence of high moisture and temperature in ASR is well-documented [8–16]. Both factors aid the transport of ions involved and the formation of ASR gel, leading to high ultimate expansion. On the other hand, low moisture conditions typically lead to a dramatic reduction in expansion. Hence, reducing available moisture has been recommended to mitigate ASR. Moisture has often been quantified using relative humidity (RH), and a threshold below 80% RH has been widely accepted as a requirement to limit ASR despite lower values cited in the literature [8,13]. Additionally, temperature, although not typically considered one of the primary factors for ASR (i.e., alkalis, silica, moisture), can influence the availability of these factors [229], the structure of ASR gel [58,107], and the expansion rate [103,111]. Furthermore, the temperature has been noted to influence the RH threshold needed for ASR. For instance, an RH threshold of 83%RH required at 23°C can fall to 73% RH upon a temperature rise to 38°C [13]. Similarly, other studies [25,26] have reported a similar reduced threshold at 40°C. The threshold could, however, be as low as 59% RH at 60°C, according to [10].

9.2.3 Effect of aggregate reactivity level and alkali content on ASR

Aggregates consist of a variety of mineral constituents. Among the reactive forms of silica are cristobalite, chalcedony, opal, and tridymite [241,242]. These forms possess high reactivity potential due to their amorphous or poorly crystalline nature, facilitating alkali penetration and ASR initiation. Furthermore, weathered feldspars found in aggregates can contribute to ASR by releasing alkali into the pore solution and exacerbating ASR [243,244]. Similarly, volcanic glasses, with their high silica content and amorphous structure, also display high reactivity in ASR [245,246]. The varying presence of these mineral constituents, among others [246] in aggregates, leads to different reactivity potentials. Consequently, aggregates used in construction, especially

those prone to ASR, have been classified into different groups based on their reactivity levels. For instance, reactive aggregates can be distinguished into nonreactive, moderately, highly, and very highly reactive aggregates based on their performance in accelerated laboratory tests such as ASTM C1260 and ASTM C1293 [247,248]. Typically, the rate and ultimate expansion increases with a rise in reactivity level. As a result, it could be safe to assume that aggregates with different levels of reactivity would require different proportions of alkali and moisture to initiate the ASR. For instance, very highly reactive aggregates might require lower alkali content in the pore solution to generate ASR gel. Furthermore, the expansive potential of the resulting gel might allow for subsequent expansion even in a low moisture environment. Hence, some studies claim that the RH threshold needed for ASR depends on aggregate reactivity [48]. On the other hand, alkali content is critical for initiating the reaction. All the existing accelerated laboratory tests for assessing the reactivity potential of aggregates are based on boosted alkali concrete mixtures. Hence, limiting the alkali content in concrete's pore solution has been proven promising in mitigating ASR [106].

As illustrated in Table 9.1, varying RH thresholds have been widely reported. Despite that, 80% RH has been widely suggested. Considering the reviewed studies, the 80% RH threshold would be effective at low temperatures and for moderately/borderline reactive aggregates. However, given the enhanced kinetics at high temperatures and highly/very highly reactive aggregates, a lower threshold might be required to mitigate the reaction. Nevertheless, a conclusion based on the reviewed studies can be nuanced since variability exists among the studies based on the test conditions (i.e., specimen sizes, temperature, alkali level, relative humidity, and reactive content type [i.e., mortar versus concrete]). Hence, to thoroughly examine how temperature and aggregate reactivity influence the moisture threshold for ASR, a comprehensive study under similar testing conditions is essential.

Table 9.1: Relative humidity thresholds

Reference	Reactive content	Sample size	Exposure conditions	Comments
[13]	Washed Hvalfjordur sand	25 x 25 x 285mm	23°C: 83-100% RH 38°C: 73-100% RH	RH threshold of 73% is required at 38°C. However, 83% RH is needed to attain 0.04% expansion at 23°C.
[26]	Andesite	75 x 75 x 400mm	40°C: 75-100% RH	Specimens in all RH conditions displayed significant expansion after 52 weeks of storage at 40°C. Hence, more than 75% RH is required to achieve the expansion threshold
[48]	Rhyolitic tuff	75 x 75 x 285mm	38°C: 70-100% RH	Expansion of 0.04% was reached at 70% RH. Hence, an RH lower than 70% is required to mitigate the reaction
	Spratt limestone			About 0.06% expansion was attained at 70% RH; as such, the aggregate type required much lower than 70% RH for mitigative measures
	Potsdam sandstone			Specimens containing this aggregate type expanded 0.00% at 80% RH and 0.06% at 90% RH. This aggregate type requires between 80 – 90% RH to mitigate ASR
	Siliceous limestone			70% RH and 80% RH attained expansions of -0.01% and 0.02%, respectively. However, 90% RH reached a high ultimate expansion of 0.145%. Hence, 80-90% RH is the minimum threshold.
[10]	Reactive limestone	20 x 160mm	60°C: 59-100% RH	All conditions expanded beyond 0.04% after 100 days of exposure. 59% RH achieved an expansion of 0.06%. Hence, the threshold for the aggregate at this temperature is lower than 59% RH
[8]	Very highly reactive siliceous sand	75 x 75 x 285mm	21-40°C: 74-100%RH	21°C: ultimate expansion at 75.5% RH is lower than 0.04%. However, 85% RH and above attained expansions greater than 0.04%. So, the threshold is higher than 75.5% RH. 30 and 40°C: all conditions from 74.6% and above reached ultimate expansions

				significantly higher than 0.04%. the lowest ultimate expansion was ~0.25% in 74.6% at 40°C. Hence, the threshold is lower than 74.6% RH
	Borderline reactive river sand		21-40°C: 49-100%RH	Ultimate expansion increases with RH and temperature. However, none of the conditions attained up to 0.04% expansion.
[93]	Very highly reactive sand (Texas)	75 x 75 x 285mm	20-40°C: 65 – 100% RH	The threshold for this aggregate falls around 75% RH in specimens stored at 30°C which reduces to around 70% RH at 40°C. Interestingly, specimens stored at 20°C failed to attain 0.04% across all RH considered.

9.2.4 Tools for assessing ASR-induced damage

All available studies on the role of exposure conditions and aggregate reactivity level on ASR and moisture threshold have been limited to expansion measurements, limiting the comprehensive understanding of the role of these factors on induced damage. Recent studies [133,249] have emphasized the need to correlate ASR-induced expansion with microscopic properties, modulus of elasticity loss, and reductions in mechanical properties for a comprehensive understanding of ASR-induced deterioration. Several tools exist for such assessment, including the multi-level assessment protocol that includes the Stiffness Damage Test (SDT), Damage Rating Index (DRI), and other mechanical property tools. The reliability of such a protocol has been widely reported [120,121,250,251] and well described in chapters seven and eight of the thesis.

9.2.5 Scope of work

Alkali silica reaction is often described as a result of a ternary interaction among unstable siliceous mineral phases, alkalis, and sufficient moisture, with temperature playing a critical role in the kinetics. Most of the available research has been limited to the influence of individual or a

combination of some of these factors on ASR kinetics (i.e., expansion) with limited emphasis on ASR-induced deterioration. Furthermore, moisture limitation has been effective in maintaining ASR-affected concrete, but varying RH thresholds have been reported. Even so, such assessment remain rooted only in ASR-induced expansion. Hence, this study aims to fill this gap by conducting a comprehensive assessment involving all these factors on the kinetics of ASR and induced damage. A testing matrix was designed incorporating three aggregates of different reactivity levels (i.e., moderately, highly, and very highly reactive), two alkali loadings (i.e., 3.82 kg/m³ and 5.25kg/m³ Na_2O_{eq}), five relative humidity conditions (i.e., 100% RH, 90% RH, 82% RH, 75% RH, and 62% RH), and three temperatures (i.e., 21°C, 38°C, and 60°C). Length changes were monitored over twelve months for specimens stored at 21°C and 38°C, while those stored at 60°C were monitored for six months. At 3 and 6 months (i.e., for 60°C) and 6 and 12 months (i.e., for 21°C and 38°C), specimens were collected for damage assessments (i.e., DRI, SDT, and compressive strength). A time-based and expansion-based damage assessment was conducted, considering the influence of moisture, temperature, alkali content, and aggregate reactivity and finally, a damage-based moisture threshold required for ASR was evaluated.

9.3 Materials and method

9.3.1 Statistical design of experiment (DOE)

The statistical DOE was implemented to investigate the effects of four variables (i.e., alkali content, aggregate reactivity, relative humidity [RH], and temperature) on the development of ASR-induced expansion and deterioration. Due to practical constraints, a partial factorial design was employed, excluding certain combinations that were impractical for this study based on the following considerations:

- For instance, Sudbury (i.e., moderately reactive aggregate) containing a low alkali content was not exposed to low RH conditions at 21°C because of its low reactivity. The reaction would not reach a significant level of expansion and deterioration within the time frame of this project.
- Springhill was not exposed to 60°C due to its very highly reactive potential.

These considerations resulted in a partial factorial design of 2x3x5x3 – (exclusions) with the following variables and factors in Table 9.2. In total, 52 combinations were experimentally tested out of 90 possibilities.

Table 9.2: Factors and associated level for the design of experiment

Factors/Levels	1	2	3	4	5
Alkali content	Boosted (5.25 kg/ <i>m</i> ³ <i>alkalis</i>)	Non-boosted - NB (3.82 kg/ <i>m</i> ³ <i>alkalis</i>)	----	----	----
Aggregates	Springhill – SPH (Very highly reactive)	Spratt – SP (Highly reactive)	Sudbury – SB (Moderately reactive)	----	----
Relative humidity (RH)	100% RH	90% RH	82% RH	75% RH	62% RH
Temperature	60°C	38°C	21°C	----	----

9.3.2 Materials

Seven concrete mixtures were manufactured in the laboratory using a mix design based on the concrete prism test (i.e., ASTM C1293). Three reactive coarse aggregates (i.e., Sudbury - moderately reactive; Spratt - highly reactive; and Springhill - very highly reactive), one

nonreactive coarse aggregate (crushed limestone), and one nonreactive fine aggregate (i.e., manufactured sand) were used. Table 9.3 provides information on the different aggregates used in this study. All mixes contained conventional Portland cement (i.e., CSA Type GU equivalent to ASTM type I) with a total alkali content of 0.86% Na_2O_{eq} by mass of cement. Concrete with two alkali levels were prepared: boosted and non-boosted (i.e., NB), each containing 5.25 kg/m^3 and $3.82 \text{ kg/m}^3 Na_2O_{eq}$, respectively by adding NaOH pellets to the mixing water. Table 9.4 displays the mix proportions for all mixtures.

Table 9.3: Aggregates used in the study

Aggregates		Location	Rock Type	Specific gravity	Absorption capacity	AMBT exp. [ASTM C1260]
Coarse	Sudbury	Canada	Greywacke and argillite	2.59	0.60	0.23
	Spratt		Siliceous limestone	2.70	0.62	0.31
	Springhill		Greywacke and argillite	2.68	0.70	0.33
	Non-reactive limestone		Limestone	2.78	0.42	0.02
Fine	Manufactured sand	2.76		0.65	0.04	

Table 9.4: Characteristics of the seven mixtures

Mixture		Cement (kg/m^3)	Water (kg/m^3)	Coarse aggregate (kg/m^3)			Fine Aggregate (kg/m^3)	Alkali loading (kg/m^3)
				4.75-9.5mm	9.5-12.5mm	12.5-19mm		
Sudbury (SB)	Boosted	420	177.40	324.86	324.86	333.70	799.52	5.25
	Non boosted (NB)							3.82

Spratt (SP)	Boosted			334.12	334.12	344.24	833.46	5.25
	Non boosted (NB)							3.82
Springhill (SPH)	Boosted			330.15	330.15	340.15	822.98	5.25
	Non boosted (NB)							3.82
Non-reactive (NR)				328.58	328.58	338.53	855.17	5.25

To perform an extensive study of the role of numerous exposure conditions and reactivity of aggregates on ASR development, five relative humidity conditions (i.e., 62% RH, 75% RH, 82% RH, 90% RH, and 100% RH) and three temperatures (i.e., 21, 38, and 60°C) were selected for this study. The relative humidity conditions were targeted and maintained using saturated salt solutions, as used by Poyet et al. [10]. Specific salt solutions for distinct RH/temperature setups were selected from ASTM E104, as presented in Table 9.5. Sensors were inserted into the storage buckets to monitor the RH and temperature over time. Specimens at 21°C and 38°C were stored for 12 months based on the concrete prism test (CPT), while the specimens at 60°C were conditioned for 6 months following the accelerated concrete prism (ACPT).

Table 9.5: Control of relative humidity

RH/Temperature	21°C	38°C	60°C
100%	Distilled water	Distilled water	Distilled water
90%	Barium chloride	Potassium nitrate	Potassium sulfate
82%	Ammonium sulfate	Potassium chloride	Potassium nitrate
75%	Sodium chloride	Sodium chloride	Sodium chloride
62%	Sodium bromide	Sodium nitrite	Sodium nitrite

Eight hundred and eighty-five (885) 100mm x 200mm concrete cylinders were fabricated. After casting, the specimens were de-molded and moist-cured at room temperature for 48 hours; holes

were drilled on both ends, and studs were installed using a fast-setting cement slurry during the first 24 hours. The initial length readings were conducted at 48 hours, and specimens were ready for storage. Concrete specimens were placed in sealed buckets, each containing four concrete cylinders, and a minimum of 12 specimens were prepared for each RH (i.e., a minimum of three buckets per RH) at each temperature for every aggregate type. The buckets at 100% RH have distilled water at the bottom to control RH, while water was replaced with the respective saturated salt solution as per ASTM E104 for RHs lower than 100%, as highlighted in Table 9.5. Length change measurements were carried out for 12 months (i.e., 21°C and 38°C) or 6 months (i.e., 60°C).

9.3.3 Experimental Methods

9.3.3.1 Stiffness Damage Test (SDT)

The SDT procedure adhered to the methodology proposed by Sanchez et al. [138], which involved subjecting concrete specimens to five loading/unloading cycles at a controlled rate of 0.10 MPa/s, with a maximum load equivalent to 40% of the 28-day concrete compressive strength. Tests were conducted after 6 and 12 months (i.e., for specimens conditioned at 21°C and 38°C) and after 3 and 6 months (i.e., for those stored at 60°C). Before the initiation of the test, specimens from each condition were stored in a humid environment at room temperature for 48 hours as per [138]. Each end of the specimens was mechanically ground to ensure a flat surface. Given the similarities between the SDI and PDI values, this study only presents the SDI results based on an average of three specimens, similar to the modulus of elasticity.

9.3.3.2 Damage Rating Index (DRI)

This study conducted a microscopic evaluation involving the conventional and extended Damage Rating Index (DRI). A time-based assessment was selected to monitor the evolution of ASR-induced expansion and damage. The concrete specimens conditioned at 21°C and 38°C were tested

at 6 and 12 months. The 60°C specimens were, however, assessed after 3 and 6 months. Before the assessment, a specimen at each predetermined age was longitudinally cut in half. One half was polished using a mechanically operated table polish with grit sizes 30, 60, 120, 240, 600, 1200, and 3000. A square grid of 1cm² was drawn on the polished surface, and the DRI was conducted using a stereomicroscope at a magnification of 16x. Considering one square at a time, the number of each damaged feature is counted as shown in Fig. 9.2. The sum of the total count per feature is multiplied by weighting factors specified by Villeneuve and Fournier [45]. The final DRI number was obtained by normalizing the grand sum of the weighted crack count to 100 cm². The extended version of the DRI was conducted without multiplying the weighting factors. Hence, the microscopic features are reported as counts.

Distress feature	Description	Weighting factor
CCA	Closed crack in aggregate	0.25
OCA	Opened crack in aggregate	2
OCA_RP	Opened crack in aggregate with reaction product	2
CAD	Debonded aggregate	3
DAP	Disaggregated/corroded aggregate particle	2
CCP	Crack in the cement paste	3
CCP_RP	Crack in the cement paste with reaction product	3

Figure 9.2: Distress features with corresponding weighting factors [140]

9.3.3.3 Compressive strength

The 28-day compressive strength of the concrete mix utilized in this study was assessed by employing the maturity concept due to the reactivity potential of the aggregate, which could potentially trigger ASR at room temperature and above, thereby impacting the strength of the concrete. Six concrete specimens from each aggregate type were enclosed in a plastic wrap and stored at 12°C for 47 days, after which they were tested (the maturity is equivalent to 28 days at

standard temperature). To assess compressive strength reductions, the specimens tested for SDT underwent an additional 48-hour reconditioning at 21°C as per [138], this approach was facilitated by the non-destructive nature of the SDT.

9.4 Results

9.4.1 ASR kinetics

ASR-induced expansion (i.e., after accounting for the shrinkage measured from non-reactive aggregate specimens) of concrete cylinders incorporating aggregates of different levels of reactivity (i.e., Sudbury[SB], Spratt[SP], and Springhill[SPH]) containing two alkali levels (i.e., 3.82kg/m³ and 5.25kg/m³Na₂O_{eq}) tested at 21°C, 38°C, and 60°C under numerous relative humidity conditions (i.e., 100%, 90%, 82%, 75%, and 62%) were measured to evaluate the effect of these factors on ASR kinetics. The “NB” in some condition’s identification (e.g., 100%RH-NB) means a concrete mixture with non-boosted alkali content (i.e., 3.82kg/m³Na₂O_{eq}).

9.4.1.1 Concrete cylinders conditioned at 21°C and 38°C

Fig. 9.3a, c, and e show the ASR-induced expansion results of concrete cylinders containing Sudbury, Spratt, and Springhill with two alkali levels stored under numerous RH at 21°C. Generally, in each aggregate type, ASR-induced expansion increases with RH at each alkali level, and the highest ultimate expansions were recorded at the highest RH and higher alkali levels.

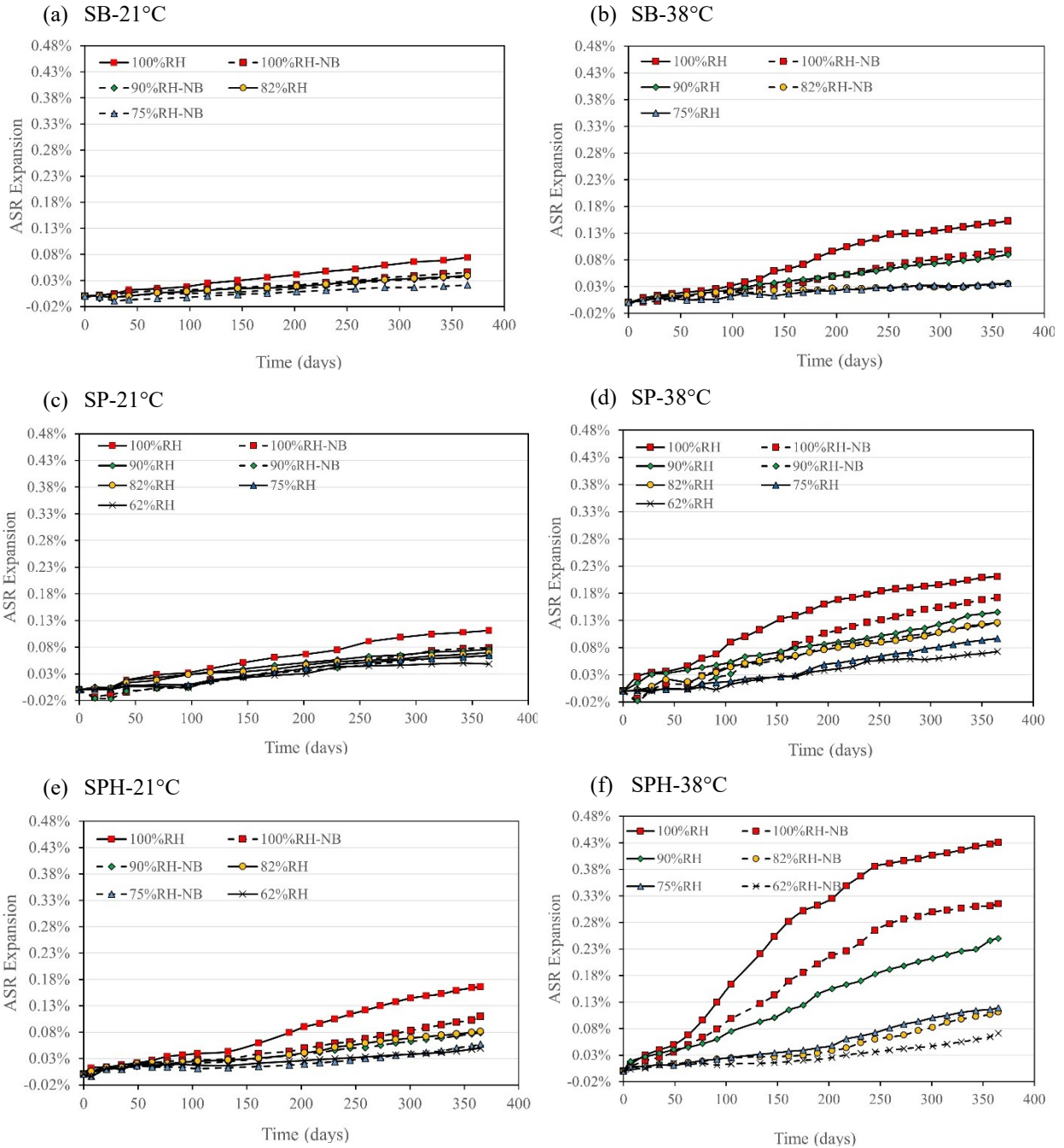


Figure 9.3: ASR expansions results at 21°C and 38°C: (a) Sudbury-21°C (b) Sudbury-38°C (c) Spratt-21°C (d) Spratt-38°C (e) Springhill-21°C (f) Springhill-38°C

As shown in Fig. 9.3a, the highest ultimate expansion for concrete cylinders containing Sudbury was recorded at 100% RH, with 0.074% expansion after 365 days. Notably, 90%RH-NB and 82%RH registered similar ultimate expansion, highlighting a possible compensatory effect between alkali level and RH. Similarly, concrete specimens containing Spratt reactive aggregates

present a similar trend at a similar duration but with higher ASR-induced expansion. The expansion trend in Springhill containing specimens behaved similarly to other aggregates, but the reaction was more aggressive than others, especially at high RH conditions.

The kinetics of the reaction is significantly enhanced with a rise in temperature to 38°C. However, the trends are similar to that presented at 21°C. Fig. 9.3b shows the 365-day expansion in concrete cylinders with Sudbury aggregates. The highest ultimate expansion was recorded at 100% RH with 0.153% expansion recorded, which is more than double that at 21°C. A similar trend can be observed in other aggregates, with Springhill presenting an exponential increase in expansion compared to other aggregates. Notably, concrete specimens containing Spratt and Springhill attained similar ASR-induced expansion at 62% RH. Hence, the likelihood that a rise in the reactivity level of the aggregates may not influence the reaction at low moisture conditions.

9.4.1.2 Concrete cylinders conditioned at 60°C

The 60°C setups were conducted for a lower duration of 182 days and were limited to Sudbury and Springhill, as mentioned earlier. Overall, the kinetics of the reaction are significantly influenced at this temperature, with higher expansion levels attained compared to 21°C but lower than 38°C in both aggregates as shown in Fig. 9.4.

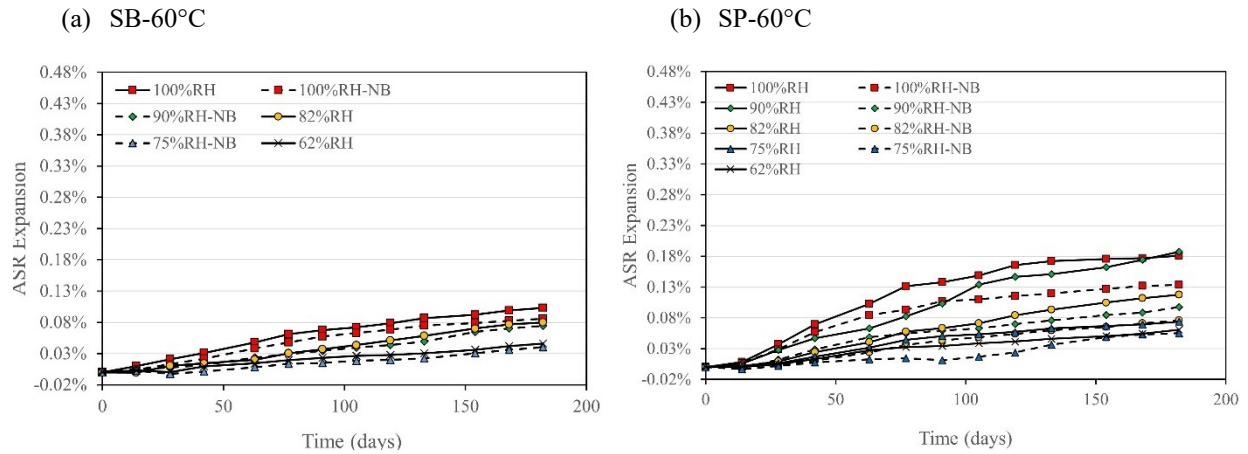


Figure 9.4: ASR expansions results at 60°C: (a) Sudbury-60°C (b) Spratt-60°C

The increase in temperature does not change the alkali and RH compensatory effect recorded at lower temperatures. Considering the expansion results, as presented in Fig. 9.4, at low alkali levels (i.e., NB), the apparent trend of an increase in expansion with a rise in RH remains true. However, specimens containing Spratt conditioned at 90% RH at high alkali levels attained a slightly higher expansion than at 100% RH, which can be attributed to alkali leaching.

Overall, RH, alkali, and aggregate reactivity levels are essential in induced expansion. The increase in these factors often leads to enhanced kinetics and higher expansions, especially at high moisture conditions. However, this may not hold true at very low RH, like 62%RH. Some compensatory effects exist between the factors, especially alkali and relative humidity. Interestingly, no significant plateau in expansion was recorded at 21°C compared to 38 and 60°C.

9.4.2 Stiffness Damage Test (SDT)

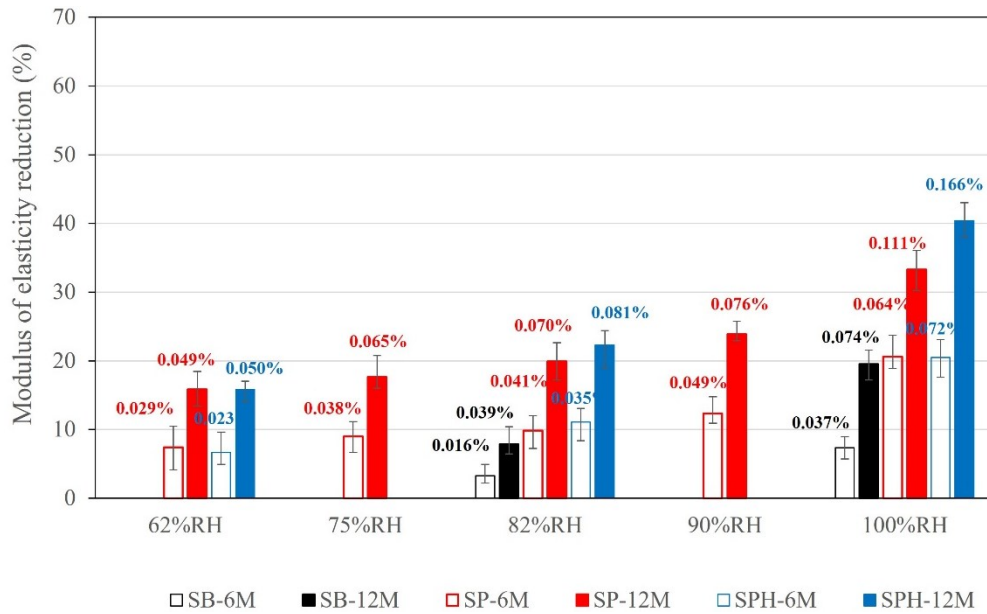
Each data point presented in this section represents an average result obtained from three concrete specimens incorporating aggregates of different reactivity levels containing two alkali levels stored at three temperatures and five relative humidity and tested at the proposed testing ages. The error bars highlight the range from the minimum to the maximum measured values, representing the

observed variability in the results. Moreover, the percentage value above each bar indicates the corresponding ASR-induced expansion for each condition.

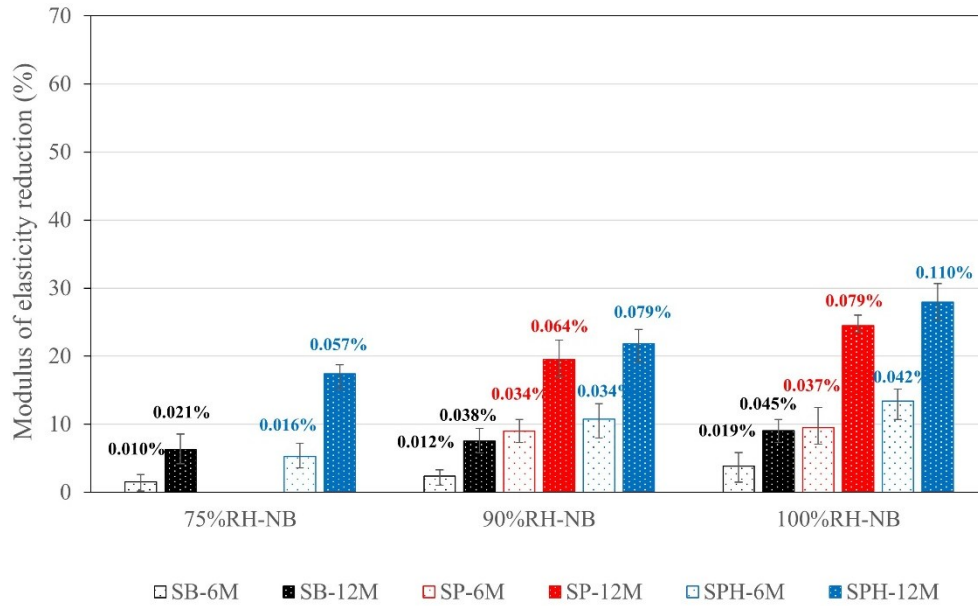
9.4.2.1 Modulus of elasticity reduction (MER)

Analyzing the modulus of elasticity reduction in Fig. 9.5, one notices that the higher the RH, the higher the modulus of elasticity reduction, with the highest modulus loss achieved at 100% RH.

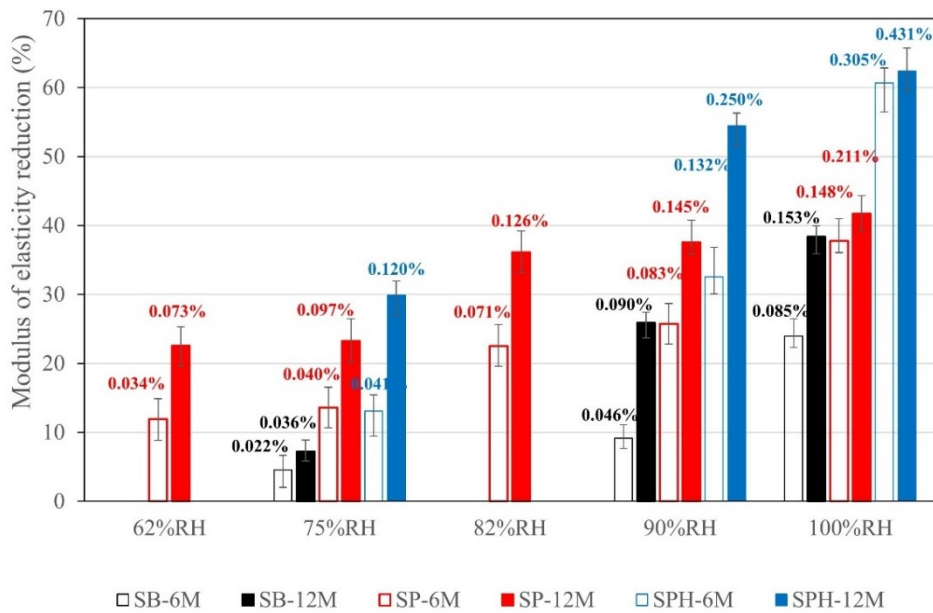
(a) 21°C - boosted alkalis



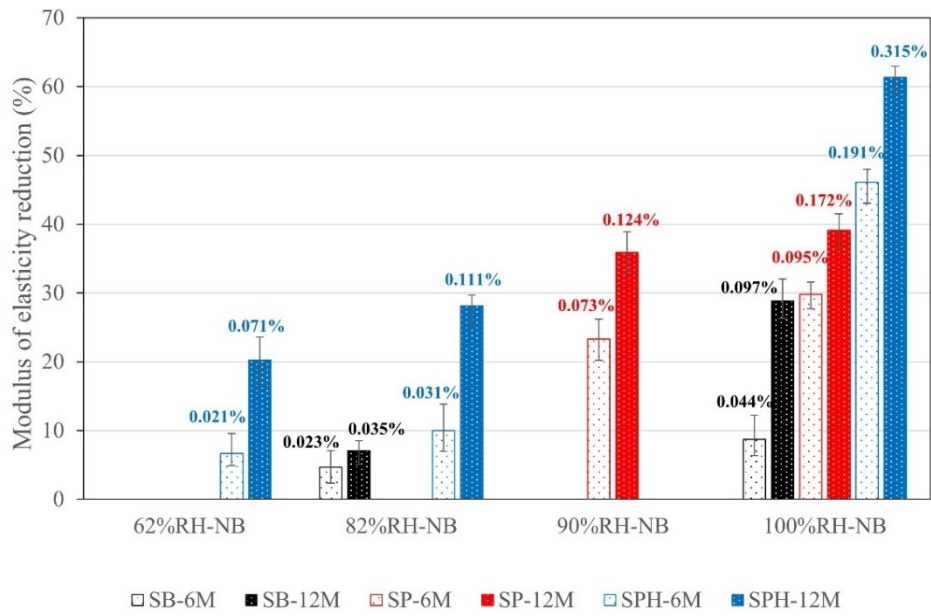
(b) 21°C - non-boosted alkalis (NB)



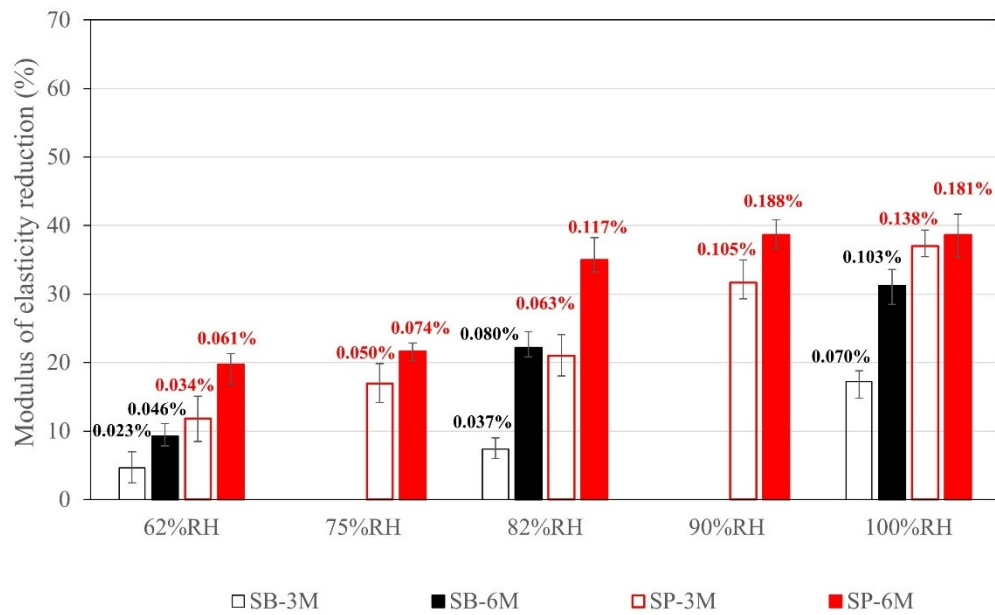
(c) 38°C - boosted alkalis



(d) 38°C - non-boosted alkalis (NB)



(e) 60°C - boosted alkalis



(f) 60°C - non boosted alkalis (NB)

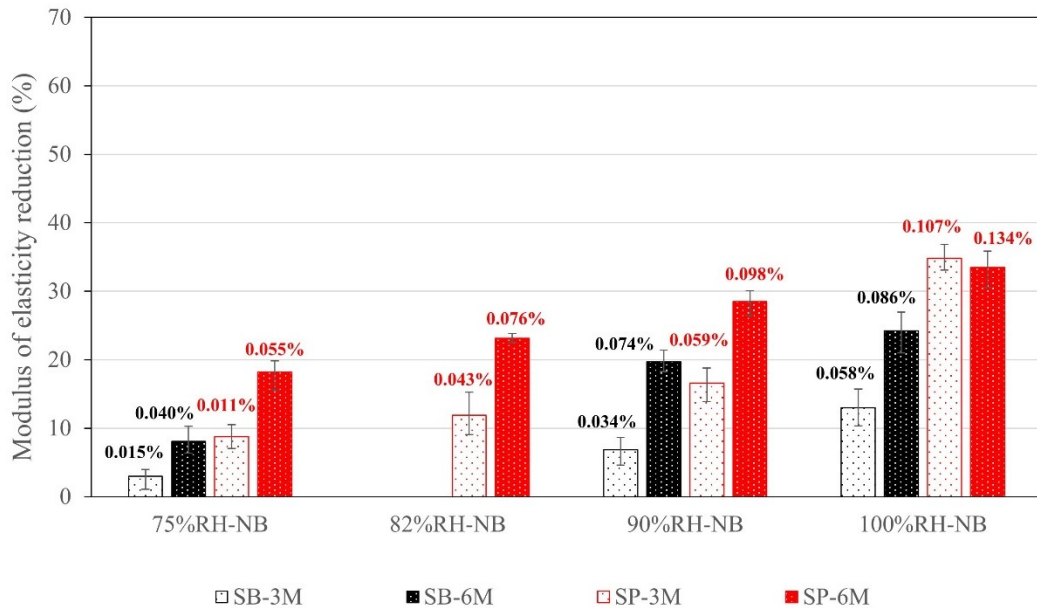


Figure 9.5: Modulus of elasticity reduction as a function of time, relative humidity and aggregates: (a) 21°C-boosted alkalis (b) 21°C-non-boosted alkalis (c) 38°C-boosted alkalis (d) 38°C-non-boosted alkalis (e) 60°C-boosted alkalis (f) 60°C-non-boosted alkalis

Considering the specimen containing Sudbury conditioned at 21°C as displayed in Fig. 9.5a and b, all conditions except 100% RH experience a $\leq 10\%$ reduction in modulus throughout the study. It is essential also to note in these exact figures that the change in alkali level from 3.82kg/m^3 to 5.25kg/m^3 Na_2O_{eq} at 100% RH condition could lead to up to 10% loss in modulus of elasticity loss. Comparing these results to Spratt and Springhill at the same temperature, Springhill-containing specimens attained the highest reductions. Furthermore, specimens containing Springhill and Sudbury stored at 62% RH present similar ME loss, replicating the earlier identified relationship in the expansion plots.

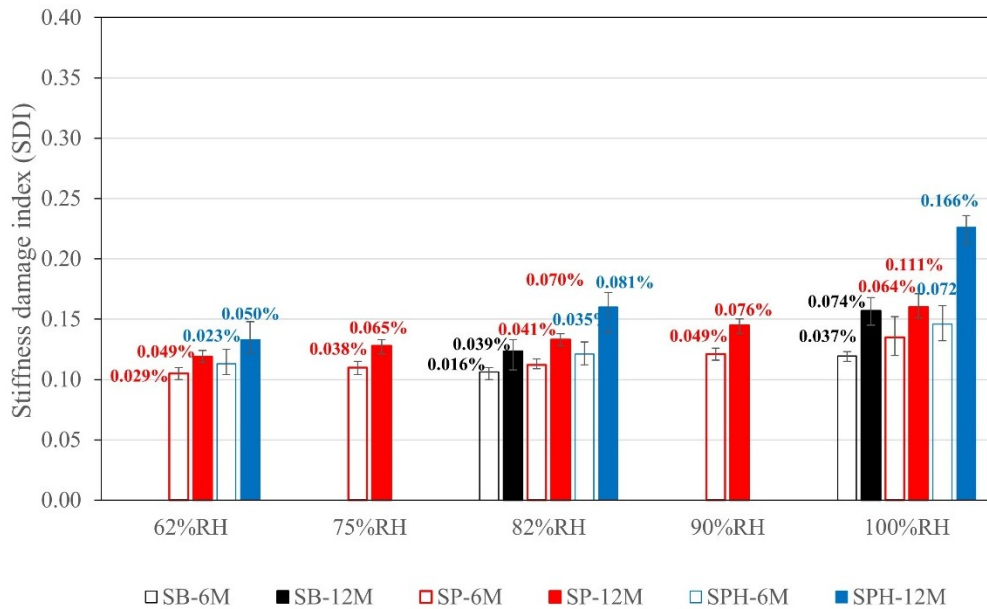
Concrete specimens conditioned at 38°C, especially those at high RH conditions, all attained higher ME losses for all concrete mixtures than their counterparts at 21°C. As Fig. 9.5c and d display for Sudbury, 100% RH attained close to 40% Modulus loss compared to 20% for the same RH at 21°C. An interesting observation can be made upon a further increase in temperature to

60°C. While the trend of increase in modulus loss with an increase in RH remains true, most conditions attained similar or lower reductions than specimens conditioned to 38°C.

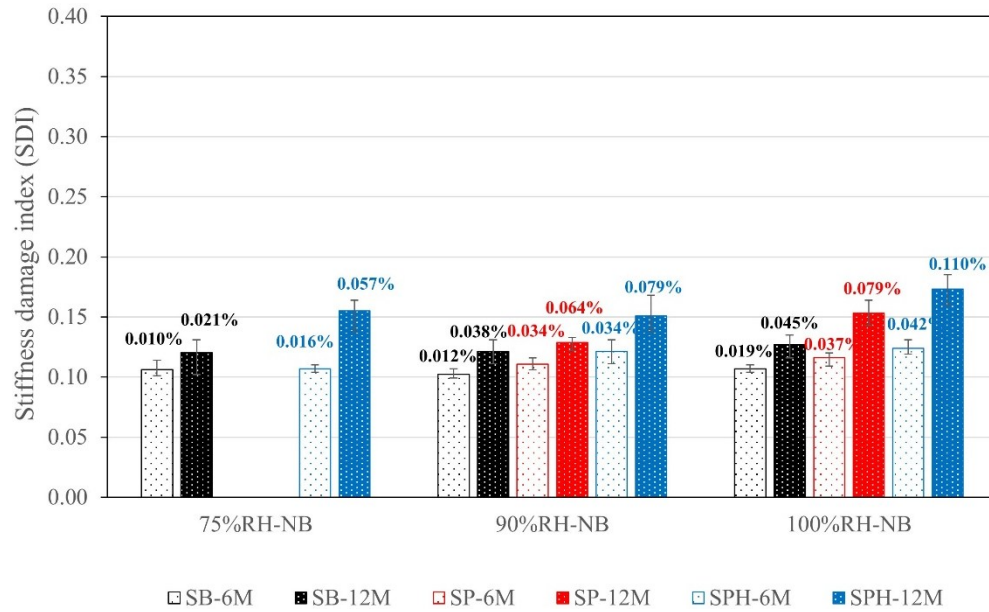
9.4.2.2 Stiffness Damage Index (SDI)

As shown in Fig. 9.6 a and b for concrete specimens containing Sudbury stored at 21°C, the average SDI values at 6 months are in the range of 0.102 – 0.120, which increases to 0.120 – 0.157 after 12 months. All RHs lower than 100% (i.e., 75% - 90%) attained similar SDI throughout the study.

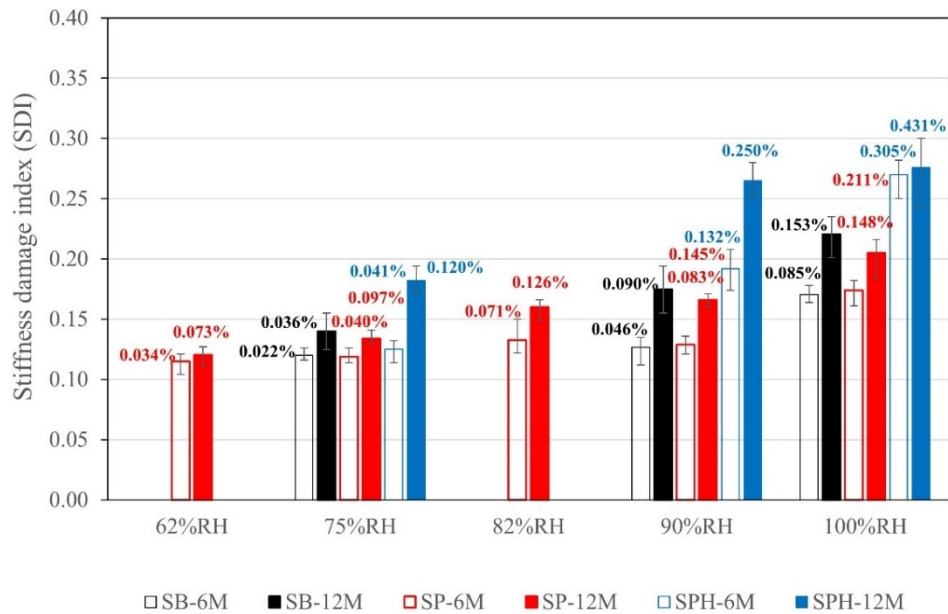
(a) 21°C - boosted alkalis



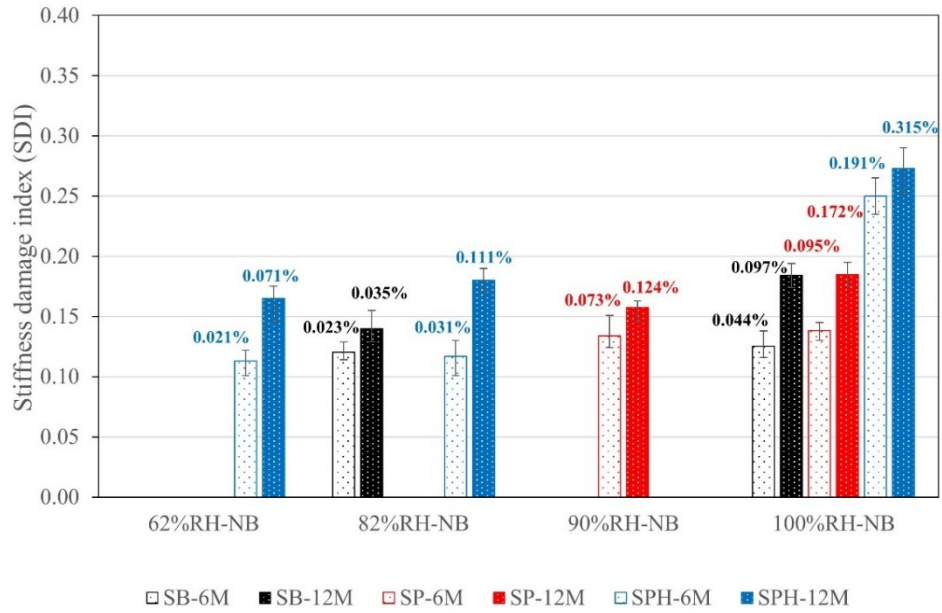
(b) 21°C - non-boosted alkalis (NB)



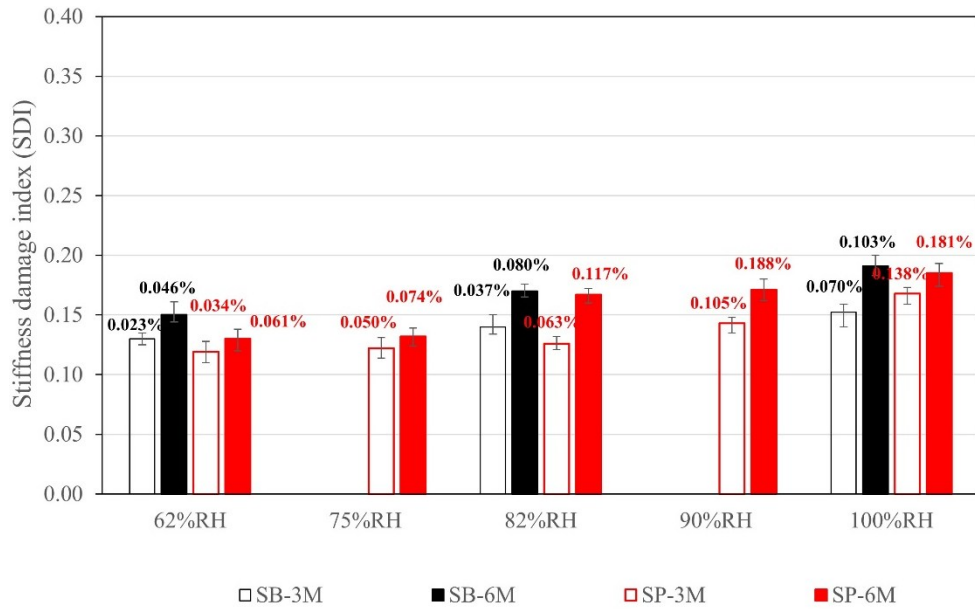
(c) 38°C - boosted alkalis



(d) 38°C - non-boosted alkalis (NB)



(e) 60°C - boosted alkalis



(f) 60°C - non-boasted alkalis (NB)

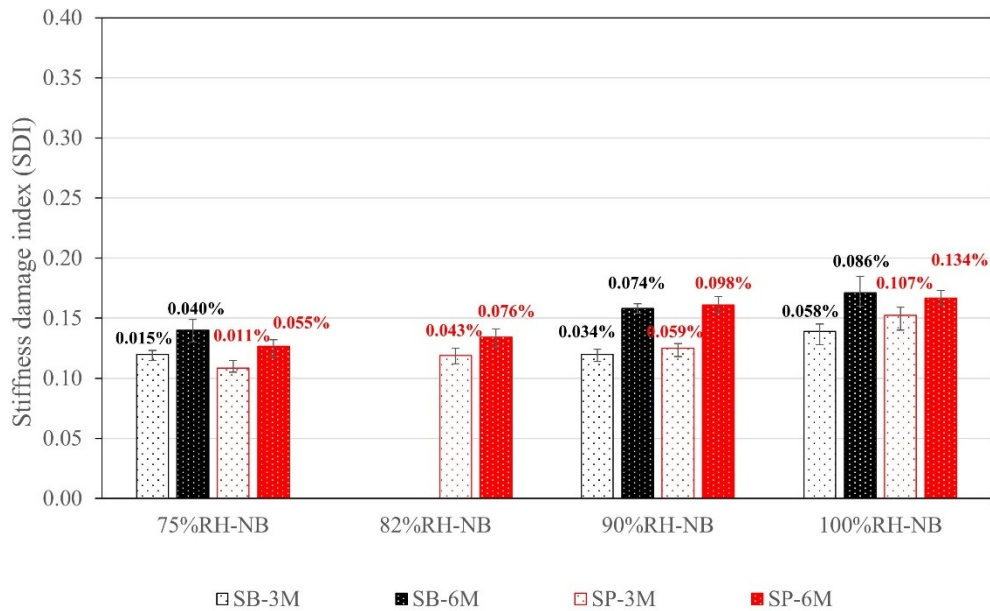


Figure 9.6: Stiffness Damage Index (SDI) as a function of time, relative humidity and aggregates: (a) 21°C-boosted alkalis (b) 21°C-non-boasted alkalis (c) 38°C-boosted alkalis (d) 38°C-non-boasted alkalis (e) 60°C-boosted alkalis (f) 60°C-non-boasted alkalis

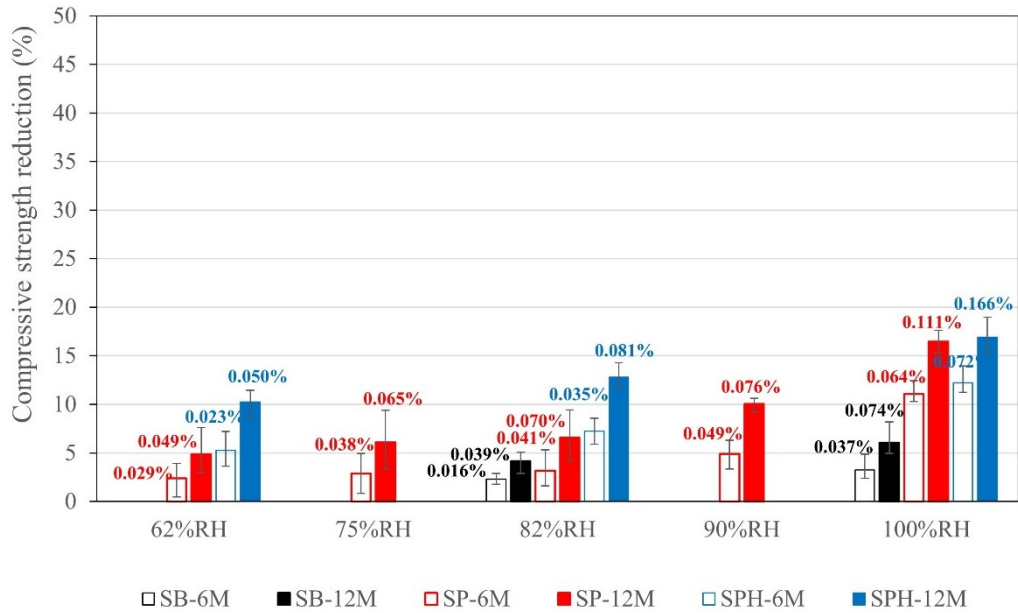
Similarly, the range of SDI in Spratt-containing specimens at 21°C is slightly higher; they fall within the range of 0.105 – 0.135 at 6 months and increase to 0.120 – 0.160 after 12 months. However, Springhill presented a much higher increment, for the same temperature. The SDI values increase from 0.107 – 0.146 to 0.133 – 0.226 from 6 to 12 months, respectively. For all aggregates, most low RHs present similar SDI values; 62% RH to 90% RH for all aggregates falls within 0.110 to 0.160, irrespective of their alkali content. However, the SDI values increase significantly at the RH rises to 100%. This trend of comparable SDI values remains true for all aggregates stored at 38°C and 60°C, as shown in Fig. 9.6c and d, except for specimens stored at RH greater than 82%. This finding suggests similar crack counts at low RH conditions irrespective of the RH.

9.4.3 Compressive strength reduction (CSR)

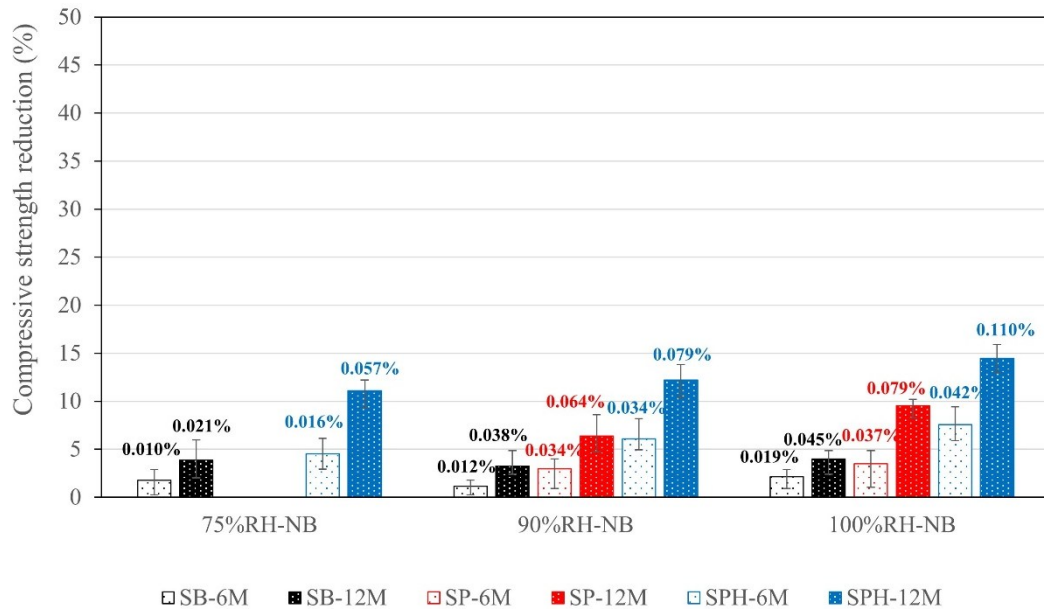
Fig. 9.7 illustrates the compressive strength reductions (CSR) as a function of RH, aggregate reactivity, and time. Overall, CSR increases with time in all conditions. As presented in Figs. 9.7a

and b for Sudbury-containing specimens, all conditions at 21°C experienced lower than 10% CSR. However, Spratt and Springhill-containing specimens present higher CSR with specimens conditioned at high RHs (i.e., RH>82%) attaining more than 10% loss after 12 months. A significant increase in reductions was recorded with an increase in temperature to 38°C, yet, most specimens containing Sudbury attained less than 10% loss. Similar findings were observed at 60°C despite the improved ASR kinetics.

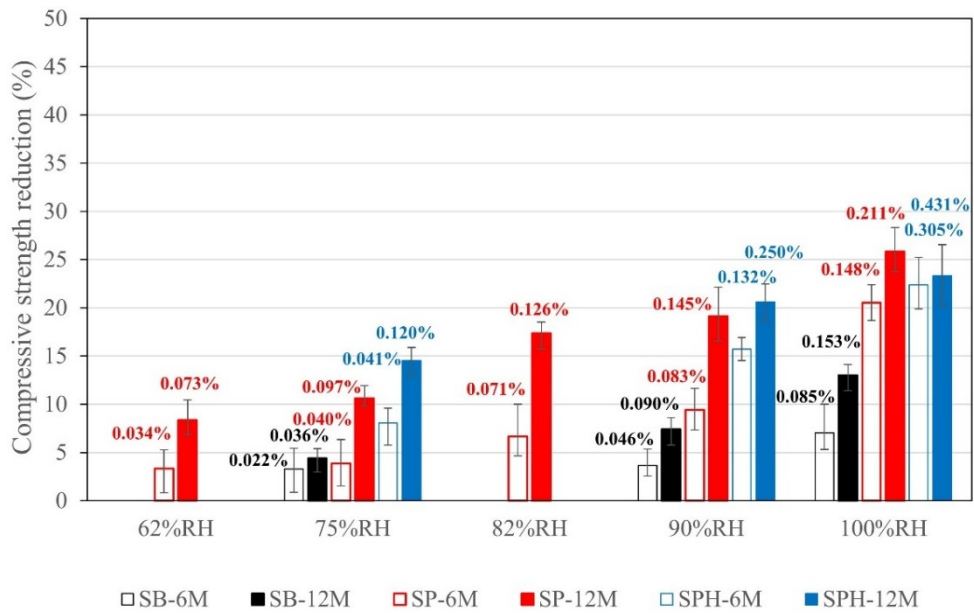
(a) 21°C - boosted alkalis



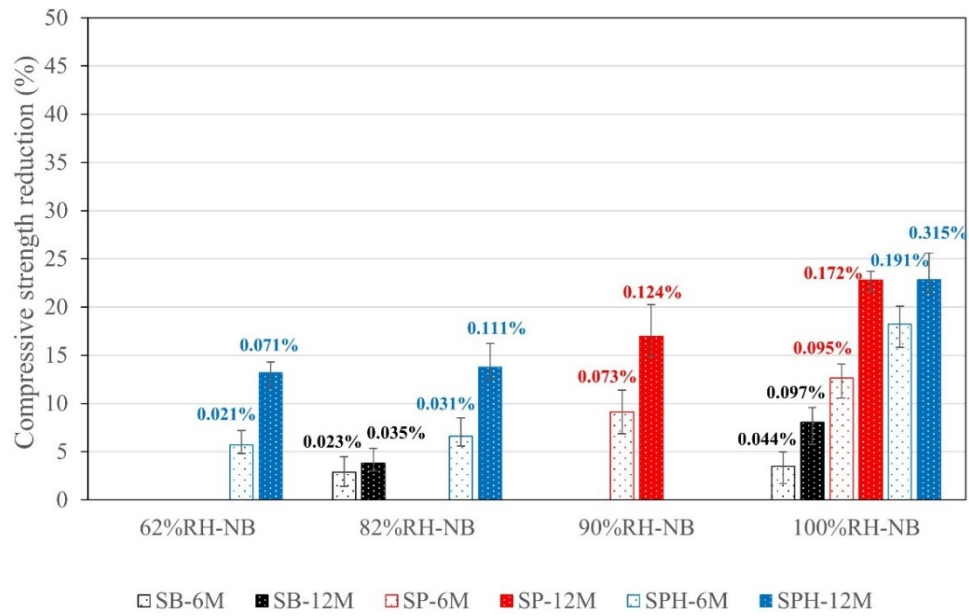
(b) 21°C - non-boosted alkalis (NB)



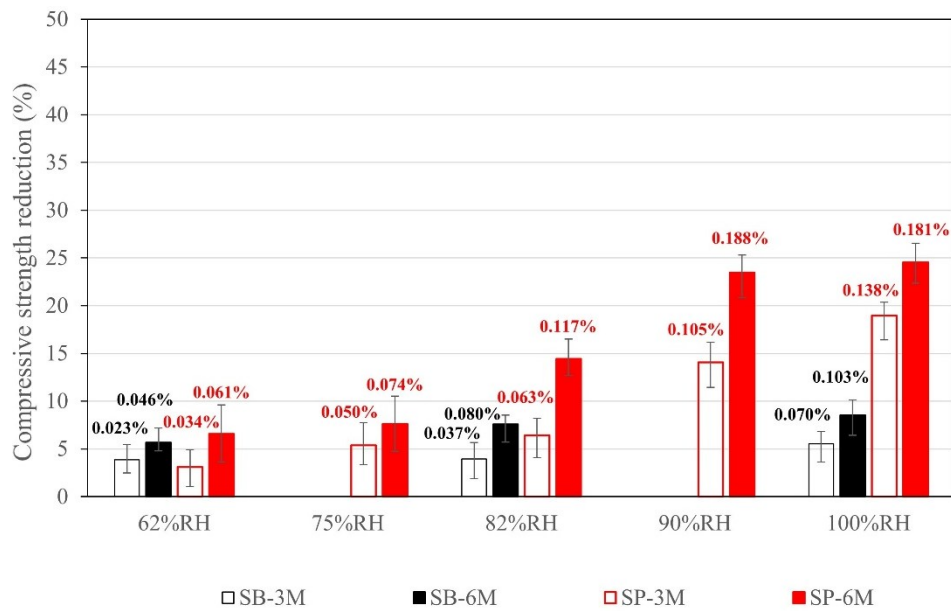
(c) 38°C - boosted alkalis



(d) 38°C - non-boosted alkalis (NB)



(e) 60°C - boosted alkalis



(f) 60°C - non-boosted alkalis (NB)

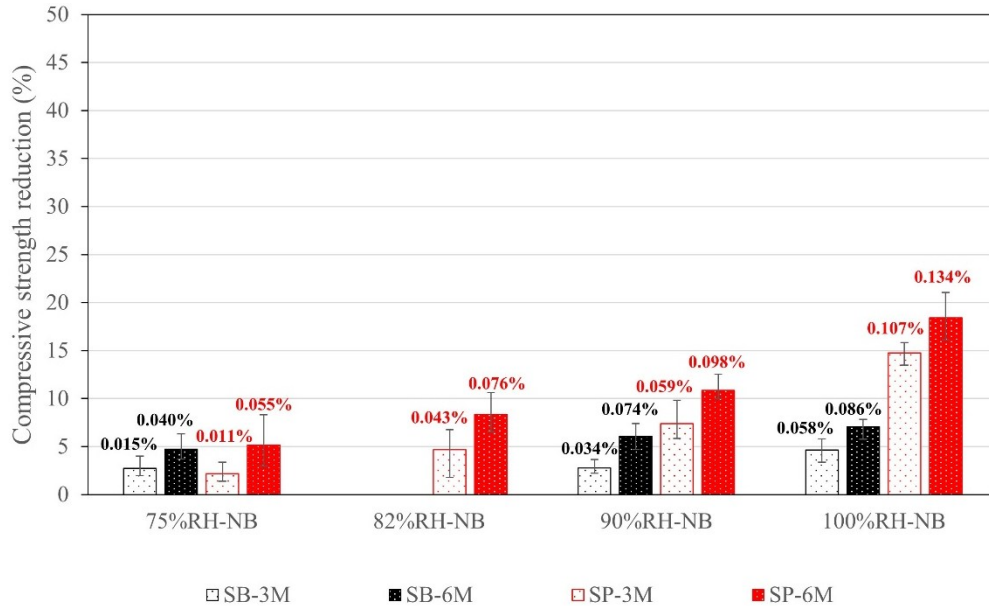


Figure 9.7: Compressive strength reduction (CSR) as a function of time, relative humidity and aggregates: (a) 21°C-boosted alkalis (b) 21°C-non-boosted alkalis (c) 38°C-boosted alkalis (d) 38°C-non-boosted alkalis (e) 60°C-boosted alkalis (f) 60°C-non-boosted alkalis

9.4.4 Damage Rating Index (DRI)

Fig. 9.8 displays the ASR-induced microscopic distress features in counts in concrete specimens containing Sudbury, Spratt, and Springhill, which contain different alkali levels under numerous exposure conditions using the extended version of the DRI. The distinct microscopic features appraised by counts are normalized to 100cm² without using the DRI weighting factors. The percentage value in front of each bar indicates the corresponding ASR-induced expansion for each condition. Overall, the most common feature in all conditions is the closed cracks in the aggregates (CCA). However, no trend exists with increased RH, alkali content, or temperature. Furthermore, although open cracks in the aggregates and cement paste (with or without reaction products) displayed some increase with these conditions, such cannot be inferred for the total microscopic feature counts.

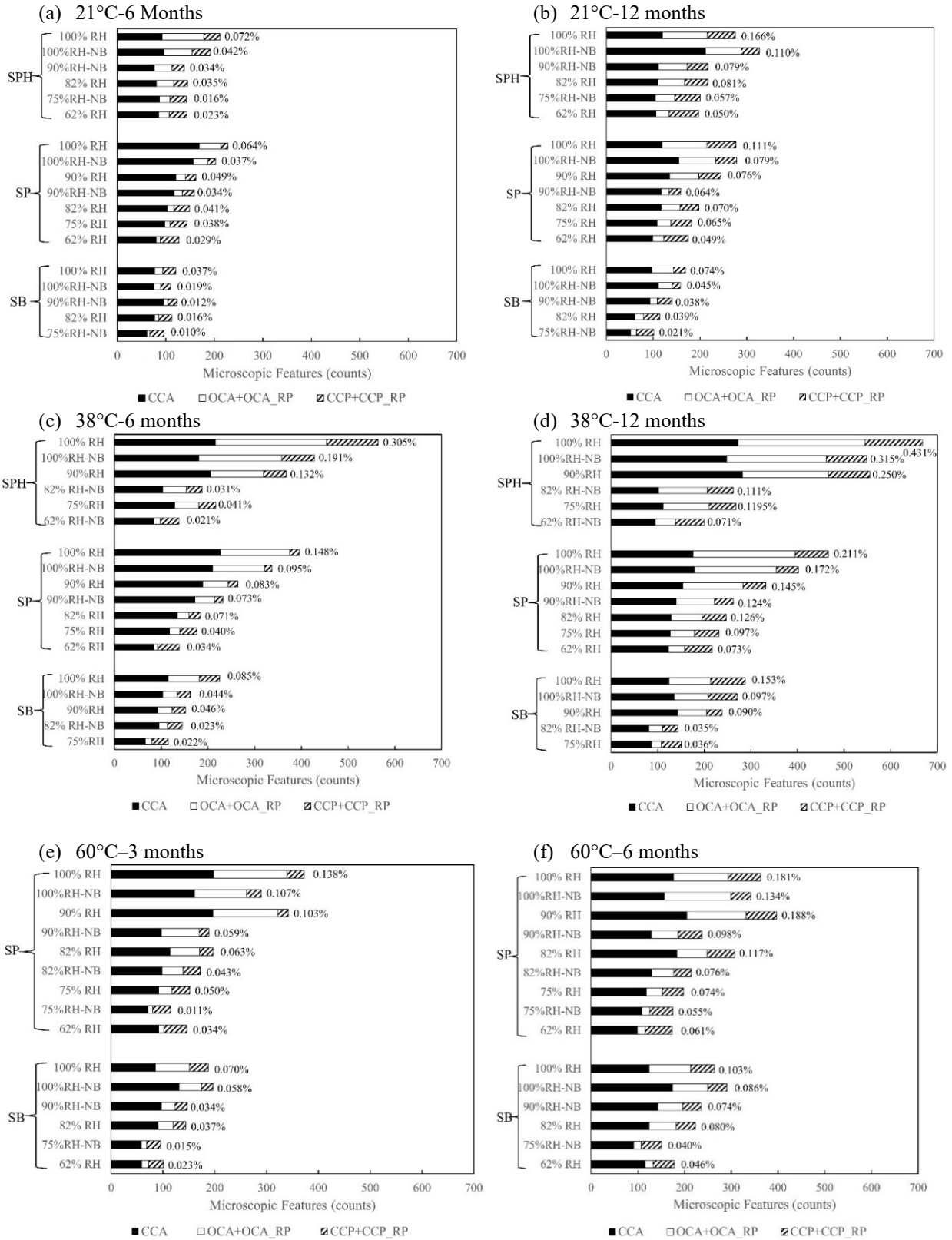


Figure 9.8: Microscopic distress features of deterioration (counts): (a) 21°C-6 Months (b) 21°C-12 Months (c) 38°C-6 Months (d) 38°C-12 Months (e) 60°C-3 Months (f) 60°C-6 Months

Fig. 9.8a and b presents the microscopic features for all aggregates at 21°C as a function of time. Overall, all aggregates (i.e., specimens containing SB, SP and SPH) experienced an increase in the total counts from 6 to 12 months. Furthermore, the total counts are affected by aggregate reactivity level, with Sudbury presenting the lowest counts across all conditions. Moreover, in each alkali level, the total microscopic features increase with RH, corresponding to the expansion trend in these conditions.

Considering the ASR-induced distress features, one will notice an increase in the OCA + OCA_RP as exposure conditions increase. However, CCP + CCP_RP does not show a clear trend. As illustrated in Fig. 9.8, the counts of CCP + CCP_RP are mostly higher at low RHs, which reduces with the rise in RH and increases again at high RH in most aggregates. Globally, the increment in total microscopic counts over time is aggregate-dependent. SPH and SP presented a more dramatic change compared to SB. For instance, at 12 months in 100% RH, SPH presents 273 counts of OCA + OCA_RP. While Spratt and Sudbury present 219 and 89, respectively.

Comparing the microscopic features across all temperatures, elevating temperature dramatically increases the microscopic feature counts with the most increment experienced in SPH and SP. At the same time, only a minimal influence was recorded in SB. Furthermore, the influence of temperature is more significant at high RHs than at low RHs. As a result, SB specimens at low RH are not significantly influenced by the change in temperature.

9.5 Discussion

9.5.1 Understanding the overall influence of aggregate reactivity, alkali loading and exposure conditions on ASR kinetics and damage development

9.5.1.1 ASR kinetics

As per Fig. 9.3 and 9.4, aggregate reactivity, alkali loading, and exposure conditions influenced the rate and ultimate expansion. This can be attributed to the abundance of alkalis, enhanced mobility of ions, solubility of silica and aggregate lithotype. Moisture has been reported to be critical to ASR. Interestingly, a general trend of increase in ASR-induced expansion with a rise in RH is consistent across all temperatures and aggregates. However, the increment from 62% to 90% RH appears gradual, with a spike in expansion noticed when the RH is increased from 90% to 100% RH. This can be related to the saturation of the pores at 100% RH. Below 90% RH, a few pores might be close to saturation conditions. Still, most pores are less saturated, limiting the movement of ions needed for ASR despite sufficient alkalis in the system. While the movement of the ions is not entirely stopped (i.e., proven by the ASR-induced expansion recorded even at 62% RH), the reduction in the number of saturated pores leads to a gradual decrease in ASR-induced expansion. Another interesting observation from the expansion results is the similar expansion recorded at low RHs (i.e., 62% RH and 75% RH) for all temperatures and aggregates. First, the ultimate expansions recorded prove that ASR cannot be stopped even at a low RH of 62%. For context, using a moderately reactive aggregate (i.e., Sudbury) at a temperature of 21°C would not halt the reaction or prevent it entirely from initiating, provided there are required alkalis and reactive silica. Secondly, reducing RH to 62% or 75% RH did not significantly change expansion depending on the aggregate type. This can be useful when considering the management of affected structures. Given the challenge of attaining a low RH of 62% in concrete exposed to the natural

environment, achieving a 75% RH might be sufficient. Nevertheless, as mentioned earlier, considering that similar expansion might lead to a difference in ASR-induced damage, it is critical to distinguish between induced damage in these RH conditions to make an informed decision.

9.5.1.2 Microscopic assessment

The overall assessment of the DRI number obtained for all aggregates and exposure conditions as a function of ASR-induced expansion is shown in Fig. 9.9.

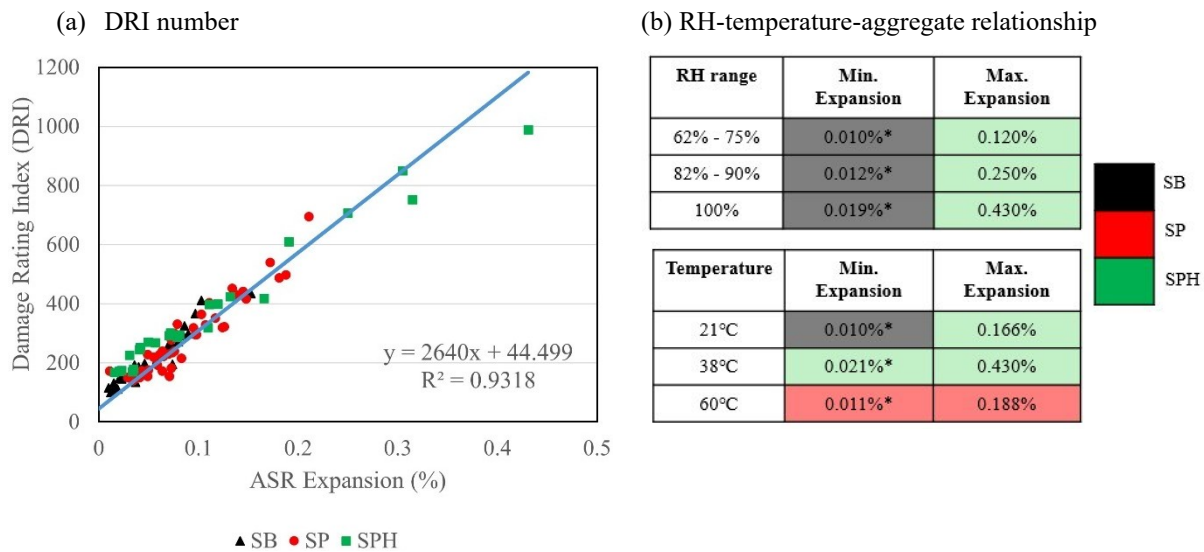


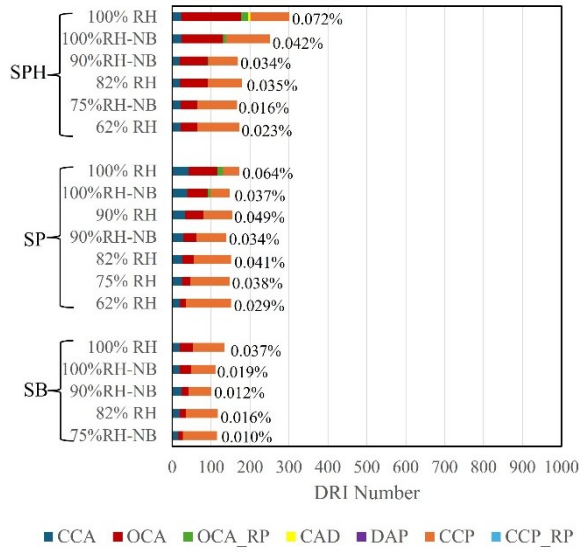
Figure 9.9: Damage Rating Index: (a) DRI number of ASR-affected concrete incorporating aggregates of different levels of reactivity at numerous exposure conditions (b) Expansion range as a function of RH, temperature, and aggregate type

Aggregate reactivity level presents a moderate influence on the DRI number. However, exposure condition strongly influences the microscopic features of affected concrete. Considering the overall influence of exposure conditions using expansion ranges highlighted in Fig. 9.9b, 62% - 75% RH attained an expansion range of 0.010% - 0.120%, leading to a DRI number of 115 – 399. The 82% - 90% RH range presents an expansion within 0.012% - 0.250% and subsequently DRI number of 100 – 706. Finally, the 100%RH presented an expansion of 0.019% - 0.430% with a DRI number within 111-988. Interestingly, the lowest RH (i.e., 62%RH) presents a slightly higher DRI number than 82% RH at similar expansion, which can be attributed to the shrinkage cracks

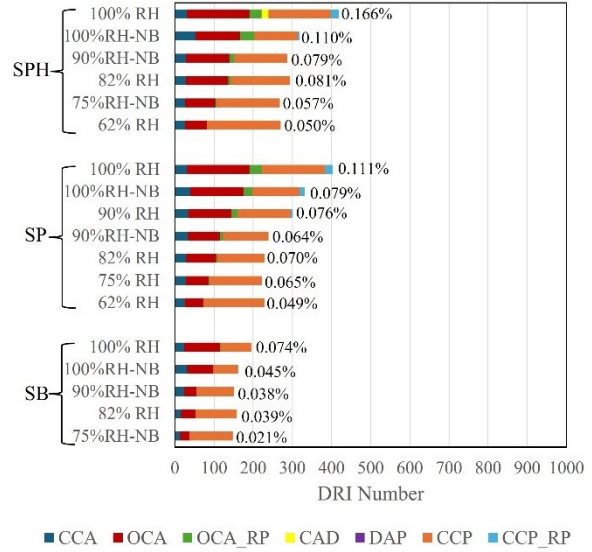
(i.e., CCP) observed at 62%RH as shown in Fig. 9.8. On the other hand, considering the influence of temperature, 21°C attained an expansion of 0.010% - 0.166%, leading to a DRI range of 115 – 418. At an increased temperature of 38°C, a higher expansion range of 0.021% - 0.430% was attained, presenting a DRI of 171 – 988. However, at 60°C, expansion of 0.011% - 0.188% attained DRI of 172 – 498. Hence, at similar expansion (i.e., 0.010% - 0.011%), a rise in temperature (i.e., from 21°C to 60°C) leads to an increase in the DRI number from 115 to 172. This can be attributed to the increased crack density at high temperatures, as highlighted in chapter eight, with the occurrence of a high number of thin and short cracks in the aggregate particles as a result of the aggressiveness of the reaction at elevated temperatures.

Fig. 9.10 is presented to further understand ASR development under the factors considered. The percentage value in front of each bar indicates the corresponding ASR-induced expansion for each condition. At a low ASR-induced expansion level (i.e., around 0.05%), ASR-induced cracks are found in the aggregate particles. However, the occurrence of shrinkage leads to the presence of isolated cracks in the cement paste.

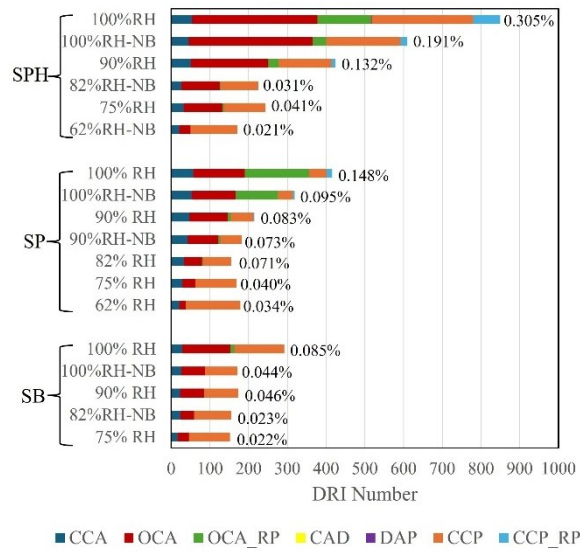
(a) 21°C-6 months



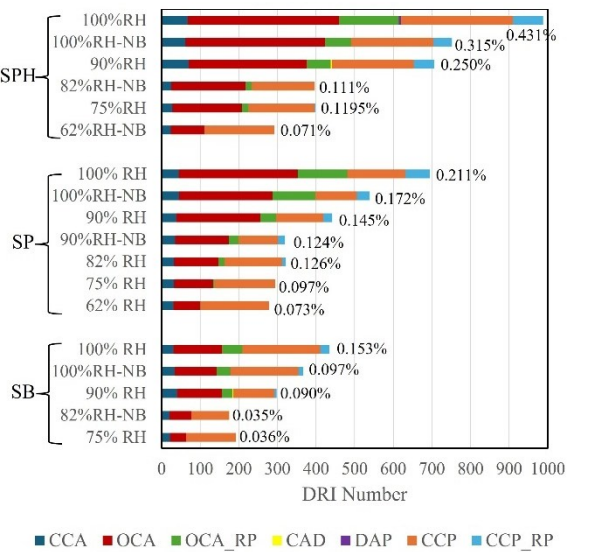
(b) 21°C-12 months



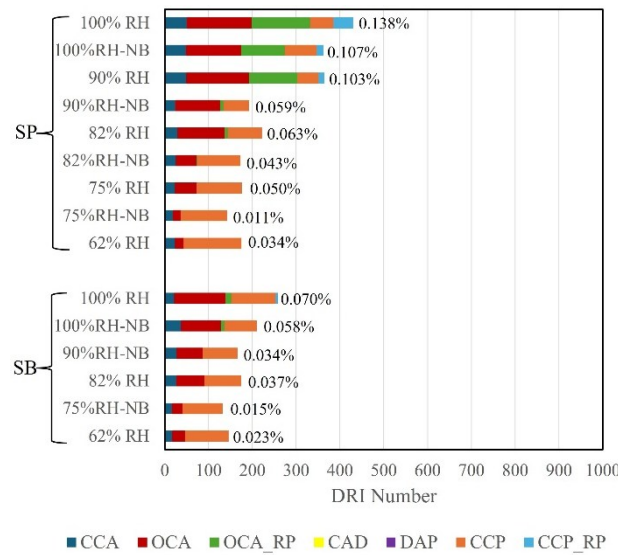
(c) 38°C-6 months



(d) 38°C-12 months



(e) 60°C-3 months



(f) 60°C-6 months

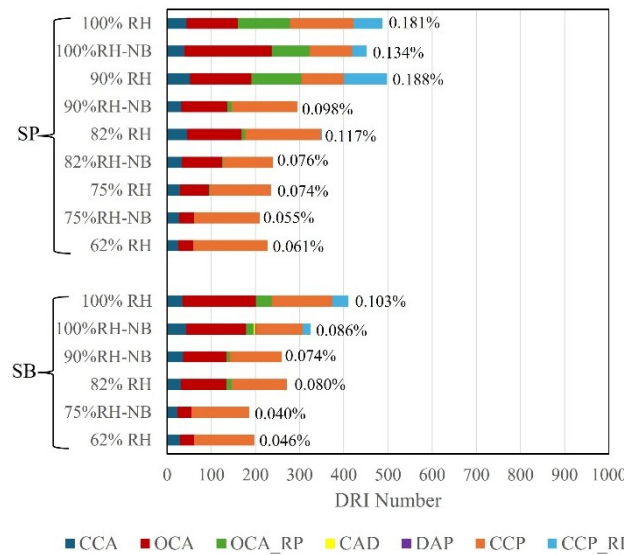


Figure 9.10: DRI results for specimens containing three aggregates (SP, SB, and SPH) with two alkali levels in numerous RH conditions: (a,b) 21°C (c,d) 38°C (e,f) 60°C

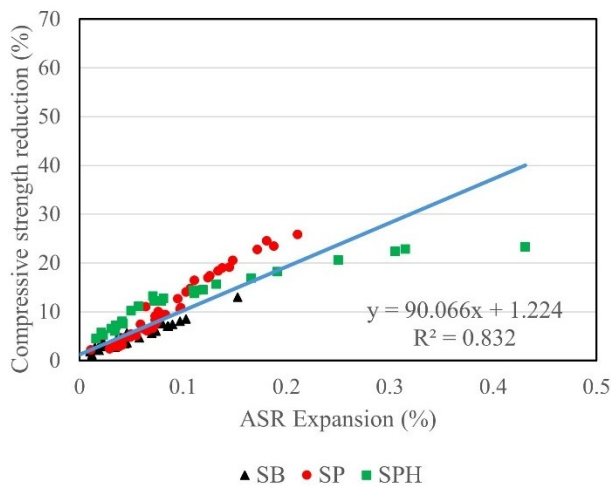
As the expansion increases to moderate levels (i.e., about 0.12%), the initial cracks within the aggregate particles experience a slight propagation into the cement paste depending on the aggregate type; the sharp cracks that are primarily seen in Springhill specimens slightly extend into the cement paste, while the onion skin cracks seen more prominently in Spratt were all within the boundary of the aggregate particles, nevertheless, they experience a growth in length at this expansion level and new cracks are generated. Furthermore, the length of the cracks is influenced by temperature; specimens at 38°C presented longer cracks compared to those at 60°C. At high and very high expansion levels of 0.20% and >0.30%, respectively, both types of cracks are present in the cement paste in all aggregate types, and considering the only specimens that attained up to 0.30% expansion, a network of cracks was noted in the cement paste [133]. Considering the descriptive model and the distress features at low RHs (e.g., 62%RH and 75%RH) for all conditions in this study, a high number of CCP is attained despite their low expansion (i.e., <0.12%), which leads to their high DRI number compared to similar expansion levels at higher RHs.

Shrinkage at low RH conditions can lead to concurrent expansive stresses from the gel in the aggregate particles and the restraining function of the aggregates to prevent the shrinkage of the cement paste, thus leading to stress redistribution. Such a phenomenon could be beneficial when ASR reaction is low, causing the relief of some internal stresses. Still, as the expansion rate increases, the expansive pressure is expected to overcome shrinkage. Furthermore, given the progressive nature of ASR, significant damage in the ITZ and microcracks can be expected as expansion increases. Considering the influence of aggregate type on this phenomenon, one will notice that SPH presents a higher amount of CCP, and SB presents the lowest amounts at similar exposure conditions. This could be attributed to the other properties not assessed in this study, such as the quality of ITZ and stress distribution. The influence of this observation will be discussed in the following section.

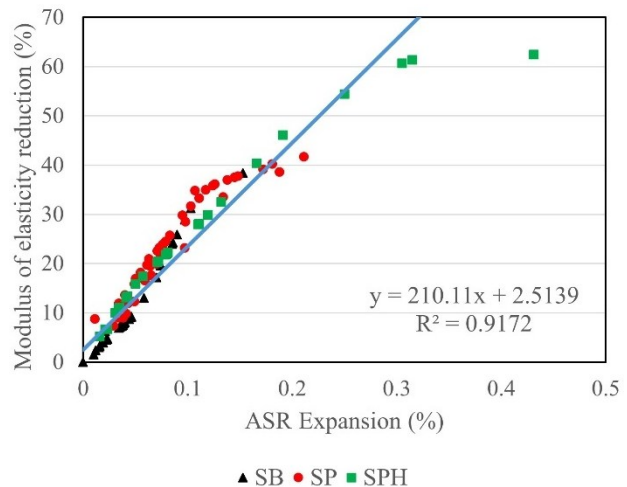
9.5.1.3 Mechanical properties

To conduct a thorough damage assessment, understanding the influence of the microstructure on mechanical properties is crucial. Fig. 9.11 displays the mechanical properties and SDT outcomes as a function of ASR-induced expansion.

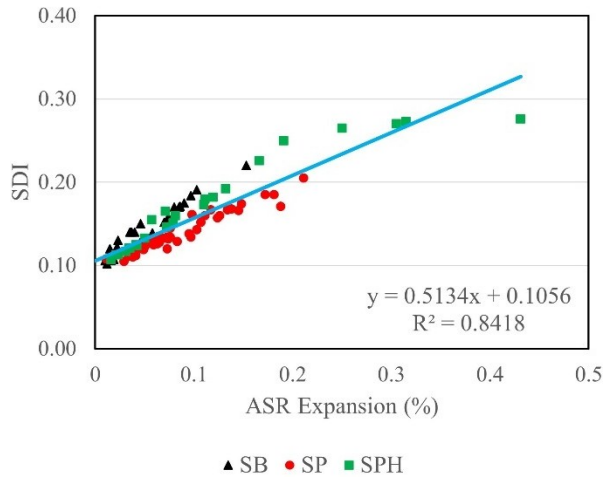
(a) Compressive strength



(b) Modulus of elasticity



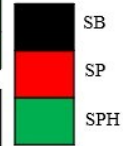
(c) Stiffness Damage Index



(d) RH-temperature-aggregate relationship

RH range	Min. Expansion	Max. Expansion
62% - 75%	0.010%*	0.120%
82% - 90%	0.012%*	0.250%
100%	0.019%*	0.430%

Temperature	Min. Expansion	Max. Expansion
21°C	0.010%*	0.166%
38°C	0.021%*	0.430%
60°C	0.011%*	0.188%



*non-boosted alkali content

Figure 9.11: Mechanical properties of ASR-affected concrete incorporating aggregates of different levels of reactivity at numerous exposure conditions: (a) compressive strength reduction (b) modulus of elasticity reduction (c) SDI (d) RH, temperature, and expansion

The occurrence of secondary cracks (i.e., shrinkage-induced cracks) and the difference in lithotype of the aggregates used are expected to influence mechanical properties. For instance, isolated shrinkage-induced cracks in the cement paste at low RHs can densify the cement matrix at high expansion level, leading to increased mechanical property losses. Furthermore, aggregate particles exhibit different crack types, such as onion skin and/or sharp cracks [7]. The evolution of these cracks differs with the progress in expansion, as shown in Fig. 9.1. Hence, their properties can impact the sensitivity of the specimens to mechanical properties reduction. Considering the compressive strength reduction and SDI results (i.e., Fig. 9.11a and c), Spratt and Springhill possess slightly different responses from Sudbury. However, a similar modulus of elasticity reduction was recorded in all aggregate types (i.e., Fig. 9.11b). Since ASR is initiated in the aggregates and given the relevance of the modulus of elasticity in aggregates, the results mean that the influence of the reaction on aggregates with different levels of reactivity is similar. However, the difference in the SDI values (i.e., related to the number of cracks within a deteriorated concrete) indicates a difference in the crack counts in the system for each aggregate type. The significance

(or location) of these cracks might vary, leading to the difference in the compressive strength reductions. As mentioned in the microscopic analysis, SPH presents a higher number of cracks in the cement paste, which can cause a higher compressive strength reduction, as illustrated in Fig. 9.11a, until an expansion close to 0.1%. Moreover, this can be related to the crack type in the aggregate particles. The sharp cracks are more frequent in the SPH specimens and propagate faster into the cement paste, leading to differences in compressive strength response compared to other aggregates. Beyond this expansion limit (i.e., 0.1%), SP presents higher compressive strength loss despite having a lower SDI value. Assessing the corresponding microscopic results at this instance, SP presents more crack counts in the cement paste (i.e., CCP + CCP_RP) than SPH beyond that expansion point; this caused a higher compressive strength loss in the SP, buttressing the hypothesis that similar crack counts might present a difference in importance depending on the location of the cracks.

9.5.2 Influence of exposure conditions, alkali loading, and aggregate reactivity on ASR damage classification degree

The conduction of the experiment in a time-based manner allows for the assessment of the influence of exposure conditions and aggregate reactivity over time. However, it remains vital to evaluate how these factors impact ASR-induced damage at similar expansion levels and how it evolves with changes in expansion. To assess this, a comprehensive evaluation of deterioration is conducted at three damage degrees (i.e., low, moderate, and high levels, as previously highlighted in paper 4), and specimens with expansions corresponding to each damage level are assessed using their deterioration outcomes and considering the influence of moisture, temperature, alkali content, and aggregate reactivity level.

Exposure conditions (i.e., moisture and temperature) play a critical role in influencing damage at low expansion levels (0.04 – 0.05% expansion), shrinkage cracks are initiated at low moisture and high temperature often induced higher distress features leading to an overall increase in ASR-induced damage which can not be captured in expansion measurement. As expansion increases to moderate levels (0.10 – 0.12% expansion), the number/significance of shrinkage cracks on the overall damage depends on temperature. The impact of these cracks is lower at high temperatures due to an improved microstructure. However, a rise in temperature at similar RH levels can influence the crack count in the aggregates and impact the mechanical properties, especially the modulus of elasticity. At moderate to high expansion levels ($0.12\% < \text{Expansion} < 0.20\%$), low moisture and high-temperature impact inner damage, and the significance of these factors on mechanical property reduction depends on the location of secondary cracks (i.e., shrinkage-induced cracks). The occurrence of a network of cracks that propagate from the aggregate particles into the cement paste and existing shrinkage cracks would increase the damage outcomes.

The influence of alkali on microscopic distress features is more evident at high temperatures and RHs, largely due to improved mobility. Typically, at similar expansion levels (typically at moderate to high expansion levels), specimen containing high alkali concentrations presents higher amounts and significance (measured by crack counts and DRI number) of cracks. A possible explanation could be slower kinetics leading to more pressure buildup and greater damage.

The influence of the lithotype of aggregates is not limited to the kinetics of the reaction. Some differences exist in the microstructure of concrete containing different aggregate types. The differences in the crack type (i.e., onion skin or sharp crack) are of particular interest. For instance, onion skin cracks are typical in Spratt reactive aggregates. The mode of propagation of this type of crack can lead to lower compressive strength when compared with aggregates with other types

of cracks, such as sharp cracks at low expansion levels. However, mechanical properties reduction can be greater at moderate to high expansion levels.

Table 9.6 shows the global classification of ASR damage from literature [141] that was computed based on damage outcomes from concrete mixtures presenting different strengths (i.e., 25, 35, and 45 MPa) containing 13 different aggregates that have often been used as a guide in the condition assessment of ASR-affected concrete [249,250,254]. However, the damage table was computed with results from tests conducted at high relative humidity (>95% RH) and 38°C. This current study identifies the occurrence of coupled mechanisms involving ASR and shrinkage at low RH conditions. Furthermore, crack properties are influenced by temperature. Hence, the damage outcomes were extensively assessed (see detailed tables on the damage classification in supplementary materials). Table 9.6 presents the summary and comparison of the results gathered in the current study with the existing proposed damage classification.

Table 9.6: Comparison of the classification of ASR-induced damage in concrete [141] (*Reproduced with permission of Elsevier*)

Expansion (ASR damage classification degree)	CS Loss		ME Loss		SDI		DRI	
	This study	Sanchez et al. [141]	This study	Sanchez et al. [141]	This study	Sanchez et al. [141]	This study	Sanchez et al. [141]
0.00-0.03 (Negligible)	1-7	-	2-12	-	0.10-0.13	0.06-0.16	100-225	100-155
0.04±0.01 (Marginal)	3-10	10-15	7-16	5-37	0.11-0.14	0.11-0.25	134-270	210-400
0.11±0.01 (Moderate)	7-17	0-20	23-36	20-50	0.13-0.19	0.15-0.31	292-411	330-500
0.20±0.01 (High)	18-26	13-25	39-46	35-60	0.17-0.25	0.19-0.32	498-695	500-765
0.30±0.01 (Very high)	22-23	20-35	61-62	40-67	0.27-0.28	0.22-0.36	752-988	600-925

Overall, the results gathered from this study follow a similar trend as per [141]. The negligible–high level presents a similar trend but with a change in range values. Notable differences include the higher DRI numbers at negligible damage, which can be attributed to shrinkage. Furthermore, low compressive strength loss was obtained at marginal damage level (i.e., 0.04 ± 0.01 expansion); this can be attributed to ongoing hydration, which increases compressive strength, as the specimens were exposed to low relative humidity (RH). At these conditions, the kinetics of ASR were slower and outweighed by the effects of continued hydration. Alternatively, this discrepancy could be explained by the limitations of compressive strength testing in accurately assessing ASR progression at low expansion levels, as noted in [17,141]. Moreover, at this level, Sudbury specimens presented lower open crack counts in the aggregates even at expansion levels similar to other aggregate types, leading to a lower range DRI number than Sanchez's results. As expansion increases to moderate, high, and very high damage levels, the influence of exposure conditions diminishes. Most of the damage indices obtained in this study fall within the reference range, with only the SDI at moderate and high expansion presenting some difference, yet within a close range. Hence, Table 9.7 (adapted from Sanchez's table) is compiled for evaluating the coupled mechanism (i.e., ASR + Shrinkage) and allows for a robust ASR-damage classification table that accounts for the influence of all the factors evaluated in this study.

Table 9.7: Classification of ASR-induced damage coupled with shrinkage in concrete [141] (*Reproduced with permission of Elsevier*)

Classification of ASR damage degree	Expansion	CS Loss	ME Loss	SDI	DRI
Negligible	0.00-0.03	1-7	2-12	0.06-0.16	100-225
Marginal	0.04±0.01	3-15	5-37	0.11-0.25	134-400
Moderate	0.11±0.01	0-20	20-50	0.13-0.31	292-500
High	0.20±0.01	13-26	35-60	0.17-0.32	498-765
Very high	0.30±0.01	20-35	40-67	0.22-0.36	600-988

9.5.3 Exploring the influence of exposure conditions, alkali loading and aggregate reactivity on ASR-induced damage using the response surface methodology (RSM)

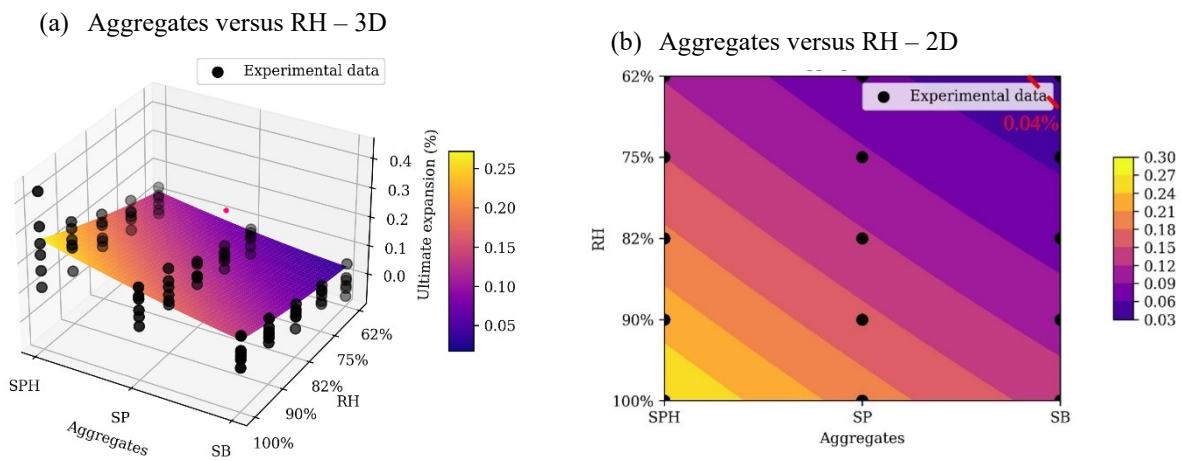
RSM is notable for its efficiency in modeling interactions. Hence, it is applied to model the interactions among temperature, RH, alkali content, and aggregate reactivity to understand how these factors jointly influence ASR kinetics and induced damage. This study utilized ultimate expansion, modulus of elasticity loss, and DRI as responses. The compressive strength is omitted due to its widely reported ineffectiveness in assessing ASR at low expansion [17,141].

The statistical analyses were conducted starting with the preprocessing of the data; since it is a partial factorial experiment, simply removing the rows or columns with missing data (i.e., listwise or pairwise deletion) would yield a significant loss of data, reducing the reliability and generalizability of the analysis. On the other hand, the imputation methods aid in retaining the entire dataset, preserving the sample size and the information contained in the dataset, and reducing the bias in the results. In this sense, the missing data were handled using the multiply imputation chained equations (MICE). MICE uses chained equations to handle different factors and missing

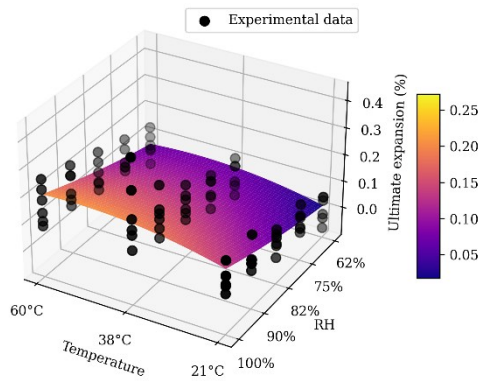
data patterns. It models each factor with missing values as a function of other factors in the dataset interactively [255]. The subpackage ‘C’ of the Python library was used to handle the missing values. The surface response methodology was then used to model the behavior of the responses (i.e., ultimate expansion, the modulus of elasticity loss, and the DRI number) under all the possible pair combinations among the factors.

The analysis of variance (ANOVA) for the responses (i.e., ultimate expansion, DRI, and modulus of elasticity) is presented in the supplementary materials. This statistical analysis was conducted using a 95% confidence level. At this confidence level, the model parameter with a p-value less than 0.05 is considered statistically significant, meaning it has a strong likelihood of affecting the results. Conversely, parameters with p-values greater than 0.05 are considered statistically non-significant, indicating they likely do not have a meaningful impact on the outcome.

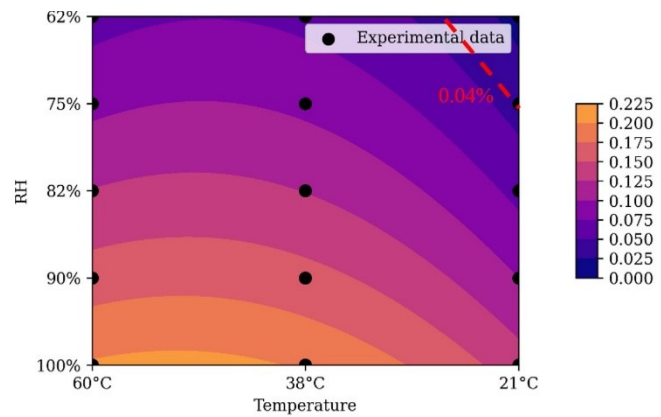
Fig. 9.12 presents the 3D surface and 2D contour, highlighting the influence of some combinations on ASR kinetics and expansion limit of 0.04%, while others can be found in the supplementary materials.



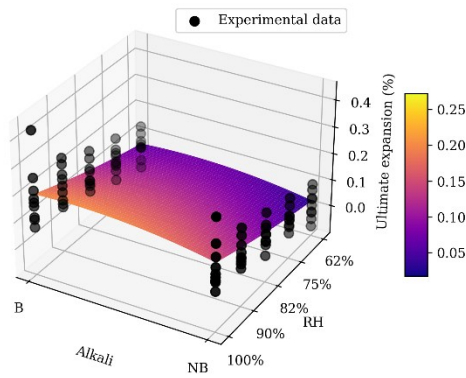
(c) Temperature versus RH – 3D



(d) Temperature versus RH – 2D



(e) Alkali loading versus RH-3D



(f) Alkali loading versus RH-2D

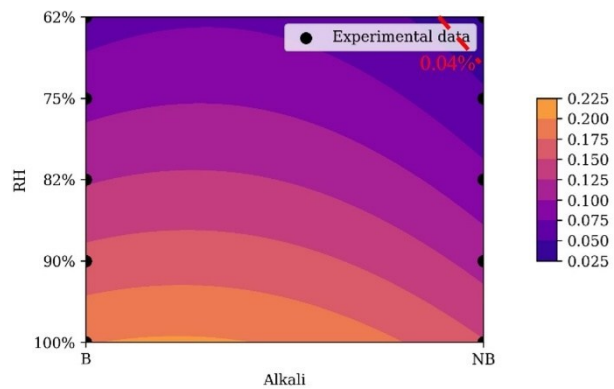


Figure 9.12: 3D surface and 2D contour plot of expansion model: (a,b) effects of aggregate reactivity and RH (c,d) effects of temperature and RH (e,f) effects of alkali content and RH

The ANOVA results show a significant interaction between aggregate reactivity and RH for ultimate expansions, while no significant interaction exists between other combinations. One will notice that the influence of aggregate reactivity (i.e., a change from Sudbury to Springhill) on ultimate expansion is not the same across all RH levels. Sufficient moisture is believed to be available at high RH (i.e., 90%-100%). Hence, the change in the reactivity of the aggregate is expected to lead to a substantial change in ultimate expansion. This is, however, not replicated at low RHs, such as 62%-75%. Although the ASR gel is formed regardless of the RH level, the induced expansion is not greatly influenced by an aggregate change due to low moisture availability. Especially considering SB and SP. This pinpoints the possibility of a moisture threshold. However, considering the ANOVA results, such interactions are absent in the DRI and

modulus loss. This highlights the differences between induced expansion and damage (i.e., associated mechanical reductions and the physical integrity of affected concrete). Hence, the need for a damage assessment rather than just expansion measurement in evaluating ASR is validated. On the other hand, the ANOVA results indicate that other combination of factors presents no significant interaction for expansion and other damage outcomes. Overall, the results imply that aggregate reactivity may significantly influence the RH threshold needed for ASR.

9.5.4 Damage-based RH threshold assessment

Having thoroughly assessed significant factors that can influence ASR-induced damage, as earlier highlighted, no known solution exists to stop ASR. The most common mitigative measure for existing concrete has been moisture limitation, prevalently quantified by an RH threshold. This threshold has been disparately claimed to depend on temperature and aggregate reactivity level. This study examined the threshold, considering these two factors by evaluating ultimate damage (i.e., a combined assessment of final expansion, DRI, and modulus of elasticity loss) in boosted specimens (i.e., containing $5.25 \text{ kg/m}^3 \text{ Na}_2\text{O}_{eq}$) as shown in Fig. 9.13. The multiply imputation chained equations (MICE) obtained missing experimental data to prepare this assessment.

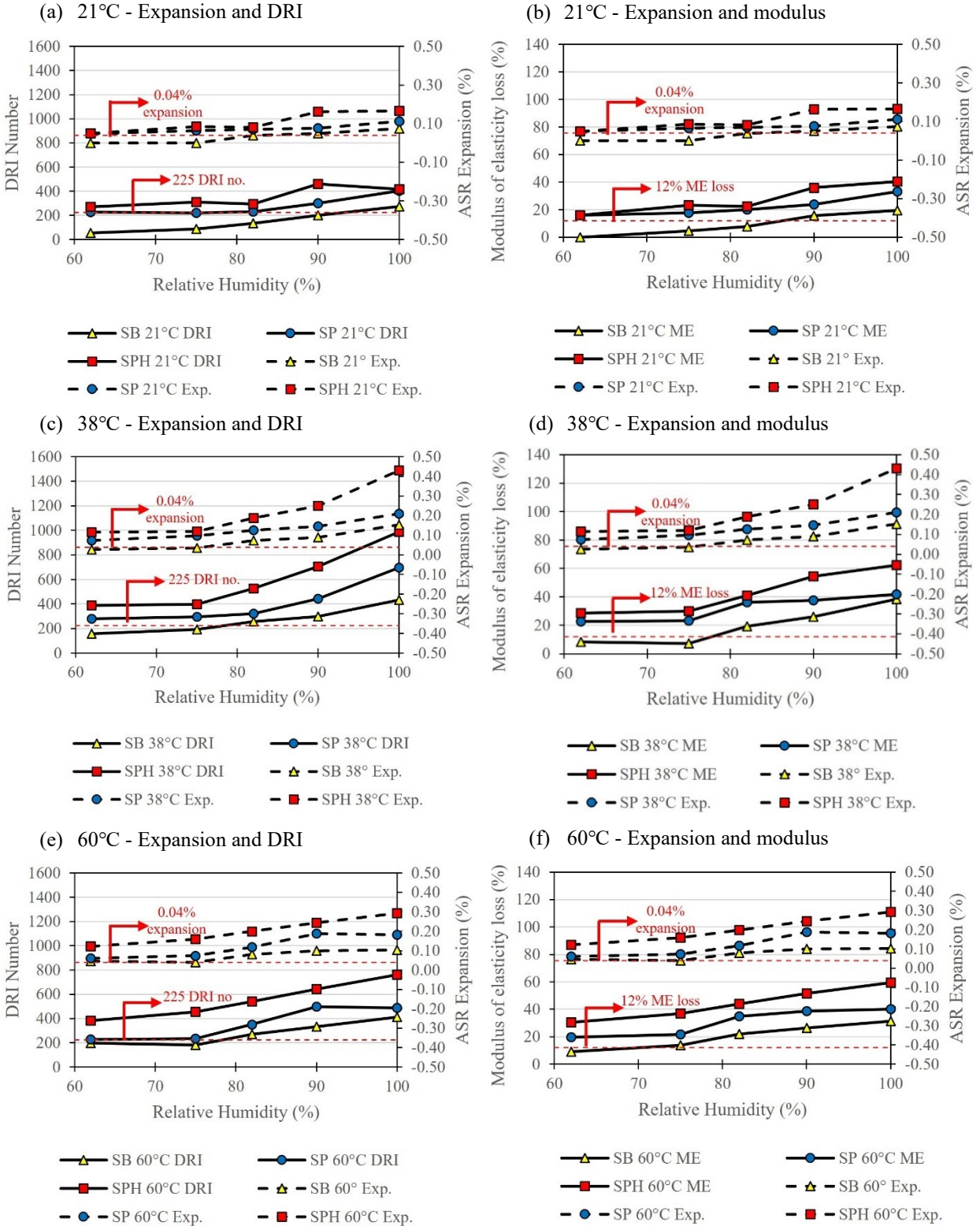


Figure 9.13: Damage-based (ultimate expansion, DRI and modulus loss) evaluation of RH threshold for ASR: (a,b) 21°C (c,d) 38°C (e,f) 60°C

Given the aggregates used in this study are reactive, all exposure conditions and aggregate types attained ultimate expansion greater than 0.04% at 100% RH. Some conditions attained expansion greater than 0.04% at the lowest RH considered (i.e., 62%). Nevertheless, the 0.04% expansion limit is selected for this assessment. Hence, any RH level with an ultimate expansion below this limit is not considered. Despite the reliability of the DRI in assessing ASR-induced deterioration, the minimum DRI number correlating to significant damage in concrete is unknown. However, according to the adapted global damage assessment table (i.e., Table 9.7), a negligible damage range presents a DRI of 100-225. Hence, a DRI number above 225 is assumed sufficient to define significant inner damage. Furthermore, the corresponding modulus of elasticity reduction of 12% loss was selected as per Table 9.7. Another worthy observation is the similarities in damage among some RH levels; hence, to confirm the significance of such similarities, Tukey's post hoc test was conducted to assess the significance of modulus of elasticity reductions in pairs of RHs. In contrast, the Chi-square test was performed for the DRI. Results from these tests are presented in the supplementary materials.

The minimum RH required to reach an expansion of 0.04% for all aggregate types at all temperatures is reported in Table 9.8. The DRI and MER assessment was conducted using the earlier criteria and a further significance assessment based on post hoc test results (see in supplementary materials). The results considering the significance assessment are displayed in parentheses. For instance, if 62% RH is identified as the threshold based on the DRI number (i.e., ≥ 225) or ME loss (i.e., $\geq 12\%$), if the damage outcomes of this RH are proven similar to that of 75% RH, a range of 62%-75% is presented in parenthesis. The overall RH threshold for each condition is selected based on the lowest RH identified.

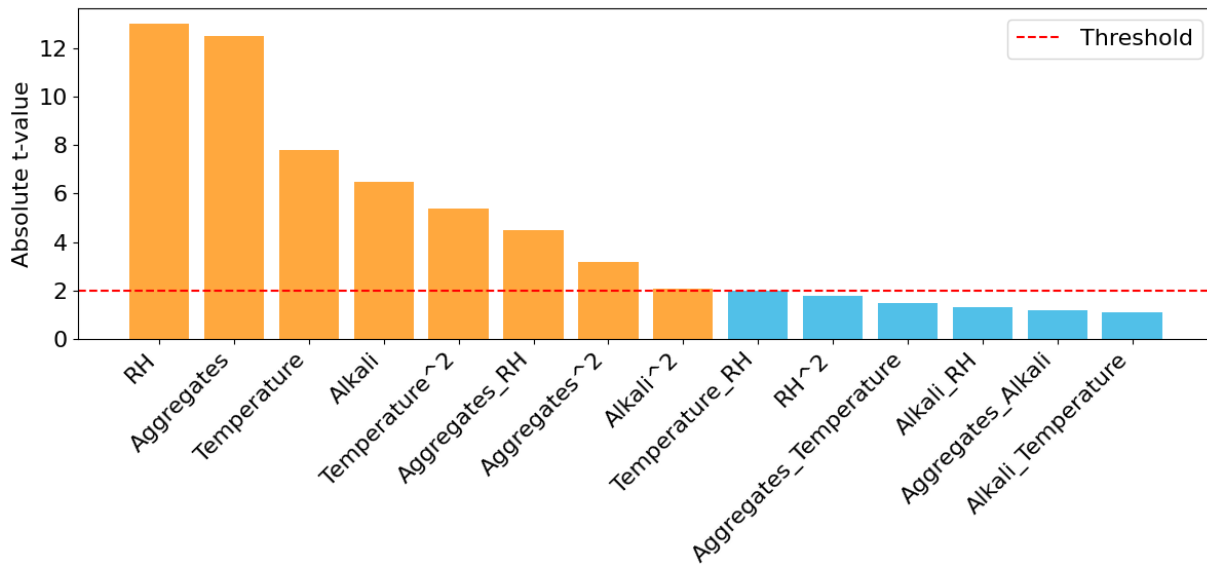
The obtained overall thresholds show that expansion, mechanical property loss, and DRI present similar RH thresholds, which validates the popular assessment of RH thresholds based on expansion. However, the popularly reported 80% RH may be limited to some specific aggregates and temperatures.

Table 9.8: Influence of temperature and aggregate reactivity on damage-based RH threshold for ASR

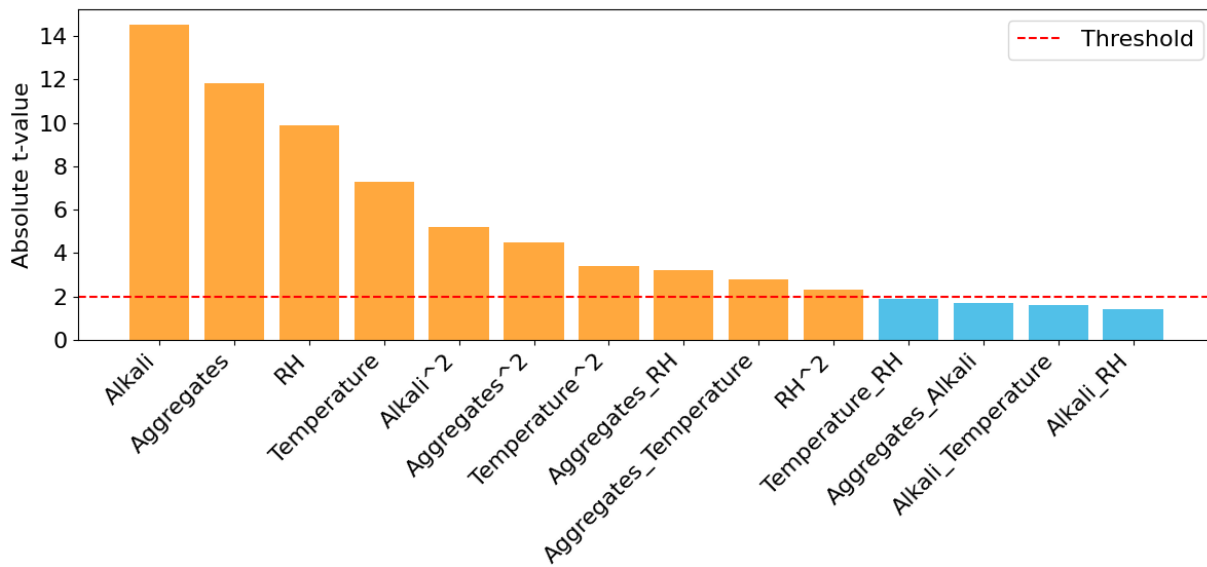
Temperature	Aggregates	Expansion Threshold	DRI Threshold	ME Threshold	Overall
21°C	SB	90% RH	90% RH	82-90% RH	90% RH
	SP	62% RH	62% (62%-75%) RH	62% (62-82%) RH	62% RH
	SPH	62% RH	62% (62%-75%) RH	62% RH	62% RH
38°C	SB	75% RH	75% RH	75-82% RH	75% RH
	SP	62% RH	62% (62%-75%) RH	62% (62%-75%) RH	62% RH
	SPH	62% RH	62% (62%-75%) RH	62% (62%-75%) RH	62% RH
60°C	SB	75% RH	75-82% (62%-82%) RH	75% RH	75% RH
	SP	62% RH	62% (62%-75%) RH	62% (62%-75%) RH	62% RH
	SPH	62% RH	62% RH	62% RH	62% RH

A Pareto plot (Fig. 9.14) was prepared to rank the tested factors and their interactions based on their absolute t-values to predict the factor with the most importance on ASR kinetics and induced damage.

(a) Expansion



(b) DRI



(c) Modulus of elasticity loss

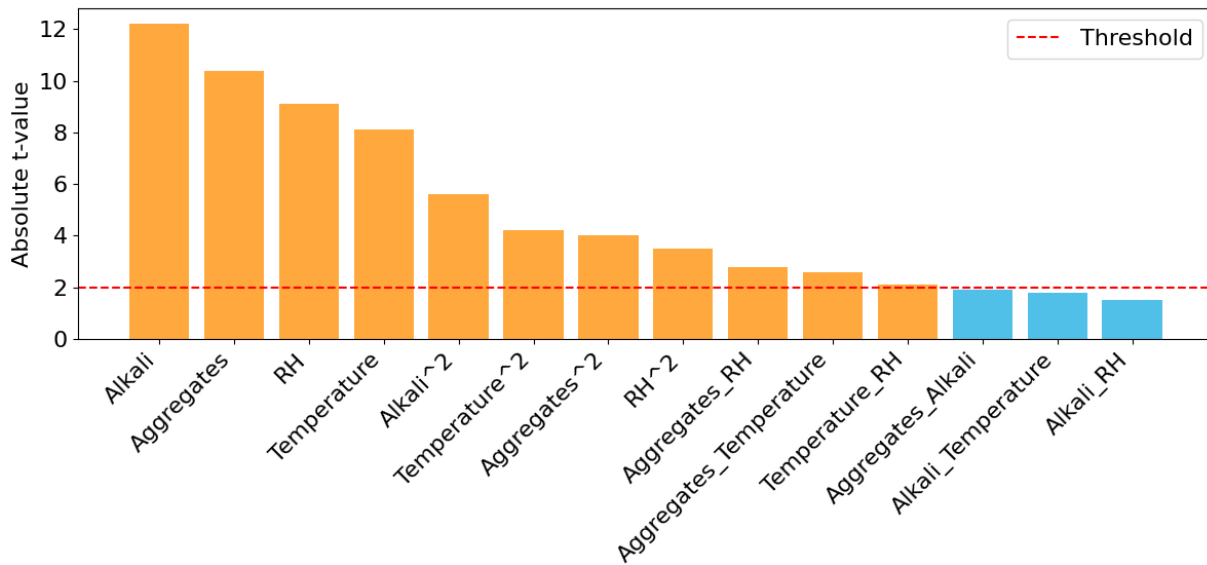


Figure 9.14: Pareto plot: (a) Expansion (b) DRI (c) Modulus

The t-values were calculated by considering the degrees of freedom and the standard errors of the model, with a threshold t-value set at 2 for significance. The absolute t-value analysis indicates that RH and Aggregates are the primary contributors to ultimate expansion, with RH showing the highest influence. Temperature and alkali content also play significant roles, though their impact is slightly less pronounced than that of RH and Aggregates. Additionally, the analysis highlights the importance of quadratic and interaction terms. The quadratic effect of temperature², aggregates², and alkali² suggests that non-linear relationships exist between these factors and expansion. In particular, the interaction between aggregates and RH demonstrates a noteworthy influence, implying that the behavior of aggregates under varying RH conditions can significantly affect expansion. This interaction likely reflects the complex interplay between moisture availability and aggregate reactivity in determining the extent of expansion.

The analysis of the deterioration due to ASR provides further insight. Interestingly, the factors influencing the deterioration response (i.e., DRI and modulus loss) can be ranked as alkali,

Aggregates, RH, Temperature, and their respective quadratic terms (alkali², aggregates², temperature²), as well as significant interaction terms such as Aggregates and Aggregates, and RH². These findings reveal the complex nature of ASR-induced deterioration, where both the individual factors and their interactions contribute to the ultimate induced damage.

This comprehensive analysis emphasizes the multifaceted role that environmental conditions and material properties play in ASR-induced deterioration. The inclusion of quadratic terms highlights that the relationship between these factors and deterioration is non-linear, suggesting that certain factors may have a more pronounced effect under specific conditions. For example, the interaction between aggregates and RH points to the importance of moisture availability in enhancing aggregate reactivity, while temperature influences higher temperatures, which may yield greater deterioration in certain aggregate types.

Overall, the aggregate reactivity is ranked to present a higher significance on ASR deterioration than temperature. Such significance can be inferred to influence the RH threshold required for ASR.

9.6 Conclusion

This study aimed to appraise the influence of moisture, temperature, and aggregate reactivity on ASR-induced damage through mechanical properties and microscopic assessments. The main conclusions drawn from the study are:

- The influence of temperature on ASR extends beyond kinetics (i.e., expansion rate). It impacts the microstructure of affected concrete. The rapid development of ASR at elevated temperatures generates higher crack counts, which can result in more significant reductions in mechanical properties at low to moderate expansion levels.

- Limiting moisture is crucial for mitigating ASR. However, low RH levels potentially cause higher ASR-induced damage due to shrinkage. Shrinkage-induced cracks are isolated within the cement paste at low expansion. They can significantly influence mechanical properties at very high expansion levels by densifying the cement matrix and forming an extended network with ASR-induced cracks propagating from the aggregate particles.
- While a minimum DRI number for significant damage in ASR-affected concrete did not exist before this study, considering all the factors evaluated therein, a DRI number of 225 can be considered a critical threshold for significant ASR-induced deterioration.
- This study proves that the driving factors for ASR kinetics and ASR-induced damage differ, emphasizing the difference between these two assessments. The kinetics of the reaction is more influenced by moisture. However, alkali content is crucial for deterioration.
- Considering the damage-based assessment conducted in this study, the ASR RH threshold depends on aggregate and temperature reactivity, but the former is more critical. Hence, no single RH threshold fit for all aggregate types. As such, the maintenance of affected concrete should be considered individually. In case of the need for a universal RH threshold that fits all conditions, this study proves that such a threshold should be lower than the 80% that has been popularly reported.

Supplementary materials

Table S9.1: Influence of RH on damage

Relative Humidity	Expansion range	CS Loss	ME Loss	SDI	DRI
62% RH	0.00-0.03	2-6	5-12	0.105-0.130	146-175
	0.04±0.01	3-10	9-16	0.119-0.133	179-228
	0.07±0.01	7-13	20-23	0.130-0.165	228-292
75% RH	0.00-0.03	2-5	2-6	0.106-0.120	115-172
	0.04±0.01	4-8	7-18	0.110-0.140	148-244
	0.07±0.01	6-8	17-22	0.128-0.155	219-268
	0.11±0.01	11-15	23-30	0.134-0.182	295-399
82% RH	0.00-0.03	2-7	3-10	0.106-0.120	117-225
	0.04±0.01	3-7	7-12	0.112-0.140	151-225
	0.07±0.01	6-13	20-23	0.126-0.170	155-271
	0.11±0.01	13-14	28-35	0.170-0.180	351-397
	0.12%<Expansion< 0.20%*	17	36	160	222
90% RH	0.00-0.03	1-6	2-11	0.102-0.121	100-169
	0.04±0.01	3-7	8-12	0.111-0.127	151-192
	0.07±0.01	6-12	20-26	0.129-0.158	182-301
	0.11±0.01	11-17	29-36	0.143-0.175	295-364
	0.14±0.01	16-19	33-38	0.166-0.192	424-442
	0.20±0.01*	23	39	0.170	498
	0.20%<Expansion< 0.30%*	21	54	0.265	706
100% RH	0.00-0.03*	2	4	0.107	111
	0.04±0.01	3-8	7-13	0.116-0.127	134-252
	0.07±0.01	5-12	13-24	0.135-0.157	172-331
	0.11±0.01	9-16	28-29	0.138-0.191	319-411
	0.14±0.01	18-21	34-38	0.168-0.220	416-452
	0.20±0.01	18-26	42-46	0.205-0.250	610-695
	0.30±0.01	22-23	61-62	0.270-0.276	752-988

*One storage condition falls in this expansion range

Table S9.2: Influence of temperature on damage

Temperature	Expansion range	CS Loss	ME Loss	SDI	DRI
21°C	0.00-0.03	1-5	2-7	0.102-0.120	111-173
	0.04±0.01	3-10	7-16	0.110-0.133	134-270
	0.07±0.01	6-13	17-22	0.129-0.157	172-331
	0.11±0.01	14-16	28-33	0.160-0.173	319-403
	0.12%<Expansion< 0.20%*	17	40	0.226	418
38°C	0.00-0.03	3-7	5-7	0.113-0.120	152-225
	0.04±0.01	3-8	7-14	0.117-0.140	175-244
	0.07±0.01	7-13	20-26	0.120-0.165	155-292
	0.11±0.01	7-15	23-36	0.138-0.182	292-397
	0.14±0.01	16-21	33-38	0.162-0.220	322-442
	0.20±0.01	18-26	42-46	0.205-0.250	610-695
	0.30±0.01*	23	62	0.276	988
60°C	0.00-0.03	2-4	3-12	0.108-0.130	132-172
	0.04±0.01	3-6	7-17	0.119-0.150	166-197
	0.07±0.01	5-8	13-23	0.125-0.170	192-271
	0.11±0.01	9-15	29-35	0.143-0.191	329-411
	0.14±0.01	18-19	34-37	0.168-0.170	430-452
	0.20±0.01*	23	39	0.190	498

*One storage condition falls in this expansion range

Table S9.3: ANOVA Table for expansion

Source	Sum of Squares (SS)	Degree of Freedom (df)	Mean Squares (MS)	F-value	p-value	Significance
Aggregates	0.0094	1	0.0094	10.6542	0.0016	Yes
Alkali	0.0704	1	0.0704	79.8797	<0.0001	Yes
Temperature	0.0078	1	0.0078	8.8966	0.0038	Yes
RH	0.0136	1	0.0136	15.3881	0.0002	Yes
Aggregates ²	0.0014	1	0.0014	1.6007	0.2097	No
Alkali ²	0.0386	1	0.0386	43.7448	<0.0001	Yes
Temperature ²	0.0148	1	0.0148	16.8122	0.0001	Yes
RH ²	0.0012	1	0.0012	1.3158	0.2549	No
Aggregates:Alkali	0.0007	1	0.0007	0.8444	0.3610	No
Aggregates:Temperature	0.0027	1	0.0027	3.0670	0.0839	No
Aggregates:RH	0.0054	1	0.0054	6.0968	0.0158	Yes
Alkali:Temperature	0.0001	1	0.0001	0.1421	0.7072	No
Alkali:RH	0.0005	1	0.0005	0.5966	0.4423	No
Temperature:RH	0.0006	1	0.0006	0.6687	0.4161	No
Residual	0.0670	76	0.0009			

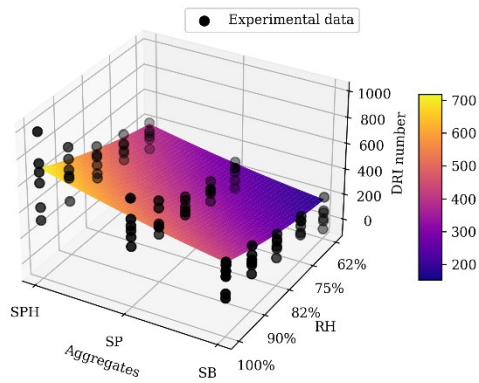
Table S9.4: ANOVA Table for DRI

Source	Sum of Squares (SS)	Degree of Freedom (df)	Mean Squares (MS)	F-value	p-value	Significance
Aggregates	47668.5624	1	47668.5624	11.5279	0.0011	Yes
Alkali	423106.2063	1	423106.2063	102.3215	<0.0001	Yes
Temperature	47057.0040	1	47057.0040	11.3800	0.0012	Yes
RH	95294.3904	1	95294.3904	23.0454	<0.0001	Yes
Aggregates ²	6387.3413	1	6387.3413	1.5447	0.2177	No
Alkali ²	216727.7852	1	216727.7852	52.4121	<0.0001	Yes
Temperature ²	86304.8062	1	86304.8062	20.8714	<0.0001	Yes
RH ²	15592.3977	1	15592.3977	3.7708	0.0559	No
Aggregates: Alkali	3594.7749	1	3594.7749	0.8693	0.3541	No
Aggregates: Temperature	5977.0341	1	5977.0341	1.4455	0.2330	No
Aggregates: RH	9755.2906	1	9755.2906	2.3592	0.1287	No
Alkali: Temperature	550.3656	1	550.3656	0.1331	0.7163	No
Alkali: RH	2715.2463	1	2715.2463	0.6566	0.4203	No
Temperature: RH	12713.1159	1	12713.1159	3.0745	0.0836	No
Residual	314265.1549	76	4135.0678			

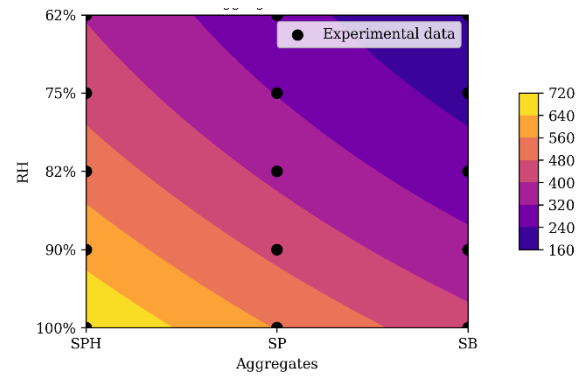
Table S9.5: ANOVA Table for modulus loss

Source	Sum of Squares (SS)	Degree of Freedom (df)	Mean Squares (MS)	F-value	p-value	Significance
Aggregates	96.1775	1	96.1775	6.0237	0.0164	Yes
Alkali	2354.9324	1	2354.9324	147.4926	<0.0001	Yes
Temperature	156.4723	1	156.4723	9.8001	0.0025	Yes
RH	400.4294	1	400.4294	25.0794	<0.0001	Yes
Aggregates ²	4.6877	1	4.6877	0.2936	0.5895	No
Alkali ²	1026.5530	1	1026.5530	64.2944	<0.0001	Yes
Temperature ²	380.3142	1	380.3142	23.8196	<0.0001	Yes
RH ²	15.2935	1	15.2935	0.9579	0.3308	No
Aggregates: Alkali	0.7320	1	0.7320	0.0458	0.8310	No
Aggregates: Temperature	51.0887	1	51.0887	3.1998	0.0776	No
Aggregates: RH	19.7321	1	19.7321	1.2358	0.2698	No
Alkali: Temperature	0.0404	1	0.0404	0.0025	0.9600	No
Alkali: RH	1.6726	1	1.6726	0.1048	0.7471	No
Temperature: RH	25.0820	1	25.0820	1.5709	0.2139	No
Residual	1213.4497	76	15.9664			

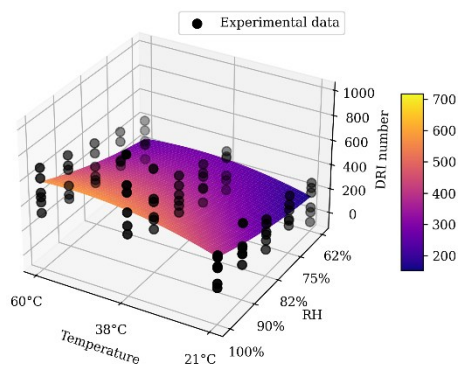
(a) Aggregates versus RH-3D



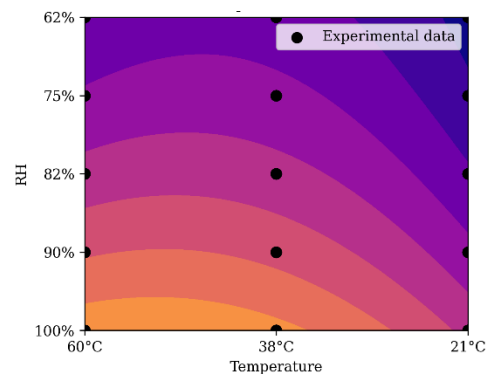
(b) Aggregates versus RH-2D



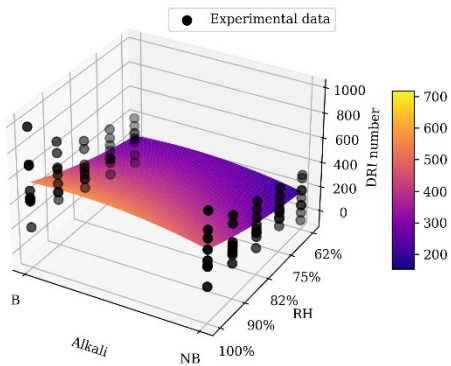
(c) Temperature versus RH-3D



(d) Temperature versus RH-2D



(e) Alkali loading versus RH-3D



(f) Alkali loading versus RH-2D

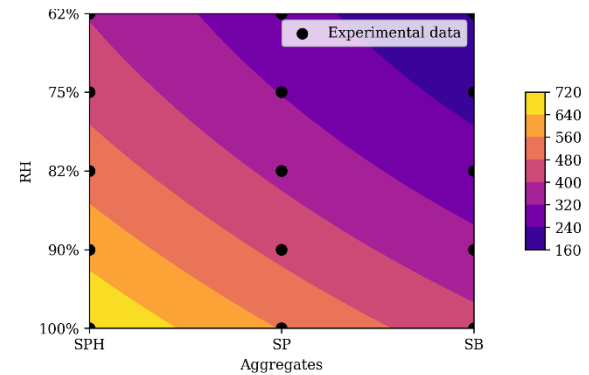
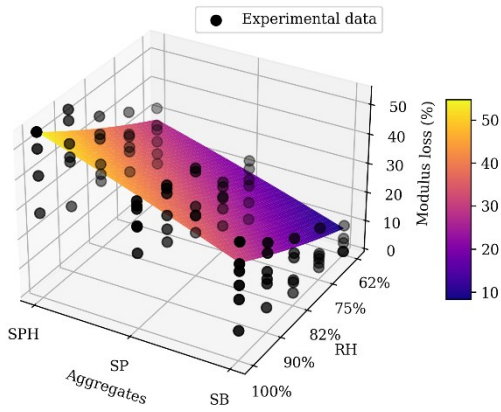
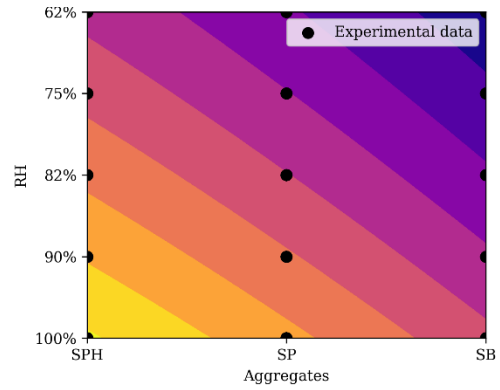


Figure S9.1: 3D surface and 2D contour plot of DRI model: (a,b) effects of aggregate reactivity and RH (c,d) effects of temperature and RH (e,f) effects of alkali loading and RH

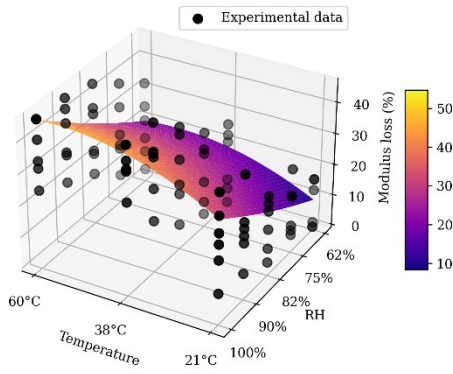
(a) Aggregates versus RH -3D



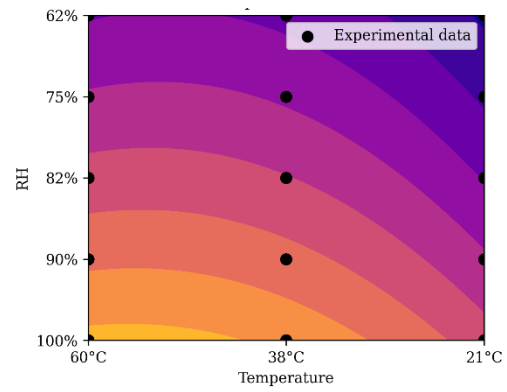
(b) Aggregates versus RH-2D



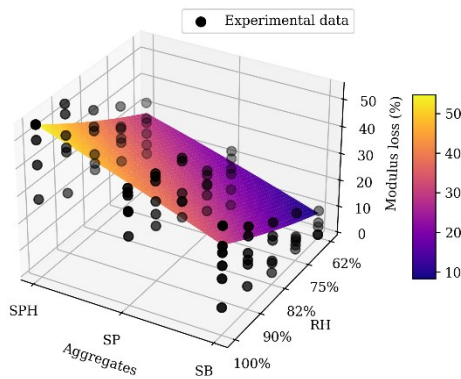
(c) Temperature versus RH-3D



(d) Temperature versus RH-2D



(e) Alkali loading versus RH-3D



(f) Alkali loading versus RH-2D

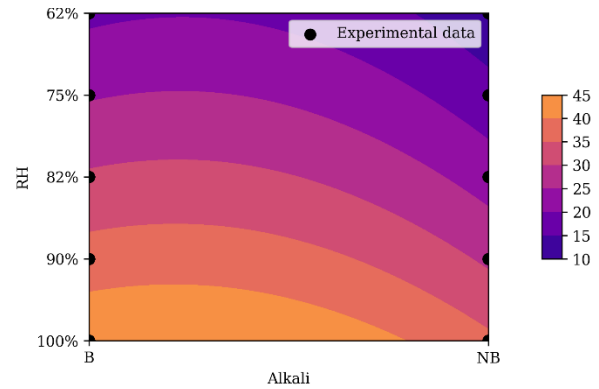


Figure S9.2: 3D surface and 2D contour plot surface of modulus of elasticity reduction model: (a,b) effects of aggregate reactivity and RH (c,d) effects of temperature and RH (e,f) effects of alkali loading and RH

Table S9.6: Tukey test for damage assessment: (a) expansion. (b) modulus of elasticity reduction. Chi-squared test for (c) DRI

(a) Pairs	Sudbury			Spratt			Springhill		
	21°C	38°C	60°C	21°C	38°C	60°C	21°C	38°C	60°C
62% versus 75%	No	No	Yes	No	No	No	Yes	No	-
62% versus 82%	Yes	Yes	Yes	No	Yes	Yes	Yes	Yes	-
62% versus 90%	Yes	Yes	Yes	Yes	Yes	Yes	Yes	Yes	-
62% versus 100%	Yes	Yes	Yes	Yes	Yes	Yes	Yes	Yes	-
75% versus 82%	No	Yes	Yes	No	Yes	Yes	Yes	Yes	-
75% versus 90%	Yes	Yes	Yes	No	Yes	Yes	Yes	Yes	-
75% versus 100%	Yes	Yes	Yes	Yes	Yes	Yes	Yes	Yes	-
82% versus 90%	Yes	Yes	Yes	No	No	No	Yes	Yes	-
82% versus 100%	Yes	Yes	Yes	Yes	No	No	Yes	Yes	-
90% versus 100%	No	Yes	No	Yes	No	No	Yes	Yes	-

(b) Pairs	Sudbury			Spratt			Springhill		
	21°C	38°C	60°C	21°C	38°C	60°C	21°C	38°C	60°C
62% versus 75%	No	No	Yes	No	No	No	Yes	No	-
62% versus 82%	Yes	Yes	Yes	No	Yes	Yes	Yes	Yes	-
62% versus 90%	Yes	Yes	Yes	Yes	Yes	Yes	Yes	Yes	-
62% versus 100%	Yes	Yes	Yes	Yes	Yes	Yes	Yes	Yes	-
75% versus 82%	No	Yes	Yes	No	Yes	Yes	No	Yes	-
75% versus 90%	Yes	Yes	Yes	No	Yes	Yes	Yes	Yes	-
75% versus 100%	Yes	Yes	Yes	Yes	Yes	Yes	Yes	Yes	-
82% versus 90%	Yes	Yes	Yes	No	No	No	Yes	Yes	-
82% versus 100%	Yes	Yes	Yes	Yes	No	No	Yes	Yes	-
90% versus 100%	No	Yes	No	Yes	No	No	No	Yes	-

(c) Pairs	Sudbury			Spratt			Springhill		
	21°C	38°C	60°C	21°C	38°C	60°C	21°C	38°C	60°C
62% versus 75%	No	Yes	No	No	No	Yes	No	No	-
62% versus 82%	Yes	Yes	No	Yes	Yes	Yes	Yes	Yes	-
62% versus 90%	Yes	Yes	Yes	Yes	Yes	Yes	Yes	Yes	-
62% versus 100%	Yes	Yes	Yes	Yes	Yes	Yes	Yes	Yes	-
75% versus 82%	Yes	Yes	No	Yes	Yes	Yes	Yes	Yes	-
75% versus 90%	Yes	Yes	No	Yes	Yes	Yes	Yes	Yes	-
75% versus 100%	Yes	Yes	Yes	Yes	Yes	Yes	Yes	Yes	-
82% versus 90%	Yes	Yes	No	No	No	Yes	Yes	Yes	-
82% versus 100%	Yes	Yes	Yes	No	No	Yes	Yes	Yes	-
90% versus 100%	Yes	No	Yes	No	No	Yes	Yes	Yes	-

Table S9.7: Experimental plan

Run	Aggregates	Alkali	Temperature	RH	Experimented
1	1	1	1	1	No
2	1	1	1	2	No
3	1	1	1	3	No
4	1	1	1	4	No
5	1	1	1	5	No
6	1	1	2	1	Yes
7	1	1	2	2	Yes
8	1	1	2	3	No
9	1	1	2	4	Yes
10	1	1	2	5	No
11	1	1	3	1	Yes
12	1	1	3	2	No
13	1	1	3	3	Yes
14	1	1	3	4	No
15	1	1	3	5	Yes
16	1	2	1	1	No
17	1	2	1	2	No
18	1	2	1	3	No
19	1	2	1	4	No
20	1	2	1	5	No
21	1	2	2	1	Yes
22	1	2	2	2	No
23	1	2	2	3	Yes
24	1	2	2	4	No
25	1	2	2	5	Yes
26	1	2	3	1	Yes
27	1	2	3	2	Yes
28	1	2	3	3	No
29	1	2	3	4	Yes
30	1	2	3	5	No
31	2	1	1	1	Yes
32	2	1	1	2	Yes
33	2	1	1	3	Yes
34	2	1	1	4	Yes
35	2	1	1	5	Yes
36	2	1	2	1	Yes
37	2	1	2	2	Yes
38	2	1	2	3	Yes
39	2	1	2	4	Yes
40	2	1	2	5	Yes
41	2	1	3	1	Yes

42	2	1	3	2	Yes
43	2	1	3	3	Yes
44	2	1	3	4	Yes
45	2	1	3	5	Yes
46	2	2	1	1	Yes
47	2	2	1	2	Yes
48	2	2	1	3	Yes
49	2	2	1	4	Yes
50	2	2	1	5	No
51	2	2	2	1	Yes
52	2	2	2	2	Yes
53	2	2	2	3	No
54	2	2	2	4	No
55	2	2	2	5	No
56	2	2	3	1	Yes
57	2	2	3	2	Yes
58	2	2	3	3	No
59	2	2	3	4	No
60	2	2	3	5	No
61	3	1	1	1	Yes
62	3	1	1	2	No
63	3	1	1	3	Yes
64	3	1	1	4	No
65	3	1	1	5	Yes
66	3	1	2	1	Yes
67	3	1	2	2	Yes
68	3	1	2	3	No
69	3	1	2	4	Yes
70	3	1	2	5	No
71	3	1	3	1	Yes
72	3	1	3	2	No
73	3	1	3	3	Yes
74	3	1	3	4	No
75	3	1	3	5	No
76	3	2	1	1	Yes
77	3	2	1	2	Yes
78	3	2	1	3	No
79	3	2	1	4	Yes
80	3	2	1	5	No
81	3	2	2	1	Yes
82	3	2	2	2	No
83	3	2	2	3	Yes
84	3	2	2	4	No

85	3	2	2	5	No
86	3	2	3	1	Yes
87	3	2	3	2	Yes
88	3	2	3	3	No
89	3	2	3	4	Yes
90	3	2	3	5	Noi

Overview of Chapter nine

Chapters 6-8 discuss the influence of moisture and temperature on ASR-induced damage, which is limited to Spratt reactive aggregate. Chapter nine focused on a rather comprehensive damage assessment that includes various aggregates with different levels of reactivity, as well as concrete with varying alkali loading. ASR-induced deterioration was reported to be influenced by aggregate type and the response surface methodology (RSM) was used to evaluate the interactions between the factors assessed. Furthermore, the RH threshold required to trigger ASR was evaluated using ASR-induced expansion, as well as results from the DRI and SDT.

CHAPTER TEN: SCIENTIFIC AND ENGINEERING CONTRIBUTIONS OF THE PHD THESIS

As previously stated, this PhD study aims to provide a better understanding of the impact of exposure conditions (i.e., moisture and temperature), alkali loading, and aggregate reactivity level on ASR-induced development. Aspects investigated were kinetics, induced expansion, physical integrity assessment based on microscopic evaluation and degradation of mechanical properties. Furthermore, a damage-based assessment of the RH threshold required to trigger and sustain ASR development can be recognized as another research achievement. The specific findings can be categorized as being either scientific or engineering contributions, as presented hereafter:

10.1 Scientific contributions

- Understanding the dynamic interaction between external and internal moisture in concrete specimens undergoing ASR;
- Understanding how shrinkage from low moisture conditions can underrepresent actual ASR-induced expansion;
- Understanding of the influence of temperature, alkali content and aggregate reactivity level on ASR-induced expansion;
- Understanding how concrete maturity influences ASR development and introduction of a metric (K-value) that evaluates moisture states in concrete and relation to ASR-induced expansion;
- Understanding the dependency of the RH threshold on temperature and aggregate reactivity;
- Understanding of the development of ASR microscopic distress features in concrete specimens containing different alkali levels and aggregate lithotypes under various exposure conditions;

- Understanding how the microscopic distress features of ASR impact the mechanical behaviour at different exposure conditions;
- Understanding how various crack types (sharp versus onion skin) can influence ASR development;
- Understanding the distinction between ASR expansion and associated deterioration.

10.2 Engineering contributions

- Demonstrating the suitability of the Stiffness Damage Test (SDT) and Damage Rating Index (DRI) as diagnostic tools for assessing ASR-induced damage in affected concrete over a wide sssrange of exposure conditions than previously examined;
- Proposal of a damage classification table fit for use under numerous exposure conditions for a comprehensive classification of ASR-induced damage using outcomes such as the DRI, modulus of elasticity reduction, SDI, and compressive strength reduction. Overall, a DRI of 225 and modulus of elasticity reduction of 12% can be used as damage outcomes indicating the occurrence of deleterious ASR in affected concrete;
- Provision of a foundation for developing predictive models focused on aggregates with different reactivity levels and over a wide range of exposure conditions;
- Insights on internal and external moisture interaction offer engineers a practical approach to managing ASR. A damage-based assessment of the critical RH needed for managing ASR-affected concrete is proposed. Engineers can now implement targeted RH controls, ensuring that concrete structures remain below the identified RH threshold, which is dependent on temperature, aggregate and alkali loading.

CHAPTER ELEVEN: CONCLUSIONS AND RECOMMENDATIONS

11.1 Conclusions

The main objective of this research was to evaluate how various critical factors, particularly moisture, temperature, aggregate reactivity, and alkali loading, influence ASR-induced expansion and deterioration. From the results obtained after a comprehensive experimental campaign, the following conclusions can be drawn:

- ASR is quite sensitive to internal RH since a change in the internal RH impacts induced development, leading to expansion or shrinkage. This suggests that maintaining lower internal RH could potentially control ASR. However, the external RH plays an important role in influencing the internal RH through a dynamic moisture exchange that varies with environmental conditions. This highlights the importance of considering the internal RH and external RH as interdependent factors in effective maintenance strategies.
- Moisture and temperature significantly influence ASR kinetics. The reaction progresses faster under high moisture and temperature conditions, leading to greater expansion within a shorter period compared to low moisture and temperature conditions. Hence, similar levels of expansion are reached at different ages.
- Moisture primarily governs ASR kinetics rather than ultimate expansion. At low RH, the reaction proceeds slower due to reduced mobility of ions and limited moisture. However, a comparison of the expansion plots suggests that the silica dissolution and gel formation remain active. However, only at a reduced pace, as highlighted by the stable expansion rates reported in this study. It can, therefore, be concluded that over extended periods, the

accumulated reaction products will likely induce ultimate expansion comparable to that observed in high RH conditions.

- Sanchez et al.'s qualitative model for ASR development, proposed in 2017, can be adapted for coupled mechanisms involving shrinkage and ASR at low moisture conditions. ASR-induced cracks propagate as described by the model; however, isolated shrinkage cracks may form in the cement paste at negligible-low expansion levels. Although these cracks are inactive, they contribute to a denser microstructure at high expansion levels, leading to greater mechanical property losses.
- The trend of microscopic and mechanical properties changes as a function ASR-induced expansion is consistent across all temperatures. However, crack properties are influenced by temperature changes. Concrete specimens at 60°C exhibit a higher crack density with shorter and narrower cracks, while those at 38°C present fewer but wider and longer cracks.
- Specimens stored at 62% RH and 75% RH exhibit similar ASR-induced deterioration. The Tukey test statistical analysis confirms no significant difference in ASR development within this RH range. This suggests that moisture change between 62% and 75% RH will not notably alter ASR-induced deterioration rates, simplifying environmental control recommendations.
- Analysis of the images captured and processed using image analysis technique revealed that the aggregate type, exposure conditions, or alkali level played an inconsequential role in the orientation of ASR-induced cracks in concrete specimens undergoing free expansion.
- Given the broader range of exposure conditions assessed in this study, it was found that low moisture can lead to a coupled mechanism and temperature influencing crack properties. The impact of these exposure conditions on the qualitative and quantitative

properties of cracks and associated reductions in mechanical properties led to the adaptation of the damage classifications proposed by Sanchez et al. in 2017. A new damage classification was proposed to account for coupled mechanisms (i.e., ASR + Shrinkage), incorporating the combined influence of moisture and temperature.

- The damage-based RH threshold assessment indicates that the widely reported 80% RH threshold depends on the aggregate reactivity level and temperature. The 80% RH applies mainly to moderately reactive aggregates at 21°C. This threshold is insufficient for very-highly reactive aggregates at elevated temperatures (e.g., Springhill at 38°C/60°C). Hence, a 62-75% RH threshold range seems to be more realistic to accommodate various aggregate reactivity levels and temperatures.
- Overall, while ASR-induced expansion and damage exhibit a similar trend, the Pareto plots show that different factors influence these phenomena. Moisture conditions predominantly impact ASR kinetics (i.e., rate of expansion), while alkali loading is most significant in terms of the extent of damage.

11.2 Recommendations

After conducting extensive experimental research on the influence of moisture and temperature on ASR-affected concrete and considering the conclusions stated above, some recommendations and suggestions for future research can be proposed as follows:

- This study only considers reactive coarse aggregates; it is well-established that reactive fine aggregates have ASR-induced cracks initiated from reactive fine particles compared to reactive coarse aggregates. Such propagation mode could present a difference in damage, especially in low moisture conditions. Further study comparing damage in

reactive coarse and fine aggregates will enhance our understanding of ASR-induced damage.

- This study confirmed the influence of moisture on ASR kinetics. However, the limited duration of the experiment limited the determination of the actual ultimate ASR-induced expansion at low RH conditions. A longer duration assessment would provide experimental confirmation of the influence of moisture on ultimate expansion.
- Concrete in service is often subjected to cycles of wet and dry conditions and varying temperatures. The influence of this condition on ASR kinetics is known. However, an evaluation of its impact on damage is unknown. Research into this will further enhance our understanding of environmental/weather conditions.
- The moisture dynamics and ASR-induced expansion and deterioration evaluation in concrete could be further explored using field-exposed specimens. Thus increasing our understanding of the damage mechanism.
- Based on the comprehensive experimental campaign conducted in this study, developing a mathematical model to predict ASR development in concrete containing aggregates of various reactivity levels and alkali loading under numerous exposure conditions is recommended. Such a model will build on the findings of this research to provide a reliable tool for forecasting ASR.

References

1. Stanton, T.E. Expansion of Concrete through Reaction between Cement and Aggregate. *Proceedings of the American Society of Civil Engineering* **1940**, *66*, 1781–1811.
2. Stokes, D.; Pappas, J.; Thomas, M.D.A.; Folliard, K.J. Field Cases Involving Treatment or Repair of ASR-Affected Concrete Using Lithium. In Proceedings of the Proceedings of the 6th CANMET/ACI International Conference on Durability of Concrete; Thessaloniki, Greece, 2003; pp. 631–642.
3. Folliard, K.J.; Thomas, M.D.A.; Ideker, J.H.; East, B.; Fournier, B. Case Studies of Treating ASR-Affected Structures with Lithium Nitrate. In Proceedings of the Proceedings of the 13th International Conference on Alkali-Aggregate Reaction in Concrete; Trondheim, Norway, 2008.
4. Durand, B. Review of Repair Methods Used at Hydro-Quebec to Inhibit AAR in Concrete Structures. In Proceedings of the AAR in Hydroelectric Plants and Dams: Proceedings of the 2nd International Conference; United States Committee on Large Dams: Chattanooga, USA, 1995; pp. 289–309.
5. De Beauchamp, T. The Progress of Remedial Measures at Chambon Dam. In Proceedings of the AAR in Hydroelectric Plants and Dams: Proceedings of the 2nd International Conference; United States Committee on Large Dams: Chattanooga, USA, 1995; pp. 209–220.
6. Sanchez, L.; Fournier, B.; Jolin, M.; Duchesne, J. Reliable Quantification of AAR Damage through Assessment of the Damage Rating Index (DRI). *Cement and Concrete Research* **2015**, *67*, 74–92, doi:10.1016/j.cemconres.2014.08.002.
7. Sanchez, L.; Fournier, B.; Jolin, M.; Bedoya, M.; Bastien, J.; Duchesne, J. Use of Damage Rating Index to Quantify Alkali-Silica Reaction Damage in Concrete: Fine versus Coarse Aggregate. *ACI Materials Journal* **2016**, *113*, doi:10.14359/51688983.
8. Deschenes, R.A.; Giannini, E.; Drimalas, T.; Fournier, B.; Hale, W.M. Effects of Moisture, Temperature, and Freezing and Thawing on Alkali-Silica Reaction. *ACI Materials Journal* **2018**, *115*, 575–584, doi:10.14359/51702192.
9. Tosun, K.; Felekoğlu, B.; Baradan, B. The Effect of Cement Alkali Content on ASR Susceptibility of Mortars Incorporating Admixtures. *Building and Environment* **2007**, *42*, 3444–3453, doi:10.1016/j.buildenv.2006.08.024.
10. Poyet, S.; Sellier, A.; Capra, B.; Thèvenin-Foray, G.; Torrenti, J.-M.; Tournier-Cognon, H.; Bourdarot, E. Influence of Water on Alkali-Silica Reaction: Experimental Study and Numerical Simulations. *J. Mater. Civ. Eng.* **2006**, *18*, 588–596, doi:10.1061/(ASCE)0899-1561(2006)18:4(588).
11. Multon, S.; Toutlemonde, F. Effect of Moisture Conditions and Transfers on Alkali Silica Reaction Damaged Structures. *Cement and Concrete Research* **2010**, *40*, 924–934, doi:10.1016/j.cemconres.2010.01.011.
12. Nilsson, L.-O. On the Role of Moisture in Degradation of Concrete Structures. In Proceedings of the Global Construction: Ultimate Concrete Opportunities; Dundee, Scotland, 2005; pp. 15–24.
13. Olafsson, H. The Effect of Relative Humidity and Temperature on Alkali Expansion of Mortar Bars. In Proceedings of the 7th International Conference on Alkali Aggregate Reaction in Concrete; Ottawa, 1986; pp. 461–465.
14. Ideker, J.H.; East, B.L.; Folliard, K.J.; Thomas, M.D.A.; Fournier, B. The Current State of the Accelerated Concrete Prism Test. *Cement and Concrete Research* **2010**, *40*, 550–555, doi:10.1016/j.cemconres.2009.08.030.
15. Gautam, B.P.; Panesar, D.K. The Effect of Elevated Conditioning Temperature on the ASR Expansion, Cracking and Properties of Reactive Spratt Aggregate Concrete. *Construction and Building Materials* **2017**, *140*, 310–320, doi:10.1016/j.conbuildmat.2017.02.104.
16. Larive, C. Apports combinés de l'expérimentation et de la modélisation à la compréhension de l'alcali-réaction et de ses effets mécaniques, 28, Presses du Laboratoire Central des Ponts et Chaussées, Paris, 1997.
17. De Souza, D.J.; Sanchez, L.; Tagliaferri de Grazia, M. Evaluation of a Direct Shear Test Setup to Quantify AAR-Induced Expansion and Damage in Concrete. *Construction and Building Materials* **2019**, *229*, doi:10.1016/j.conbuildmat.2019.116806.
18. Marzouk, H.; Langdon, S. The Effect of Alkali-Aggregate Reactivity on the Mechanical Properties of High and Normal Strength Concrete. *Cement and Concrete Composites* **2003**, *25*, 549–556, doi:10.1016/S0958-9465(02)00094-X.

19. Mohammadi, A.; Ghiasvand, E.; Nili, M. Relation between Mechanical Properties of Concrete and Alkali-Silica Reaction (ASR); a Review. *Construction and Building Materials* **2020**, *258*, 1–16, doi:10.1016/j.conbuildmat.2020.119567.
20. Diab, S.H.; Soliman, A.M.; Nokken, M.R. Changes in Mechanical Properties and Durability Indices of Concrete Undergoing ASR Expansion. *Construction and Building Materials* **2020**, *251*, 118951, doi:10.1016/j.conbuildmat.2020.118951.
21. Zhang, K.; Zhou, J.; Yin, Z. Experimental Study on Mechanical Properties and Pore Structure Deterioration of Concrete under Freeze–Thaw Cycles. *Materials* **2021**, *14*, 6568, doi:10.3390/ma14216568.
22. Rajabipour, F.; Giannini, E.; Dunant, C.; Ideker, J.H.; Thomas, M.D.A. Alkali–Silica Reaction: Current Understanding of the Reaction Mechanisms and the Knowledge Gaps. *Cement and Concrete Research* **2015**, *76*, 130–146, doi:10.1016/j.cemconres.2015.05.024.
23. Nilsson, L.-O. On the Role of Moisture in Degradation of Concrete Structures.; Thomas Telford, 2005; pp. 15–24.
24. Stark, D.; Okamoto, P.; Diamond, S. *Eliminating or Minimizing Alkali-Silica Reactivity*; Strategic Highway Research Program, SHRP-C; Washington, DC, 1993; ISBN 978-0-309-05603-8.
25. Kurihara, T.; Katawaki, K. Effects of Moisture Control and Inhibition on Alkali Silica Reaction. In Proceedings of the 8th International Conference on Alkali-Aggregate Reaction; Kyoto, Japan, 1989; pp. 629–634.
26. Tomosawa, F.; Tamura, K.; Abe, M. Influence of Water Content of Concrete on Alkali-Aggregate Reaction. In Proceedings of the 8th International Conference on Alkali-Aggregate Reaction; Kyoto, Japan, 1989; pp. 881–885.
27. Stark, D. The Moisture Condition of Field Concrete Exhibiting Alkali–Silica Reactivity. In Proceedings of the Second International Conference on Durability of Concrete; ACI Publication SP, 1991; pp. 973–987.
28. Rajabipour, F.; Giannini, E.; Dunant, C.; Ideker, J.H.; Thomas, M.D.A. Alkali–Silica Reaction: Current Understanding of the Reaction Mechanisms and the Knowledge Gaps. *Cement and Concrete Research* **2015**, *76*, 130–146, doi:10.1016/j.cemconres.2015.05.024.
29. Tragardh, J.; Lagerblad, B. Influence of ASR Expansion on the Frost Resistance of Concrete. In Proceedings of the 10th International Conference on Alkali Aggregate Reaction in Concrete; Melbourne, Australia, 1996; pp. 853–860.
30. Boddy, A.M.; Hooton, R.D.; Thomas, M.D.A. The Effect of the Silica Content of Silica Fume on Its Ability to Control Alkali–Silica Reaction. *Cement and Concrete Research* **2003**, *33*, 1263–1268, doi:10.1016/S0008-8846(03)00058-9.
31. Diamond, S. Effects of Two Danish Flyashes on Alkali Contents of Pore Solutions of Cement-Flyash Pastes. *Cement and Concrete Research* **1981**, *11*, 383–394, doi:10.1016/0008-8846(81)90110-1.
32. Duchesne, J.; Bérubé, M.A. The Effectiveness of Supplementary Cementing Materials in Suppressing Expansion Due to ASR: Another Look at the Reaction Mechanisms Part 2: Pore Solution Chemistry. *Cement and Concrete Research* **1994**, *24*, 221–230, doi:10.1016/0008-8846(94)90047-7.
33. Ramlochan, T.; Thomas, M.; Gruber, K.A. The Effect of Metakaolin on Alkali–Silica Reaction in Concrete. *Cement and Concrete Research* **2000**, *30*, 339–344, doi:10.1016/S0008-8846(99)00261-6.
34. Venkatachalam, S.; Raja, K.; Vishnuvardhan, K.; Suchithra, S.; Maniarsan, S.K.; Saravanan, M.M.; Miruna, M.; Prabanjan, S. The ASR Mechanism in Concrete and the Influence of Lithium in Mitigating It: A Critical Review. *Materials Today: Proceedings* **2022**, *65*, A1–A6, doi:10.1016/j.matpr.2022.07.327.
35. Kaladharan, G.; Szeles, T.; Stoffels, S.M.; Rajabipour, F. Novel Admixtures for Mitigation of Alkali-Silica Reaction in Concrete. *Cement and Concrete Composites* **2021**, *120*, 104028, doi:10.1016/j.cemconcomp.2021.104028.
36. Feng, X.; Thomas, M.D.A.; Bremner, T.W.; Balcom, B.J.; Folliard, K.J. Studies on Lithium Salts to Mitigate ASR-Induced Expansion in New Concrete: A Critical Review. *Cement and Concrete Research* **2005**, *35*, 1789–1796, doi:10.1016/j.cemconres.2004.10.013.
37. Leemann, A.; Lörtscher, L.; Bernard, L.; Le Saout, G.; Lothenbach, B.; Espinosa-Marzal, R.M. Mitigation of ASR by the Use of LiNO₃—Characterization of the Reaction Products. *Cement and Concrete Research* **2014**, *59*, 73–86, doi:10.1016/j.cemconres.2014.02.003.
38. Diaz-Loya, I.; Juenger, M.; Seraj, S.; Minkara, R. Extending Supplementary Cementitious Material Resources: Reclaimed and Remediated Fly Ash and Natural Pozzolans. *Cement and Concrete Composites* **2019**, *101*, 44–51, doi:10.1016/j.cemconcomp.2017.06.011.

39. Oey, T.; La Plante, E.C.; Falzone, G.; Hsiao, Y.-H.; Wada, A.; Monfardini, L.; Bauchy, M.; Bullard, J.W.; Sant, G. Calcium Nitrate: A Chemical Admixture to Inhibit Aggregate Dissolution and Mitigate Expansion Caused by Alkali-Silica Reaction. *Cement and Concrete Composites* **2020**, *110*, 103592, doi:10.1016/j.cemconcomp.2020.103592.
40. Xiao, R.; Huang, B.; Zhou, H.; Ma, Y.; Jiang, X. A State-of-the-Art Review of Crushed Urban Waste Glass Used in OPC and AAMs (Geopolymer): Progress and Challenges. *Cleaner Materials* **2022**, *4*, 100083, doi:10.1016/j.clema.2022.100083.
41. Bérubé, M.-A.; Chouinard, D.; Pigeon, M.; Frenette, J.; Rivest, M.; Vézina, D. Effectiveness of Sealers in Counteracting Alkali–Silica Reaction in Highway Median Barriers Exposed to Wetting and Drying, Freezing and Thawing, and Deicing Salt. *Canadian Journal of Civil Engineering* **2002**, *29*, 329–337, doi:DOI: 10.1139/L02-010.
42. Lute, R.D.; Folliard, K.J.; Drimalas, T.; Rust, C.K. Coatings and Sealers for Mitigation of Alkali-Silica Reaction and/or Delayed Ettringite Formation. In Proceedings of the 15th International Conference on Alkali-Aggregate Reaction 15th International Conference on Alkali-Aggregate Reaction; São Paulo, Brazil, 2016; p. 10.
43. Murray, C.D. Durability of Silane Sealer in a Highly Alkaline Environment. Graduate Theses and Dissertations, University of Arkansas: Fayetteville, 2014.
44. Schindler, A.; Johnson, D.; Warnock, R.; Barnes, R. Effectiveness of Silane to Mitigate Alkali-Silica Reaction in a Historical Bridge. *MATEC Web Conf.* **2018**, *199*, 03009, doi:10.1051/mateconf/201819903009.
45. Thomas, M.; Folliard, K.; Fournier, B.; Rivard, P.; Drimalas, T. *Methods for Evaluating and Treating ASR-Affected Structures: Results of Field Application and Demonstration Projects Volume I: Summary of Findings and Recommendations Final Report*; FHWA Office of Pavement Technology: Washington, DC 20590, 2013;
46. Ludwig, U. Effects of Environmental Conditions on Alkali-Aggregate Reaction. In Proceedings of the 8th International Conference on Alkali-Aggregate Reaction; Kyoto, Japan, 1989; pp. 583–596.
47. Poyet, S.; Sellier, A.; Capra, B.; Thèvenin-Foray, G.; Torrenti, J.-M.; Tournier-Cognon, H.; Bourdarot, E. Influence of Water on Alkali-Silica Reaction: Experimental Study and Numerical Simulations. *J. Mater. Civ. Eng.* **2006**, *18*, 588–596, doi:10.1061/(ASCE)0899-1561(2006)18:4(588).
48. Pedneault, A. Development of Testing and Analytical Procedures for the Evaluation of the Residual Potential of Reaction, Expansion, and Deterioration of Concrete Affected by ASR, Laval University: Quebec City, Canada, 1996.
49. Sanchez, L.; Fournier, B.; Drimalas, T.; Bastien, J.; Mitchell, D.; Noel, M. Semi-Quantitative Condition Assessment of Concrete Distress through the Damage Rating Index. In Proceedings of the 15th International Conference on Alkali-Aggregate Reaction; Brazil, 2016; pp. 1–10.
50. Sanchez, L.F.M.; Drimalas, T.; Fournier, B. Assessing Condition of Concrete Affected by Internal Swelling Reactions (ISR) through the Damage Rating Index (DRI). *Cement* **2020**, *1–2*, 100001, doi:10.1016/j.cement.2020.100001.
51. Owsiak, Z.; Zapala-Sławeta, J.; Czapik, P. Diagnosis of Concrete Structures Distress Due to Alkali-Aggregate Reaction. *Bulletin of the Polish Academy of Sciences, Technical Sciences* **2015**, *63*, 23–29, doi:10.1515/bpasts-2015-0003.
52. Juliana, M.M. da F.; Vanessa Karla Barbosa, de S.; Deborah Grasielly Cipriano, da S.; Dione Luiza, da S.; Eliana Cristina, B.M. Alkali-Aggregate Reaction: Definition, Influence and Control. *EAS* **2018**, *3*, 12–20, doi:10.11648/j.eas.20180301.13.
53. Du, H.; Tan, K.H. Effect of Particle Size on Alkali–Silica Reaction in Recycled Glass Mortars. *Construction and Building Materials* **2014**, *66*, 275–285, doi:10.1016/j.conbuildmat.2014.05.092.
54. Fernandes, I.; Broekmans, M.A.T.M. Alkali–Silica Reactions: An Overview. Part I. *Metallogr. Microstruct. Anal.* **2013**, *2*, 257–267, doi:10.1007/s13632-013-0085-5.
55. Hou, X.; Struble, L.J.; Kirkpatrick, R.J. Formation of ASR Gel and the Roles of C-S-H and Portlandite. *Cement and Concrete Research* **2004**, *34*, 1683–1696, doi:10.1016/j.cemconres.2004.03.026.
56. Wang, H.; Gillott, J.E. Mechanism of Alkali-Silica Reaction and the Significance of Calcium Hydroxide. *Cement and Concrete Research* **1991**, *21*, 647–654, doi:10.1016/0008-8846(91)90115-X.
57. Frýbort, A.; Všianský, D.; Štulířová, J.; Stryk, J.; Gregerová, M. Variations in the Composition and Relations between Alkali-Silica Gels and Calcium Silicate Hydrates in Highway Concrete. *Materials Characterization* **2018**, *137*, 91–108, doi:10.1016/j.matchar.2018.01.012.

58. Leemann, A.; Shi, Z.; Lindgård, J. Characterization of Amorphous and Crystalline ASR Products Formed in Concrete Aggregates. *Cement and Concrete Research* **2020**, *137*, 106190, doi:10.1016/j.cemconres.2020.106190.
59. Powers, T.C.; Steinour, H.H. An Interpretation of Some Published Researches on the Alkali–Aggregate Reaction; Part 1 — the Chemical Reactions and Mechanisms of Expansion. *Journal of the American Concrete Institute* **1955**, *26*, 497–516.
60. Chatterji, S.; Jensen, A.D.; Thaulow, N.; Christensen, P.; Denmark, T. Studies of Alkali–Silica Reaction. Part 3. Mechanism by Which NaCl and Ca (OH)₂ Affect the Reaction. *Cement and Concrete Research* **1986**, *16*, 246–254.
61. Cai, Y.; Xuan, D.; Poon, C.S. Effects of Nano-SiO₂ and Glass Powder on Mitigating Alkali-Silica Reaction of Cement Glass Mortars. *Construction and Building Materials* **2019**, *201*, 295–302, doi:10.1016/j.conbuildmat.2018.12.186.
62. Gause, G.R.; Tucker, J. Method for Determining the Moisture Condition in Hardened Concrete. *J. RES. NATL. BUR. STAN.* **1940**, *25*, 403, doi:10.6028/jres.025.019.
63. González, J.A.; López, W.; Rodríguez, P. Effects of Moisture Availability on Corrosion Kinetics of Steel Embedded in Concrete. *Corrosion* **1993**, *49*, 1004–1010, doi:10.5006/1.3316021.
64. Chen, X.; Huang, W.; Zhou, J. Effect of Moisture Content on Compressive and Split Tensile Strength of Concrete. *Indian J Eng. Mater. Sci.* **2012**, *9*.
65. Lura, P.; Winnefeld, F.; Fang, X. A Simple Method for Determining the Total Amount of Physically and Chemically Bound Water of Different Cements. *J Therm Anal Calorim* **2017**, *130*, 653–660, doi:10.1007/s10973-017-6513-z.
66. Hundt, J.; Buschmann, J. Moisture Measurement in Concrete: Analysis of the Results of a RILEM Inquiry Carried out by the B.A.M. *Mat. Constr.* **1971**, *4*, 253–256, doi:10.1007/BF02478952.
67. Kumara, W.A.S.; Halvorsen, B.M.; Melaaen, M.C. Single-Beam Gamma Densitometry Measurements of Oil–Water Flow in Horizontal and Slightly Inclined Pipes. *International Journal of Multiphase Flow* **2010**, *36*, 467–480, doi:10.1016/j.ijmultiphaseflow.2010.02.003.
68. De Jong, S.M.; Heijnen, R.A.; Nijland, W.; van der Meijde, M. Monitoring Soil Moisture Dynamics Using Electrical Resistivity Tomography under Homogeneous Field Conditions. *Sensors* **2020**, *20*, 5313, doi:10.3390/s20185313.
69. Andrade, C.; Sarria, J.; Alonso, C. Relative Humidity in the Interior of Concrete Exposed to Natural and Artificial Weathering. *Cement and Concrete Research* **1999**, *29*, 1249–1259, doi:10.1016/S0008-8846(99)00123-4.
70. Nilsson, L.-O. *Methods of Measuring Moisture in Building Materials and Structures*; RILEM State-of-the-Art Reports; Springer International Publishing: Cham, 2018; Vol. 26; ISBN 978-3-319-74230-4.
71. Zeilinger, A.; Hübner, R. Measurement of Moisture Motion Under a Temperature Gradient in a Concrete for SNR-300 Using Thermal Neutrons. In Proceedings of the Concrete Properties Relevant to PCRV; IASMiRT: London, UK, 1975; pp. 1–9.
72. Pandey, T.; Bhuiya, T.; Singh, B.; Harsh, R. A Review on Microwave Based Moisture Measurement System for Granular Materials. *IOSR Journal of Electronics and Communication Engineering (IOSR-JECE)* **2012**, *3*, 37–41.
73. Grinzato, E.; Ludwig, N.; Cadelano, G.; Bertucci, M.; Gargano, M.; Bison, P. Infrared Thermography for Moisture Detection: A Laboratory Study and In-Situ Test. *Materials Evaluation* **2011**, *69*.
74. Derome, D.; Fazio, P. Experimental Setup for the Study of Air Leakage Patterns. In Proceedings of the Thermal Performance of the Exterior Envelopes of Buildings VII; American Society of Heating, Refrigerating and Air-Conditioning Engineers, Inc.: Atlanta, 1998; pp. 99–108.
75. Lindgård, J.; Rodum, E.; Pedersen, B. Alkali-Silica Reactions in Concrete - Relationship between Water Content and Observed Damage on Structures. *ACI Symposium Publication* **2006**, *234*, doi:10.14359/15934.
76. Yang, Q. Inner Relative Humidity and Degree of Saturation in High-Performance Concrete Stored in Water or Salt Solution for 2 Years. *Cement and Concrete Research* **1999**, *29*, 45–53, doi:10.1016/S0008-8846(98)00174-4.
77. Zhang, J.; Wang, J.; Han, Y. Simulation of Moisture Field of Concrete with Pre-Soaked Lightweight Aggregate Addition. *Construction and Building Materials* **2015**, *96*, 599–614, doi:10.1016/j.conbuildmat.2015.08.058.

78. Zhang, J.; Gao, Y.; Han, Y.; Sun, W. Shrinkage and Interior Humidity of Concrete under Dry–Wet Cycles. *Drying Technology* **2012**, *30*, 583–596, doi:10.1080/07373937.2011.653614.
79. Geiker, M.R.; Laugesen, P. On the Effect of Laboratory Conditioning and Freeze/Thaw Exposure on Moisture Profiles in HPC. *Cement and Concrete Research* **2001**, *31*, 1831–1836, doi:10.1016/S0008-8846(01)00643-3.
80. Lindgård, J.; Andiç-Çakır, Ö.; Fernandes, I.; Rønning, T.F.; Thomas, M.D.A. Alkali–Silica Reactions (ASR): Literature Review on Parameters Influencing Laboratory Performance Testing. *Cement and Concrete Research* **2012**, *42*, 223–243, doi:10.1016/j.cemconres.2011.10.004.
81. Wardeh, G.; Perrin, B. Relative Permeabilities of Cement-Based Materials: Influence of the Tortuosity Function. *Journal of Building Physics* **2006**, *30*, 39–57, doi:10.1177/1744259106064597.
82. Chaudhry, R.H. Determination of Air Voids, Capillary, and Gel Porosity in Hardened Concrete Using Mass-Based Saturation Techniques. Master of Applied Science Thesis, University of Toronto: Canada, 2018.
83. Weiss, J. *Relating Transport Properties to Performance in Concrete Pavements*; Moving Advancements into Practice; 2014; pp. 1–6.
84. Olajide, O.; Nokken, M.; Sanchez, L. A Review on the Role of Moisture and Temperature in Alkali-Silica Reaction (ASR). In Proceedings of the 16th International Conference on Alkali-Aggregate Reaction in Concrete (ICAAR); Lisbon, Portugal, May 31 2022.
85. Saccani, A.; Bonora, V.; Monari, P. Laboratory Short-Term Evaluation of ASR A Contribution. *Cement and Concrete Research* **2001**.
86. Lenzner, D. Influence of the Amount of Mixing Water on the Alkali-Silica Reaction. In Proceedings of the 5th International Conference on Alkali-Aggregate Reaction; Cape Town, South Africa, 1981; pp. 1–6.
87. Nilsson, L.-O.; Peterson, O. *A Moisture Problem Causing Pop-Outs in Concrete Floors*; Alkali Silica Reactions in Scania, Sweden; Division of Building Materials, LTH, Lund University: Lund Sweden, 1983; pp. 1–106.
88. Multon, S.; Seignol, J.-F.; Toutlemonde, F. Structural Behavior of Concrete Beams Affected by Alkali-Silica Reaction. *MJ* **2005**, *102*, 67–76, doi:10.14359/14299.
89. Lindgård, J.; Thomas, M.D.A.; Sellevold, E.J.; Pedersen, B.; Andiç-Çakır, Ö.; Justnes, H.; Rønning, T.F. Alkali–Silica Reaction (ASR)—Performance Testing: Influence of Specimen Pre-Treatment, Exposure Conditions and Prism Size on Alkali Leaching and Prism Expansion. *Cement and Concrete Research* **2013**, *53*, 68–90, doi:10.1016/j.cemconres.2013.05.017.
90. Bažant, Z.P.; Steffens, A. Mathematical Model for Kinetics of Alkali–Silica Reaction in Concrete. *Cement and Concrete Research* **2000**, *30*, 419–428, doi:10.1016/S0008-8846(99)00270-7.
91. Hashemi, A.; Donnell, K.M.; Zoughi, R.; Kurtis, K.E. Effect of Humidity on Dielectric Properties of Mortars with Alkali-Silica Reaction (ASR) Gel. In Proceedings of the 2015 IEEE International Instrumentation and Measurement Technology Conference (I2MTC) Proceedings; IEEE: Pisa, Italy, May 2015; pp. 1502–1506.
92. *BCA The Diagnosis of Alkali–Silica Reaction-Report of a Working Party*; British Cement Association: Wexham Springs, Slough, U.K., SL3 6PL, 1992; p. 36.
93. Reed, R.G. Measuring Relative Humidity in Concrete Pavements as a Method to Assess ASR Mitigation Measures. Civil Engineering Undergraduate Honors Theses, University of Arkansas: Fayetteville, 2016.
94. Gudmundsson, B.; Asgeirsson, H. Some Investigations on Alkali Aggregate Reaction. *Cement and Concrete Research* **1975**, *5*, 211–220.
95. Sinno, N.; Shehata, M.H. Role of Temperature on Alkali-Silica Reaction and the Efficacy of Supplementary Cementitious Materials. *Construction and Building Materials* **2021**, *313*, 125427, doi:10.1016/j.conbuildmat.2021.125427.
96. Guo, J.-J.; Liu, P.-Q.; Wu, C.-L.; Wang, K. Effect of Dry–Wet Cycle Periods on Properties of Concrete under Sulfate Attack. *Applied Sciences* **2021**, *11*, 888, doi:10.3390/app11020888.
97. Farny, J.A.; Kerkhoff, B. Diagnosis and Control of Alkali-Aggregate Reactions in Concrete. *Portland Cement Association* **2007**, 1–26.
98. Kagimoto, H.; Kawamura, M. Measurements of Strain and Humidity within Massive Concrete Cylinders Related to the Formation of ASR Surface Cracks. *Cement and Concrete Research* **2011**, *41*, 808–816, doi:doi:10.1016/j.cemconres.2011.03.010.
99. Kagimoto, H.; Yasuda, Y.; Kawamura, M. Effects of Expansion Behavior of ASR-Affected Concrete in Atmospheres with Various Values of Relative Humidity on Surface Cracking. In Proceedings of the 15th International Conference on Alkali Aggregate Reaction in Concrete; Sao Paulo, Brazil, 2016; pp. 1–10.

100. Gautam, B.P.; Panesar, D.K. The Effect of Elevated Conditioning Temperature on the ASR Expansion, Cracking and Properties of Reactive Spratt Aggregate Concrete. *Construction and Building Materials* **2017**, *140*, 310–320, doi:10.1016/j.conbuildmat.2017.02.104.
101. Deschenes, R.A.Jr. Mitigation and Evaluation of Alkali-Silica Reaction (ASR) and Freezing and Thawing in Concrete Transportation Structures. *Theses and Dissertations. 2467* **2017**, 273.
102. Gillott, J.E. Alkali-Aggregate Reactions in Concrete. *Engineering Geology* **1975**, *9*, 303–326.
103. Helmuth, R.; Stark, D.; Diamond, S.; Moranville-regourd, M. Alkali-Silica Reactivity: An Overview of Research. In Proceedings of the National Research Council; Washington D.C, USA, 1993.
104. Lu, D.; Zhou, X.; Xu, Z.; Lan, X.; Tang, M.; Fournier, B. Evaluation of Laboratory Test Method for Determining the Potential Alkali Contribution from Aggregate and the ASR Safety of the Three-Gorges Dam Concrete. *Cement and Concrete Research* **2006**, *36*, 1157–1165, doi:10.1016/j.cemconres.2006.01.004.
105. Bérubé, M.-A.; Duchesne, J.; Dorion, J.F.; Rivest, M. Laboratory Assessment of Alkali Contribution by Aggregates to Concrete and Application to Concrete Structures Affected by Alkali–Silica Reactivity. *Cement and Concrete Research* **2002**, *32*, 1215–1227, doi:10.1016/S0008-8846(02)00766-4.
106. Drolet, C.; Duchesne, J.; Fournier, B. Effect of Alkali Release by Aggregates on Alkali-Silica Reaction. *Construction and Building Materials* **2017**, *157*, 263–276, doi:10.1016/j.conbuildmat.2017.09.085.
107. Maia Neto, F.M.; Andrade, T.W.C.O.; Gomes, R.M.; Leal, A.F.; Almeida, A.N.F.; Lima Filho, M.R.F.; Torres, S.M. Considerations on the Effect of Temperature, Cation Type and Molarity on Silica Degradation and Implications to ASR Assessment. *Construction and Building Materials* **2021**, *299*, 123848, doi:10.1016/j.conbuildmat.2021.123848.
108. Ideker, J.H.; East, B.L.; Folliard, K.J.; Thomas, M.D.A.; Fournier, B. The Current State of the Accelerated Concrete Prism Test. *Cement and Concrete Research* **2010**, *40*, 550–555, doi:10.1016/j.cemconres.2009.08.030.
109. Fournier, B.; Chevrier, R.; Grosbois, M.; Lisella, R.; Folliard, K.; Ideker, J.; Shehatad, M.; Thomas, M.; Baxter, S. The Accelerated Concrete Prism Test (60°C): Variability of the Test Method and Proposed Expansion Limits. *Researchgate* **2014**.
110. Sanchez, L.; Kuperman, S.C.; Helene, P. Using the Accelerated Brazilian Concrete Prism Test (ABCPT) to Evaluate Alkali Aggregate Reaction (AAR). *IBRACON Structures and Materials Journal* **2011**, *4*, 575–581.
111. Kawabata, Y.; Dunant, C.; Yamada, K.; Scrivener, K. Impact of Temperature on Expansive Behavior of Concrete with a Highly Reactive Andesite Due to the Alkali–Silica Reaction. *Cement and Concrete Research* **2019**, *125*, 105888, doi:10.1016/j.cemconres.2019.105888.
112. Kim, T.; Olek, J.; Jeong, H. Alkali–Silica Reaction: Kinetics of Chemistry of Pore Solution and Calcium Hydroxide Content in Cementitious System. *Cement and Concrete Research* **2015**, *71*, 36–45, doi:10.1016/j.cemconres.2015.01.017.
113. Li, B.; Wang, Z.-R.; Liu, H.-B.; Liu, X.-Z.; Li, H.; Chen, X. Meso-Mechanical Research on Alkali-Silica Reaction Expansion in Pyrex Glass and Silica Sand at Different Temperatures and Curing Times. *Construction and Building Materials* **2019**, *223*, 377–393, doi:10.1016/j.conbuildmat.2019.06.232.
114. Folliard, K J; Ideker, J.H.; Thomas, M.D.; Fournier, B. Assessing Aggregate Reactivity Using the Accelerated Concrete Prism Test. In Proceedings of the 7th CANMET/ACI International Conference on Recent Advances in Concrete Technology; Ottawa, 2004; pp. 269–283.
115. Li, B.; Baingam, L.; Kurumisawa, K.; Nawa, T.; XiaoZhou, L. Micro-Mechanical Modelling for the Prediction of Alkali-Silica Reaction (ASR) Expansion: Influence of Curing Temperature Conditions. *Construction and Building Materials* **2018**, *164*, 554–569, doi:10.1016/j.conbuildmat.2018.01.007.
116. Golmakani, F.; Hooton, R.D. Impact of Pore Solution Concentration on the Accelerated Mortar Bar Alkali-Silica Reactivity Test. *Cement and Concrete Research* **2019**, *121*, 72–80, doi:10.1016/j.cemconres.2019.02.008.
117. Kawabata, Y.; Yamada, K.; Sagawa, Y.; Ogawa, S. Alkali-Wrapped Concrete Prism Test (AW-CPT) – New Testing Protocol toward a Performance Test against Alkali-Silica Reaction–. *ACT* **2018**, *16*, 441–460, doi:10.3151/jact.16.441.
118. Lindgård, J.; Nixon, P.J.; Borchers, I.; Schouenborg, B.; Wigum, B.J.; Haugen, M.; Åkesson, U. The EU “PARTNER” Project — European Standard Tests to Prevent Alkali Reactions in Aggregates: Final Results and Recommendations. *Cement and Concrete Research* **2010**, *40*, 611–635, doi:10.1016/j.cemconres.2009.09.004.

119. De Grazia, M.T.; Goshayeshi, N.; Gorga, R.; Sanchez, L.F.M.; Santos, A.C.; Souza, D.J. Comprehensive Semi-Empirical Approach to Describe Alkali Aggregate Reaction (AAR) Induced Expansion in the Laboratory. *Journal of Building Engineering* **2021**, *40*, 102298, doi:10.1016/j.jobbe.2021.102298.
120. Cukierski, D. Quantifying Alkali-Silica Reaction in Concrete: Damage Rating Index. In Proceedings of the Concrete Institute of Australia's Biennial National Conference; Australia, 2021; pp. 1–6.
121. Rivard, P.; Ballivy, G. Assessment of the Expansion Related to Alkali-Silica Reaction by the Damage Rating Index Method. *Construction and Building Materials* **2005**, *19*, 83–90, doi:10.1016/j.conbuildmat.2004.06.001.
122. Sanchez, L.; Fournier, B.; Jolin, M. Sanchez, L.F.M., Fournier, B., Jolin M, Bustamante, M.A. B. Evaluation of the Microscopic ASR Features through the Damage Rating Index (DRI) for Different Concrete Strengths and Aggregate Types (Fine and Coarse Reactive Aggregates). In Proceedings of the 14th Euroseminar on Microscopy Applied to Building Materials; Denmark, June 1 2013.
123. Wang, Y.; Gao, P.; Su, H.; Qin, Y.; Wang, Y.; Xue, G. Failure Criteria and Microstructure Evolution Mechanism of the Alkali-Silica Reaction of Concrete. *Reviews on Advanced Materials Science* **2023**, *62*, 20230102, doi:10.1515/rams-2023-0102.
124. Shakoorioskooie, M.; Griffa, M.; Leemann, A.; Zboray, R.; Lura, P. Quantitative Analysis of the Evolution of ASR Products and Crack Networks in the Context of the Concrete Mesostructure. *Cement and Concrete Research* **2022**, *162*, 106992, doi:10.1016/j.cemconres.2022.106992.
125. Glinicki, M.A.; Józwiak-Niedźwiedzka, D.; Antolik, A.; Dziedzic, K.; Dąbrowski, M.; Bogusz, K. Diagnosis of ASR Damage in Highway Pavement after 15 Years of Service in Wet-Freeze Climate Region. *Case Studies in Construction Materials* **2022**, *17*, e01226, doi:10.1016/j.cscm.2022.e01226.
126. Antolik, A.; Józwiak-Niedźwiedzka, D. Assessment of the Alkali-Silica Reactivity Potential in Granitic Rocks. *Construction and Building Materials* **2021**, *295*, 123690, doi:10.1016/j.conbuildmat.2021.123690.
127. Fernandes, I. Composition of Alkali-Silica Reaction Products at Different Locations within Concrete Structures. *Materials Characterization* **2009**, *60*, 655–668, doi:10.1016/j.matchar.2009.01.011.
128. Rößler, C.; Möser, B.; Giebson, C.; Ludwig, H.-M. Application of Electron Backscatter Diffraction to Evaluate the ASR Risk of Concrete Aggregates. *Cement and Concrete Research* **2017**, *95*, 47–55, doi:10.1016/j.cemconres.2017.02.015.
129. Boehm-Courjault, E.; Barbotin, S.; Leemann, A.; Scrivener, K. Microstructure, Crystallinity and Composition of Alkali-Silica Reaction Products in Concrete Determined by Transmission Electron Microscopy. *Cement and Concrete Research* **2020**, *130*, 105988, doi:10.1016/j.cemconres.2020.105988.
130. Sanchez, L.F.M.; Drimalas, T.; Fournier, B.; Mitchell, D.; Bastien, J. Comprehensive Damage Assessment in Concrete Affected by Different Internal Swelling Reaction (ISR) Mechanisms. *Cement and Concrete Research* **2018**, *107*, 284–303, doi:10.1016/j.cemconres.2018.02.017.
131. Joo, H.E.; Takahashi, Y. Analytical and Experimental Studies on Alkali-Silica Reaction Mechanism: Aggregate Cracking and Chemical Composition Change of Gel. *Cement and Concrete Composites* **2023**, *139*, 105003, doi:10.1016/j.cemconcomp.2023.105003.
132. Sanchez, L.; Fournier, B.; Mitchell, D.; Bastien, J. Condition Assessment of an ASR-Affected Overpass after Nearly 50 Years in Service. *Construction and Building Materials* **2019**, *236*, doi:10.1016/j.conbuildmat.2019.117554.
133. Sanchez, L.; Drimalas, T.; Fournier, B.; Mitchell, D.; Bastien, J. Comprehensive Damage Assessment in Concrete Affected by Different Internal Swelling Reaction (ISR) Mechanisms. *Cement and Concrete Research* **2018**, *107*, 284–303, doi:10.1016/j.cemconres.2018.02.017.
134. Walsh, J.B. The Effect of Cracks on the Uniaxial Elastic Compression of Rocks. *Journal of Geophysical Research* **1965**, *70*, 399–411.
135. Crouch, R.S. *Specification for the Determination of Stiffness Damage Parameters from the Low Cyclic Uniaxial Compression of Plain Concrete Core*; Mott Hay & Anderson, Special Services Division, 1987;
136. Chrisp, T.M.; Waldron, P.; Wood, J.G.M. Development of a Non-Destructive Test to Quantify Damage in Deteriorated Concrete. *Magazine of Concrete Research* **1993**, *45*, 247–256, doi:10.1680/mac.1993.45.165.247.
137. Smaoui, N.; Bérubé, M.-A.; Fournier, B.; Bissonnette, B.; Durand, B. Evaluation of the Expansion Attained to Date by Concrete Affected by Alkali-Silica Reaction. Part I: Experimental Study. *Can. J. Civ. Eng.* **2004**, *31*, 826–845, doi:10.1139/104-051.

138. Sanchez, L.F.M.; Fournier, B.; Jolin, M.; Bastien, J. Evaluation of the Stiffness Damage Test (SDT) as a Tool for Assessing Damage in Concrete Due to ASR: Test Loading and Output Responses for Concretes Incorporating Fine or Coarse Reactive Aggregates. *Cement and Concrete Research* **2014**, *56*, 213–229, doi:10.1016/j.cemconres.2013.11.003.
139. Grattan-Bellew, P.; Danay, A. Comparison of Laboratory and Field Evaluation of Alkali- Silica Reaction in Large Dams. In Proceedings of the Proceedings of the International Conference on Concrete Alkali–Aggregate Reactions in Hydroelectric Plants and Dams; Fredericton, NB, 1992; Vol. 18.
140. Villeneuve, V.; Fournier, B. Determination of the Damage in Concrete Affected by ASR – the Damage Rating Index (DRI). In Proceedings of the 14th ICAAR - International Conference on Alkali-Aggregate Reaction in Concrete; Austin, Texas, USA, May 20 2012.
141. Sanchez, L.; Fournier, B.; Jolin, M.; Mitchell, D.; Bastien, J. Overall Assessment of Alkali-Aggregate Reaction (AAR) in Concretes Presenting Different Strengths and Incorporating a Wide Range of Reactive Aggregate Types and Natures. *Cement and Concrete Research* **2017**, *93*, 17–31, doi:10.1016/j.cemconres.2016.12.001.
142. Zahedi, A.; Sanchez, L. Effect of Confinement on ASR-Induced Expansion and Damage. In Proceedings of the 16th International Conference on Alkali-Aggregate Reaction in Concrete (ICAAR); Lisbon, Portugal, June 2 2022.
143. Zahedi, A.; Trottier, C.; Sanchez, L.; Noël, M. Microscopic Assessment of ASR-Affected Concrete Under Confinement Conditions. *Cement and Concrete Research* **2021**, *145*, 106456, doi:10.1016/j.cemconres.2021.106456.
144. Zahedi, A.; Trottier, C.; Sanchez, L.F.M.; Noël, M. Microscopic Assessment of ASR-Affected Concrete under Confinement Conditions. *Cement and Concrete Research* **2021**, *145*, 106456, doi:10.1016/j.cemconres.2021.106456.
145. Sanchez, L.; Fournier, B.; Jolin, M.; Pouliot, N.; Hovington, A. Evaluation of Damage in the Concrete Elements of the Viaduct “Robert-Bourassa Charest” after Nearly 50 Years in Service. In Proceedings of the International Conference on Alkali-Aggregate Reaction (ICAAR); Austin, Texas, USA, May 1 2012.
146. Bui, T.T.; Nana, W.S.A.; Abouri, S.; Limam, A.; Tedoldi, B.; Roure, T. Influence of Uniaxial Tension and Compression on Shear Strength of Concrete Slabs without Shear Reinforcement under Concentrated Loads. *Construction and Building Materials* **2017**, *146*, 86–101, doi:10.1016/j.conbuildmat.2017.04.068.
147. Haskett, M.; Oehlers, D.J.; Mohamed Ali, M.S.; Sharma, S.K. Evaluating the Shear-Friction Resistance across Sliding Planes in Concrete. *Engineering Structures* **2011**, *33*, 1357–1364, doi:10.1016/j.engstruct.2011.01.013.
148. Barr, B.; Hasso, E.B.D. Development of a Compact Cylindrical Shear Test Specimen. *J Mater Sci Lett* **1986**, *5*, 1305–1308, doi:10.1007/BF01729401.
149. Barbosa, R.A.; Hansen, K.K.; Hoang, L.C.; Maag, I. Alkali-Silica Reaction in Reinforced Concrete Structures, Part II: XXII Nordic Concrete Research Symposium. *Proceedings of the XXII Nordic Concrete Research Symposium* **2014**, 69–72.
150. ASTM E 104 Standard Practice for Maintaining Constant Relative Humidity by Means of Aqueous Solution 1985.
151. QA Supplies iButton Temp & Humidity Logger Available online: <https://qasupplies.com/ibutton-temp-humidity-logger/> (accessed on 30 December 2023).
152. Granja, J.L.; Azenha, M.; de Sousa, C.; Faria, R.; Barros, J. Hygrometric Assessment of Internal Relative Humidity in Concrete: Practical Application Issues. **2014**, *12*.
153. Fournier, B.; Rogers, C.; MacDonald, C.-A. Multi Laboratory Study of the Concrete Prism and Accelerated Mortar Bar Expansion Tests with Spratt Aggregate. In Proceedings of the 15th International Conference on Alkali-Aggregate Reaction in Concrete (ICAAR); Sao Paulo, Brazil, 2016.
154. Smith, A.D.H.; Crabtree, D.R.; Bilzon, J.L.J.; Walsh, N.P. The Validity of Wireless iButtons® and Thermistors for Human Skin Temperature Measurement. *Physiol. Meas.* **2010**, *31*, 95–114, doi:10.1088/0967-3334/31/1/007.
155. Sanchez, L.; Fournier, B.; Jolin, M.; Bastien, J.; Mitchell, D. Practical Use of the Stiffness Damage Test (SDT) for Assessing Damage in Concrete Infrastructure Affected by Alkali-Silica Reaction. *Construction and Building Materials* **2016**, *125*, 1178–1188, doi:10.1016/j.conbuildmat.2016.08.101.
156. Deschenes, R.; Waidner, M.; Hale, W.M. Mitigation of Alkali-Silica Reaction in Concrete Pavements by Silane Treatment.

157. Fournier, B.; Ideker, J.H.; Folliard, K.J.; Thomas, M.D.A.; Nkinamubanzi, P.-C.; Chevrier, R. Effect of Environmental Conditions on Expansion in Concrete Due to Alkali–Silica Reaction (ASR). *Materials Characterization* **2009**, *60*, 669–679, doi:10.1016/j.matchar.2008.12.018.
158. Zhou, J.K.; Chen, X.D.; Zhang, J.; Kan, X.W. Measurement of the Internal Relative Humidity Distribution in Concrete. *AMR* **2010**, *163–167*, 1409–1413, doi:10.4028/www.scientific.net/AMR.163-167.1409.
159. Jensen, V. In-Situ Measurement of Relative Humidity and Expansion of Cracks in Structures Damaged by AAR. *12*.
160. Zhang, J.; Huang, Y.; Qi, K.; Gao, Y. Interior Relative Humidity of Normal- and High-Strength Concrete at Early Age. *J. Mater. Civ. Eng.* **2012**, *24*, 615–622, doi:10.1061/(ASCE)MT.1943-5533.0000441.
161. Figueira, R.B.; Sousa, R.; Coelho, L.; Azenha, M.; de Almeida, J.M.; Jorge, P.A.S.; Silva, C.J.R. Alkali-Silica Reaction in Concrete: Mechanisms, Mitigation and Test Methods. *Construction and Building Materials* **2019**, *222*, 903–931, doi:10.1016/j.conbuildmat.2019.07.230.
162. Chatterji, S. Chemistry of Alkali–Silica Reaction and Testing of Aggregates. *Cement and Concrete Composites* **2005**, *27*, 788–795, doi:10.1016/j.cemconcomp.2005.03.005.
163. Al-Jabari, M. 1 - Introduction to Concrete Chemistry. In *Integral Waterproofing of Concrete Structures*; Al-Jabari, M., Ed.; Woodhead Publishing Series in Civil and Structural Engineering; Woodhead Publishing, 2022; pp. 1–36 ISBN 978-0-12-824354-1.
164. Hover, K.C. The Influence of Water on the Performance of Concrete. *Construction and Building Materials* **2011**, *25*, 3003–3013, doi:10.1016/j.conbuildmat.2011.01.010.
165. Santos, A.R.; Veiga, M. do R.; Santos Silva, A.; de Brito, J. Microstructure as a Critical Factor of Cement Mortars' Behaviour: The Effect of Aggregates' Properties. *Cement and Concrete Composites* **2020**, *111*, 103628, doi:10.1016/j.cemconcomp.2020.103628.
166. Sant, G.; Bentz, D.; Weiss, J. Capillary Porosity Depercolation in Cement-Based Materials: Measurement Techniques and Factors Which Influence Their Interpretation. *Cement and Concrete Research* **2011**, *41*, 854–864, doi:10.1016/j.cemconres.2011.04.006.
167. Joshaghani, A.; Balapour, M.; Ramezani-pour, A.A. Effect of Controlled Environmental Conditions on Mechanical, Microstructural and Durability Properties of Cement Mortar. *Construction and Building Materials* **2018**, *164*, 134–149, doi:10.1016/j.conbuildmat.2017.12.206.
168. Zhang, J.; Gao, Y.; Han, Y. Interior Humidity of Concrete under Dry-Wet Cycles. *J. Mater. Civ. Eng.* **2012**, *24*, 289–298, doi:10.1061/(ASCE)MT.1943-5533.0000382.
169. Zhang, H.; Li, J.; Kang, F. Real-Time Monitoring of Humidity inside Concrete Structures Utilizing Embedded Smart Aggregates. *Construction and Building Materials* **2022**, *331*, 127317, doi:10.1016/j.conbuildmat.2022.127317.
170. Honglei, C.; Zuquan, J.; Tiejun, Z.; Benzhen, W.; Zhe, L.; Jian, L. Capillary Suction Induced Water Absorption and Chloride Transport in Non-Saturated Concrete: The Influence of Humidity, Mineral Admixtures and Sulfate Ions. *Construction and Building Materials* **2020**, *236*, 117581, doi:10.1016/j.conbuildmat.2019.117581.
171. Wu, Z.; Wong, H.S.; Buenfeld, N.R. Transport Properties of Concrete after Drying-Wetting Regimes to Elucidate the Effects of Moisture Content, Hysteresis and Microcracking. *Cement and Concrete Research* **2017**, *98*, 136–154, doi:10.1016/j.cemconres.2017.04.006.
172. Jin, H.; Fan, X.; Li, Z.; Zhang, W.; Liu, J.; Zhong, D.; Tang, L. An Experimental Study on the Influence of Continuous Ambient Humidity Conditions on Relative Humidity Changes, Chloride Diffusion and Microstructure in Concrete. *Journal of Building Engineering* **2022**, *59*, 105112, doi:10.1016/j.jobe.2022.105112.
173. Grasley, Z.C.; Lange, D.A.; D'Ambrosia, M.D. Internal Relative Humidity and Drying Stress Gradients in Concrete. *Mater Struct* **2006**, *39*, 901–909, doi:10.1617/s11527-006-9090-3.
174. Taheri, S. A Review on Five Key Sensors for Monitoring of Concrete Structures. *Construction and Building Materials* **2019**, *204*, 492–509, doi:10.1016/j.conbuildmat.2019.01.172.
175. Zhang, J.; Dongwei, H.; Wei, S. Experimental Study on the Relationship between Shrinkage and Interior Humidity of Concrete at Early Age. *Magazine of Concrete Research* **2010**, *62*, 191–199, doi:10.1680/mac.2010.62.3.191.
176. Kim, J.-K.; Lee, C.-S. Moisture Diffusion of Concrete Considering Self-Desiccation at Early Ages. *Cement and Concrete Research* **1999**, *29*, 1921–1927, doi:10.1016/S0008-8846(99)00192-1.

177. Zhou, F.; Li, W.; Hu, Y.; Huang, L.; Xie, Z.; Yang, J.; Wu, D.; Chen, Z. Moisture Diffusion Coefficient of Concrete under Different Conditions. *Buildings* **2023**, *13*, 2421, doi:10.3390/buildings13102421.
178. Ryu, D.-W.; Ko, J.-W.; Noguchi, T. Effects of Simulated Environmental Conditions on the Internal Relative Humidity and Relative Moisture Content Distribution of Exposed Concrete. *Cement and Concrete Composites* **2011**, *33*, 142–153, doi:10.1016/j.cemconcomp.2010.09.009.
179. Wilson, C.; Weiss, J. The Measurement of the Internal Relative Humidity of Concrete at Early Ages. *Advances in Civil Engineering Materials* **2019**, *8*, 655–669, doi:10.1520/ACEM20190109.
180. Zhou, J.K.; Chen, X.D.; Zhang, J.; Kan, X.W. Measurement of the Internal Relative Humidity Distribution in Concrete. *AMR* **2010**, *163–167*, 1409–1413, doi:10.4028/www.scientific.net/AMR.163-167.1409.
181. ASTM C 1293 ASTM International, West Conshohocken, PA, USA. *Standard Test Method for Determination of Length Change of Concrete Due to Alkali-Silica Reaction (Concrete Prism Method)*; **2008**.
182. A23.2-14A *Potential Expansivity of Aggregates (Procedure for Length Change Due to Alkali-Aggregate Reaction in Concrete Prisms at 38 °C)*; 246–256; Mississauga, ON, CA, **2004a**.
183. Rivard, P.; Bérubé, M.A.; Ollivier, J.P.; Ballivy, G. Decrease of Pore Solution Alkalinity in Concrete Tested for Alkali-Silica Reaction. *Mater Struct* **2007**, *40*, 909–921, doi:10.1617/s11527-006-9191-z.
184. Zhang, Q.; Kang, Z.; Ling, Y.; Chen, H.; Li, K. Influence of Temperature on the Moisture Transport in Concrete. *Crystals* **2021**, *11*, 8, doi:10.3390/cryst11010008.
185. Keskin, Ö.K.; Keskin, S.B.; Tekin, K. Predicting the Ultimate Properties of Engineered Cementitious Composites by Maturity Method. *ACT* **2023**, *21*, 735–747, doi:10.3151/jact.21.735.
186. Soutsos, M.; Kanavaris, F. The Modified Nurse-Saul (MNS) Maturity Function for Improved Strength Estimates at Elevated Curing Temperatures. *Case Studies in Construction Materials* **2018**, *9*, e00206, doi:10.1016/j.cscm.2018.e00206.
187. Yikici, T.A.; Chen, H.-L. (Roger) Use of Maturity Method to Estimate Compressive Strength of Mass Concrete. *Construction and Building Materials* **2015**, *95*, 802–812, doi:10.1016/j.conbuildmat.2015.07.026.
188. Zhang, J.; Cusson, D.; Monteiro, P.; Harvey, J. New Perspectives on Maturity Method and Approach for High Performance Concrete Applications. *Cement and Concrete Research* **2008**, *38*, 1438–1446, doi:10.1016/j.cemconres.2008.08.001.
189. Waller, V.; d’Aloia, L.; Cussigh, F.; Lecrux, S. Using the Maturity Method in Concrete Cracking Control at Early Ages. *Cement and Concrete Composites* **2004**, *26*, 589–599, doi:10.1016/S0958-9465(03)00080-5.
190. Poyet, S.; Sellier, A.; Capra, B.; Foray, G.; Torrenti, J.-M.; Cognon, H.; Bourdarot, E. Chemical Modelling of Alkali Silica Reaction: Influence of the Reactive Aggregate Size Distribution. *Mater Struct* **2007**, *40*, 229–239, doi:10.1617/s11527-006-9139-3.
191. Reinhardt, H.W.; Özkan, H.; Mielich, O. Changes in Mechanical Properties of Concrete Due to ASR. *Hormigón y Acero* **2018**, S0439568918300172, doi:10.1016/j.hya.2018.02.001.
192. Esposito, R.; Anaç, C.; Hendriks, M.A.N.; Çopuroğlu, O. Influence of the Alkali-Silica Reaction on the Mechanical Degradation of Concrete. *J. Mater. Civ. Eng.* **2016**, *28*, 04016007, doi:10.1061/(ASCE)MT.1943-5533.0001486.
193. Na, O.; Xi, Y.; Ou, E.; Saouma, V.E. The Effects of Alkali-Silica Reaction on the Mechanical Properties of Concretes with Three Different Types of Reactive Aggregate. *Structural Concrete* **2016**, *17*, 74–83, doi:10.1002/suco.201400062.
194. Diamond, S. Alkali Silica Reactions — Some Paradoxes. *Cement and Concrete Composites* **1997**, *19*, 391–401, doi:10.1016/S0958-9465(97)00004-8.
195. Yang, L.; Pathirage, M.; Su, H.; Alnaggar, M.; Di Luzio, G.; Cusatis, G. Computational Modeling of Temperature and Relative Humidity Effects on Concrete Expansion Due to Alkali-Silica Reaction. *Cement and Concrete Composites* **2021**, *124*, 104237, doi:10.1016/j.cemconcomp.2021.104237.
196. Deschenes, R.A.; Murray, C.D.; Hale, W.M. Prevention and Mitigation of ASR in Median Barriers with Varying Degrees of Damage. In Proceedings of the T&DI Congress 2014; American Society of Civil Engineers: Orlando, Florida, May 29 2014; pp. 111–120.
197. Zahedi, A.; Trottier, C.; Sanchez, L.; Noël, M. Evaluation of the Induced Mechanical Deterioration of Alkali-Silica Reaction Affected Concrete under Distinct Confinement Conditions through the Stiffness Damage Test. *Cement and Concrete Composites* **2021**, 104343, doi:10.1016/j.cemconcomp.2021.104343.
198. Kongshaug, S.S.; Oseland, O.; Kanstad, T.; Hendriks, M.A.N.; Rodum, E.; Markeset, G. Experimental Investigation of ASR-Affected Concrete – The Influence of Uniaxial Loading on the Evolution of Mechanical

- Properties, Expansion and Damage Indices. *Construction and Building Materials* **2020**, *245*, 118384, doi:10.1016/j.conbuildmat.2020.118384.
199. Gholizadeh-Vayghan, A.; Rajabipour, F. The Influence of Alkali–Silica Reaction (ASR) Gel Composition on Its Hydrophilic Properties and Free Swelling in Contact with Water Vapor. *Cement and Concrete Research* **2017**, *94*, 49–58, doi:10.1016/j.cemconres.2017.01.006.
 200. Fournier, B.; Bérubé, M.-A. Alkali–Aggregate Reaction in Concrete: A Review of Basic Concepts and Engineering Implications. *Canadian Journal of Civil Engineering* **2000**, *27*, 167–191, doi:10.1139/cjce-27-2-167.
 201. Wu, S.; Chen, X.; Zhou, J. Tensile Strength of Concrete under Static and Intermediate Strain Rates: Correlated Results from Different Testing Methods. *Nuclear Engineering and Design* **2012**, *250*, 173–183, doi:10.1016/j.nucengdes.2012.05.004.
 202. Yurtdas, I.; Chen, D.; Hu, D.W.; Shao, J.F. Influence of Alkali Silica Reaction (ASR) on Mechanical Properties of Mortar. *Construction and Building Materials* **2013**, *47*, 165–174, doi:10.1016/j.conbuildmat.2013.04.046.
 203. Giaccio, G.; Zerbino, R.; Ponce, J.M.; Batic, O.R. Mechanical Behavior of Concretes Damaged by Alkali-Silica Reaction. *Cement and Concrete Research* **2008**, *38*, 993–1004, doi:10.1016/j.cemconres.2008.02.009.
 204. Ahmed, T.; Burley, E.; Rigden, S.; Abu-Tair, A.I. The Effect of Alkali Reactivity on the Mechanical Properties of Concrete. *Construction and Building Materials* **2003**, *17*, 123–144, doi:10.1016/S0950-0618(02)00009-0.
 205. Swartz, S.E.; Taha, N.M. Mixed Mode Crack Propagation and Fracture in Concrete. *Engineering Fracture Mechanics* **1990**, *35*, 137–144, doi:10.1016/0013-7944(90)90191-I.
 206. Ziapourrazlighi, R.; Trottier, C.; Zahedi, A.; Sanchez, L. Assessment of Effects of ASR-Induced Cracking on Direct Shear Strength of Recycled Concrete. *Materiales de Construcción* **2022**, *72*, e280, doi:10.3989/mc.2022.17621.
 207. Munir, M.J.; Abbas, S.; Qazi, A.U.; Nehdi, M.L.; Kazmi, S.M.S. Ga. *Proceedings of the Institution of Civil Engineers - Construction Materials* **2018**, *171*, 203–221, doi:10.1680/jcoma.16.00058.
 208. Islam, M.S.; Ghafoori, N. Relation of ASR-Induced Expansion and Compressive Strength of Concrete. *Mater Struct* **2015**, *48*, 4055–4066, doi:10.1617/s11527-014-0465-6.
 209. Kawabata, Y.; Dunant, C.; Nakamura, S.; Yamada, K.; Kawakami, T. Effects of Temperature on Expansion of Concrete Due to the Alkali-Silica Reaction: A Simplified Numerical Approach. *materconstrucc* **2022**, *72*, e282, doi:10.3989/mc.2022.17121.
 210. Nasir, M.; Alimi, W.O.; Adeoluwa Oladapo, E.; Imran, M.; Kazmi, Z.A. Behavior of Drying and Plastic Shrinkage of Portland Cement Concrete Prepared and Cured under Harsh Field. *Developments in the Built Environment* **2023**, *16*, 100252, doi:10.1016/j.dibe.2023.100252.
 211. Maruyama, I. Impact of Drying on Concrete and Concrete Structures. *RILEM Tech Lett* **2022**, *7*, 1–11, doi:10.21809/rilemtechlett.2022.154.
 212. Nixon, P.J.; Sims, I. RILEM Recommended Test Method: AAR-4.1—Detection of Potential Alkali-Reactivity—60 °C Test Method for Aggregate Combinations Using Concrete Prisms. In *RILEM Recommendations for the Prevention of Damage by Alkali-Aggregate Reactions in New Concrete Structures: State-of-the-Art Report of the RILEM Technical Committee 219-ACS*; Nixon, P.J., Sims, I., Eds.; Springer Netherlands: Dordrecht, 2016; pp. 99–116 ISBN 978-94-017-7252-5.
 213. Lindgård, J.; Andiç-Çakır, Ö.; Fernandes, I.; Rønning, T.F.; Thomas, M.D.A. Alkali–Silica Reactions (ASR): Literature Review on Parameters Influencing Laboratory Performance Testing. *Cement and Concrete Research* **2012**, *42*, 223–243, doi:10.1016/j.cemconres.2011.10.004.
 214. Costa, U.; Mangialardi, T.; Paolini, A.E. Minimizing Alkali Leaching in the Concrete Prism Expansion Test at 38 °C. *Construction and Building Materials* **2017**, *146*, 547–554, doi:10.1016/j.conbuildmat.2017.04.116.
 215. Strack, C.M.; Thornell, T.L.; Jefcoat, J.A.; Borne, G.J.; Alapati, P.; Kurtis, K.E.; Moser, R.D. The Viscoelastic Behavior of Synthetic Alkali-Silica Gels at Ambient Temperature. *Cement and Concrete Research* **2023**, *165*, 107069, doi:10.1016/j.cemconres.2022.107069.
 216. Diamond, S. A Review of Alkali-Silica Reaction and Expansion Mechanisms 2. Reactive Aggregates. *Cement and Concrete Research* **1976**, *6*, 549–560, doi:10.1016/0008-8846(76)90083-1.
 217. Winnicki, A.; Pietruszczak, S. On Mechanical Degradation of Reinforced Concrete Affected by Alkali-Silica Reaction. *J. Eng. Mech.* **2008**, *134*, 611–627, doi:10.1061/(ASCE)0733-9399(2008)134:8(611).

218. Salim, M.U.; Mosaberpanah, M.A. The Mechanism of Alkali-Aggregate Reaction in Concrete/Mortar and Its Mitigation by Using Geopolymer Materials and Mineral Admixtures: A Comprehensive Review. *European Journal of Environmental and Civil Engineering* **2022**, *26*, 6766–6806, doi:10.1080/19648189.2021.1960899.
219. Matteini, I.; Noyce, P.; Crevello, G. ASR: Practical Investigative Techniques and Field Monitoring Systems Used to Assess ASR for Service Life Modeling. *MATEC Web Conf.* **2019**, *289*, 08004, doi:10.1051/mateconf/201928908004.
220. Multon, S.; Sellier, A. Multi-Scale Analysis of Alkali–Silica Reaction (ASR): Impact of Alkali Leaching on Scale Effects Affecting Expansion Tests. *Cement and Concrete Research* **2016**, *81*, 122–133, doi:10.1016/j.cemconres.2015.12.007.
221. Marko, M.; Hrubý, P.; Janča, M.; Kříkala, J.; Hajzler, J.; Šoukal, F.; Vojtíšek, J.; Doležal, M. Monitoring of Ion Mobility in the Cement Matrix to Establish Sensitivity to the ASR Caused by External Sources. *Materials* **2022**, *15*, 4730, doi:10.3390/ma15144730.
222. Saccani, A.; Bignozzi, M.C. ASR Expansion Behavior of Recycled Glass Fine Aggregates in Concrete. *Cement and Concrete Research* **2010**, *40*, 531–536, doi:10.1016/j.cemconres.2009.09.003.
223. Fernandes, I.; Broekmans, M.A.T.M. Alkali–Silica Reactions: An Overview. Part I. *Metallogr. Microstruct. Anal.* **2013**, *2*, 257–267, doi:10.1007/s13632-013-0085-5.
224. Comi, C.; Pignatelli, R. On Damage Modeling of Concrete Affected by Alkali- Silica Reaction in the Presence of Humidity Gradients. In Proceedings of the XVIII GIMC Conference; Siracusa, 2010; pp. 1–4.
225. Reinhardt, H.W.; Mielich, O. A Fracture Mechanics Approach to the Crack Formation in Alkali-Sensitive Grains. *Cement and Concrete Research* **2011**, *41*, 255–262, doi:10.1016/j.cemconres.2010.11.008.
226. Ponce, J.M.; Batic, O.R. Different Manifestations of the Alkali-Silica Reaction in Concrete According to the Reaction Kinetics of the Reactive Aggregate. *Cement and Concrete Research* **2006**, *36*, 1148–1156, doi:10.1016/j.cemconres.2005.12.022.
227. Sanchez, L.F.M.; Fournier, B.; Jolin, M.; Duchesne, J. Reliable Quantification of AAR Damage through Assessment of the Damage Rating Index (DRI). *Cement and Concrete Research* **2015**, *67*, 74–92, doi:10.1016/j.cemconres.2014.08.002.
228. Sinno, N.; Shehata, M.H. Role of Temperature on Alkali-Silica Reaction and the Efficacy of Supplementary Cementitious Materials. *Construction and Building Materials* **2021**, *313*, 125427, doi:10.1016/j.conbuildmat.2021.125427.
229. Lothenbach, B.; Winnefeld, F.; Alder, C.; Wieland, E.; Lunk, P. Effect of Temperature on the Pore Solution, Microstructure and Hydration Products of Portland Cement Pastes. *Cement and Concrete Research* **2007**, *37*, 483–491, doi:10.1016/j.cemconres.2006.11.016.
230. Fournier, B.; Ideker, J.H.; Folliard, K.J.; Thomas, M.D.A.; Nkinamubanzi, P.-C.; Chevrier, R. Effect of Environmental Conditions on Expansion in Concrete Due to Alkali–Silica Reaction (ASR). *Materials Characterization* **2009**, *60*, 669–679, doi:10.1016/j.matchar.2008.12.018.
231. Krüger, M.E.; Heisig, A.; Heinz, D.; Machner, A. Effect of Cement Composition and the Storage Conditions on the Morphology of ASR Products in Concrete. *ce/papers* **2023**, *6*, 1151–1159, doi:10.1002/cepa.2943.
232. Bissonnette, B.; Pierre, P.; Pigeon, M. Influence of Key Parameters on Drying Shrinkage of Cementitious Materials. *Cement and Concrete Research* **1999**, *29*, 1655–1662, doi:10.1016/S0008-8846(99)00156-8.
233. Tapas, M.J.; Sofia, L.; Vessalas, K.; Thomas, P.; Sirivivatnanon, V.; Scrivener, K. Efficacy of SCMs to Mitigate ASR in Systems with Higher Alkali Contents Assessed by Pore Solution Method. *Cement and Concrete Research* **2021**, *142*, 106353, doi:10.1016/j.cemconres.2021.106353.
234. Adams, M.P.; Ideker, J.H. Using Supplementary Cementitious Materials to Mitigate Alkali-Silica Reaction in Concrete with Recycled-Concrete Aggregate. *Journal of Materials in Civil Engineering* **2020**, *32*, 04020209, doi:10.1061/(ASCE)MT.1943-5533.0003277.
235. Akhnoukh, A.; Namian, M.; Skinner, P.; Elia, H. Impact of Supplementary Cementitious Materials on Alkali-Silica Reactivity of Concrete. In Proceedings of the Proceedings of 59th Annual Associated Schools of Construction International Conference; Vol. 4, pp. 280–270.
236. Thomas, M. The Effect of Supplementary Cementing Materials on Alkali-Silica Reaction: A Review. *Cement and Concrete Research* **2011**, *41*, 1224–1231, doi:10.1016/j.cemconres.2010.11.003.
237. De Souza, D.J.; Sanchez, L.F.M. Evaluating the Efficiency of SCMs to Avoid or Mitigate ASR-Induced Expansion and Deterioration through a Multi-Level Assessment. *Cement and Concrete Research* **2023**, *173*, 107262, doi:10.1016/j.cemconres.2023.107262.

238. Nsiah-Baafi, E.; Tapas, M.J.; Vessalas, K.; Thomas, P. Mitigation of ASR Using Aggregate Fines as an Alternative for SCMs. In Proceedings of the 16th International Conference on Alkali Aggregate Reaction in Concrete; Lisbon, Portugal, 2021; pp. 431–438.
239. Ghafari, E.; Feys, D.; Khayat, K. Feasibility of Using Natural SCMs in Concrete for Infrastructure Applications. *Construction and Building Materials* **2016**, *127*, 724–732, doi:10.1016/j.conbuildmat.2016.10.070.
240. Mahmood, A.H.; Afroz, S.; Kashani, A.; Kim, T.; Foster, S.J. The Efficiency of Recycled Glass Powder in Mitigating the Alkali-Silica Reaction Induced by Recycled Glass Aggregate in Cementitious Mortars. *Mater Struct* **2022**, *55*, 156, doi:10.1617/s11527-022-01989-7.
241. Esteves, H.; Fernandes, I.; Janeiro, A.; Santos Silva, A.; Pereira, M.; Medeiros, S.; Nunes, J. Potentially Reactive Forms of Silica in Volcanic Rocks Using Different Analytical Approaches. *IOP Conference Series: Earth and Environmental Science* **2017**, *95*, 022040, doi:10.1088/1755-1315/95/2/022040.
242. Fanijo, E.; Kolawole, J.; Almakrab, A. Alkali-Silica Reaction (ASR) in Concrete Structures: Mechanisms, Effects and Evaluation Test Methods Adopted in the United States. *Case Studies in Construction Materials* **2021**, *15*, e00563, doi:10.1016/j.cscm.2021.e00563.
243. Constantiner, D.; Diamond, S. Alkali Release from Feldspars into Pore Solutions. *Cement and Concrete Research* **2003**, *33*, 549–554, doi:10.1016/S0008-8846(02)01001-3.
244. Leemann, A.; Holzer, L. Alkali-Aggregate Reaction—Identifying Reactive Silicates in Complex Aggregates by ESEM Observation of Dissolution Features. *Cement and Concrete Composites* **2005**, *27*, 796–801, doi:10.1016/j.cemconcomp.2005.03.007.
245. Kazemi, P.; Nikudel, M.R.; Khomehchiyan, M.; Giri, P.; Taheri, S.; Clark, S.M. Assessment of Alkali–Silica Reaction Potential in Aggregates from Iran and Australia Using Thin-Section Petrography and Expansion Testing. *Materials (Basel)* **2022**, *15*, 4289, doi:10.3390/ma15124289.
246. Saha, A.K.; Khan, M.N.N.; Sarker, P.K.; Shaikh, F.A.; Pramanik, A. The ASR Mechanism of Reactive Aggregates in Concrete and Its Mitigation by Fly Ash: A Critical Review. *Construction and Building Materials* **2018**, *171*, 743–758, doi:10.1016/j.conbuildmat.2018.03.183.
247. Lu, D.; Fournier, B.; Grattan-Bellew, P.E. Evaluation of Accelerated Test Methods for Determining Alkali-Silica Reactivity of Concrete Aggregates. *Cement and Concrete Composites* **2006**, *28*, 546–554, doi:10.1016/j.cemconcomp.2006.03.001.
248. Lu, D.; Fournier, B.; Grattan-Bellew, P.E.; Xu, Z.; Tang, M. Development of a Universal Accelerated Test for Alkali-Silica and Alkali-Carbonate Reactivity of Concrete Aggregates. *Mater Struct* **2008**, *41*, 235–246, doi:10.1617/s11527-007-9232-2.
249. Zahedi, A.; Trottier, C.; Sanchez, L.; Noël, M. Condition Assessment of Alkali-Silica Reaction Affected Concrete under Various Confinement Conditions Incorporating Fine and Coarse Reactive Aggregates. *Cement and Concrete Research* **2022**, *153*, 106694, doi:10.1016/j.cemconres.2021.106694.
250. Zahedi, A.; Trottier, C.; Sanchez, L.; Noël, M. Evaluation of the Induced Mechanical Deterioration of Alkali-Silica Reaction Affected Concrete under Distinct Confinement Conditions through the Stiffness Damage Test. *Cement and Concrete Composites* **2021**, 104343, doi:10.1016/j.cemconcomp.2021.104343.
251. Giannini, E.; Sanchez, L.; Tuinukuafe, A.; Folliard, K. Characterization of Concrete Affected by Delayed Ettringite Formation Using the Stiffness Damage Test. *Construction and Building Materials* **2018**, *162*, 253–264, doi:10.1016/j.conbuildmat.2017.12.012.
252. Olajide, O.; Nokken, M.; Sanchez, L. Effect of Moisture History on ASR Expansion and Microstructural Properties. In Proceedings of the 16th International Conference on Durability of Building Materials and Components; CIMNE, 2023.
253. Olajide, O.D.; Nokken, M.R.; Sanchez, L.F.M. Efficiency of the Dynamic Resonance Frequency in Assessing ASR Induced Damage at Numerous Exposure Conditions. In Proceedings of the Proceedings of the 17th International Conference on Alkali-Aggregate Reaction in Concrete; Sanchez, L.F.M., Trottier, C., Eds.; Springer Nature Switzerland: Cham, 2024; pp. 28–35.
254. Zahedi, A.; Sanchez, L.; Noël, M. Appraisal of Visual Inspection Techniques to Understand and Describe ASR-Induced Development under Distinct Confinement Conditions. *Construction and Building Materials* **2022**, *323*, 126549, doi:10.1016/j.conbuildmat.2022.126549.
255. Azur, M.J.; Stuart, E.A.; Frangakis, C.; Leaf, P.J. Multiple Imputation by Chained Equations: What Is It and How Does It Work? *Int J Methods Psychiatr Res* **2011**, *20*, 40–49, doi:10.1002/mpr.329.